

RANGELAND FORAGE GROWTH PREDICTION, LOGISTICS, ENERGY, AND ECONOMICS
ANALYSIS AND TOOL DEVELOPMENT USING OPEN-SOURCE SOFTWARE

A Dissertation
Submitted to the Graduate Faculty
of the
North Dakota State University
of Agriculture and Applied Science

By

Subhashree Navaneetha Srinivasagan

In Partial Fulfillment of the Requirements
for the Degree of
DOCTOR OF PHILOSOPHY

Major Department:
Agricultural and Biosystems Engineering

March 2022

Fargo, North Dakota

NORTH DAKOTA STATE UNIVERSITY

Graduate School

Title

RANGELAND FORAGE GROWTH PREDICTION, LOGISTICS, ENERGY, AND
ECONOMICS ANALYSIS AND TOOL DEVELOPMENT USING
OPEN-SOURCE SOFTWARE

By

Subhashree Navaneetha Srinivasagan

The supervisory committee certifies that this dissertation complies with North Dakota State University's regulations and meets the accepted standards for the degree of

DOCTOR OF PHILOSOPHY

SUPERVISORY COMMITTEE:

Dr. Igathinathane Cannayen

Chair

Dr. Adnan Akyuz

Dr. Md Saidul Borhan

Dr. Simone Ludwig

Approved:

03/10/2022

Date

Dr. Leon Schumacher

Department Chair

ABSTRACT

Forage availability was crucial for livestock production across the United States. Rangelands occupied vast areas (31 %) of land and were the primary source of forage for livestock. However, extreme climatic conditions such as drought affect rangeland forage production and pose a serious threat to the rangeland enterprise. This increases the need to monitor forage in vast rangelands and adapt to other measures such as cultivating or buying forage to balance demand and supply. Despite this need, resources (studies and tools) on rangeland forage monitoring and existing forage production, handling, and economics were scattered and scarce. Therefore, a comprehensive systematic literature review was performed to gather the current understanding of the technology and resources used for monitoring and economics of forage production. Remote sensing technologies were widely used in recent research for their ability to scout vast areas frequently and machine learning (ML) in successfully comprehending complex relationships. Forage production economics was predominantly available for alfalfa forage crop, but other crops and bale collection logistics during production were ignored. Bale collection using conventional tractor carrying 1 and 2 bales/trip (BPT) and automatic bale picker (8–23 BPT) was simulated mathematically and analyzed with open-source R software using realistic equipment turning scenarios. Fuel consumption based on aggregation distance for ABP decreased on average by 72 % and 53 % compared to the tractor with 1 and 2 BPT. A web-based calculator tool was developed using open-source HTML, CSS, and JavaScript software for forage economic analysis including more than 10 varieties of forage crops involving the economics of bale collection (tractor and ABP). Pasture biomass yield prediction was performed with

R software using vegetation index (VI) and climate data through ML approaches. Recursive feature selection (RFE) and random forest (RF) model for forage yield emerged as the best methodology based on accuracy. A web-based interactive tool was developed using Shiny package in R to accommodate “field-specific,” pasture-scale inputs for predicting biomass yield. In conclusion, these successful results demonstrate the possibility of using open-source software for simulating logistics, developing models, and building tools for forage monitoring and analyzing the economics of forage production.

ACKNOWLEDGEMENTS

I would like to express my deepest appreciation and thanks to my major advisor and Doctoral Committee Chair Dr. Igathinathane Cannayen (Igathi), Associate Professor, Department of Agricultural and Biosystems Engineering (ABEN). His patience, knowledge, and motivation have made this journey an inspiring experience. As my mentor, he has led by example to show that anything was possible if we set our sincere efforts and time to it. This has helped me to break inhibitions, explore many opportunities, and learn new skills. His passion for research and technical writing has made me realize the importance of communicating research with the audience, in terms of peer-reviewed journal articles, and technical oral and poster presentations, and I am grateful for his efforts in teaching me this skill. His approach of solving an issue “Break it down — start simple!” has been a valuable lesson and it is something that I will carry with me for the rest of my career. His persistent and enthusiastic nature in solving a research problem is what I aspire to be as a researcher. Without his guidance and support, this research and dissertation would have not been possible. I would like to extend my thanks to Dr. S Pugalendhi, Professor, Tamil Nadu Agricultural University for introducing me to Dr. Igathi.

I would also like to record my appreciation to my doctoral dissertation committee members, Dr. Adnan Akyuz, Dr. Simone Ludwig, and Dr. Md Saidul Borhan for their valuable suggestions, time, guidance, and encouragement throughout this research. I would like to gratefully acknowledge my funding supports, USDA-ARS (FAR0020464 and FAR0028541), and in part by the USDA, NIFA, NDSU Hatch Projects through my advisor’s effort (ND01472 and ND01481).

I would like to thank Northern Great Plains Research Laboratory (NGPRL), USDA-ARS, Mandan for providing research and office facilities. I highly appreciate the help extended by the staff of NGPRL. I am grateful and thankful to the NGPRL scientists Drs. David Archer, John Hendrickson, Mark Liebig, Scott Kronberg, David Toledo, Jonathan Halvorson, and other researchers for their constant support and valuable guidance. I would like to thank my co-authors of the manuscripts during my time at NDSU. I would like to thank Julie Meissner for the discussion and support during my stay at NGPRL.

I want to thank Drs. Kevin Sedivec, NDSU, and Dannele Peck, USDA Climate Hub, for their insights and field data. I want to thank Mark Hayek and Jeff Printz, USDA-NRCS, for their constant support and suggestions on the developed tool. I am thankful to the farmers participating in the case studies and sharing their data. I thank Julie Bietz, Sara Ogundolani, Melissa Selders-Ortez, and Jim Moose, for their help during my time at the NDSU.

I am ever grateful to Dr. Sunoj Shajahan, Postdoctoral Research Associate, Cornell University, for inspiring me to pursue my doctoral degree. He has encouraged and helped me in every step of the way and has always been available for research discussions. I would like to extend my thanks to my advisor's family, Lalida akka, Srividhya, and Raghav for their care and kindness during my stay at Bismarck. I would like to thank Robin Malik, Sujitha Soundararajan, Amritha Raveendran, Pradeepika Chintla, and Harsh Pathak for their friendship and kind support during my stay at Fargo.

I would like to thank my family, my parents Navaneetha Srinivasagan Lalapuram Guruvappan and Umamaheswari Subbian, brother Ajay Guru, husband Vijay Kiran Rajamannar, mother-in-law Sathyabama Rajamannar, grandmother Mangaiyarkarasi, aunt

Vasuki Subbian, uncle Ulaganathan Perumal, and sisters Manju Narmada and Sindana Ulaganathan for their support in every step of my career.

Finally, I would like to thank all the faculty and staff at ABEN, NDSU, and friends who have been warm and supportive and any of this would have not been possible without them.

DEDICATION

This thesis is dedicated to my parents,

Navaneetha Srinivasagan Lalapuram Guruvappan and Umamaheswari Subbian

TABLE OF CONTENTS

ABSTRACT	iii
ACKNOWLEDGEMENTS	v
DEDICATION	viii
LIST OF TABLES	xv
LIST OF FIGURES	xvi
LIST OF ABBREVIATIONS	xxi
LIST OF SYMBOLS	xxvi
LIST OF APPENDIX TABLES	xxviii
LIST OF APPENDIX FIGURES	xxix
1. GENERAL INTRODUCTION	1
1.1. Significance of Rangeland Forage for Livestock Production	1
1.2. Current Technologies for Rangeland Monitoring	2
1.3. The Production, Logistics, and Economics of Forage	3
1.4. Problem Statement	4
1.5. Statement of Hypothesis	6
1.6. Statement of Objectives	7
1.7. Dissertation Organization	8
1.8. References	10
2. RANGELAND FORAGE GROWTH PREDICTION AND ECONOMIC ANALYSIS TOOLS — A SYSTEMATIC LITERATURE REVIEW	13
2.1. Abstract	13
2.2. Introduction	14
2.3. Review Methodology	17
2.3.1. Defining Research Questions	19
2.3.2. Strategy for Searching Literature	19

2.3.3. Exclusion Criteria	19
2.4. Results and Discussion	21
2.4.1. Important Features Predicting Grass/Forage Yield	21
2.4.2. Overview of Forage/Grass Prediction Models	33
2.4.3. Existing Tools for Grass/Forage Prediction	35
2.4.4. Tools Available for Forage Economics Analysis	44
2.5. Research Gaps and Future Recommendations	54
2.6. Conclusions	56
2.7. References	57
3. BIOMASS BALES INFIELD AGGREGATION LOGISTICS ENERGY FOR TRACTORS AND AUTOMATIC BALE PICKERS — A SIMULATION STUDY	76
3.1. Abstract	76
3.2. Introduction	77
3.3. Materials and Methods	80
3.3.1. Mathematical Simulation of Infield Bales Aggregation	82
3.3.2. Parameters Considered in the Simulation	84
3.3.3. Bale Aggregation Energy Through Fuel Consumption	84
3.3.4. Total Tractor Load of Fuel Consumption Methods	85
3.3.5. Fuel Quantity Calculation	89
3.3.6. Statistical Analysis	90
3.3.7. Development of Prediction Models	91
3.4. Results and Discussion	92
3.4.1. Bale Collection Using Tractor and ABP	92
3.4.2. Field Parameters Influence on Bale Aggregation Logistics Distances	94
3.4.3. Statistical Model Development for Logistics Distance and Time	94
3.4.4. Comparison of Fuel Consumption Methods - General vs Fuel Efficiency	98
3.4.5. Effect of Field Parameters on Fuel Quantity	100
3.4.6. Statistical Model Development for Fuel Quantity	106
3.5. Model Validation and Future Recommendation	109

3.6. Conclusions	110
3.7. References	111
4. DEVELOPMENT OF FORAGE ECONOMICS CALCULATOR WEB TOOL	118
4.1. Abstract	118
4.2. Introduction	119
4.3. Overview of the Web Tool	122
4.4. Web Tool Development	123
4.4.1. Web Tool Sections	124
4.4.2. User Interface and Web Tool Features	126
4.4.3. Web Tool Inputs	129
4.4.4. Web Tool Generated Results	133
4.5. Case Studies With Actual Farmers	140
4.5.1. Case Study Inputs	141
4.5.2. Case Study Results	141
4.5.3. ABP Inclusion in Case Studies	144
4.6. Scenario Analysis	145
4.6.1. Equipment Purchase Decision Scenario	146
4.6.2. Forage Crop Type Scenario	148
4.6.3. Low-Inputs Scenario	150
4.7. Conclusions	153
4.8. References	155
5. BIOMASS YIELD PREDICTION FOR PASTURES USING REMOTELY SENSED VEG- ETATION INDEX AND CLIMATE DATA THROUGH MACHINE LEARNING	158
5.1. Abstract	158
5.2. Introduction	159
5.3. Materials and Methods	163
5.3.1. Study Site Description	163
5.3.2. Data Acquisition	163
5.3.3. Data Processing	168

5.3.4.	Estimation of Vegetation Indices	169
5.3.5.	Modeling Approaches	172
5.3.6.	Feature Selection	172
5.3.7.	Linear and Machine Learning Prediction Models	174
5.3.8.	High-Performance Computing Resources Used	177
5.3.9.	Model Performance Assessment	178
5.4.	Results and Discussion	180
5.4.1.	Feature Ranking Results	180
5.4.2.	Feature Selection and Model Performance Comparison	182
5.4.3.	Application of the Developed Methodology and Model	186
5.5.	Conclusions	194
5.6.	References	196
6.	DEVELOPMENT OF A USER-FRIENDLY RANGELAND FORAGE YIELD PREDICTION WEB TOOL	207
6.1.	Abstract	207
6.2.	Introduction	208
6.3.	Application Methodology	210
6.4.	RangeForage Prediction Tool	212
6.4.1.	Data Collection and Processing	212
6.4.2.	Shiny User Interface	216
6.4.3.	Shiny Server	217
6.5.	RangeForage Tool Application - A Demonstration	218
6.5.1.	Loading Tool Inputs	218
6.6.	Conclusions	222
6.7.	References	223
7.	GENERAL CONCLUSIONS AND SUGGESTIONS FOR FUTURE WORK	225
7.1.	General Conclusions	225
7.2.	Suggestions for Future Work	228

APPENDIX A. BALE COLLECTION LOGISTICS ENERGY - EFFECT OF FIELD PARAMETERS ON AGGREGATION LOGISTICS DISTANCE	230
A.1. Effect of Field Parameters on Logistics Distance	230
A.1.1. Effect of Field Area on Logistics Distance	230
A.1.2. Effect of BPT on Logistics Distance	232
A.1.3. Effect of Biomass Yield on Logistics Distance	233
A.1.4 Effect of Outlet Location on Logistics Distance	235
A.2. Tukey’s HSD R Source Code	238
A.3. Tukey’s HSD Results	240
A.3.1. Aggregation Logistics Distance Influenced by the Field Parameters BPT and Biomass Yield	240
A.3.2. Fuel Quantity Influenced by Parameter Field Area	241
A.3.3. Fuel Quantity Influenced by Field Parameter BPT and Biomass Yield .	242
APPENDIX B. FORAGE ECONOMICS CALCULATOR - SIX-STEP USER INSTRUCTION	243
B.1. Web Tool User Instructions	244
APPENDIX C. FORAGE ECONOMICS CALCULATOR - STANDARD ECONOMICS CALCULATIONS	254
C.1. Total Fixed Cost	254
C.1.1. Depreciation (D)	254
C.1.2. Taxing, Housing, and Insurance (THI)	256
C.1.3. Interest (I)	256
C.1.4. Total Field Area Rent (TFAR)	257
C.2. Total Variable Cost	257
C.2.1. Repair and Maintenance (RMC)	258
C.2.2. Total Fuel Cost (TFC)	258
C.2.3. Total Labor Cost (TLC)	259
C.2.4. Total Bale Transportation Cost (TBTC)	259
APPENDIX D. FORAGE ECONOMICS CALCULATOR - HTML, CSS, AND JS SOURCE CODE	260
D.1. Cascading Style Sheet (CSS) for Styling Calculator	260

D.2. JavaScript - User-Defined Functions for Calculation Operation	266
D.3. JavaScript - User-Defined Functions for Data Visualization	281
APPENDIX E. BIOMASS YIELD PREDICTION - SHAPEFILE CREATION AND SATELLITE DATA COLLECTION	283
E.1. Creating Shapefile Using QGIS Software	283
E.2. Collecting Landsat and Sentinel Data From the GEE Archive	284
APPENDIX F. BIOMASS YIELD PREDICTION - R SOURCE CODES FOR SATELLITE BAND EXTRACTION, DATA SIMULATION AND MACHINE LEARNING APPROACHES	285
F.1. User-Defined Function to Extract the Raster (Satellite) Image Values Based on the Pasture Shapefile	285
F.2. Band Data Simulation Using Loess Fit Performed for Each Pasture	286
F.3. Combining Simulated Band Data Into a Data Frame and Filtering Using Date	286
F.4. Estimating Vegetation Indices	287
F.5. Machine Learning - Recursive Feature Elimination and Random Forest	288
APPENDIX G. RANGEFORAGE WEB TOOL - R SOURCE CODES FOR USER INTERFACE AND SERVER	290
G.1. User Interface R Code for Tool Development	290
G.2. Server R Code for Tool Development	292

LIST OF TABLES

<u>Table</u>	<u>Page</u>
2.1. Identified search item strings for systematic literature review.	20
2.2. Distribution of collected and screened literature based on the database sources in the chosen knowledge domain.	21
2.3. Details of selected articles through systematic literature review and their citation scores.	22
2.4. Distribution of screened literature based on the satellite platforms.	29
3.1. Fuel efficiency of different tractor loads (part and full) and different diesel types engines in kW h L^{-1} (hp h gal^{-1}) (Hunt, 2008).	89
3.2. Effect of field parameters on bale aggregation logistics distance.	95
3.3. Fuel consumption calculation for tractor and ABP using two methods.	99
3.4. ANOVA of field area, BPT, biomass yield, and equipment speed on the bale aggregation fuel quantity.	102
4.1. Brief description of the forage economics calculator web tool (FECWT) input options.	130
4.2. Field case studies using forage economics calculator web tool (FECWT) analyz- ing a perennial and annual forage crop.	142
4.3. Effect of including automatic bale picker (ABP) in case studies.	145
5.1. Climate and remote sensing data considered for the study.	167
5.2. List of RGB and multispectral based vegetation indices.	171
5.3. Feature rank from recursive feature elimination for satellite platforms.	191

LIST OF FIGURES

<u>Figure</u>	<u>Page</u>
1.1. Overview of the whole research on rangeland enterprise showing the objectives of different component studies.	8
2.1. Flowchart for conducting systematic literature review showing planning, conducting, and reporting stages of the review.	18
2.2. Vegetation indices versus number of literature collected from publication database sources. Frequency of vegetation indices is sorted from lowest to highest.	30
2.3. Distribution of screened literature on the application of climate and soil features for grass and forage prediction.	32
2.4. Box plot of prediction performance (R^2) for the eight most used regression and machine learning methods. ANN - artificial neural network, GB - gradient boosting, kNN - k-nearest neighbor, LR - linear regression, MLR - multiple linear regression, PLSR - partial least square regression, RF - random forest, and SVM - support vector machine.	34
2.5. Previous version of the ND drought calculator rainfall input page for predicting forage growth potential from three growth zones.	36
2.6. Updated no-macro ND drought calculator dashboard for predicting forage growth potential using monthly precipitation for two growth zones.	37
2.7. US Drought Monitor map categorized into abnormally dry (D0), moderate (D1), severe (D2), extreme (D3), and exceptional (D4). Last accessed on: February 24, 2022.	39
2.8. Grass-Cast maps with 3 scenarios; if precipitation is above normal (left map), is near-normal (middle map), and below normal (right map). Last accessed on: February 24, 2022.	41
2.9. Range analysis platform — interactive web-based tool for forbs and grass percentage cover and herbaceous biomass yield.	43
2.10. Alfalfa profitability and fertilizer cost calculator developed by University of Wisconsin-Extension.	46
2.11. Haying system enterprise budgeting estimate the operating and ownership costs developed by Montana State University Extension.	48
2.12. Alfalfa budget workbook guidelines reference developed by Washington State University Extension.	49

2.13. Price of standing hay crop from buyer and grower perspectives developed by PennState Extension.	51
2.14. Decision support tool for producing versus purchasing grass and alfalfa hay developed by Natural Resource Conservation Service (NRCS).	52
2.15. Forage economic calculator developed by North Dakota State University and NGPRL, USDA-ARS, Mandan, ND.	53
3.1. Examples of common and modern bale aggregation equipment: (A) Tractor equipped with bale spears at the front and rear (capacity = 1–2 bales); and (B) An automatic bale picker (ABP) with loading arm (capacity up to 23) — Image sources: https://www.himac.com.au and https://www.farm-king.com	81
3.2. Flowchart showing the details of the developed algorithm for the R program simulation to compare the tractor and ABP (automatic bale picker) performances based on the generated logistics distances and fuel consumption.	83
3.3. Logarithmic model ($R^2 > 0.99$) to predict the fuel efficiency (kWh/L) using the predictor variable of tractor load (%).	90
3.4. Bale aggregation equipment simulation results: (A) Tractor, BPT (bales/trip) = 1; (B) Tractor, BPT = 2; and (C) Automatic bale picker, BPT = 8; Simulation data: area = 2 ha; turning radius, $r_t = 10$ m; biomass yield/ha = 10 Mg; bale mass = 500 kg; harvester swath = 9 m; field aspect ratio = 1.0 ; random variation in biomass yield = 15 %; and random number seed used = 2016.	93
3.5. Fuel consumption methods comparison at two engine powers.	100
3.6. Effect of field area on the fuel quantity required for selected BPT (bales/trip) for tractor (1 and 2 BPT) and automatic bale picker (8, 11, 17, and 23 BPT), and field areas (8, 32, 65, 129, and 259 ha) with 10 Mg ha ⁻¹ biomass yield.	101
3.7. Effect of BPT (bales/trip) on the fuel quantity required by tractor and ABP (automatic bale picker) for aggregating 1–23 BPT for selected field areas of 8, 32, 65, 129, and 259 ha with 10 Mg ha ⁻¹ biomass yield.	103
3.8. Effect of biomass yield on the fuel quantity required by ABP (automatic bale picker) for aggregating 8 BPT (bales/trip) for selected field areas of 8, 32, 65, 129, and 259 ha.	105
3.9. Effect of equipment speed on the fuel quantity required to aggregate 8 BPT (bales/trip) for selected field areas of 8, 32, 65, 129, and 259 ha.	106
3.10. Fuel quantity utilized in bale aggregation as affected by field area and biomass yield at a selected equipment speed of 6.4 km h ⁻¹ . (A) Tractor with 1 BPT (bales/trip; tractor minimum); (B) Tractor with 2 BPT (tractor maximum); (C) ABP with 8 BPT (recommended); and (D) ABP (automatic bale picker) with 23 BPT (maximum).	108

4.1. Information flow and overall features of forage economics calculator web tool (FECWT) showing the user-inputs, FECWT processes and features, and the generated results using imperial units. The \$ represents US dollars (USD).	123
4.2. Overview of the forage economics calculator web tool (FECWT): A. home page of FECWT with web tool user-count feature; B. user instructions and manual section with downloadable 6-step instructions and detailed manual; C. calculator section of FECWT with 29 inputs, 37 output results, and a dynamic graph. .	125
4.3. Forage economics calculator web tool (FECWT) user interface and features showing the inputs column and results column: A. tooltip info, B. drop-down box, C. checkbox option, D. input slider, E. read-only text box, F. dynamic plot, G. profit-based color output, H. equipment-based output (tractor or automatic bale picker), I. view chart, J. download report.	127
4.4. Downloadable graphical visualization chart comparing total revenue, total cost, and net return. Other prominent economics outputs are presented in text. . . .	143
4.5. Equipment purchase scenario analysis for alfalfa forage crop: Effect of field area sections (8, 32, 65, 129, and 259 ha) on payback period (cycles) for equipment: tractor and ABP, tractor only, and ABP only. Tractor only = 2 BPT; ABP only and tractor and ABP = 8 BPT.	147
4.6. Forage crop type net return scenario: Effect of forage crop types (exclusive forage and grain-forage crops) economics showing grain revenue, total (grain + forage) revenue, total cost, and net return.	149
4.7. Low-inputs scenario analysis for alfalfa and grass on the effect of forage percent yield potential (alfalfa: 5000 lb/ac; grass: 3000 lb/ac) on net return for tractor only (bales/trip = 2) for field areas between 8 and 259 ha.	151
4.8. Low-inputs scenario analysis with 50 % forage yield potential (2500 lb/ac) for alfalfa crop: Effect of field area sections (8 ha–259 ha) on normal net return and low-inputs net return for tractor only (bales/trip = 2) and tractor and automatic bale picker (ABP) combined (bales/trip = 8).	153
5.1. Study site pastures located at Northern Great Plains Research Laboratory (NGPRL; USDA-ARS), Mandan, ND. Polygonal shapefiles of the study pastures are overlaid on the map. CWP: crested wheat pasture, HGP: highly grazed pasture, MGP: moderately grazed pasture. Inset: Mandan, ND, USA.	164
5.2. Overall process methodology including data extraction, processing, and developing biomass prediction models using climate and remote sensing data. NDAWN - North Dakota Agricultural Weather Network and NGPRL - Northern Great Plains Research Laboratory.	165
5.3. Feature (52 total) ranking results from backward elimination, Boruta, and recursive feature elimination feature selection methods.	181

5.4. Feature ranking from backward elimination, Boruta, and recursive feature elimination feature selection methods. MLR - multiple linear regression, kNN - k-nearest neighbor, SVR - support vector regression, and RF - random forest. . . .	183
5.5. A. Area under the curve for feature selection methods and ML models (kNN: k-Nearest Neighbor, MLR = multiple linear regression, RF - random forest, SVR - support vector regression; B. absolute RMSE deviation for recursive feature elimination feature selection method and random forest model).	185
5.6. Observed versus predicted biomass for the developed machine learning model for the pastures mildly grazed pasture (MGP), highly grazed pasture (HGP), and crested wheat pasture (CWP).	188
5.7. Satellite imagery with spatial resolution for moderately grazed pasture at Northern Great Plains Research Laboratory; A. Landsat 30 m (July 31, 2018); B. Sentinel 10 m (July 13, 2018); C: PlanetScope’s CubSat 3 m (July 14, 2018). . . .	190
5.8. Landsat, Sentinel, and CubeSat satellite comparison using performance metrics coefficient of determination (R^2) and root mean square error (RMSE).	191
5.9. Alfalfa forage fields H1 and G2 represented as polygon shapefiles located at Northern Great Plains Research Laboratory, (NGPRL; USDA-ARS), Mandan, ND, USA.	193
5.10. Observed versus predicted yields for alfalfa forage (hay crop) for different years (2017, 2018, and 2020), cuts (1–3), and fields (H1 and G2; fig. 5.9).	194
6.1. Shiny R framework of RangeForage tool consisting on user interface and server components.	212
6.2. User interface of RangeForage web tool showing inputs (left) and results panel (right).	213
6.3. Creating a new polygon shapefile layer using QGIS software.	214
6.4. Downloading raster images; A. PlanetScope’s filter search dialog box; B. raster image tile (captured by the satellite) available for the selected extent (shown in blue).	215
6.5. Weather variables selected using North Dakota agricultural weather network (NDAWN).	216
6.6. Shiny widgets used in the RangeForage prediction tool; A. file upload, B. slider, C. action button, and D. checkbox.	217
6.7. Loading shapefile; A. file upload from a local system, and B. extent of shapefile overlaid on the base map.	219
6.8. Loading raster file; A. file upload from a local system, and B. raster and shapefile overlaid on the base map.	219

6.9. Weather variable input using slider shiny widget.	220
6.10. Extracted band values, estimated vegetation indices, forage yield results presented in tool's main panel.	221
6.11. Extracted band values, estimated vegetation indices, forage yield results presented in tool's main panel.	222

LIST OF ABBREVIATIONS

ABP.....	Automatic Bale Picker
AIC.....	Akaike Information Criterion
ANN.....	Artificial Neural Network
ARS.....	Agricultural Research Service
ARVI.....	Atmospherically Resistant Vegetation Index
AVHRR.....	Advanced Very High Resolution Radiometer
B.....	Blue
BCC.....	Blue Chromatic Coordinate
B-G.....	Blue-Green Difference
BIBLMM.....	Biomass Infield Bale Logistics Multivariate Model
BPT.....	Bales Per Trip
BRVI.....	Blue Red Vegetation Index
C1.....	Exclusion Criteria 1
C2.....	Exclusion Criteria 2
C3.....	Exclusion Criteria 3
C4.....	Exclusion Criteria 4
CCAST.....	Center for Computationally Assisted Science and Technology
CIC.....	Crop Input Cost
CIVE.....	Colour Index of Vegetation
CO.....	Coloration Index
CSS.....	Cascading Style Sheets
CSV.....	Comma Separated Value
CWP.....	Crested Wheat Pasture
DC.....	Drought Calculator
DVI.....	Difference Vegetation Index

EOSDIS	Earth Observing System Data and Information System
ETM	Enhanced Thematic Mapper
EVI	Enhanced Vegetation Index
EVI2	Two-Band Enhanced Vegetation Index
ExG	Excess Green
ExG2	Normalized Excess Green
ExGR	Excess Green Minus Excess Red
ExR	Excess Red
FECWT	Forage Economics Calculator Web Tool
FGP	Forage Growth Potential
G	Green
G/R	Green-Red Ratio
GARI	Green Atmospherically Resistance Vegetation Index
GB	Gradient Boosting
GBVI	Green Blue Vegetation Index
GCC	Green Chromatic Coordinate
GCI	Green Chlorophyll Index
GEE	Google Earth Engine
GIS	Geographic Information System
GNDVI	Green Normalized Difference Vegetation Index
G-R	Green-Red Difference
GRVI	Green and Red Ratio Vegetation Index
HCC	Harvest and Collection Cost
HGP	Highly Grazed Pasture
HTML	Hypertext Markup Language
IDE	Integrated Development Environment
kNN	k-Nearest Neighbor
L	Length

LIDAR	Light Detection and Ranging
LR	Linear Regression
LSWI	Land Surface Water Index
MAE	Mean Absolute Error
MGP	Moderately Grazed Pasture
MGRVI	Modified Green Red Vegetation Index
MIRA	Maximal Importance of Random Features
ML	Machine Learning
MLR	Multiple Linear Regression
MODIS	Moderate Resolution Imaging Spectroradiometer
MSAVI	Modified Soil-Adjusted Vegetation Index
MSI	Multi-Spectral Instrument
NASS	National Agricultural Statistics Service
ND	North Dakota
NDAWN	North Dakota Agricultural Weather Network
NDMC	National Drought Mitigation Center
NDMI	Normalized Difference Moisture Index
NDPI	Normalized Difference Phenology Index
NDSU	North Dakota State University
NDVI	Normalized Difference Vegetation Index
NDWI	Normalized Difference Water Index
NGP	Northern Great Plains
NGPRL	Northern Great Plains Research Laboratory
NIR	Near-Infrared
NOAA	National Oceanic and Atmospheric Administration
NRCS	Natural Resource Conservation Service
NRI	National Resource Inventory
NSAVI	Modified Soil Adjusted Vegetation Index

OOB	Out-of-Bag
OSAVI	Optimized Soil-Adjusted Vegetation Index
PDF	Portable Document Format
PDSI	Palmer Drought Severity Index
PET	Potential Evapotranspiration
PLS	Partial Least Square
PLSR	Partial Least Square Regression
PTO	Power Take Off
Q1	Research Question 1 of Systematic Literature Review
Q2	Research Question 2 of Systematic Literature Review
Q3	Research Question 3 of Systematic Literature Review
Q4	Research Question 4 of Systematic Literature Review
R	Red
RAP	Rangeland Analysis Platform
RCC	Red Chromatic Coordinate
RF	Random Forest
RFE	Recursive Feature Elimination
RMSE	Root Mean Square Error
ROI	Return on Investment
RS	Remote Sensing
RVI	Relative Vigor Index
SAVI	Soil-Adjusted Vegetation Index
SIPI	Structure Intensive Pigment Index
SLR	Systematic Literature Review
SPI	Standard Precipitation Index
SR	Simple Ratio

SR.....	Simple Ratio Index
sUAS.....	Small Unmanned Aerial System
SVM.....	Support Vector Machine
SVR.....	Support Vector Regression
SWIR.....	Short-Wave Infrared
SWIR1.....	Short-Wave Infrared 1
SWIR2.....	Short-Wave Infrared 2
TBC.....	Total Baling Cost
TC.....	Total Cost
TCC.....	Total Combined Chemical + Application Cost
TFC.....	Total Fixed Cost
TFRC.....	Total Combined Fertilizer + Application Cost
THC.....	Total Harvest Cost
TM.....	Thematic Mapper
TPC.....	Total Bale Production Cost
TSC.....	Total Combined Seed + Application Cost
TVC.....	Total Variable Cost
UAV.....	Unmanned Aerial Vehicle
USD.....	United States Dollars
USDA.....	United States Department of Agriculture
USDM.....	US Drought Monitor
VARI.....	Visible Atmospherically Resistant Index
VDVI.....	Visible-Band Difference Vegetation Index
VI.....	Vegetation Index
W.....	Width
WI.....	Woebbecke Index

LIST OF SYMBOLS

A_F	Field area (ha)
Avg.T	Average air temperature ($^{\circ}\text{C}$)
Avg.WD	Average wind direction ($^{\circ}$)
Avg.WindS	Average wind speed (km/h)
AvgB_Soil	Average bare soil temperature ($^{\circ}$)
AvgT_Soil	Average turf soil temperature ($^{\circ}$)
a, a', b'', c''	Model coefficients
a'	Constant $0.0434 \text{ (gal hp}^{-1}\text{h}^{-1}\text{)}$
B_T	Bales per trip
b' and a''	Model constants
b, c, c', d''	Exponents of the models
C_{F1}	Fuel consumption at partial and full tractor load (gal h^{-1})
C_{F2}	Fuel consumption using energy efficiency method (L h^{-1})
C_T	Tractor capacity (kW)
D_L	Total bale aggregation logistics distance (km)
Dew_P	Dew point ($^{\circ}\text{C}$)
Di_TR	Diurnal air temperature ($^{\circ}\text{C}$)
E_F	Fuel efficiency (kW h L^{-1})
F_C	Fuel quantity for bale collection
F_{LU}	Fuel quantity for loading and unloading
h	hour
JH_PET	Potential evapotranspiration (Jensen–Haise, mm)
L_T	Total tractor load (%)
L_E	Empty tractor load (%)

L_B	Bale load (%)
M_B	Bale mass (kg)
Max_T	Maximum air temperature (°C)
Max_WS	Maximum wind speed (km/h)
Min_T	Minimum air temperature (°C)
Min_Wind_Chill	Minimum wind chill (°C)
N_B	Number of bales
N_F	Number of fields
%	Percentage
Pen_PT	Penman potential evapotranspiration (mm)
p	Probability value
P_R	Rated power take off (PTO) power (hp)
X	Ratio of equivalent available PTO power based on tractor load to the rated PTO power
P_A	Available PTO power based on the part and full tractor load (hp)
Q_F	Fuel quantity (L)
R^2	Coefficient of determination
S_p	Equipment speed (km h ⁻¹)
Tot_Sol_R	Total solar radiation (Ly)
T_C	Bale collection time
T_L	Loading time per bale
T_{LU}	Total bale loading and unloading time
T_{OT}	Total bale movement time
T_U	Unloading time per bale
Wind_Chill	Average wind chill (°C)
y	Dependent variable
Y_B	Biomass yield (Mg ha ⁻¹)

LIST OF APPENDIX TABLES

<u>Table</u>	<u>Page</u>
A1. ANOVA of field area, BPT, and biomass yield on bale aggregation logistics distances.	231
A2. Tukey's HSD analysis results of aggregation logistics distance influenced by the field parameters BPT and biomass yield.	240
A3. Tukey's HSD analysis results of fuel quantity influenced by the field area.	241
A4. Tukey's HSD analysis results of fuel quantity influenced by BPT and biomass yield.	242

LIST OF APPENDIX FIGURES

<u>Figure</u>	<u>Page</u>
A1. Effect of field area on the aggregation logistics distances generated for selected BPT (bales/trip) for tractor (1 and 2 BPT) and automatic bale picker (8, 11, 17, and 23 BPT), and field areas (8, 32, 65, 129, and 259 ha) with biomass yield at 10 Mg.ha ⁻¹	231
A2. Effect of BPT (bales/trip) on the aggregation logistics distance generated for selected field areas (8, 32, 65, 129, and 259 ha) for tractor (0–5 BPT) and automatic bale picker (ABP; 8–23 BPT) with biomass yield at 10 Mg ha ⁻¹	232
A3. Effect of biomass yields (3–40 Mg ha ⁻¹) on the aggregation logistics distance generated for selected field areas (8, 32, 65, 129, and 259 ha) using automatic bale picker (ABP) with 8 BPT (bales/trip).	234
A4. Effect of outlet location on bale aggregation; Simulation data: area = 4 ha; BPT = 8; turning radius, r _t = 10 m; biomass yield/ha = 10 Mg; bale mass = 500 kg; harvester swath = 9 m; field aspect ratio = 1.0 ; random variation in biomass yield = 15 %; and random number seed used = 2016.	236
A5. Outlet locations effect on logistics distance (km). O:M = field middle; O:W = along mid-width edge; O:L = along mid-length edge; O:O = field origin; Simulation data: field area = 65 ha, BPT = 8, biomass yield = 10 Mg ha ⁻¹ , and rest of the data were similar to fig. A4.	237
E1. Creating polygon shapefile using QGIS software.	284

1. GENERAL INTRODUCTION

1.1. Significance of Rangeland Forage for Livestock Production

In the United States, the rangelands contribute to about 31 % of the total land area, approximately about 308 million ha (Havstad et al., 2007) and serve as a key resource for ecological and economic impact. Natural grassland, savannas, pastures, shrublands, marshes, and wet meadows fall under the category of rangeland (Reeves et al., 2015). Rangeland is a naturally managed ecosystem often described as the land consisting of indigenous vegetation which is predominantly grasses. Rangelands were the primary base for grazing forages and therefore crucial for livestock production. For ages, forages has been an essential source of nutrients in maintaining animal health and is a rich source of fiber that facilitates proper digestion in the animals consuming forage. With the conversion of livestock into milk and meat products, the forages continue to remain as one of the primary sources of nutrients in the human diet as well.

The forage production in rangeland depends on multiple drivers such as climate, soil, and topography which aids in regulating the plant-available water. Numerous studies have explored the influence of factors controlling the forage production, temperature was observed to be the important feature affecting the four stages of growth such as germination, winter, spring, and peak forage production (Becchetti et al., 2016). Studies have also reported a strong link between precipitation and forage production (Allred et al., 2014; Lang et al., 2019).

Several rangelands in the Northern Great Plains are rain-fed and therefore are vulnerable to irregular precipitation trends (Sloat et al., 2018). With increasing climate vari-

ability, drought conditions are prevalent and pose a serious threat to livestock production. With reduced production of forage during drought season, the animal stocking rate is affected and the value of cattle drops down. In addition, the rangeland system is overworked during drought season and the lost plant cover leads to soil erosion (Herrick et al., 2018). The varying climate intensifies the need for monitoring the forage production in rangelands and adapting to drought conditions through cultivating and securing forage for later use (Angerer, 2012).

1.2. Current Technologies for Rangeland Monitoring

Monitoring of rangeland forage has evolved over the years from traditional methods to the use of modern remote sensing using unmanned aerial vehicles (UAVs) and satellites. The traditional methods include clip-dry-weigh, rising plate meter, visual estimation (Psomas et al., 2011). These methods are subjective, laborious, time-consuming, of a smaller scale, and were not comparable to remote sensing technology. The remote sensing technology provides spatio-temporal information of the rangeland, and the state of the environment can be easily captured over a large landscape more frequently. Availability of large imagery data has facilitated the understanding of land cover, plant health, and monitoring change in the rangeland landscape (Chen and Gillieson, 2009).

The selection of the type of remote sensing data is based on the scale and scope of the research. Using high spatial resolution (<10 m) was ideal for extracting rangeland biomass; however, consistently using high spatial resolution for a large landscape is limited by several factors (e.g., computational resources and storage). The satellites with a coarse spatial resolution with high frequency revisit time, such as Moderate Resolution Imaging Spectroradiometer (MODIS) was efficient in evaluating biomass on a county,

national, or global scales; however, was not successful with field-scale level since the resolution of MODIS satellite (500 m) was larger than an average pasture size. Over the last few decades, the Landsat 5, 7, and 8 (30 m) and Sentinel-2 10 m satellite imagery was widely used for biomass estimation in rangelands for its large spatial coverage, increased revisit frequency, and relatively high resolution. A comparison study between the satellite imagery reported that Sentinel-2 images assessed and monitored pasture biomass better than Landsat 8 data (Sibanda et al., 2015). Few tools such as spread-sheets-based, map-based, and interactive web-based were available to monitor and estimate biomass at a larger scale.

1.3. The Production, Logistics, and Economics of Forage

In drought-prone regions, to balance the demand and supply of forage and to overcome seasonal shortfalls, farmers and ranchers resort to cultivating or buying forage for storage. Forage production economics that includes operating cost, seeding, harvesting, baling, and storing contributes significantly to the annual livestock production cost (Horrocks and Valentine, 1999; Nayigihugu et al., 2007).

The cultivated forage is left on the field as bales randomly and is collected using a traditional tractor that can carry 1–2 bales per trip or an advanced automatic bale picker that can load about 8–23 bales/trip. This bale aggregation logistics represents significant effort and economics associated with it. Including operating costs for bale collection operation would provide farmers with realistic economics. Economic analysis of forage production aids in making management decisions such as selection of crops, fixing forage prices, and efficient operations and plays a vital role in reducing the risk involved in an agricultural enterprise. Several spreadsheet-based calculators were available, but

predominantly dealing with alfalfa forage crop, which aids farmers and ranchers with the economic analysis of their operation.

1.4. Problem Statement

Considering the overview provided on the current grazing scenario in producing forage crops and rangeland monitoring, handling the harvested forages in bale form, the economics of forage production and logistics, tools available dealing with the forage yield monitoring/prediction and economics, there are several issues and research gaps which can be addressed efficiently using modeling techniques and developing user-friendly web tool for the ranchers, ranch managers, and farmers. The problems existing with the present forage production, handling, and economics and the proposed solution in this research are outlined briefly hereunder:

First, a consolidated review on technology and advancement in rangeland forage yield prediction, forage logistics, and tools available for the users will be helpful in understanding the current knowledge domain and identifying research gaps. It also helps in identifying the features influencing the forage yield. The features generally include the climate and remotely sensed vegetation indices. Furthermore, collective information on the technologies such as sensors, type of models, and existing tools was scarce. Therefore, a need for a systematic literature review on the aforementioned aspects exists.

Second, farmers cultivating forage crops often ignore bale collection logistics operations in their economics calculations. However, collecting bales is an intensive operation as the machinery makes overlapping multiple trips collecting bales from the field and transporting them to the field outlet. There was machinery operating costs involved, including fuel and labor during the collection operation. The fuel used during this process was es-

estimated based on the distance traveled, speed of the machinery used, and machinery's fuel consumption characteristics. Therefore, there exists a need for developing a research work to evaluate energy consumption, in terms of fuel for bale collection operation. This research can be further used in economic analysis for a realistic representation of the costs and profits involved.

Third, forage economic analysis involves numerous variables and complex calculations which are difficult to perform using manual methods. Though a few available spreadsheet-based calculators for economic analysis are available, some of the disadvantages of using those include, scattered resources lead to downloading more than one spreadsheet; most spreadsheets calculators are macro-enabled, which possess a high risk of malware attack; mostly developed for the predominant forage crop, namely alfalfa; and focused on operation costs, such as harvesting and baling, while machinery, fuel, and labor cost associated with bale collection, which is an intensive field operation, are often ignored. Therefore, there exists a need for developing a safe, user-friendly web-based tool for forage economics analysis inclusive of various forage crops and bale collection operation costs. This tool will be useful for ranchers, forage producers, commercial bale operators, and others involved in the production and handling of forage.

Fourth, ranchers and rangeland managers on the US Great Plains face drought periods that range from mild to severe and can last for a season to multiple years. Drought in rangeland can significantly reduce the amount of forage available for the livestock. Monitoring forage and estimating the forage yield throughout the growing season with the consideration of weather parameters is of key importance for rangeland management decisions. The existing forage prediction models are developed for large-scale regression-

based prediction using coarse resolution satellites for monitoring thus failing to address the weather variability and native grass varieties responses specific to a local area. Therefore, new advanced machine learning (ML) approaches can be explored to predict biomass using vegetation indices from the fine-resolution satellite in combination with local weather parameters is desirable for a “field-specific” forage prediction.

Fifth, ranchers and ranch managers will benefit from a decision support tool for planning animal stocking rates based on the available forage. A functional tool should be developed that was easy to use and require only information that is readily available as user inputs. The existing forage prediction tools are developed for larger scale landscapes, visually presented, and allow minimal interaction from the user. Therefore, a simple ranch prediction forage web tool that allows users to input “field-specific” climatic and remote sensing inputs to predict more realistic forage yields using open-source platforms will be useful and appreciated by the stakeholders.

1.5. Statement of Hypothesis

1. A systematic review can be performed on the existing models and tools available for rangeland forage estimation and economic analysis to identify research gaps and formulate future research directions.
2. Energy expensed during the intensive forage bale collection logistics operation can be studied and modeled through mathematical simulation.
3. A user-friendly forage analysis web tool can be developed for major forage varieties with sensitivity analysis features and downloadable results using open-source platforms.

4. Recent advancements such as a finer spatial satellite in combination with local weather variables and ML modeling can be used to estimate field-specific rangeland forage yields.
5. A ranch forage prediction user-friendly web tool can be developed using the developed ML forage prediction models for the ranchers and range managers to aid in management decisions.

1.6. Statement of Objectives

The specific objectives of this research are to (fig. 1.1):

1. Perform systematic literature review on remote sensing platforms, vegetation indices, weather parameters, prediction models for monitoring forage along with tools available for prediction of forage yield and economic analysis of forage production and handling.
2. Develop prediction models using field parameters to evaluate logistics distance, operation time, and energy involved in terms of fuel requirements during bale collection processes through mathematical simulation.
3. Build user-friendly forage economic web tool with sensitivity analysis and downloadable results using open-source platform resources.
4. Identifying overall methodology of best features selected and best ML model for rangeland forage yield prediction.
5. Build ranch forage prediction web tool using the developed prediction model with user-friendly features for ranchers, farmers, and other stakeholders.

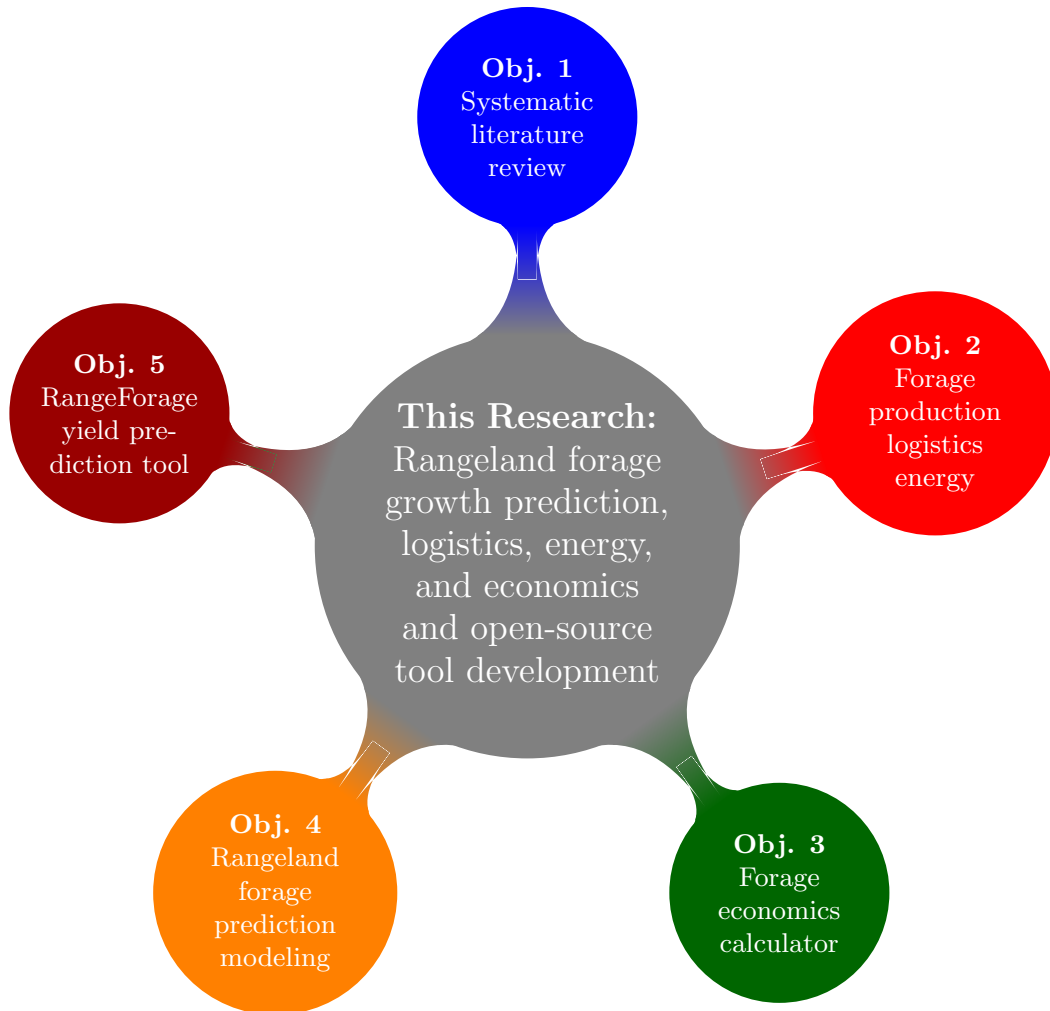


Figure 1.1. Overview of the whole research on rangeland enterprise showing the objectives of different component studies.

1.7. Dissertation Organization

The dissertation is organized into chapters that consist of the general introduction (Chapter 1), and the research objectives are presented in the form of peer-reviewed journal articles (Chapters 2–6) with individual chapter references, and the general conclusion (Chapter 7), and appendices covering various additional information of the regular chapter materials.

Chapter 1, this general introduction (this chapter) provides an overall significance of rangeland forage production for livestock production, current technologies used for rangeland monitoring, forage yield production and logistics, and economics of cultivated forage. It also includes the problem statement, statement of hypothesis, and statement of objectives.

Chapter 2, deals with the systematic literature review on economic analysis tools and forage growth prediction models and tools available (Paper 1), titled: “Rangeland forage growth prediction and economic analysis tools — a systematic literature review.” The review covers various remote sensing platforms, vegetation indices, climate features, prediction models and tools used for forage yield prediction, and forage economic analysis tools.

Chapter 3, deals with the mathematical simulation of bale collection operation using tractor and automatic bale picker (Paper 2), titled: “Biomass bales infield aggregation logistics energy for tractors and automatic bale pickers — a simulation.” The study used kinematics and analytical geometry principles and simulated field parameters for developing prediction models to evaluate the aggregation distance and time involved in the bale collection process.

Chapter 4, deals with the user-friendly web-based tool developed for forage economic analysis of several forage crops (Paper 3), titled: “Development of forage economics calculator web tool.” The chapter contains the overview, structure, styling, and development of the web tool. Individual sections, inputs, background models, results, and features of the web tool are explained in detail. The chapter also contains real field case studies conducted to validate the performance of the developed web-based calculator.

Chapter 5, deals with the selection of the best methodology for forage yield prediction (Paper 4), titled: “Biomass yield prediction for pastures using remotely sensed vegetation index and climate data through machine learning.” The study used ground-truth biomass data, spatial data from Landsat, Sentinel, and CubeSat satellites for estimating the best methodology of influential features and best-performing ML model.

Chapter 6, deals with the development of a web tool, named RangeForage, for rangeland forage prediction based on the trained ML models developed (Paper 4), titled: “Development of rangeland forage yield prediction tool.” The chapter contains the need for the rangeland prediction tool, methodology, user interface input widgets, server functions, developed application and its demonstration.

1.8. References

- Allred, B. W., Scasta, J. D., Hovick, T. J., Fuhlendorf, S. D., & Hamilton, R. G. (2014). Spatial heterogeneity stabilizes livestock productivity in a changing climate. *Agric. Ecosyst. Environ.*, 193, 37–41.
- Angerer, J. P. (2012). 12. Gobi forage livestock early warning system. *Nt. Feed Assess.*, 115.
- Becchetti, T., George, M., McDougald, N., Dudley, D., Connor, M., Flavel, D., Vaughn, C., Forero, L., Frost, W., Oneto, S., et al. (2016). Annual range forage production. *Calif. Agric.*, 8018.
- Chen, Y., & Gillieson, D. (2009). Evaluation of landsat TM vegetation indices for estimating vegetation cover on semi-arid rangelands: A case study from Australia. *Can. J. Remote Sens.*, 35(5), 435–446.

- Havstad, K. M., Peters, D. P., Skaggs, R., Brown, J., Bestelmeyer, B., Fredrickson, E., Herrick, J., & Wright, J. (2007). Ecological services to and from rangelands of the united states. *Ecol. Econ.*, *64*(2), 261–268.
- Herrick, J., Weltz, M., Reeder, J., Schuman, C., & Simanton, J. (2018). Rangeland soil erosion and soil quality: Role of soil resistance, resilience, and disturbance regime. *Soil Qual. Soil Ero.* (pp. 209–233). CRC press.
- Horrocks, R. D., & Valentine, J. F. (1999). *Harvested Forages*. Academic Press, Cambridge, MA, USA.
- Lang, B., Geiger, A., Oyunbileg, M., Ahlborn, J., von Wehrden, H., Wesche, K., Oyuntsetseg, B., & Römermann, C. (2019). Intraspecific trait variation patterns along a precipitation gradient in Mongolian rangelands. *Flora*, *254*, 135–146.
- Naygihugu, V., Schleicher, A., Koch, D., Held, L., Flake, J., & Hess, B. (2007). Beef cattle production, nutritional quality, and economics of windrowed forage vs. baled hay during winter. *Agron. J.*, *99*(4), 944–951.
- Psomas, A., Kneubühler, M., Huber, S., Itten, K., & Zimmermann, N. (2011). Hyperspectral remote sensing for estimating aboveground biomass and for exploring species richness patterns of grassland habitats. *Int. J. Remote Sens.*, *32*(24), 9007–9031.
- Reeves, M. C., Robert, A., Angerer, J., Hunt Jr, E. R., Wasantha, R., & Kumar, L. (2015). Global view of remote sensing of rangelands: Evolution, applications, future pathways. *Land Resour. Monit. Model. Mapp. Remote Sens.*, 237–266.
- Sibanda, M., Mutanga, O., & Rouget, M. (2015). Examining the potential of Sentinel-2 MSI spectral resolution in quantifying above ground biomass across different fertilizer treatments. *SPRS J. Photogramm. Remote Sens.*, *110*, 55–65.

Sloat, L. L., Gerber, J. S., Samberg, L. H., Smith, W. K., Herrero, M., Ferreira, L. G., Godde, C. M., & West, P. C. (2018). Increasing importance of precipitation variability on global livestock grazing lands. *Nat. Clim. Change*, 8(3), 214–218.

2. RANGELAND FORAGE GROWTH PREDICTION AND ECONOMIC ANALYSIS TOOLS — A SYSTEMATIC LITERATURE REVIEW *

2.1. Abstract

Farmers and ranchers heavily depend on the annual production of natural forage and herbage from the grassland for livestock grazing. Many regression and machine learning (ML) prediction models have been developed for grass and forage to understand the seasonal variability in the forage production, build management practices, and plan the animal stocking rate. Besides, decision-support tools aid farmers in comparing management practices and developing forecast scenarios. Although numerous individual studies on forage growth, models, predictions, economics, tools were available, a comprehensive review for forage growth prediction and economic analysis tools was not available. Therefore, in this study, a systematic literature review (SLR) was performed to establish comprehensive knowledge and identify research gaps in this knowledge domain to serve better the stakeholders. The input features (vegetation index (VI), climate, and soil), various models (regression and ML), and relevant tools for grass and forage prediction and tools developed for forage economic analysis were analyzed. Based on the search criteria and from the three publication databases, we retrieved 147 relevant peer-reviewed manuscripts of the current period (2010 – 2021), of which only 85 were screened after applying exclusion criteria for further analysis and reporting. The most frequently used remote sensing satellite

* This paper will be submitted to the *Biomass and Bioenergy* journal in 2022. Authors: Srinivasagan N. Subhashree, C. Igathinathane, A. Akyuz, Md. Borhan, J. Hendrickson, D. Archer, M. Liebig, D. Toledo, K. Sedevic, S. Kronberg, and J. Halvorson. Subhashree performed the systematic literature review and wrote the manuscript. Dr. Igathinathane Cannayen is the major advisor, principal investigator, and the corresponding author who worked with Subhashree throughout the research and manuscript development. All the co-authors have assisted in the research direction and review of the manuscript.

platform was MODIS based on the review. The most commonly used input features were normalized difference vegetation index (NDVI), precipitation, and soil moisture. Among the ML models, the most widely used and with better performance, for estimating grass and forage yield was the random forest. Four existing tools use inputs such as precipitation, evapotranspiration, and NDVI available for larger-scale grass and forage prediction and monitoring. Most tools available for forage economic analysis were spreadsheet-based and focused on alfalfa. Suggestions for future research in this knowledge domain include the use of high-resolution satellites, combined VI and climate features, advanced ML models, development of field-specific prediction, and development of interactive, user-friendly, web-based tools and smartphone applications in this knowledge domain.

2.2. Introduction

Pastures dominate the landscape of western and central United States, covering more than 60% of the land surface (M. C. Reeves and Mitchell, 2011). Grasslands, rangelands, shrublands, meadows, steppes, and woodlands fall under the category of pastures and were maintained to support various operations but predominantly the livestock industry. The Northern Great Plains comprises states such as Montana, Wyoming, Colorado, North Dakota, South Dakota, and Nebraska, which are primarily rural areas, and the region consists of 25% of the nation's livestock population (Derner et al., 2018). Forages are crucial in maintaining livestock health as they aid in providing essential nutrients and enhancing proper digestion in the animals. Therefore, ranchers and farmers have to ensure a continuous supply of forage through adequate monitoring and management practice for rangeland and pastureland and making effective agricultural enterprise decisions through performing economic analysis.

Although several individual scientific studies on forage growth, models, predictions, economics, tools were available, a comprehensive review on the knowledge domain of forage growth prediction and economic analysis tools was not available. Therefore, this study reviews the scientific literature, specifically peer-reviewed journal articles of the current period from years 2010 to 2021, to provide comprehensive knowledge and research gaps for serving the stakeholders better.

Ranchers rely on natural forage, herbaceous plants, and shrubs that predominantly grow in range and pastureland. These lands are feeding grounds for beef cattle, dairy cattle, sheep, goats, horses, and other domestic livestock. Therefore, estimating forage potential (forage growth prediction) months in advance aid ranchers and range managers in resource planning and management. In addition to ensuring forage availability and productivity, effective management practices also benefit the ecosystem of the pastures. One of the primary indicators for the pasture ecosystem is the biomass yield which is traditionally measured using destructive methods, such as clipping and drying that are constrained to small areas due to the nature, time, and labor involved (Feng et al., 2020; Jin et al., 2014).

A possible replacement for the traditional methods for estimating pasture biomass is the non-destructive methods such as remote sensing (RS) after suitable validation/calibration. Satellites and unmanned aerial vehicles (UAVs) fall under the RS technology, and the green vegetation was monitored using its spectral reflectance properties (Atzberger, 2013). The satellite information can be of high value when large areas are studied, the time and labor were significantly reduced. The satellite datasets can be easily obtained, and reproducible studies can be performed. The wavelengths from optical sensors, at-

tached to the satellite platforms efficiently collected and secured the information, can be used for applications, such as detecting greenness, estimating vegetation density, distinguishing different vegetation classes, among others (Hashim et al., 2019; Pal et al., 2018; Xie et al., 2019). The most commonly used optical sensor satellites are Landsat, Sentinel-2, MODIS, and AVHRR.

In recent years, the use of satellites for monitoring pasture biomass steadily increased since the data was readily available and freely accessible. Vegetation indices (VI) estimated from the spectral wavelength data were used as a proxy for the biomass yield in pastures (Dos Reis et al., 2020). Other than remote sensing methodology, many studies have explored the influence of soil and climate features in predicting biomass yield (Krueger et al., 2021; Y. Liu et al., 2021). A simple linear relationship was helpful to understand the importance of VI, soil, or climate feature in predicting pasture biomass individually. However, complex and interlinked connections between the features and biomass were better explained using machine learning (ML) approaches.

Building interactive tools were critical to farmers' success since it helps them to make real-time decisions, devise management strategy, and plan budget (Garg et al., 2022; Leroux et al., 2018). The developed prediction models and economic analysis can be delivered as a user-friendly tool that puts farmers at the driver's seat in making decisions. For example, tools using a developed prediction model might aid farmers in monitoring pastures and planning livestock stocking rates. Economic analysis tools were vital in aspects such as measuring farm profit, evaluating the effectiveness of management strategies, and analyzing scenarios.

The objective of this study was to review the input features (VI, soil, and climate), prediction models (regression and ML), and tools applied to grass and forage estimation and economic analysis tools using systematic literature review (SLR) process. The SLR was designed to be replicable; therefore, all the required steps of conducting SLR and the results will be presented for transparency. The review included responses to the research questions framed during the initial stage of the review. Potential research gaps in a specific knowledge domain were effectively identified using SLR. These identified research gaps are expected to serve as a guide to researchers pursuing new research in this subject area and add information to the knowledge domain.

2.3. Review Methodology

The review methodology followed the systematic literature review (SLR) guidelines as outlined by Keele et al. (2007). A review protocol is emphasized in SLR which includes developing specific research questions to be addressed and planning the methods for successfully performing the review (fig. 2.1). The SLR relies on a defined search strategy that helps to find as much as the relevant literature for answering the research questions. The database sources that were used for selecting relevant literature include, Science Direct, Web of Science, Scopus, and Google Scholar. The selected literature were screened using various inclusion or exclusion criteria; this aids in assessing the importance of incorporating a study addressing a specific research question. According to SLR, the review process can be classified into three stages; (i) plan, (ii) conduct, and (iii) report the review.

Scope for conducting the review and research questions was identified during the planning stage. With the scope identified a draft review protocol that details the steps and procedures to be followed during the review process was developed. The draft protocol

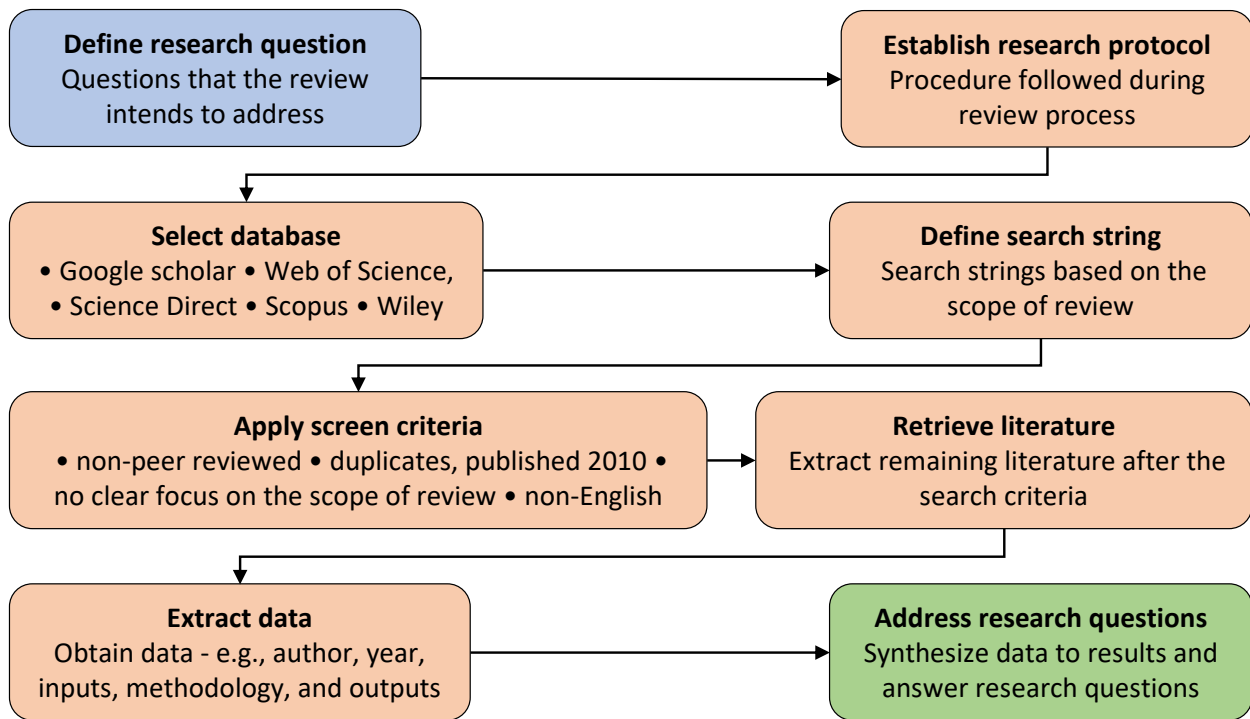


Figure 2.1. Flowchart for conducting systematic literature review showing planning, conducting, and reporting stages of the review.

is then validated to assess if the approach was viable. Other information such as publication databases, search strings, and selection criteria were defined. The protocol was further revised and finalized based on the available research question and information. Data were extracted from the selected literature from various publication sources during the review stage. Basic information regarding the authors, year of publication, and more research-related information such as the type of research, methodology, results, and recommendations were stored. The stored data were analyzed to provide an outline of the relevant literature published. The final stage was review reporting, where the results were used to answer the developed research questions and the review was concluded.

2.3.1. Defining Research Questions

This review aims to focus on the literature published in the domain of “*Biomass yield prediction models and tools for pasture grass and forage and economic analysis tools for forage.*” The research questions have been developed with the objective to gain insights into this knowledge domain. For this SLR based review, the developed research questions were:

Q1: What are the significant factors influencing grass and forage biomass yield prediction?

Q2: What are the regression and machine learning modeling techniques used for biomass yield prediction?

Q3: What are the currently available tools for grass/forage monitoring and yield prediction?

Q4: What are the existing tools for forage economics analysis?

2.3.2. Strategy for Searching Literature

Searching in the broader aspect of the chosen knowledge domain might yield a lot many published literature which are not in the scope of this review. Therefore, searching should include basic concepts from the research questions that are relevant to the review scope. A primary search was conducted to identify and list the search item and their synonyms for individual search aspects based on the literature abstracts. The search items identified were used as “search strings” in the publication databases (table 2.1).

2.3.3. Exclusion Criteria

Irrelevant studies that were outside the scope of this review were excluded based on the following set criteria to perform SLR. There was no exclusion in the geographic location of the publication.

Table 2.1. Identified search item strings for systematic literature review.

Search Aspect	Search item strings
Grassland	grassland*, pasture*, steppe*, rangeland*, meadow*
Climate	precipitation, rainfall, evapo-transpiration, humidity, solar radiation, temperature, soil temperature
Remote Sensing	remote sensing, satellite, drone*, UAV*
Vegetation indices	vegetation ind*, NDVI, GNDVI, EVI
Methodology	machine learning, artificial intelligence, regression
Yield	biomass, produc*, monitoring, harvest, cut, quantity, yield

Note: * indicates placeholder that captures other forms (e.g., plurals).

C1: Literature that do not have clear focus on grass or forage prediction

C2: Literature not in English

C3: Duplicate literatures already retrieved from another database source

C4: Literature published before 2010 (latest 10+ years considered)

C5: Literature including conference papers and magazines

The total number of literature entities (manuscripts) downloaded from the selected four database sources was 147 (table 2.2). Only 85 manuscripts qualified for further analysis after applying all the five criteria. Among the databases, more relevant manuscripts were retrieved from Google Scholar (64%) followed by Web of Science (17%), and Science Direct (table 2.2).

Table 2.2. Distribution of collected and screened literature based on the database sources in the chosen knowledge domain.

Database	Downloaded	Screened	Selected (%)
Google Scholar	83	46	54
Web of Science	36	20	24
Science Direct	28	19	22
Total	147	85	100

The data from the qualified manuscripts were extracted based on the research questions developed in (section 2.3.1). The data from the final screened literature was obtained for data analysis and the results are presented in the subsequent section.

2.4. Results and Discussion

2.4.1. Important Features Predicting Grass/Forage Yield

To address research question 1 (Q1), data from the selected literature were extracted (table 2.3) to analyze the most significant features used in the prediction of pasture grass or forage. A collection of the screened literature ($n = 85$) with information such as publication database, year published, literature title, citations generated, and reference illustrated the greater interest in the subject based on the increased number of citations (table 2.3). The significant remotely sensed vegetation index (VI) and soil, as well as climate features, were individually analyzed and reported.

2.4.1.1. Vegetation indices

The satellite sensors used in capturing the grass and forage production in grassland, pasture, rangelands, meadow, and steppe were recorded from the collected and screened 52 manuscripts. The term Landsat included platforms such as Landsat 5, 7, and 8 while Sentinel included Sentinel 1 and 2. Analyzing the satellites revealed that MODIS, Landsat,

Table 2.3. Details of selected articles through systematic literature review and their citation scores.

S.No.	Database	Year	Title	Citations	Reference
1	Sci-Dir	2022	A non-destructive method for rapid acquisition of grassland aboveground biomass for satellite ground verification using UAV RGB images	*	H. Zhang et al. (2022)
2	Sci-Dir	2022	Classification of Zambian grasslands using random forest feature importance selection during the optimal phenological period	1	Zhao et al. (2022)
3	Sci-Dir	2022	Estimating pasture quality of Mediterranean grasslands using hyperspectral narrow bands from field spectroscopy by Random Forest and PLS regressions	*	Fernández-Habas et al. (2022)
4	Sci-Dir	2022	Monitoring standing herbaceous biomass and thresholds in semiarid rangelands from harmonized Landsat 8 and Sentinel-2 imagery to support within-season adaptive management	*	Kearney et al. (2022)
5	Sci-Dir	2022	Monitoring the available forage using Sentinel 2-derived NDVI data for sustainable rangeland management	*	İleri and Koç (2022)
6	Goo-Sch	2021	A machine learning method for predicting vegetation indices in China	3	X. Li et al. (2021)
7	Sci-Dir	2021	A novel UAV-based approach for biomass prediction and grassland structure assessment in coastal meadow	7	Pecina et al. (2021)
8	Goo-Sch	2021	A practical satellite-derived vegetation drought index for arid and semi-arid grassland drought monitoring	5	Chang et al. (2021)
9	Goo-Sch	2021	Applicability of different vegetation indices for pasture biomass estimation in the north-central region of Mongolia	*	Bayaraa et al. (2021)
10	Sci-Dir	2021	Changes and controls of aboveground net primary production in response to grassland policy in Inner Mongolian grasslands of China	*	Zheng et al. (2021)
11	Sci-Dir	2021	Comparing vegetation indices from Sentinel-2 and Landsat 8 under different vegetation gradients based on a controlled grazing experiment	*	Qin et al. (2021)
12	Goo-Sch	2021	Enhanced drought detection and monitoring using sun-induced chlorophyll fluorescence over Hulun Buir Grassland,China	4	Y. Liu et al. (2021)
13	Goo-Sch	2021	Estimating pasture biomass using Sentinel-2 imagery and machine learning	9	Y. Chen et al. (2021)

continued ...

Table 2.3 Details of selected articles through systematic literature review and their citation scores — (continued)

S.No.	Database	Year	Title	Citations	Reference
14	Goo-Sch	2021	Estimation of rangeland production in the arid oriental region (Morocco) combining remote sensing vegetation and rainfall Indices: Challenges and lessons learned	2	Lang et al. (2021)
15	Goo-Sch	2021	Grassland productivity estimates informed by Soil moisture measurements: Statistical and mechanistic approaches	2	Krueger et al. (2021)
16	Goo-Sch	2021	Improving the estimation of alpine grassland fractional vegetation cover using optimized algorithms and multi-dimensional features	*	Lin et al. (2021)
17	Goo-Sch	2021	Monitoring rainfed alfalfa growth in semiarid agrosystems using Sentinel-2 imagery	*	Echeverría et al. (2021)
18	Web-Sci	2021	National mapping of New Zealand pasture productivity using temporal Sentinel-2 data	4	Amies et al. (2021)
19	Goo-Sch	2021	Precipitation rather than evapotranspiration determines the warm-season water supply in an alpine shrub and an alpine meadow	5	H. Li et al. (2021)
20	Sci-Dir	2021	Remote sensing inversion of grassland aboveground biomass based on high accuracy surface modeling	5	Zhou et al. (2021)
21	Goo-Sch	2021	Remote sensing of aboveground grass biomass between protected and non-protected areas in savannah rangelands	*	Dube et al. (2021)
22	Web-Sci	2021	Remote-sensing inversion method for aboveground biomass of typical steppe in inner Mongolia, China	4	Lyu et al. (2021)
x23	Sci-Dir	2021	The superiority of the normalized difference phenology index (NDPI) for estimating grassland aboveground fresh biomass	3	Xu et al. (2021)
24	Goo-Sch	2021	Cool-season grass productivity estimation model evaluating the effects of global warming and climate adaptation strategies	1	Tarumi et al. (2021)
25	Web-Sci	2021	A new method for grassland degradation monitoring by vegetation species composition using hyperspectral remote sensing	12	Lyu et al. (2020)
26	Goo-Sch	2020	Estimating grassland parameters from Sentinel-2: a model comparison study	6	Schwieder et al. (2020)
27	Sci-Dir	2020	Effects of climate change on the growing season of alpine grassland in Northern Tibet, China	5	X. Zhang et al. (2020)

continued . . .

Table 2.3 Details of selected articles through systematic literature review and their citation scores — (continued)

S.No.	Database	Year	Title	Citations	Reference
28	Goo-Sch	2020	Estimating plant pasture biomass and quality from UAV imaging across Queensland's Rangelands	10	Barnetson et al. (2020)
29	Goo-Sch	2020	Influence of climate variability on the potential forage production of a mown permanent grassland in the French Massif Central	7	Gómara et al. (2020)
30	Goo-Sch	2020	Long-term grass biomass estimation of pastures from satellite data	4	Clementini et al. (2020)
31	Goo-Sch	2020	Monitoring and modeling rangeland health with remote sensing	1	Soubry and Guo (2020)
32	Goo-Sch	2020	Monitoring pasture aboveground biomass and canopy height in an integrated crop livestock system using textural information from PlanetScope imagery	8	Dos Reis et al. (2020)
33	Goo-Sch	2020	Remote sensing applications for insurance: a predictive model for pasture yield in the presence of systemic weather	6	Brock Porth et al. (2020)
34	Goo-Sch	2020	Spatial and temporal pasture biomass estimation integrating electronic plate meter, Planet CubeSats and Sentinel-2 satellite data	9	Gargiulo et al. (2020)
35	Goo-Sch	2020	The fusion of spectral and structural datasets derived from an airborne multispectral sensor for estimation of pasture dry matter yield at paddock scale with time	10	Karunaratne et al. (2020)
36	Goo-Sch	2020	Estimating natural grassland biomass by vegetation indices using Sentinel 2 remote sensing data	34	Guerini Filho et al. (2020)
37	Goo-Sch	2019	A new approach to predict normalized difference vegetation index using time-delay neural network in the arid and semi-arid grassland	8	T. Wu et al. (2019)
38	Sci-Dir	2019	Application of the MODIS MOD 17 net primary production product in grassland carrying capacity assessment	24	De Leeuw et al. (2019)
39	Web-Sci	2019	Canopy height measurements and non-destructive biomass estimation of Lolium perenne swards using UAV imagery	31	Borra-Serrano et al. (2019)
40	Goo-Sch	2019	Drought-induced decline of productivity in the dominant grassland species Lolium perenne L. depends on soil type and prevailing climatic conditions	15	Buttler et al. (2019)
41	Goo-Sch	2019	Effect of irrigation management on pasture yield and nitrogen losses	20	Vogeler et al. (2019)

continued ...

Table 2.3 Details of selected articles through systematic literature review and their citation scores — (continued)

S.No.	Database	Year	Title	Citations	Reference
42	Web-Sci	2019	Estimating grassland aboveground biomass on the Tibetan Plateau using a random forest algorithm	21	Zeng et al. (2019)
43	Web-Sci	2019	Estimating leaf area index and aboveground biomass of grazing pastures using Sentinel-1, Sentinel-2 and Landsat images	85	Wang et al. (2019)
44	Goo-Sch	2019	Estimating rangeland forage production using remote sensing data from a small unmanned aerial system (sUAS) and PlanetScope satellite	18	(H. Liu et al., 2019)
45	Goo-Sch	2019	Yield estimates by a two-step approach using hyperspectral methods in grasslands at high latitudes	11	Ancin-Murguzur et al. (2019)
46	Goo-Sch	2019	Estimating the basis risk of rainfall index insurance for pasture, rangeland, and forage	21	Yu et al. (2019)
47	Web-Sci	2019	Evaluation of grass quality under different soil management scenarios using remote sensing techniques	21	Askari et al. (2019)
48	Web-Sci	2019	Grassland ecosystem services in a changing environment: The potential of hyperspectra monitoring	19	Obermeier et al. (2019)
49	Goo-Sch	2019	Integrating traditional ecological knowledge and remote sensing for monitoring rangeland dynamics in the Altai Mountain region	12	Paltsyn et al. (2019)
50	Web-Sci	2019	LIDAR provides novel insights into the effect of pixel size and grazing intensity on measures of spatial heterogeneity in a native bunchgrass ecosystem	10	Jansen et al. (2019)
51	Sci-Dir	2019	Quantitative estimation of biomass of alpine grasslands using hyperspectral remote sensing	14	Kong et al. (2019)
52	Sci-Dir	2019	The classification of grassland types based on object-based image analysis with multisource data	9	Xu et al. (2019)
53	Web-Sci	2018	Grassland canopy cover and aboveground biomass in Mongolia and Inner Mongolia: Spatiotemporal estimates and controlling factors	65	John et al. (2018)
54	Goo-Sch	2018	A novel machine learning method for estimating biomass of grass swards using a photogrammetric canopy height model, images and vegetation indices captured by a drone	108	Viljanen et al. (2018)
55	Web-Sci	2018	Characterizing the spatio-temporal variations of C3 and C4 dominated grasslands aboveground biomass in the Drakensberg, South Africa	15	Shoko et al. (2018)

continued . . .

Table 2.3 Details of selected articles through systematic literature review and their citation scores — (continued)

S.No.	Database	Year	Title	Citations	Reference
56	Web-Sci	2018	Estimates of grassland biomass and turnover time on the Tibetan Plateau	35	Xia et al. (2018)
57	Web-Sci	2018	Estimating vegetation biomass and cover across large plots in shrub and grass dominated drylands using terrestrial lidar and machine learning	57	Anderson et al. (2018)
58	Goo-Sch	2018	Innovation in rangeland monitoring: annual, 30 m, plant functional type percent cover maps for us rangelands, 1984–2017.	115	Jones et al. (2018)
59	Web-Sci	2018	Modeling grassland above-ground biomass based on artificial neural network and remote sensing in the Three-River Headwaters Region	105	Yang et al. (2018)
60	Goo-Sch	2018	Modelling inter-annual variation in dry matter yield and Precipitation use efficiency of perennial pastures and annual forage crops sequences	25	Ojeda et al. (2018)
61	Sci-Dir	2018	Predicting habitat quality of protected dry grasslands using Landsat NDVI phenology	36	Weber et al. (2018)
62	Goo-Sch	2018	Remote sensing as a tool to assess botanical composition, structure, quantity and quality of temperate grasslands	4	Wachendorf et al. (2018)
63	Goo-Sch	2018	Spatial and temporal variability of grassland yield and its response to climate change and anthropogenic activities on the Tibetan Plateau from 1988 to 2013	28	H. Zhang et al. (2018)
64	Goo-Sch	2017	Constructing Italian ryegrass yield prediction model based on climatic data by locations in South Korea	17	Peng et al. (2017)
65	Sci-Dir	2017	Estimating grassland LAI using the Random Forests approach and Landsat imagery in the meadow steppe of Hulunber, China	36	LI et al. (2017)
66	Sci-Dir	2017	Estimation and prediction of grassland cover in western Mongolia using MODIS-Derived vegetation indices	6	Paltsyn et al. (2017)
67	Goo-Sch	2017	Evaluation of remote sensing inversion error for the above-ground biomass of alpine meadow grassland based on multi-source satellite data	32	Meng et al. (2017)
68	Goo-Sch	2017	Multi-model simulation of soil temperature, soil water content and biomass in Euro-Mediterranean grasslands: Uncertainties and ensemble performance	52	Sandor et al. (2017)
69	Goo-Sch	2017	Identification of high nature value grassland with remote sensing and minimal field data	54	Stenzel et al. (2017)

continued ...

Table 2.3 Details of selected articles through systematic literature review and their citation scores — (continued)

S.No.	Database	Year	Title	Citations	Reference
70	Goo-Sch	2017	Remote sensing of above-ground biomass	119	Kumar and Mutanga (2017)
71	Goo-Sch	2017	The relationship between soil moisture and temperature vegetation on Kirklareli City Luleburgaz District a natural pasture vegetationPasture Vegetation	5	Sen and Ozturk (2017)
72	Goo-Sch	2017	The signature of sea surface temperature anomalies on the dynamics of semiarid grassland productivity.	21	M. Chen et al. (2017)
73	Goo-Sch	2017	Modelling biomass of mountainous grasslands by including a species composition map	23	Magiera et al. (2017)
74	Web-Sci	2016	Modeling managed grassland biomass estimation by using multitemporal remote sensing data—A machine learning approach	80	Ali et al. (2016)
75	Goo-Sch	2016	Calibration of GrassMaster II to estimate green and dry matter yield in Mediterranean pastures: effect of pasture moisture content	24	Serrano et al. (2016)
76	Web-Sci	2016	Comparison of machine-learning methods for above-ground biomass estimation based on Landsat imagery	52	C. Wu et al. (2016)
77	Web-Sci	2016	Grassland and cropland net ecosystem production of the US Great Plains: Regression tree model development and comparative analysis	10	Wylie et al. (2016)
78	Sci-Dir	2016	Modeling grassland aboveground biomass using a pure vegetation index	50	F. Li et al. (2016)
79	Web-Sci	2016	Application of synthetic NDVI time series blended from Landsat and MODIS data for grassland biomass estimation	76	B. Zhang et al. (2016)
80	Goo-Sch	2016	Modeling phenological responses of Inner Mongolia grassland species to regional climate change	24	Q. Li et al. (2016)
81	Sci-Dir	2015	Estimating above-ground biomass on mountain meadows and pastures through remote sensing	64	Barrachina et al. (2015)
82	Web-Sci	2015	Estimating plant traits of grasslands from UAV-acquired hyperspectral images: a comparison of statistical approaches	98	Capolupo et al. (2015)
83	Goo-Sch	2015	Water use efficiency of six rangeland grasses under varied Soil moisture content levels in the arid Tana River County, Kenya	19	Koech et al. (2015)
84	Goo-Sch	2013	The drought calculator: decision support tool for predicting forage growth during drought.	8	Dunn et al. (2013)

continued ...

Table 2.3 Details of selected articles through systematic literature review and their citation scores — (continued)

S.No.	Database	Year	Title	Citations	Reference
85	Sci-Dir	2010	Using remote sensing and GIS technologies to estimate grass yield and livestock carrying capacity of alpine grasslands in Golog Prefecture, China	98	Long et al. (2010)

Note: Sci-Dir - Science Direct; Goo-Sch - Google Scholar; Web-Sci - Web of Science; * Citations not reported for these latest publications.

and Sentinel were mostly applied in the literature predicting pasture or forage yield (table 2.4). The finer spatial resolution recorded using PlanetScope satellite was used in literature published after 2019. Unmanned aerial vehicle (UAV) equipped with hyperspectral sensors were also widely used for grass and forage yield prediction.

Table 2.4. Distribution of screened literature based on the satellite platforms.

Satellite platforms	Frequency
MODIS	16
Landsat	15
Sentinel	12
UAV	9
PlanetScope	5
LIDAR	2
EOSDIS	1
NOAA/AVHRR	1
PROBA-V	1

The traditional methods of monitoring biomass involved the destructive process of hand clipping and drying the biomass from the randomly placed quadrats across a large landscape (Catchpole and Wheeler, 1992). The traditional method was time-consuming and laborious process, therefore, not performed frequently. While, surface reflectance properties of vegetation recorded by satellite sensors were used to develop VI for large-scale, timely, and non-destructive methods of biomass prediction and plant health monitoring. Therefore, with the advances in remote sensing over the recent years, studies on using vegetation indices as proxies for predicting and large-scale monitoring the spatial and temporal patterns of the grassland were explored among other studies.

Among the literature collected, normalized difference vegetation index (NDVI) was the most frequently used VI (28 %) in predicting grass and forage (fig. 2.2) followed by

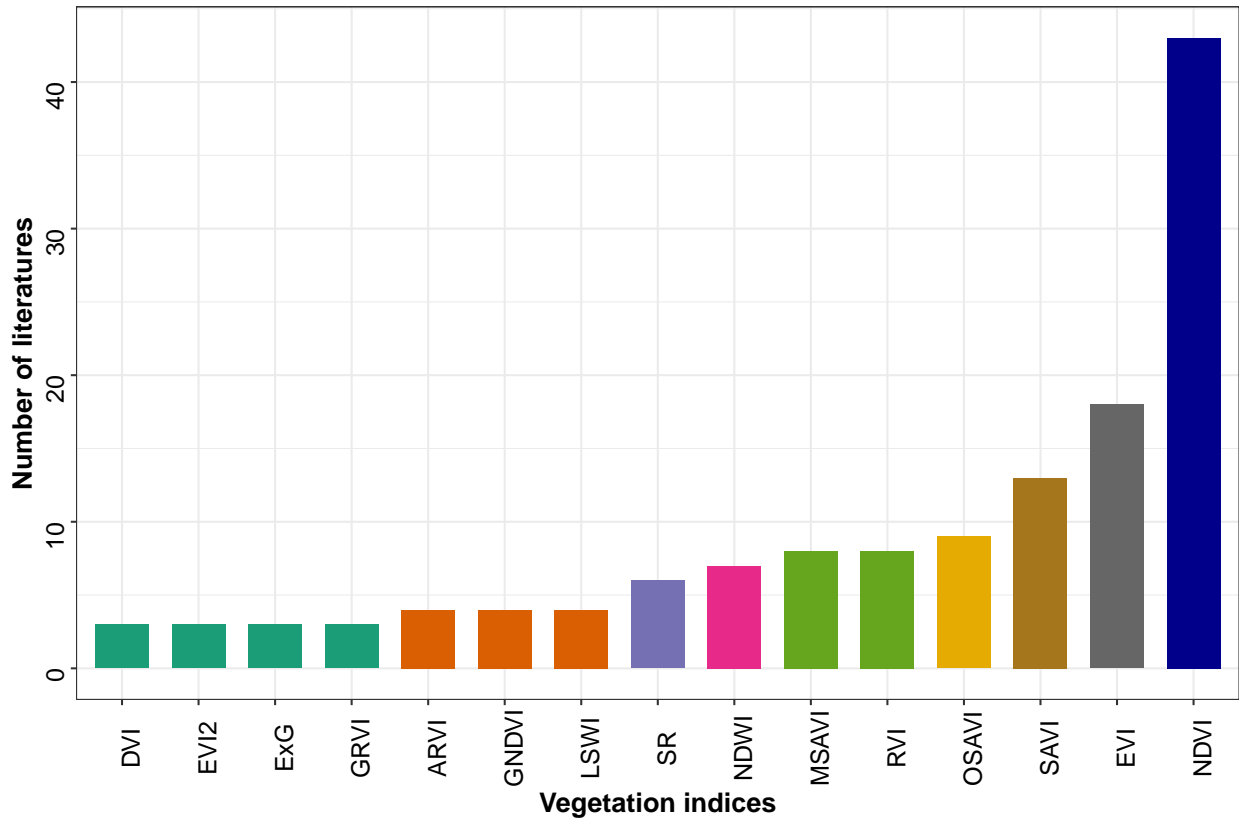


Figure 2.2. Vegetation indices versus number of literature collected from publication database sources. Frequency of vegetation indices is sorted from lowest to highest. NDVI - normalized difference vegetation index, EVI - enhanced vegetation index, SAVI - soil-adjusted vegetation index, OSAVI - optimized soil-adjusted vegetation index, RVI - relative vigor index, MSAVI - modified soil-adjusted vegetation index, NDWI - normalized difference water index, SR - simple ratio, LSWI - land surface water index, GNDVI - green NDVI, ARVI - atmospherically resistant vegetation index, GRVI - green and red ratio vegetation index, ExG - excess green, EVI2 - 2-band EVI, DVI - difference vegetation index.

enhanced vegetation index (EVI), soil-adjusted vegetation index (SAVI), and optimized soil-adjusted vegetation index (OSAVI).

A study comparing eight VIs derived from Sentinel 2 and Landsat 8 satellite data showed that the prediction models developed using the EVI, NDVI, SAVI correlated well

($R^2 = 0.61\text{--}0.65$) with the above-ground biomass and leaf area index (Qin et al., 2021). Another recent study on estimating the pasture biomass revealed that NDVI best estimated the pasture biomass with a prediction performance of R^2 between 0.74 and 0.94 using Sentinel 2 and PlanetScope images (Gargiulo et al., 2020). For a drone-based forage biomass estimation study, modified soil-adjusted vegetation index (MSAVI) produced good correlation ($r = 0.94\text{--}0.99$) in predicting forage and dry matter yield (Viljanen et al., 2018).

2.4.1.2. Climate and soil features

Many studies have explored the use of climate and soil features in forecasting the annual forage yield which aided in making appropriate decisions on livestock stocking rate and monitoring the desired plant community. In the collected literature, climate features mostly used included air temperature, precipitation, solar radiation, relative humidity, and wind speed. The solar information contains, minimum, average, and maximum air temperature and solar radiation observations while the term precipitation included rainfall and snow. The soil moisture, pH, organic matter, and soil nutrients were categorized under soil variables.

Based on the collected literature, mostly used climate and soil features in predicting forage and grass biomass were precipitation, air temperature, and soil moisture that contributes to the 33 %, 21 %, and 15 %, respectively (fig. 2.3). Other predominant variables include relative humidity, soil temperature, and solar radiation (6 %). The features used less for grass and forage prediction were soil pH, organic matter, and soil nutrients.

A study conducted to estimate the stability of forage covers with respect to climate revealed that annual precipitation influences the dry matter yield of sequence oats-maize

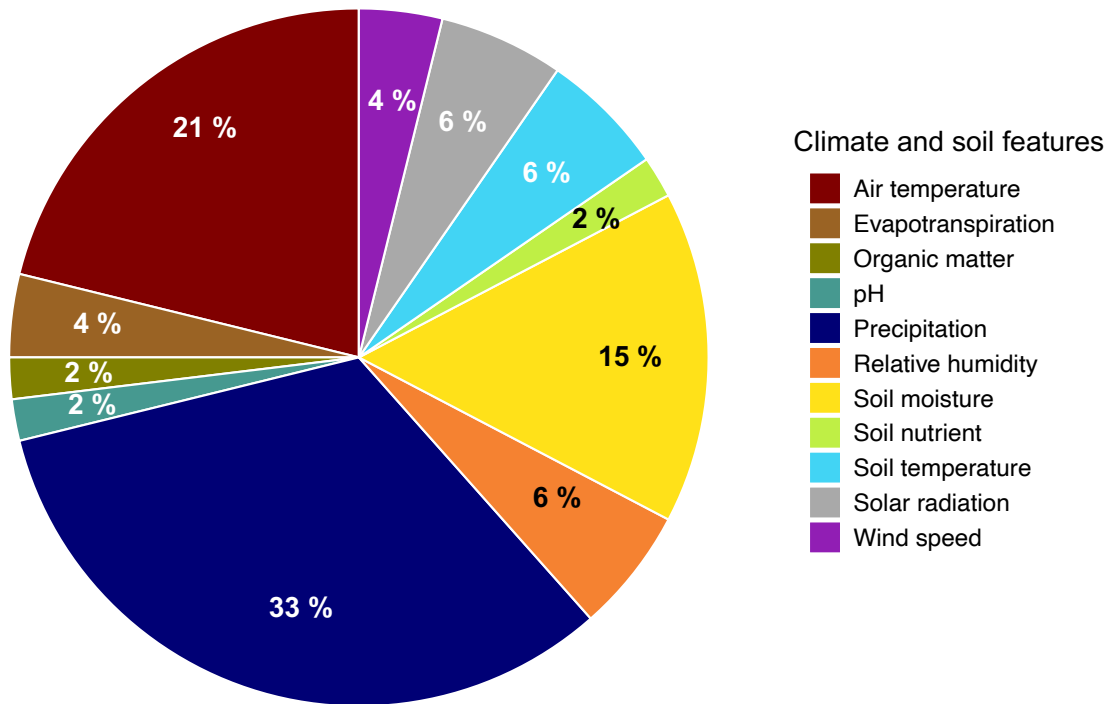


Figure 2.3. Distribution of screened literature on the application of climate and soil features for grass and forage prediction.

and pure alfalfa (Ojeda et al., 2018). Another study in Alpine grassland showed that the start growing season (January to May) was positively correlated to the mean air temperature and was negatively correlated to cumulative precipitation (X. Zhang et al., 2020). The effects of soil features on herbage yield were studied in different pastures where a decrease in yield was observed with the decrease in soil moisture and increase in soil temperature (Şen, 2018).

Overall, more recent literature focused on VI ($n = 55$) than climate features ($n = 26$), this shows a steady increasing trend in the adoption of remote sensing technology for monitoring forage and grass yield. To address Q1, the major VI, soil, and climate factors commonly used for grass and forage yield prediction were NDVI, precipitation, air temperature, and soil moisture.

2.4.2. Overview of Forage/Grass Prediction Models

The yield prediction of forage and grass was a complex relationship between the climate, soil, and or VI features. Studies have reported using linear regression (LR) for cases where the yield was correlated to individual features and also multiple linear regression (MLR) and partial least square regression (PLSR) where the features are combined for yield prediction. In the last few years, with the intricate connections between forage yield and the influencing features, new approaches have been developed such as machine learning (ML) to capture the non-linear relationships.

The common ML methods used in predicting grass or forage yield were artificial neural network (ANN), gradient boosting (GB), k-nearest neighbor (kNN), random forest (RF), and support vector machine (SVM). Based on the collected literatures published in the most recent years (since 2015), large volume of literatures were found using RF ($n = 21$), followed by LR ($n = 15$), MLR ($n = 10$), PLSR ($n = 6$), SVM as well as ANN ($n = 4$), and GB as well as kNN ($n = 3$; fig. 2.4).

The highest median R^2 was obtained with PLSR (0.75) closely followed by LR (0.73). High highest median R^2 was observed for LR models since the biomass prediction was based on individual VI or climate feature, however, this was not desirable since forage and grass biomass yield was influenced by combination of features. Among the ML prediction models, ANN and RF produced the highest median R^2 value (0.72). The absolute minimum R^2 among all methods was obtained using kNN (0.48). In the literature that used multiple prediction models, ML models (especially RF) predominantly performed better than the LR models. For example, a model comparison study conducted to estimate grass biomass using drone-based VI showed RF ($r = 0.77$) model consistently performed

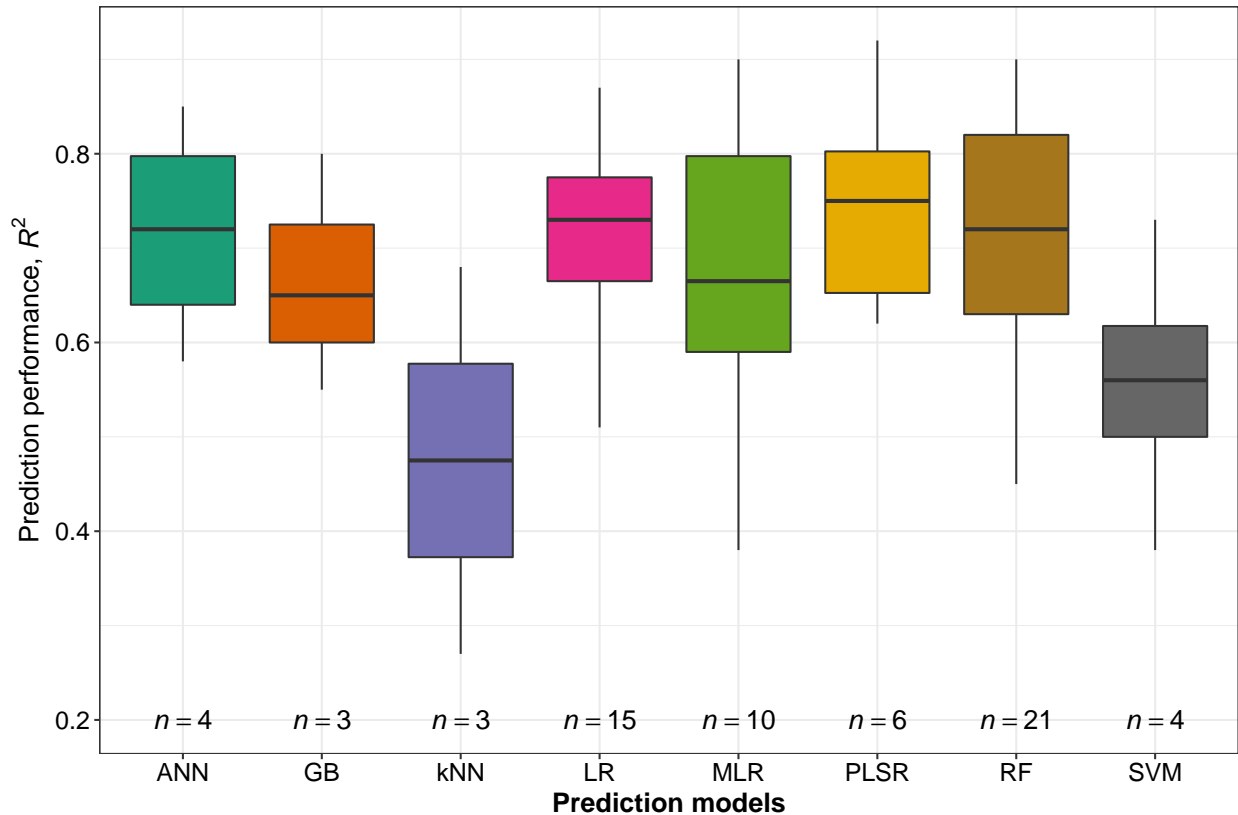


Figure 2.4. Box plot of prediction performance (R^2) for the eight most used regression and machine learning methods. ANN - artificial neural network, GB - gradient boosting, kNN - k-nearest neighbor, LR - linear regression, MLR - multiple linear regression, PLSR - partial least square regression, RF - random forest, and SVM - support vector machine.

better than MLR (Viljanen et al., 2018). Another study comparing linear regression and ML models to predict grassland biomass established that the RF model produced the best prediction accuracy ($R^2 = 0.63$) than linear regression, SVM, and kNN methods (C. Wu et al., 2016).

In general, to answer the research question Q2, based on the analysis results of the literature data showed that the RF ML model is widely used for its proven performance over other ML models and regression models.

2.4.3. Existing Tools for Grass/Forage Prediction

Few user-interactive tools that use the above-described grass and forage yield prediction models were built. These tools aid ranchers to compare management practices, aid decision-making, develop forecast scenarios, and plan livestock stocking rate. The existing tools mostly use climate features such as precipitation as inputs for predicting the biomass yield. Following are the tools developed for forage and grass prediction that include spreadsheet- and web-based applications.

2.4.3.1. Drought calculator

The drought calculator (DC) was a spreadsheet-based linear decision tool developed by the United States Department of Agriculture (USDA) Agricultural Research Service (ARS) and USDA Natural Resources Conservation Service (NRCS) to predict the reduction in forage production influenced by drought (Dunn, 2013). The DC used an average of monthly precipitation to predict the forage growth potential (FGP), based on generic forage/biomass growth curves of specific zones, for the ranchers and ranch managers to aid in stocking decisions early during the drought years (fig. 2.5).

The FGP represented the above-ground forage biomass during the growing season and was measured using the peak standing crop factor. The prediction was based on simple linear regression models developed using standardized forage production and monthly precipitation data. The calculator tool was developed and evaluated using the data from the Great Plains of the US, Colorado, North Dakota, and Wyoming. The overall accuracy of the DC tool was approximately 75 % (Dunn et al., 2013).

This spreadsheet tool was recently updated and the “dashboard and no-macro” version, developed by Agricultural and Biosystems Engineering, North Dakota State University

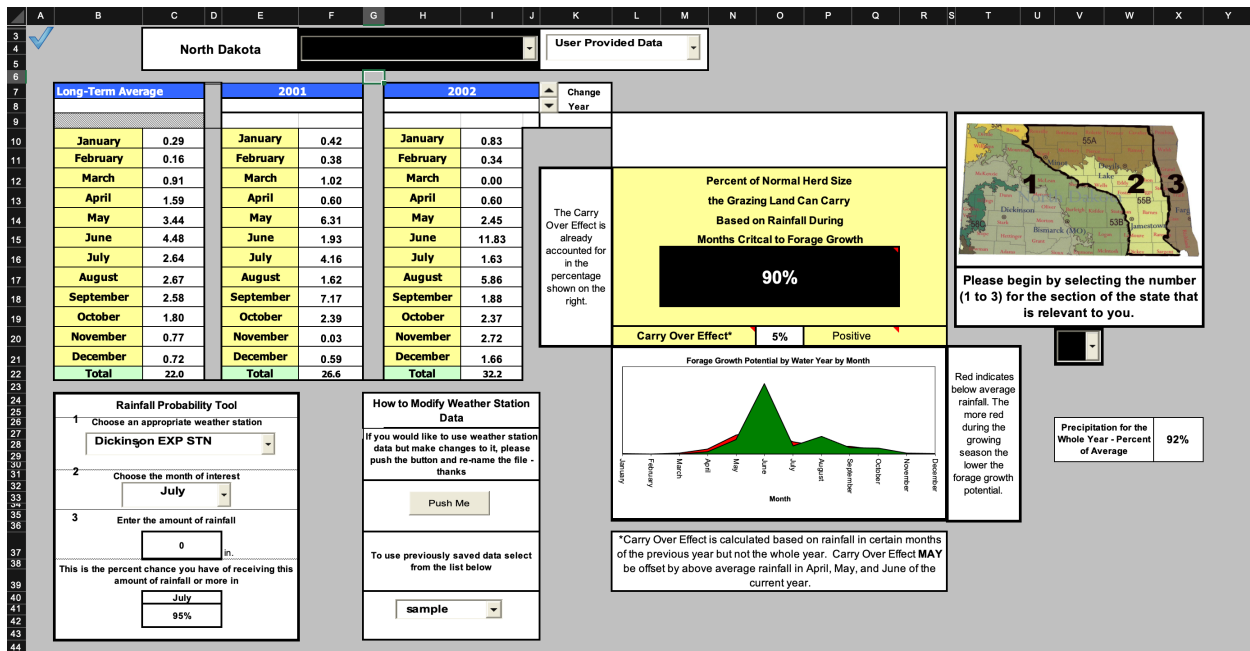


Figure 2.5. Previous version of the ND drought calculator rainfall input page for predicting forage growth potential from three growth zones.

(NDSU), can be downloaded and run using Microsoft Excel (fig. 2.6). The original DC was not active for the past few years hence sparking the development of the updated tool. The updated tool was a stripped-down version of the original and developed as a direct tool without macros and Visual Basic programming (no-macro) that ensured better security. The updated tool's inputs included information on the weather station, county, zone, year, and choice of user data. The tool can perform automatic FGP calculations based on the data stored from 150 weather stations present in North Dakota. The user data option with YES allows the users to feed in their precipitation data to be used in the analysis. The user data and information stored in the user's computer (e.g., local precipitation, and long-term precipitation average) can be used as input and the session data can be saved for future access and reference. The tool's output was a printable summary report that included infor-

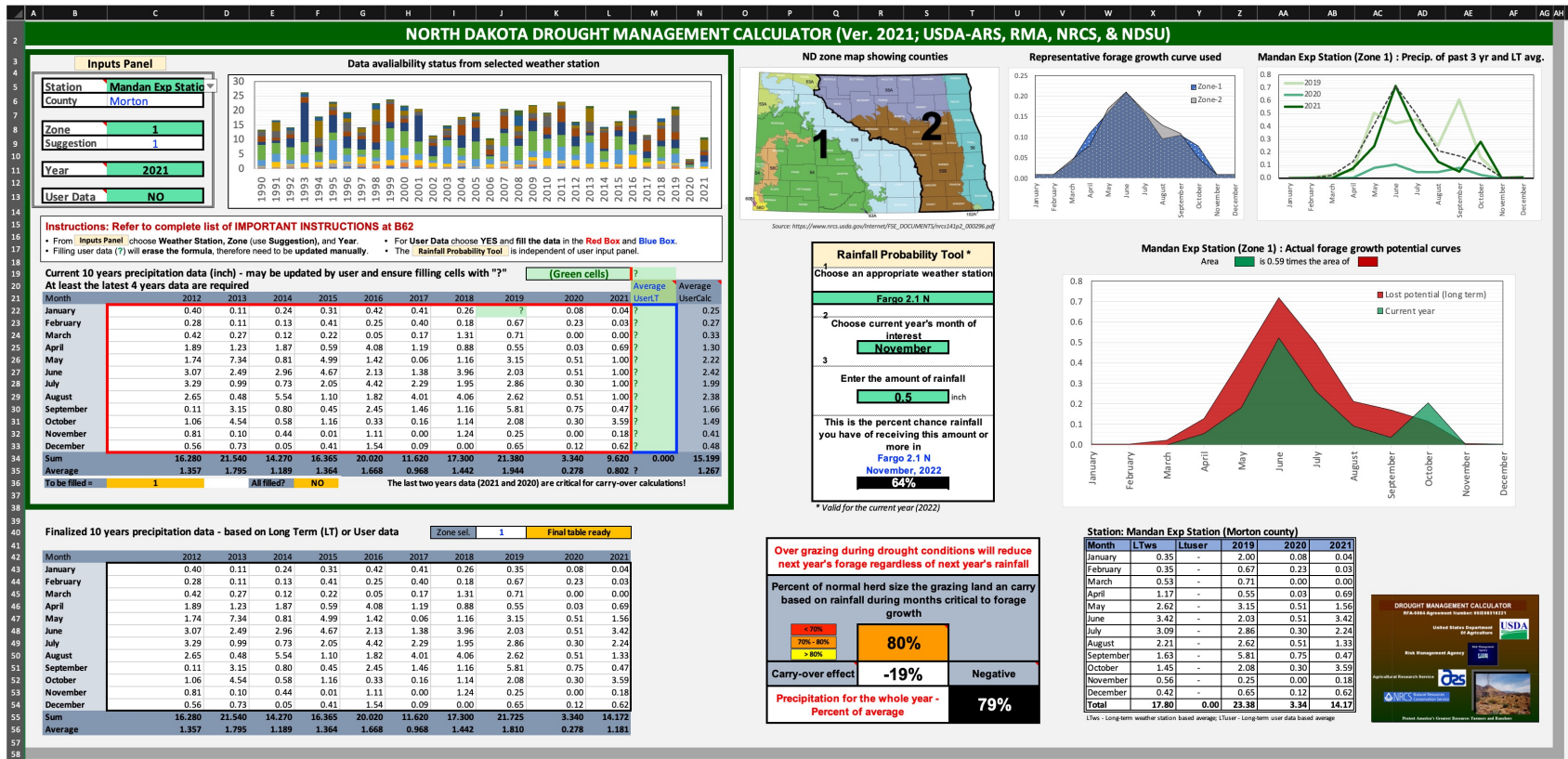


Figure 2.6. Updated no-macro ND drought calculator dashboard for predicting forage growth potential using monthly precipitation for two growth zones.

mation on the predicted FGP, precipitation data used, and a comparison between the recent and long-term potential for the selected county was presented as graphs.

The DC tool was recommended as a decision-making tool for ranchers for cattle production by adapting to the varying weather and climatic conditions in the northern great plains area (J. L. Reeves et al., 2015). Another study that reviewed drought management options for ranchers to fight against climate risk also suggested using the DC tool since it was developed based on the direct relationship between precipitation and forage growth (Shrum et al., 2018). In general, the DC was considered as a science-based tool that aids livestock producers in North Dakota at an individual level to incorporate suitable plans based on the information accessible to them (Kichler et al., 2011).

2.4.3.2. US drought monitor

The US Drought Monitor (USDM) is a web-based map tool providing weekly updates of the regions in the united states affected by drought (USDM, 1999). The USDM was functional since 1999 and maintained and operated by a team involving agencies such as the USDA, National Drought Mitigation Center (NDMC) at the University of Nebraska-Lincoln, and the National Oceanic and Atmospheric Administration (NOAA). The primary users of this tool are banks, farm service agencies, and internal revenue services.

Drought was classified into five different zones on the map namely, abnormally dry (D0), moderate (D1), severe (D2), extreme (D3), and exceptional (D4, fig. 2.7). The categorization of the different drought zones is not based on statistical or forecasting models; however, input variables such as temperature, soil moisture, snow cover, and indices such as standard precipitation index (SPI) and palmer drought severity index (PDSI) were involved in determining the drought zones. These input variables were analyzed by the

U.S. Drought Monitor

February 22, 2022
(Released Thursday, Feb. 24, 2022)
Valid 7 a.m. EST

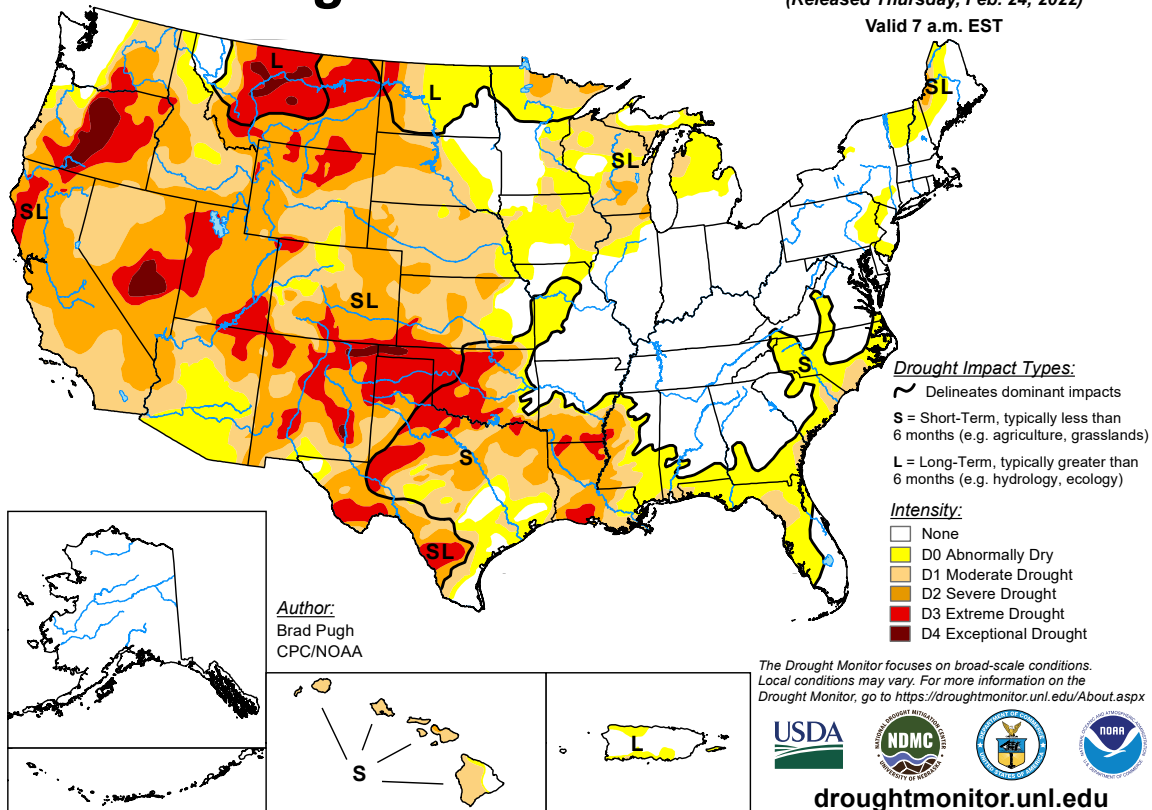


Figure 2.7. US Drought Monitor map categorized into abnormally dry (D0), moderate (D1), severe (D2), extreme (D3), and exceptional (D4). Last accessed on: February 24, 2022.

drought experts and were compared with their long-term averages to produce drought maps.

The outputs of the USDM tool include (i) side-by-side comparison and slider options for drought maps of consecutive weeks with a selectable area type, area, and statistical type, (ii) visualization of time-series analysis (2000 – 2022) of different USDM indexes, (iii) map archive consists of all the maps published weekly since 2000, (iv) animated drought maps for drought conditions over the selected period which can be downloaded

in a 'gif' version, and (v) in addition to the maps, the data were also accessible and downloadable in table format from the tabular data archive section.

A study conducted to estimate the drought impact as defined by USDM on field crops and income showed that in the High Plains, Midwest, and South regions, the USDM better correlated with the yield than the Northeast and Southeast regions (Kuwayama et al., 2019). Another study predicted the drought categories of USDM in the US with the initial conditions derived from the USDM and seasonal climate forecast from North American Multimodel Ensemble (Hao et al., 2017). Since forage biomass is dependent on the drought condition, the USDM was prescribed for ranchers as an information tool; and USDM helps the ranchers to adopt a management framework to adjust their cattle population based on the available drought condition (Derner and Augustine, 2016).

2.4.3.3. Grass-Cast

The Grass-Cast tool was developed exclusively to forecast grassland productivity in the Great Plains and Southwest regions. This web-based tool was developed in collaboration between Colorado State University, the US Department of Agriculture (USDA), National Drought Mitigation Center, and the University of Arizona (Peck, 2018). Potential users of this web tool are researchers, extension specialists, producers, land managers, and others.

The Grass-Cast tool (fig. 2.8) employs a reliable grassland ecological model, Day-Cent, to forecast forage biomass of grasslands using 38 years of historical weather and vegetation growth data along with the current weather data and seasonal climate outlook data from NOAA climate prediction center (M. Chen et al., 2017; M. Chen et al., 2019; Hartman et al., 2020; Peck et al., 2019).

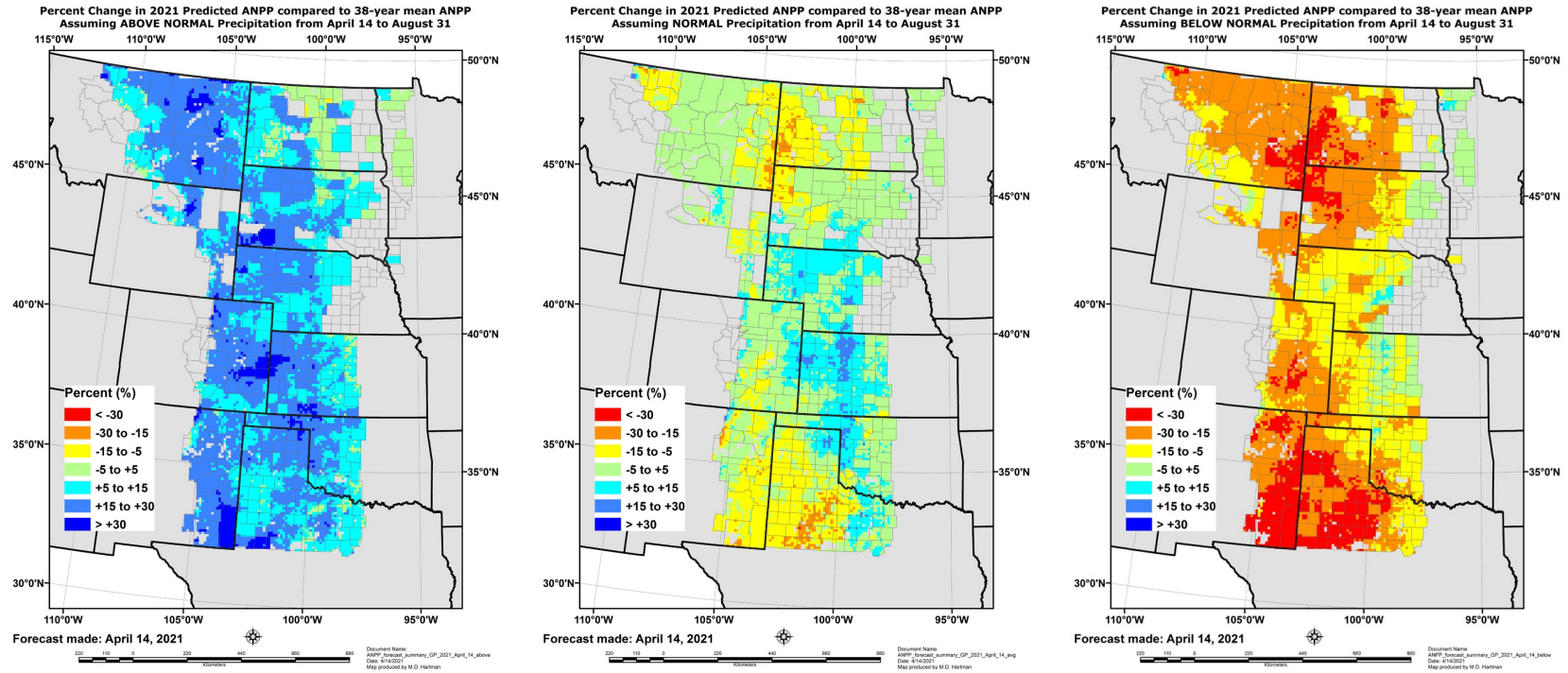


Figure 2.8. Grass-Cast maps with 3 scenarios; if precipitation is above normal (left map), is near-normal (middle map), and below normal (right map). Last accessed on: February 24, 2022.

The outcomes of the model include forecasting whether productivity in pounds/acre (for a spatial grid size of 10 km × 10 km, or ~6 miles × 6 miles) is above-normal, near-normal, or below-normal when compared to their 30 year history data of their respective area. The tool provides three different maps for the users, such as above-normal, near-normal, and below-normal.

The choropleth colors indicate the possibility of the grassland vegetation of the cell's grid to be higher or lower than its more than 30 years of historical data. The Grass-Cast forecast maps are first published at the beginning of the Spring (April) and until the end of summer (August). During this period, the maps are published every two weeks to include recently observed weather data in the model. Therefore, the accuracy of the model increases with time. Printer-friendly versions of the maps are available with the web tool, and the previous maps and CSV data (since 2017) can be accessed from the archive option of the tool.

A comparison study between Grass-Cast and MODIS NDVI (data used for validation) in predicting the plant production revealed that the model performed better with increased accuracy from May to mid-June (Parton et al., 2020). Another work on studying the critical decision dates for drought management in the rangelands belonging to Central and Northern Great Plains recommends Grass-Cast as a forage prediction tool for the ranchers to match the animal demand to the forage availability (Derner et al., 2020; Smart et al., 2021).

2.4.3.4. Rangeland analysis platform

Rangeland analysis platform (RAP) is a free online interactive tool that provides quick access to geospatial data for the United States' rangelands (fig. 2.9). The RAP tool

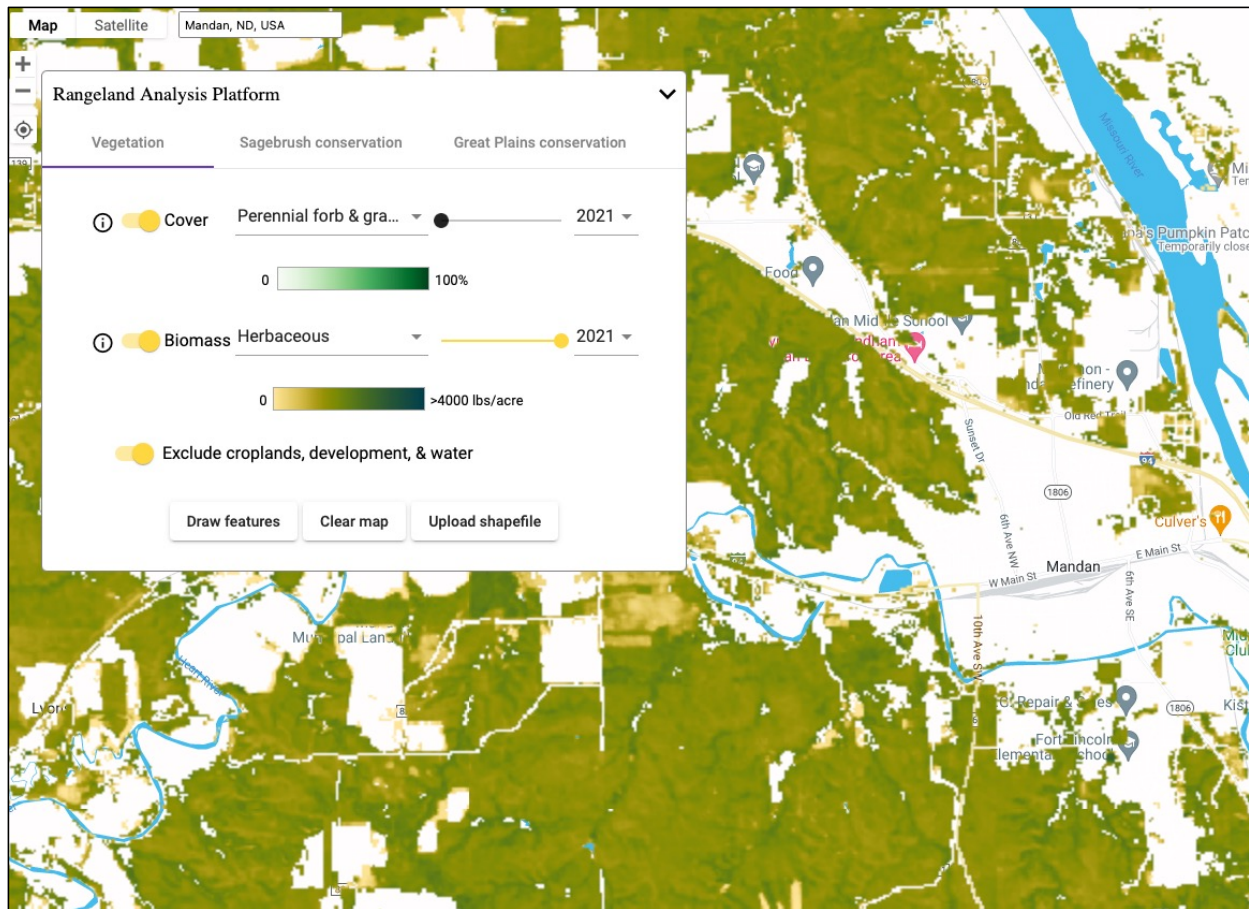


Figure 2.9. Range analysis platform — interactive web-based tool for forbs and grass percentage cover and herbaceous biomass yield.

tool is a collaborative product of the University of Montana, Department of Interior’s Bureau of Land Management, and USDA – Natural Resources Conservation Service (B. Allred, 2019). This web tool’s target audience was anyone in need to make a land management decision that could include ranchers, landowners, managers, and conservationists.

Datasets from nearly 57 000 field plots from sources such as the National Resources Conservation Service’s National Resource Inventory (NRI) and Bureau of Land Management Assessment, Inventory, and Monitoring (AIM) are combined with the historical Landsat database are used in RAP. The tool uses the power of cloud computing and machine

learning techniques (temporal convolutional network) to monitor rangelands in real-time (B. W. Allred et al., 2021; Jones et al., 2018; Jones et al., 2021; Robinson et al., 2019). The RAP monitors the rangeland vegetation from 1984 to the current at pasture, landscape, or regional scale.

The web tool provides options such as upload shapefile or draw feature to select the area of interest upon selection. The tool generates time series analysis results based on the chosen location, which show the trend in the vegetation cover (%) and the biomass availability (lb/ac) for the selected area (fig. 2.9). The generated results can be downloaded in PDF, and the respective data can be downloaded in CSV or Excel formats for future reference and use.

Several studies on monitoring grassland and estimating the expansion of grass species used geospatial products from RAP. For instance, the study on tracking the spread of exotic grasses in the Western United States used RAP's geospatial data from 1985 to 2018 (Pastick et al., 2021). Another similar study used remote sensing products of RAP to quantify the rate of spread of annual grass dominance in the Great Basin area of United States (Smith et al., 2022).

2.4.4. Tools Available for Forage Economics Analysis

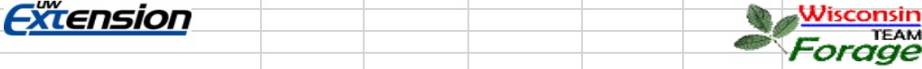
Along with the knowledge of the forage/biomass potential yield prediction, the most significant information for the producers/farmers is the bottom-line economics of the ranching or agricultural enterprise. However, the number of studies in the domain of economic analysis is scarce. Furthermore, the ranchers/farmers constantly evaluate the decision of growing or buying the forage for grazing or feeding their livestock population in a sustainable manner.

Though grasses and forages are naturally available in pastures, grasslands, ranches, meadows, and steppe; however, to meet the year-long feed supply to the livestock, some forages are cultivated and stored by farmers. Remaining hay after the grain harvest was also collected and used as animal feed. Studies show that a large portion of the livestock production cost is attributed to producing, harvesting, baling, and storing of forage (Horrocks and Valentine, 1999; Nayigihugu et al., 2007). Therefore, economic analysis of forage operations was critical for the forage growers in making informed decisions on aspects such as equipment purchases for farm operations and forage sale price. Economic analysis of forage includes numerous variables and complex calculations which are difficult to perform manually (by-hand), tedious, and time-consuming. Following were the few existing spreadsheet-based calculators replacing the manual estimation.

2.4.4.1. Alfalfa cost calculator

Based on the study conducted in a research trial of the University of Wisconsin-Extension that established that short rotations of alfalfa were more profitable than long term rotations, a spreadsheet-based calculator was developed (Undersander and Barnett, 2008). The economic analysis uses fixed and variable costs (including machinery cost and land rent) of a four-year stand alfalfa crop (fig. 2.10).

The study was extended, again as a spreadsheet calculator, where the inputs included factors, such as alfalfa yield, price, fertilizer cost, and land rent cost (Barnett, 2009). The costs of alfalfa production from year one to four are analyzed and provided in the calculator as default choices to calculate the profit.



Enter most values in yellow boxes.

Enter alfalfa base yield: (tdm/A)
(For established fields) **4.00**

Enter alfalfa hay price: (\$/ton) **\$130.00**

Enter fertilizer costs in blue cells: (\$/ton)

Enter chosen phosphorus fertilizer cost:

Phosphorous	MAP	DAP	TSP
Price/ton	\$0.00	\$590.00	\$0.00
% P ₂ O ₅	52	46	46
Cost / unit P ₂ O ₅	\$0.00	\$0.64	\$0.00

Phosphorus **\$0.64**

Enter potassium fertilizer cost:

Potash	
Price/ton	\$860.00
% K ₂ O	60
Cost / unit K ₂ O	\$0.72

Potassium **\$0.72**

Enter land cost: (\$/a) **\$85.00**

Enter cost choice (cells B50 to G50 in green) **2**

For costs to establish, produce and harvest the alfalfa (fuel, depreciation, etc) , use the following default values based on base yield ranges or enter your values –

Cost choice	1	2	3	4	5	6
Yield range	2.6-3.5	3.6-4.5	4.6-5.5	5.6-6.5	6.6-7.5	My Costs
	tdm/A	tdm/A	tdm/A	tdm/A	tdm/A	tdm/A
	(\$/A)	(\$/A)	(\$/A)	(\$/A)	(\$/A)	(\$/A)
Establishment Yr.	\$242.33	\$242.33	\$242.33	\$242.33	\$242.33	
Alfalfa - Yr. 1	\$137.79	\$137.79	\$137.79	\$137.79	\$137.79	
Alfalfa - Yr. 2	\$137.79	\$137.79	\$137.79	\$137.79	\$137.79	
Alfalfa - Yr. 3	\$137.79	\$137.79	\$137.79	\$137.79	\$137.79	
Alfalfa - Yr. 4	\$137.79	\$137.79	\$137.79	\$137.79	\$137.79	

Your Expected Alfalfa Yield and Profit per Acre

	Yield (tdm/A)	Gross Income (\$/A)	Total Costs ¹ (\$/A)	Profit (\$/A)
Establishment Yr. (-45%)	2.20	\$328.75	\$418.58	(\$89.83)
Alfalfa - Yr. 1 (0%)	4.00	\$597.72	\$426.79	\$170.93
Alfalfa - Yr. 2 (+2%)	4.08	\$609.67	\$426.79	\$182.88
Alfalfa - Yr. 3 (-17%)	3.39	\$506.57	\$377.39	\$129.18
Alfalfa - Yr. 4 (-34%)	2.69	\$401.97	\$377.39	\$24.58

¹ All establishment, production and harvesting costs (fuel, depreciation, etc) including fertilizer and land charges.

For further details on the values used in this spreadsheet, refer to the paper "[Value of Short Rotations for Alfalfa Productivity](#)".

Developed by Ken Barnett, April 2009
University of Wisconsin Center for Dairy Profitability

Figure 2.10. Alfalfa profitability and fertilizer cost calculator developed by University of Wisconsin-Extension.

2.4.4.2. *Haying system enterprise budgeting*

The Montana State University Extension developed a detailed calculator to determine the operating and ownership cost of different haying systems for alfalfa (Brence and Griffith, 2012). The general inputs of the tool were total acres of hay grown, estimated yield, cuttings per year, number of times the machine operated per year, and fuel price (fig. 2.11). In addition, other specific machinery information (speed, field efficiency, type of fuel, and percent utilized) for tractor, swather, rake, baling, hauling information were collected as inputs. The machine cost per ton and the operating and ownership costs were calculated based on the inputs. The tool also generated enterprise budgeting for irrigated alfalfa hay establishments. The inputs and the generated results were printable for future use.

2.4.4.3. *Enterprise budgeting for producing irrigated alfalfa*

A study was conducted by the Washington State University Extension to analyze the economics of establishing a central pivot irrigation system and producing alfalfa (Norberg and Neibergs, 2012). The results were based on a 120 acre central pivot irrigation of the alfalfa field. The study revealed that for irrigated alfalfa the cumulative net returns recaptured the irrigation establishment cost at the end of the third year. Since the establishment cost is met, the net return of alfalfa significantly increased past three years. The budgets from this study were presented in an Excel spreadsheet and served as a reference for growers to compare and analyze their own cost data (fig. 2.12). The reference spreadsheet included operational costs for fertilizing, irrigation, herbicide, and pesticide. Other costs included were haying cost (swath, rake, baling, and haul), fixed, variable, and land cost.

Hay/Forage Production System Cost Worksheet

by Larry Brence & Duane Griffith
 Montana State University Extension Service
<http://www.montana.edu/softwaredownloads/cropdown>

	Total Acres of Hay Grown Annually	200
	Estimated Annual Yield Tons/Acre	7.0
	Average Number of Cuttings Per Year	3.0
Help	Total Acres Covered by machinery (times over * acres)	600
	Tons Harvested Annually (Acres Hay * Avg. Yield/Ac)	1,400
	Fuel Price--Gasoline (On Farm Price)	\$2.25
	Fuel Price--Diesel (On Farm Price)	\$2.50
	Discount Rate (Interest Rate minus Inflation Rate)	5%
Help	Millage Rate (Local Mill Levee Rate, for Tax Calculation)	300
Help	Insurance Cost (Dollars per \$1000 of Machine value)	\$4.50
Help	Taxable Value Rate	4.00%

Tractor Information, Select up to 5 tractors that are used in the haying operation

Tractors (Choose up to 5)

Model	Power Unit #	Gas/Diesel (G or D)	Annual Use (hours)
26 180 HP 2WD, DUALS	1	d	400
14 115 HP MFWD	2	d	400
10 95 HP MFWD	3	d	250
00 None	4		
00 None	5		

View or Change Tractor Database

Cutting Hay -- Select the number and type of Swathers used.

Self Propelled Swathers (Choose up to 3)

Model	Speed MPH	Field Efficiency	Gas/Diesel	Percent Utilized	Cost/Acre	Cost/Ton
11 Swather 120 HP 14 Ft	4	80%	d	100%	\$ 17.03	\$ 2.43
00 None					\$ -	\$ -
00 None					\$ -	\$ -

View or

Pull Type Swather (Choose up to 3)

Model	Speed MPH	Field Efficiency	Power Unit #	Percent Utilized	Cost/Acre	Cost/Ton
00 None					\$ -	\$ -
00 None					\$ -	\$ -
00 None					\$ -	\$ -

View

Bi-directional tractor with cutter head plus a pull type swather (enter the bi-directional tractor as a power unit)

Pull type, pulled with a bi-directional	Speed MPH	Field Efficiency	Power Unit #	Percent Utilized	Cost/Acre	Cost/Ton
00 None					\$ -	\$ -

Cutter Head for the bi-directional

00 None					\$ -	\$ -
---------	--	--	--	--	------	------

Check sum 100%

Figure 2.11. Haying system enterprise budgeting estimate the operating and ownership costs developed by Montana State University Extension.

TABLE 13. SHORT FORM YEARS 2 and 3 FULL PRODUCTION SMALL 2 TIE BALES

GROSS RETURNS:	YIELD Tons/acre	PRICE \$/ton	GROSS RETURN \$/acre	YOUR FIGURES
Alfalfa Hay	8	\$220.00	\$1,760.00	_____
CULTURAL OPERATIONS:	LABOR, MACHINERY, CUSTOM HIRE \$/acre	MATERIALS \$/acre	TOTAL \$/acre	YOUR FIGURES
Fertilizing	\$9.30	\$206.58	\$215.88	_____
Herbicide Ap. (2 lb/a Velpar Alfamax)	\$9.00	\$33.40	\$42.40	_____
Irrigation (Labor and Pivot Expenses)	\$65.00	\$45.00	\$110.00	_____
Gopher Control	\$3.00	\$2.00	\$5.00	_____
HAYING:				
Swathing 4X	\$20.00		\$80.00	_____
Raking 4X	\$10.00		\$40.00	_____
Baling (\$0.95/bale 80 lb bales)	\$0.95		\$190.00	_____
Haul and Stack (\$0.40/bale)	\$0.40		\$80.00	_____
Tarping (\$7.00/ton)	\$7.00		\$56.00	_____
Hay Insurance		\$16.00	\$16.00	_____
OTHER CHARGES:				
Fuel, Repairs, Labor and other expenses	\$1.80	\$9.92	\$11.72	_____
General Overhead 5% of variable costs			\$42.35	_____
Operating Capital Interest 6.50%, 6 mo			\$27.53	_____
Fixed Costs - Depreciation, Insurance, Taxes, etc.			\$11.29	_____
Management Return			\$61.41	_____
Land Cost			\$300.00	_____
Amortized Establishment Cost			\$193.77	_____
TOTAL COST PER ACRE PER YEAR			\$1,483.35	_____
NET RETURN PER ACRE PER YEAR			\$276.65	_____
Notes:				

Figure 2.12. Alfalfa budget workbook guidelines reference developed by Washington State University Extension.

2.4.4.4. Price standing hay crop forage

A spreadsheet calculator was developed by PennState Extension to estimate prices for standing hay crop forage from buyer and grower perspectives based on current hay price, estimated hay yield/acre, and dry matter of haylage (Ishler, 2020). From the grower's perspective, cost aspects for mowing, conditioning, raking, baling, and wrapping were considered. And from the buyer's standpoint, a comparison of costs for buying silo haylage versus standing dry hay was provided (fig. 2.13). The machinery costs involved in the cost analysis were custom rates for the year 2016 published by NASS for Pennsylvania.

2.4.4.5. Decision support tool for hay production vs. hay cost

A decision support spreadsheet tool was developed by Natural Resource Conservation Service (NRCS) for alfalfa and grass hay (Kirwan, 2020). This tool helped farmers and ranchers to evaluate profitable operations by producing or purchasing hay (fig. 2.14). Two default examples on the production estimation for alfalfa and grass hay were provided as a reference. Provision for entering users' data was included. Costs of land rent, fertilizer, seed, herbicide, and their respective machinery were provided as direct inputs. This tool helped farmers to compare the estimates and make informed decisions. Another feature of this tool was determining the hay requirement after storage loss, which helps farmers explore the cost and benefits of hay storage. The storage loss analysis and worksheet were developed by Iowa State University.

Price per ton of Dry hay	\$	203.00	\$/ton	\$	0.091	Price per lb of Dry Matter	
Potential Dry Hay Yield (tons/acre)		1.25	tons/acre		2,500	lbs of dry matter harvested/acre	
Dry Matter of Harvested Silage		50.00	%	\$	228.38	Value of dry matter harvested per acre	
Market price for haylage	\$	91.35	\$/ton	\$	114.19	Moisture-adjusted value per acre	
Hay Quality Discount (\$ per ton)	\$	-	\$/ton	\$	91.35	Value per ton of haylage	
Hay Grower's Perspective				Buyer's Perspective			
(to Net the same amount from selling Standing Hay as if harvesting dry hay)				(to Pay the same as buying haylage from a silo)			
		Per Acre	Per Ton			Buy Standing Hay Per Ton	
Grower's Gross Income (ton x price)	\$	253.75	\$ 203.00	Price of haylage from silo*	\$	91.35 *includes delivery charge	
Mowing and Conditioning, Raking	- \$	25.85	\$ 20.68	Mowing and Conditioning, Raking	- \$	10.34	
Baling and Wrapping Cost	- \$	41.90	\$ 33.52	Chop/Haul/Fill	- \$	8.10	
Hay Delivery Charge	- \$	5.00	\$ 4.00	Storage Cost	- \$	5.05	
Hay Quality Discount (\$/ton)	- \$	-	\$ -	Dry Matter Loss ¹	- \$	7.31	
Total Dry Hay Net	= \$	181.00	\$ 144.80	Subtotal	= \$	60.55	
Standing Forage price, breakeven with dry hay	= \$	72.40	\$ 57.92				
Potential chopped haylage yield (Tons/acre)		2.50					
Price per Ton of Standing Hay Crop needed to Equal Dry Hay Net	= \$	57.92		Price per Ton of Standing Hay Crop Forage	= \$	60.55	
Hay Making Costs:				Silage Making Costs:			
		Your Farm:				Your Farm:	
Mowing and Conditioning		16.40	\$/acre	Mowing and Conditioning	\$	16.40	\$/acre
Raking		9.45	\$/acre	Raking	\$	9.45	\$/acre
Baling Cost	\$	7.70	\$/bale	Chop/Haul/Fill	\$	8.10	\$/Ton
Bale Weight		895	lbs.	Storage Cost Silage (Bagging or Silo Cost)	\$	5.05	\$/Ton
Wrapping Bales	\$	7.30	\$/bale	Dry Matter Loss ¹		8	%
Hay Delivery Charge	\$	4.00	\$/ton	Silage Delivery Charge	\$	5.00	\$/Ton
Bales per acre		2.79	/acre				
Baling and Wrapping per acre	\$	41.90	/acre				

Figure 2.13. Price of standing hay crop from buyer and grower perspectives developed by PennState Extension.

Alfalfa Hay Production Costs Calculation

Costs Based Upon 8.5 T/A (High Management Default Example)					
	Establish	year 2	year 3	year 4	
Rent (\$/Acre)	\$ 300.00	\$ 300.00	\$ 300.00	\$ 300.00	
Lime (\$/Acre)	\$ 36.00				
Fertilizer (\$/Acre)	\$ 88.75	\$ 266.68	\$ 266.68	\$ 266.68	
Micronutrients (\$/Acre)		\$ 20.00	\$ 20.00		
Insecticides (\$/Acre)			\$ 16.00		
Seed (\$/Acre)	\$ 140.00				
Herbicides (\$/Acre)	\$ 24.38	\$ 17.25	\$ 17.25	\$ 17.25	
Apply fert (\$/Acre)	\$ 5.65	\$ 16.95	\$ 16.95	\$ 11.30	
Apply chem (\$/Acre)	\$ 5.65	\$ 5.65	\$ 11.30	\$ 5.65	
Work ground (\$/Acre)	\$ 18.80				
Plant (\$/Acre)	\$ 15.00				
TOTAL	\$ 634.23	\$ 626.53	\$ 648.18	\$ 600.88	
Mow/co (\$20.70/A x 2)	\$ 41.40	x4 cut \$ 82.80	\$ 82.80	\$ 82.80	
Tedder (\$7.80/A x 2)	\$ 15.60	x4 cut \$ 31.20	\$ 31.20	\$ 31.20	
Rake (\$6.70/A x 2)	\$ 13.40	x4 cut \$ 26.80	\$ 26.80	\$ 26.80	
Bale (\$24.60/A x 2)	\$ 49.20	x4 cut \$ 98.40	\$ 98.40	\$ 98.40	
Stack/store (\$8/T x 4.25T)	\$ 34.00	8.5T \$ 68.00	\$ 68.00	\$ 68.00	
TOTAL	\$ 153.60	\$ 307.20	\$ 307.20	\$ 307.20	
Grand Total per Year	\$ 787.83	\$ 933.73	\$ 955.38	\$ 908.08	
Grand Total all years	\$3,585.02				
total production (Tons)	29.75				
(assumes full production years 2-4, 1/2 production in year 1)					
\$Cost/Ton	\$ 120.50				

Costs Based Upon 3.5T/A (Average Management Default Example)					
	Establish	year 2	year 3	year 4	
Rent (\$/Acre)	\$ 300.00	\$ 300.00	\$ 300.00	\$ 300.00	
Lime (\$/Acre)	\$ 36.00				
Fertilizer (\$/Acre)	\$ 88.75	\$ 115.63	\$ 115.63	\$ 115.63	
Micronutrients (\$/Acre)					
Insecticides (\$/Acre)					
Seed (\$/Acre)	\$ 140.00				
Herbicides (\$/Acre)	\$ 24.38	\$ 17.25			
Apply fert (\$/Acre)	\$ 5.65	\$ 16.95	\$ 11.30		
Apply chem (\$/Acre)	\$ 5.65	\$ 5.65			
Work ground (\$/Acre)	\$ 18.80				
Plant (\$/Acre)	\$ 15.00				
TOTAL	\$ 634.23	\$ 455.48	\$ 415.63	\$ 415.63	
Mow/co (\$20.70/A x 2)	\$ 41.40	x4 cut \$ 82.80	\$ 82.80	\$ 82.80	
Tedder (\$7.80/A x 2)	\$ 15.60	x4 cut \$ 31.20	\$ 31.20	\$ 31.20	
Rake (\$6.70/A x 2)	\$ 13.40	x4 cut \$ 26.80	\$ 26.80	\$ 26.80	
Bale (\$24.60/A x 2)	\$ 49.20	x4 cut \$ 98.40	\$ 98.40	\$ 98.40	
Stack/store (\$8/T x 1.75T)	\$ 14.00	3.5T \$ 28.00	\$ 28.00	\$ 28.00	
TOTAL	\$ 133.60	\$ 267.20	\$ 267.20	\$ 267.20	
Grand Total per Year	\$ 767.83	\$ 722.68	\$ 682.83	\$ 682.83	
Grand Total all years	\$2,856.17				
total production (Tons)	12.25				
(assumes full production years 2-4, 1/2 production in year 1)					
\$Cost/Ton	\$ 233.16				

YOUR COSTS				
Enter your input values in shaded cells.				
	Establish	year 2	year 3	year 4
Rent (\$/Acre)				
Lime (\$/Acre)				
Fertilizer (\$/Acre)				
Micronutrients (\$/Acre)				
Insecticides (\$/Acre)				
Seed (\$/Acre)				
Herbicides (\$/Acre)				
Apply fert (\$/Acre)				
Apply chem (\$/Acre)				
Work ground (\$/Acre)				
Plant (\$/Acre)				
TOTAL	\$ -	\$ -	\$ -	\$ -
Mow/co (\$/A x cut)				
Tedder (\$/A x cut)				
Rake (\$/A x cut)				
Bale (\$/A x cut)				
Stack/store (\$/T x Tons)				
TOTAL	\$ -	\$ -	\$ -	\$ -
Grand Total per Year	\$ -	\$ -	\$ -	\$ -
Grand Total all years	\$ -			
Total production (Tons)				
\$Cost/Ton	#DIV/0!			

Figure 2.14. Decision support tool for producing versus purchasing grass and alfalfa hay developed by Natural Resource Conservation Service (NRCS).

2.4.4.6. Forage economics calculator

The forage economics calculator is a user-friendly web-based tool developed by North Dakota State University in collaboration with NGSRL, USDA-ARS, Mandan (fig. 2.15).

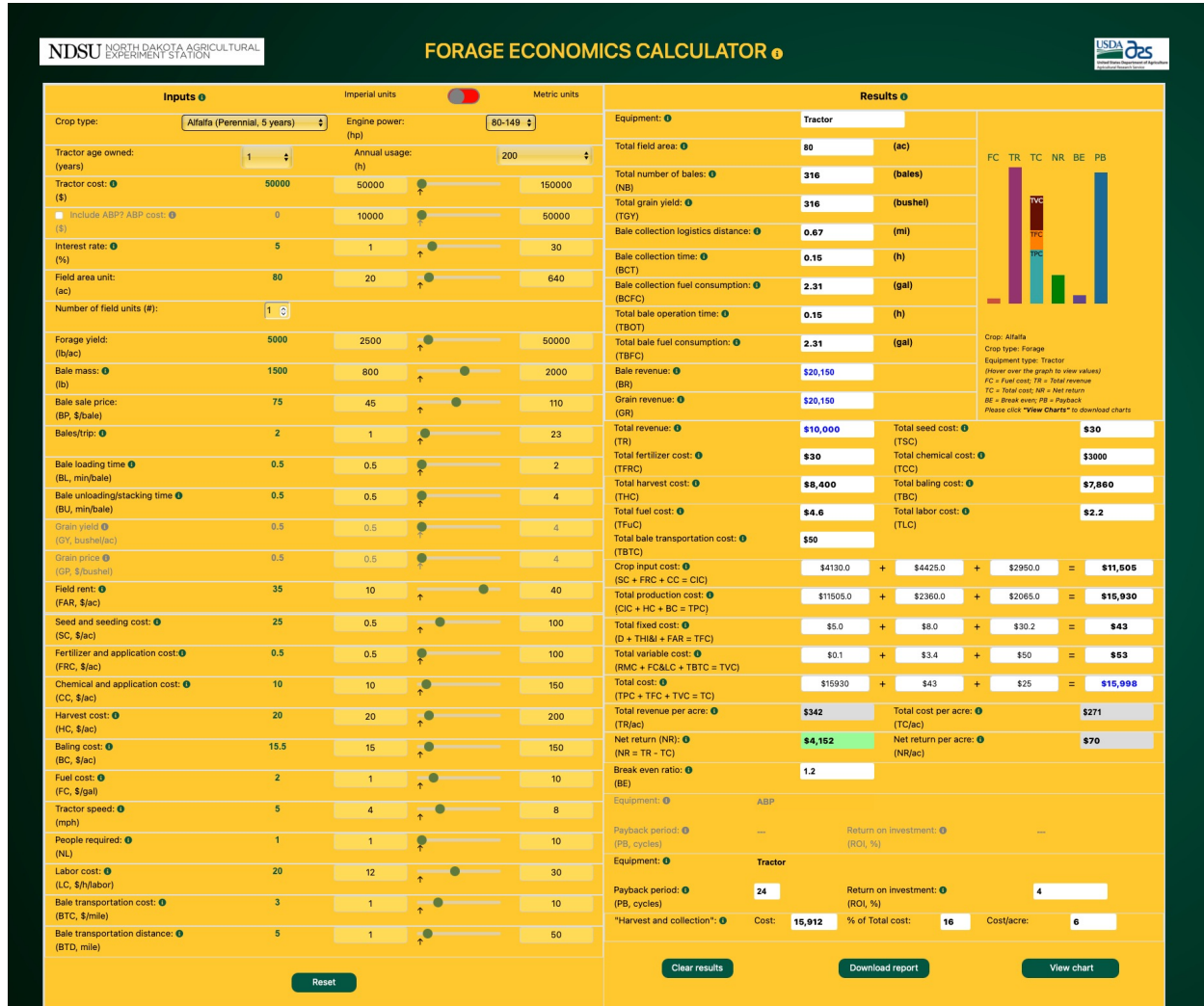


Figure 2.15. Forage economic calculator developed by North Dakota State University and NGSRL, USDA-ARS, Mandan, ND.

The tool focuses on the bale collection logistics operation, which is often ignored but a labor-intensive operation that significantly influences the economic outcomes (Subhashree et al., 2021). Other operations such as harvesting, baling, and hauling are pro-

vided as direct inputs. The tool accommodates 10 different forage types, including annual and perennial forage and grain forage (remaining hay after grain harvest). The tool takes 29 input variables and generates 37 output parameters dynamically. It serves as a decision support tool as scenario analysis can be performed, which helps the farmers to make informed decisions.

A downloadable and printable report was one of the tool's outputs which consisted of selected inputs and estimated outputs. The potential users of this tool include hay producers, farmers, custom hay operators, financial personnel, educators, and others interested in the economics of handling bales. More information on this tool's scope, development, case studies, and scenario analysis are presented in detail in chapter 4.

To answer the research question Q4, though fewer in number, spreadsheet-based tools, and one web-based tool were available for economic analysis of forage. Most of the spreadsheet tools were developed for alfalfa forage crop while the web-based tool included ten different forage crop varieties.

2.5. Research Gaps and Future Recommendations

In the study, based on the literature collected and analyzed data to predict forage and grass yields, following the SLR methodology, about 49% of the collected literature used MODIS and Landsat remote sensing satellites which have a low spatial resolution of 10–30 m, while only 8% of the literature used PlanetScope with a high spatial resolution of 3 m). Fine spatial resolution represents more detailed information obtained from the ground and should perform better in biomass yield predictions. Also, most studies used either VI or climate features in predicting biomass. However, using both VI and climate can help understand the influence of the input features as predictors and are expected to

yield better prediction results. In recent years, ML methods have proved their prediction performance for non-linear problems; therefore, more ML models need to be examined to evaluate the best model in predicting grass and forage yield. In the future, studies focused on (i) comparison between different satellite platforms for determining the influence of spatial resolution (ii) using both VI and climate features and evaluating the best features for predicting forage and grass biomass (iii) application of other advanced ML models (e.g., deep learning) to compare and evaluate the forage and grass yield prediction performance, were recommended.

The available forage prediction tools primarily focused on a county or state level using satellite images. When the prediction tools were developed for a larger scale, the weather, soil, and plant species variation were lost. These variabilities, specific to a location (e.g., producer's field), play a vital role in rangeland forage prediction. Therefore, there is scope for developing models for "field-specific" prediction using the local weather, soil, and plant species composition based on the ground truth and satellite data available. As a recommendation for future research, user-friendly web tools should be developed which allow the users to input location-specific variables for better and more realistic predictions of grass and forage yields. Since the existing tools on forage economics analysis were predominantly developed for alfalfa forage, incorporation of more forage crops was recommended. Most of the tools were spreadsheet-based; therefore, the development of more interactive, user-friendly, web-based tools was recommended for easy management and avoiding critical errors and security issues of spreadsheet programs.

2.6. Conclusions

The systematic review methodology was successfully followed to plan, conduct, gain insights, and report the results for forage yield prediction (input features, models, and tools) and for economic analysis tools. In total, 85 qualified research manuscripts were reviewed in this knowledge domain from years 2010 to 2022. Among the selected database sources, Google Scholar yielded most literature ($n = 46$) for the search terms considered. More literature were available for forage yield prediction using vegetation index (VI) which are remotely sensed ($n = 55$) than the climate features ($n = 26$) which shows a strong increasing trend of remote monitoring of grasslands and pastures. Reported forage and grass yield prediction studies either used VI or climate features but not both.

The frequencies of studies using satellite platforms were unequally distributed; among the satellites, MODIS ($n = 16$) was the most used followed by Landsat, and Sentinel. Mostly a single satellite platform was used for prediction; however, comparison between the satellites will be useful in assessing the importance of spatial resolution. About 28 % of the literature collected on remote sensing prediction of grass and forage yield used normalized difference vegetation index (NDVI) and was mostly used VI. Precipitation (33 %) and soil moisture (15 %) were the most frequently used features in the grass and forage prediction. The prediction performance of machine learning (ML) models dominated the linear and multiple linear regression models. Among ML models, the random forest model was widely used ($n = 21$) and produced the highest median R^2 of 0.72.

Existing grass and forage prediction tools were Drought Calculator, U.S. Drought Monitor, Grass-Cast, and Rangeland Analysis Platform, and they focused on large-scale prediction, where variability within individual producer's field that is of interest can be

lost. Current tools on forage economics analysis deal with alfalfa production, haying system enterprise, enterprise budgeting for production of irrigated alfalfa, price of standing hay crop, decision support tool for hay production vs hay cost, and forage economics calculator. Most of the forage economics tools were predominantly spreadsheet-based and were developed for cropped alfalfa; however, the NDSU forage economics calculator was interactive and web-based dealing with 10 forage crops.

Overall, based on the gained insights, the potential future research scope includes (i) comparison between satellite platforms to assess the influence of spatial resolution on grass and forage yield prediction and the tradeoffs; (ii) usage of the combination of vegetation index and climate features to predict biomass yield; (iii) inclusion of more robust as well as advanced ML models and comparison of prediction performance; (iv) development of interactive and user-friendly forage prediction tools for field-specific applications using local weather, soil, and plant species; (v) creation of web-based for forage economics tools including all operations and more forage crop varieties; and (vi) development of smartphone applications both for forage prediction and economics to increase the impact and visibility of these outputs to the farming, ranching, and other related sectors.

2.7. References

- Ali, I., Cawkwell, F., Dwyer, E., Barrett, B., & Green, S. (2016). Satellite remote sensing of grasslands: From observation to management. *J. Plant Ecol.*, 9(6), 649–671.
- Allred, B. (2019). *Rangeland Analysis Platform, 2019*. Retrieved March 14, 2022, from <https://rangelands.app/>.
- Allred, B. W., Bestelmeyer, B. T., Boyd, C. S., Brown, C., Davies, K. W., Duniway, M. C., Ellsworth, L. M., Erickson, T. A., Fuhlendorf, S. D., Griffiths, T. V., et al. (2021).

- Improving Landsat predictions of rangeland fractional cover with multitask learning and uncertainty. *Methods Ecol. Evol.*, 12(5), 841–849.
- Amies, A. C., Dymond, J. R., Shepherd, J. D., Pairman, D., Hoogendoorn, C., Sabetizade, M., & Belliss, S. E. (2021). National mapping of New Zealand pasture productivity using temporal Sentinel-2 data. *Remote Sens.*, 13(8), 1481.
- Ancin-Murguzur, F. J., Taff, G., Davids, C., Tømmervik, H., Mølmann, J., & Jørgensen, M. (2019). Yield estimates by a two-step approach using hyperspectral methods in grasslands at high latitudes. *Remote Sens.*, 11(4), 400.
- Anderson, K. E., Glenn, N. F., Spaete, L. P., Shinneman, D. J., Pilliod, D. S., Arkle, R. S., McIlroy, S. K., & Derryberry, D. R. (2018). Estimating vegetation biomass and cover across large plots in shrub and grass dominated drylands using terrestrial lidar and machine learning. *Ecol. Indic.*, 84, 793–802.
- Askari, M. S., McCarthy, T., Magee, A., & Murphy, D. J. (2019). Evaluation of grass quality under different soil management scenarios using remote sensing techniques. *Remote Sens.*, 11(15), 1835.
- Atzberger, C. (2013). Advances in remote sensing of agriculture: Context description, existing operational monitoring systems and major information needs. *Remote Sens.*, 5(2), 949–981.
- Barnetson, J., Phinn, S., & Scarth, P. (2020). Estimating plant pasture biomass and quality from UAV imaging across Queensland's Rangelands. *AgriEng.*, 2(4), 523–543.
- Barnett, K. (2009). *Hay Price Calculator - University of Wisconsin-Madison: Team Forage, Division of Extension*. Retrieved March 14, 2022, from <https://fyi.extension.wisc.edu/forage/economics/>.

- Barrachina, M., Cristóbal, J., & Tulla, A. F. (2015). Estimating above-ground biomass on mountain meadows and pastures through remote sensing. *Int. J. Appl. Earth Obs. Geoinf.*, *38*, 184–192.
- Bayaraa, B., Hirano, A., Purevtseren, M., Vandansambuu, B., Damdin, B., & Natsagdorj, E. (2021). Applicability of different vegetation indices for pasture biomass estimation in the North-Central region of Mongolia. *Geocarto Int.*, 1–16.
- Borra-Serrano, I., De Swaef, T., Muylle, H., Nuytens, D., Vangeyte, J., Mertens, K., Saeys, W., Somers, B., Roldán-Ruiz, I., & Lootens, P. (2019). Canopy height measurements and non-destructive biomass estimation of *Lolium perenne* swards using UAV imagery. *Grass Forage Sci.*, *74*(3), 356–369.
- Brence, L., & Griffith, D. (2012). *Montana State University Extension Economics*. Retrieved March 14, 2022, from <https://tinyurl.com/4naemjn7/>.
- Brock Porth, C., Porth, L., Zhu, W., Boyd, M., Tan, K. S., & Liu, K. (2020). Remote sensing applications for insurance: A predictive model for pasture yield in the presence of systemic weather. *North Am. Actuarial J.*, *24*(2), 333–354.
- Buttler, A., Mariotte, P., Meisser, M., Guillaume, T., Signarbieux, C., Vitra, A., Preux, S., Mercier, G., Quezada, J., Bragazza, L., et al. (2019). Drought-induced decline of productivity in the dominant grassland species *Lolium perenne* L. depends on soil type and prevailing climatic conditions. *Soil Biol. Biochem.*, *132*, 47–57.
- Capolupo, A., Kooistra, L., Berendonk, C., Boccia, L., & Suomalainen, J. (2015). Estimating plant traits of grasslands from UAV-acquired hyperspectral images: A comparison of statistical approaches. *ISPRS Int. J. Geo-Inf.*, *4*(4), 2792–2820.

- Catchpole, W., & Wheeler, C. (1992). Estimating plant biomass: A review of techniques. *Aust. J. Ecol.*, *17*(2), 121–131.
- Chang, S., Chen, H., Wu, B., Nasanbat, E., Yan, N., & Davdai, B. (2021). A practical satellite-derived vegetation drought index for arid and semi-arid grassland drought monitoring. *Remote Sens.*, *13*(3), 414.
- Chen, M., Parton, W. J., Del Grosso, S. J., Hartman, M. D., Day, K. A., Tucker, C. J., Derner, J. D., Knapp, A. K., Smith, W. K., Ojima, D. S., et al. (2017). The signature of sea surface temperature anomalies on the dynamics of semiarid grassland productivity. *Ecosphere*, *8*(12), e02069.
- Chen, M., Parton, W. J., Hartman, M. D., Del Grosso, S. J., Smith, W. K., Knapp, A. K., Lutz, S., Derner, J. D., Tucker, C. J., Ojima, D. S., et al. (2019). Assessing precipitation, evapotranspiration, and NDVI as controls of US Great Plains plant production. *Ecosphere*, *10*(10), e02889.
- Chen, Y., Guerschman, J., Shendryk, Y., Henry, D., & Harrison, M. T. (2021). Estimating pasture biomass using Sentinel-2 imagery and machine learning. *Remote Sens.*, *13*(4), 603.
- Clementini, C., Pomete, A., Latini, D., Kanamaru, H., Vuolo, M. R., Heureux, A., Fujisawa, M., Schiavon, G., & Del Frate, F. (2020). Long-term grass biomass estimation of pastures from satellite data. *Remote Sens.*, *12*(13), 2160.
- De Leeuw, J., Rizayeva, A., Namazov, E., Bayramov, E., Marshall, M. T., Etzold, J., & Neudert, R. (2019). Application of the MODIS MOD 17 net primary production product in grassland carrying capacity assessment. *Int. J. Appl. Earth Obs. Geoinf.*, *78*, 66–76.

- Derner, J. D., & Augustine, D. J. (2016). Adaptive management for drought on rangelands. *Rangelands*, 38(4), 211–215.
- Derner, J. D., Briske, D., Reeves, M. C., Brown-Brandl, T., Meehan, M., Blumenthal, D., Travis, W., Augustine, D., Wilmer, H., Scasta, D., et al. (2018). Vulnerability of grazing and confined livestock in the Northern Great Plains to projected mid-and late-twenty-first century climate. *Clim. Change*, 146(1-2), 19–32.
- Derner, J. D., Raynor, E. J., Reeves, J. L., Augustine, D. J., & Milchunas, D. G. (2020). Climatic and management determinants of large herbivore production in semiarid grassland. *Agric. Ecosyst. Environ.*, 290, 106761.
- Dos Reis, A. A., Werner, J. P., Silva, B. C., Figueiredo, G. K., Antunes, J. F., Esquerdo, J. C., Coutinho, A. C., Lamparelli, R. A., Rocha, J. V., & Magalhães, P. S. (2020). Monitoring pasture aboveground biomass and canopy height in an integrated crop–livestock system using textural information from planetscope imagery. *Remote Sens.*, 12(16), 2534.
- Dube, T., Shoko, C., & Gara, T. W. (2021). Remote sensing of aboveground grass biomass between protected and non-protected areas in savannah rangelands. *Afr. J. Ecol.*, 59(3), 687–695.
- Dunn, G. H. (2013). *Drought calculator*. Retrieved March 14, 2022, from https://www.nrcs.usda.gov/wps/portal/nrcs/detailfull/nd/home/?cid=nrcs141p2_001670/.
- Dunn, G. H., Gutwein, M., Green, T. R., Menger, A., & Printz, J. (2013). The drought calculator: Decision support tool for predicting forage growth during drought. *Rangeland Ecol. Manage.*, 66(5), 570–578.

- Echeverría, A., Urmeneta, A., González-Audícana, M., & González, E. M. (2021). Monitoring rainfed alfalfa growth in semiarid agrosystems using Sentinel-2 imagery. *Remote Sens.*, *13*(22), 4719.
- Feng, L., Zhang, Z., Ma, Y., Du, Q., Williams, P., Drewry, J., & Luck, B. (2020). Alfalfa yield prediction using UAV-based hyperspectral imagery and ensemble learning. *Remote Sens.*, *12*(12), 2028.
- Fernández-Habas, J., Cañada, M. C., Moreno, A. M. G., Leal-Murillo, J. R., González-Dugo, M. P., Oar, B. A., Gómez-Giráldez, P. J., & Fernández-Rebollo, P. (2022). Estimating pasture quality of mediterranean grasslands using hyperspectral narrow bands from field spectroscopy by random forest and PLS regressions. *Comput. Electron. Agric.*, *192*, 106614.
- Garg, A., Sapkota, A., & Haghverdi, A. (2022). Samz-desert: A satellite-based agricultural management zoning tool for the desert agriculture region of Southern California. *Comput. Electron. Agric.*, *194*, 106803.
- Gargiulo, J., Clark, C., Lyons, N., de Veyrac, G., Beale, P., & Garcia, S. (2020). Spatial and temporal pasture biomass estimation integrating electronic plate meter, planet cubesats and Sentinel-2 satellite data. *Remote Sens.*, *12*(19), 3222.
- Gómara, I., Bellocchi, G., Martin, R., Rodríguez-Fonseca, B., & Ruiz-Ramos, M. (2020). Influence of climate variability on the potential forage production of a mown permanent grassland in the French Massif Central. *Agric. For. Meteorol.*, *280*, 107768.
- Guerini Filho, M., Kuplich, T. M., & Quadros, F. L. D. (2020). Estimating natural grassland biomass by vegetation indices using Sentinel 2 remote sensing data. *Int. J. Remote Sens.*, *41*(8), 2861–2876.

- Hao, Z., Xia, Y., Luo, L., Singh, V. P., Ouyang, W., & Hao, F. (2017). Toward a categorical drought prediction system based on US Drought Monitor (USDM) and climate forecast. *J. Hydrol.*, *551*, 300–305.
- Hartman, M. D., Parton, W. J., Derner, J. D., Schulte, D. K., Smith, W. K., Peck, D. E., Day, K. A., Del Grosso, S. J., Lutz, S., Fuchs, B. A., et al. (2020). Seasonal grassland productivity forecast for the US Great Plains using Grass-Cast. *Ecosphere*, *11*(11), e03280.
- Hashim, H., Abd Latif, Z., & Adnan, N. A. (2019). Urban vegetation classification with NDVI threshold value method with very high resolution (VHR) pleiades imagery. *ISPRS Ann. Photogramm. Remote Sens. Spatial Inf. Sci.*, *42*, 237–240.
- Horrocks, R. D., & Valentine, J. F. (1999). *Harvested Forages*. Academic Press, Cambridge, MA, USA.
- İleri, O., & Koç, A. (2022). Monitoring the available forage using Sentinel 2-derived NDVI data for sustainable rangeland management. *J. Arid. Environ.*, *200*, 104727.
- Ishler, V. A. a. (2020). *Penn State Extension*. Retrieved March 14, 2022, from <https://extension.psu.edu/spreadsheet-to-price-standing-hay-crop-forage/>.
- Jansen, V., Kolden, C., Greaves, H., & Eitel, J. (2019). Lidar provides novel insights into the effect of pixel size and grazing intensity on measures of spatial heterogeneity in a native bunchgrass ecosystem. *Remote Sens. Environ.*, *235*, 111432.
- Jin, Y., Yang, X., Qiu, J., Li, J., Gao, T., Wu, Q., Zhao, F., Ma, H., Yu, H., & Xu, B. (2014). Remote sensing-based biomass estimation and its spatio-temporal variations in temperate grassland, Northern China. *Remote Sens.*, *6*(2), 1496–1513.

- John, R., Chen, J., Giannico, V., Park, H., Xiao, J., Shirkey, G., Ouyang, Z., Shao, C., Laforzezza, R., & Qi, J. (2018). Grassland canopy cover and aboveground biomass in Mongolia and Inner Mongolia: Spatiotemporal estimates and controlling factors. *Remote Sens. Environ.*, 213, 34–48.
- Jones, M. O., Allred, B. W., Naugle, D. E., Maestas, J. D., Donnelly, P., Metz, L. J., Karl, J., Smith, R., Bestelmeyer, B., Boyd, C., et al. (2018). Innovation in rangeland monitoring: Annual, 30 m, plant functional type percent cover maps for us rangelands, 1984–2017. *Ecosphere*, 9(9), e02430.
- Jones, M. O., Robinson, N. P., Naugle, D. E., Maestas, J. D., Reeves, M. C., Lankston, R. W., & Allred, B. W. (2021). Annual and 16-day rangeland production estimates for the western united states. *Rangeland Ecol. Manage.*, 77, 112–117.
- Karunaratne, S., Thomson, A., Morse-McNabb, E., Wijesingha, J., Stayches, D., Copland, A., & Jacobs, J. (2020). The fusion of spectral and structural datasets derived from an airborne multispectral sensor for estimation of pasture dry matter yield at paddock scale with time. *Remote Sens.*, 12(12), 2017.
- Kearney, S. P., Porensky, L. M., Augustine, D. J., Gaffney, R., & Derner, J. D. (2022). Monitoring standing herbaceous biomass and thresholds in semiarid rangelands from harmonized Landsat 8 and Sentinel-2 imagery to support within-season adaptive management. *Remote Sens. Environ.*, 271, 112907.
- Keele, S. et al. (2007). *Guidelines for performing systematic literature reviews in software engineering* (tech. rep.). Technical Report, Ver. 2.3 EBSE Technical Report. EBSE.

- Kichler, C., Fulton, J., Raper, R., McDonald, T., & Zech, W. (2011). Effects of transmission gear selection on tractor performance and fuel costs during deep tillage operations. *Soil Tillage Res.*, *113*(2), 105–111.
- Kirwan, B. (2020). *NRCS - Hay Production vs. Buying*. Retrieved March 14, 2022, from <https://www.nrcs.usda.gov/wps/portal/nrcs/main/national/technical/econ/tools/>.
- Koech, O., Kinuthia, R., Karuku, G., Mureithi, S., & Wanjogu, R. (2015). Water use efficiency of six rangeland grasses under varied soil moisture content levels in the arid Tana River County, Kenya. *Afr. J. Environ. Sci. Technol.*, *9*(7), 632–640.
- Kong, B., Yu, H., Du, R., & Wang, Q. (2019). Quantitative estimation of biomass of alpine grasslands using hyperspectral remote sensing. *Rangeland Ecol. Manage.*, *72*(2), 336–346.
- Krueger, E. S., Ochsner, T. E., Levi, M. R., Basara, J. B., Snitker, G. J., & Wyatt, B. M. (2021). Grassland productivity estimates informed by soil moisture measurements: Statistical and mechanistic approaches. *Agron. J.*, *113*(4), 3498–3517.
- Kumar, L., & Mutanga, O. (2017). Remote sensing of above-ground biomass. *Remote Sens.*, *9*(9), 935.
- Kuwayama, Y., Thompson, A., Bernknopf, R., Zaitchik, B., & Vail, P. (2019). Estimating the impact of drought on agriculture using the US Drought Monitor. *Am. J. Agric. Econ.*, *101*(1), 193–210.
- Lang, M., Mahyou, H., & Tychon, B. (2021). Estimation of rangeland production in the arid oriental region (Morocco) combining remote sensing vegetation and rainfall indices: Challenges and lessons learned. *Remote Sens.*, *13*(11), 2093.

- Leroux, C., Jones, H., Pichon, L., Guillaume, S., Lamour, J., Taylor, J., Naud, O., Crestey, T., Lablee, J.-L., & Tisseyre, B. (2018). Geofis: An open source, decision-support tool for precision agriculture data. *Agriculture*, 8(6), 73.
- Li, F., Zeng, Y., Luo, J., Ma, R., & Wu, B. (2016). Modeling grassland aboveground biomass using a pure vegetation index. *Ecol. Indic.*, 62, 279–288.
- Li, H., Zhang, F., Zhu, J., Guo, X., Li, Y., Lin, L., Zhang, L., Yang, Y., Li, Y., Cao, G., et al. (2021). Precipitation rather than evapotranspiration determines the warm-season water supply in an alpine shrub and an alpine meadow. *Agric. For. Meteorol.*, 300, 108318.
- Li, Q., Xu, L., Pan, X., Zhang, L., Li, C., Yang, N., & Qi, J. (2016). Modeling phenological responses of Inner Mongolia grassland species to regional climate change. *Environ. Res. Lett.*, 11(1), 015002.
- Li, X., Yuan, W., & Dong, W. (2021). A machine learning method for predicting vegetation indices in China. *Remote Sens.*, 13(6), 1147.
- LI, Z.-w., XIN, X.-p., Huan, T., Fan, Y., CHEN, B.-r., & ZHANG, B.-h. (2017). Estimating grassland LAI using the random forests approach and Landsat imagery in the meadow steppe of Hulunber, China. *J. Integr. Agric.*, 16(2), 286–297.
- Lin, X., Chen, J., Lou, P., Yi, S., Qin, Y., You, H., & Han, X. (2021). Improving the estimation of alpine grassland fractional vegetation cover using optimized algorithms and multi-dimensional features. *Plant Methods*, 17(1), 1–18.
- Liu, H., Dahlgren, R. A., Larsen, R. E., Devine, S. M., Roche, L. M., O'Geen, A. T., Wong, A. J., Covello, S., & Jin, Y. (2019). Estimating rangeland forage production using

- remote sensing data from a small unmanned aerial system (sUAS) and planetscope satellite. *Remote Sens.*, 11(5), 595.
- Liu, Y., Dang, C., Yue, H., Lyu, C., & Dang, X. (2021). Enhanced drought detection and monitoring using sun-induced chlorophyll fluorescence over Hulun Buir Grassland, China. *Sci. Total Environ.*, 770, 145271.
- Long, Y., Li, Z., Wei, L., & Hua-Kun, Z. (2010). Using remote sensing and GIS technologies to estimate grass yield and livestock carrying capacity of alpine grasslands in Golog Prefecture, China. *Pedosphere*, 20(3), 342–351.
- Lyu, X., Li, X., Dang, D., Dou, H., Xuan, X., Liu, S., Li, M., & Gong, J. (2020). A new method for grassland degradation monitoring by vegetation species composition using hyperspectral remote sensing. *Ecol. Indic.*, 114, 106310.
- Lyu, X., Li, X., Gong, J., Li, S., Dou, H., Dang, D., Xuan, X., & Wang, H. (2021). Remote-sensing inversion method for aboveground biomass of typical steppe in Inner Mongolia, China. *Ecol. Indic.*, 120, 106883.
- Magiera, A., Feilhauer, H., Waldhardt, R., Wiesmair, M., & Otte, A. (2017). Modelling biomass of mountainous grasslands by including a species composition map. *Ecol. Indic.*, 78, 8–18.
- Meng, B., Ge, J., Liang, T., Yang, S., Gao, J., Feng, Q., Cui, X., Huang, X., & Xie, H. (2017). Evaluation of remote sensing inversion error for the above-ground biomass of alpine meadow grassland based on multi-source satellite data. *Remote Sens.*, 9(4), 372.
- Nayigihugu, V., Schleicher, A., Koch, D., Held, L., Flake, J., & Hess, B. (2007). Beef cattle production, nutritional quality, and economics of windrowed forage vs. baled hay during winter. *Agron. J.*, 99(4), 944–951.

- Norberg, S., & Neiberger, S. J. (2012). *Irrigated alfalfa hay budget under center pivot in the Columbia Basin - Washington Extension Publication FS133E*. Retrieved March 14, 2022, from <https://tinyurl.com/2p83dm4h/>.
- Obermeier, W. A., Lehnert, L. W., Pohl, M., Gianonni, S. M., Silva, B., Seibert, R., Laser, H., Moser, G., Müller, C., Luterbacher, J., et al. (2019). Grassland ecosystem services in a changing environment: The potential of hyperspectral monitoring. *Remote Sens. Environ.*, *232*, 111273.
- Ojeda, J. J., Caviglia, O. P., Irisarri, J. G. N., & Agnusdei, M. G. (2018). Modelling inter-annual variation in dry matter yield and precipitation use efficiency of perennial pastures and annual forage crops sequences. *Agric. For. Meteorol.*, *259*, 1–10.
- Pal, S. C., Chakraborty, R., Malik, S., & Das, B. (2018). Application of forest canopy density model for forest cover mapping using LISS-IV satellite data: A case study of Sali watershed, West Bengal. *Model. Earth Syst. Environ.*, *4*(2), 853–865.
- Paltsyn, M. Y., Gibbs, J. P., Iegorova, L. V., & Mountrakis, G. (2017). Estimation and prediction of grassland cover in western Mongolia using MODIS-derived vegetation indices. *Rangeland Ecol. Manage.*, *70*(6), 723–729.
- Paltsyn, M. Y., Gibbs, J. P., & Mountrakis, G. (2019). Integrating traditional ecological knowledge and remote sensing for monitoring rangeland dynamics in the Altai Mountain region. *J. Environ. Manage.*, *64*(1), 40–51.
- Parton, W., Hartman, M., Peck, D., Derner, J. D., Smith, W., Del Grosso, S. J., & Fuchs, B. (2020). Grass-cast: Using grassland productivity forecast to link ecology and ecosystem management. *2020 ESA Annual Meeting (August 3-6)*.

- Pastick, N. J., Wylie, B. K., Rigge, M. B., Dahal, D., Boyte, S. P., Jones, M. O., Allred, B. W., Parajuli, S., & Wu, Z. (2021). Rapid monitoring of the abundance and spread of exotic annual grasses in the western united states using remote sensing and machine learning. *AGU Adv.*, 2(2), e2020AV000298.
- Pecina, M. V., Bergamo, T. F., Ward, R., Joyce, C., & Sepp, K. (2021). A novel UAV-based approach for biomass prediction and grassland structure assessment in coastal meadows. *Ecol. Indic.*, 122, 107227.
- Peck, D. (2018). *Grass-Cast: Grassland production forecast*. Retrieved March 14, 2022, from <https://grasscast.unl.edu/>.
- Peck, D., Derner, J. D., Parton, W., Hartman, M., & Fuchs, B. (2019). Flexible stocking with grass-cast: A new grassland productivity forecast to translate climate outlooks for ranchers. *Western Economics Forum*, 17(1837-2019-973), 24–39.
- Peng, J., Kim, M., Kim, Y., Jo, M., Kim, B., Sung, K., & Lv, S. (2017). Constructing Italian ryegrass yield prediction model based on climatic data by locations in South Korea. *Grassland Sci.*, 63(3), 184–195.
- Qin, Q., Xu, D., Hou, L., Shen, B., & Xin, X. (2021). Comparing vegetation indices from Sentinel-2 and Landsat 8 under different vegetation gradients based on a controlled grazing experiment. *Ecol. Indic.*, 133, 108363.
- Reeves, J. L., Derner, J. D., Sanderson, M. A., Kronberg, S. L., Hendrickson, J. R., Vermeire, L. T., Petersen, M. K., & Irisarri, J. G. (2015). Seasonal weather-related decision making for cattle production in the Northern Great Plains. *Rangelands*, 37(3), 119–124.

- Reeves, M. C., & Mitchell, J. E. (2011). Extent of coterminous us rangelands: Quantifying implications of differing agency perspectives. *Rangeland Ecol. Manage.*, 64(6), 585–597.
- Robinson, N. P., Jones, M. O., Moreno, A., Erickson, T. A., Naugle, D. E., & Allred, B. W. (2019). Rangeland productivity partitioned to sub-pixel plant functional types. *Remote Sens.*, 11(12), 1427.
- Sandor, R., Barcza, Z., Acutis, M., Doro, L., Hidy, D., Köchy, M., Minet, J., Lellei-Kovács, E., Ma, S., Perego, A., et al. (2017). Multi-model simulation of soil temperature, soil water content and biomass in euro-mediterranean grasslands: Uncertainties and ensemble performance. *Eur. J. Agron.*, 88, 22–40.
- Schwieder, M., Buddeberg, M., Kowalski, K., Pfoch, K., Bartsch, J., Bach, H., Pickert, J., & Hostert, P. (2020). Estimating grassland parameters from Sentinel-2: A model comparison study. *PFG- J. Photogramm. Remote Sens. Geoinf. Sci.*, 88(5), 379–390.
- Sen, C., & Ozturk, O. (2017). The relationship between soil moisture and temperature vegetation on Kirklareli City Luleburgaz District a natural pasture vegetation. *Int. J. Environ. Agric. Res.*, 3(3), 21–29.
- Şen, C. (2018). The effects of soil moisture and temperature on vegetation composition and yield at different pasture sites. *Int. J. Agric. Sci. Vet. Med.*, 5(2), 1–10.
- Serrano, J., Shahidian, S., & da Silva, J. M. (2016). Calibration of GrassMaster II to estimate green and dry matter yield in Mediterranean pastures: Effect of pasture moisture content. *Crop Pasture Sci.*, 67(7), 780–791.

- Shoko, C., Mutanga, O., Dube, T., & Slotow, R. (2018). Characterizing the spatio-temporal variations of C3 and C4 dominated grasslands aboveground biomass in the drakensberg, South Africa. *Int. J. Appl. Earth Obs. Geoinf.*, *68*, 51–60.
- Shrum, T. R., Travis, W. R., Williams, T. M., & Lih, E. (2018). Managing climate risks on the ranch with limited drought information. *Clim. Risk Manage.*, *20*, 11–26.
- Smart, A. J., Harmoney, K., Scasta, J. D., Stephenson, M. B., Volesky, J. D., Vermeire, L. T., Mosley, J. C., Sedivec, K., Meehan, M., Haigh, T., et al. (2021). Critical decision dates for drought management in central and northern great plains rangelands. *Rangeland Ecology & Management*, *78*, 191–200.
- Smith, J. T., Allred, B. W., Boyd, C. S., Davies, K. W., Jones, M. O., Kleinhesselink, A. R., Maestas, J. D., Morford, S. L., & Naugle, D. E. (2022). The elevational ascent and spread of exotic annual grass dominance in the Great Basin, USA. *Divers. Distrib.*, *28*(1), 83–96.
- Soubry, I., & Guo, X. (2020). Monitoring and modeling rangeland health with remote sensing. *Univ. Saskatchewan: Saskatoon, SK, Canada*.
- Stenzel, S., Fassnacht, F. E., Mack, B., & Schmidtlein, S. (2017). Identification of high nature value grassland with remote sensing and minimal field data. *Ecological indicators*, *74*, 28–38.
- Subhashree, S. N., Igathinathane, C., Liebig, M., Halvorson, J., Archer, D., Hendrickson, J., & Kronberg, S. (2021). Biomass bales infield aggregation logistics energy for tractors and automatic bale pickers – A simulation study. *Biomass Bioenerg.*, *144*, 105915.

- Tarumi, E., Tsuiki, M., & Mori, A. (2021). Cool-season grass productivity estimation model evaluating the effects of global warming and climate adaptation strategies. *Grassland Sci.*, 67(3), 234–240.
- Undersander, D., & Barnett, K. (2008). *Value of short rotations for alfalfa profitability*. Retrieved March 14, 2022, from <https://fyi.extension.wisc.edu/forage/value-of-short-rotations-for-alfalfa-profitability/>.
- USDM. (1999). *United states drought monitor*. Retrieved March 14, 2022, from <https://droughtmonitor.unl.edu/Maps/CompareTwoWeeks.aspx/>.
- Viljanen, N., Honkavaara, E., Näsi, R., Hakala, T., Niemeläinen, O., & Kaivosoja, J. (2018). A novel machine learning method for estimating biomass of grass swards using a photogrammetric canopy height model, images and vegetation indices captured by a drone. *Agriculture*, 8(5), 70.
- Vogeler, I., Thomas, S., & van der Weerden, T. (2019). Effect of irrigation management on pasture yield and nitrogen losses. *Agric. Water Manage.*, 216, 60–69.
- Wachendorf, M., Fricke, T., & Möckel, T. (2018). Remote sensing as a tool to assess botanical composition, structure, quantity and quality of temperate grasslands. *Grass Forage Sci.*, 73(1), 1–14.
- Wang, J., Xiao, X., Bajgain, R., Starks, P., Steiner, J., Doughty, R. B., & Chang, Q. (2019). Estimating leaf area index and aboveground biomass of grazing pastures using Sentinel-1, Sentinel-2 and Landsat images. *SPRS J. Photogramm. Remote Sens.*, 154, 189–201.
- Weber, D., Schaepman-Strub, G., & Ecker, K. (2018). Predicting habitat quality of protected dry grasslands using Landsat NDVI phenology. *Ecol. Indic.*, 91, 447–460.

- Wu, C., Shen, H., Shen, A., Deng, J., Gan, M., Zhu, J., Xu, H., & Wang, K. (2016). Comparison of machine-learning methods for above-ground biomass estimation based on Landsat imagery. *J. Appl. Remote Sens.*, *10*(3), 035010.
- Wu, T., Fu, H., Feng, F., & Bai, H. (2019). A new approach to predict normalized difference vegetation index using time-delay neural network in the arid and semi-arid grassland. *Int. J. Remote Sens.*, *40*(23), 9050–9063.
- Wylie, B., Howard, D., Dahal, D., Gilmanov, T., Ji, L., Zhang, L., & Smith, K. (2016). Grassland and cropland net ecosystem production of the US Great Plains: Regression tree model development and comparative analysis. *Remote Sens.*, *8*(11), 944.
- Xia, J., Ma, M., Liang, T., Wu, C., Yang, Y., Zhang, L., Zhang, Y., & Yuan, W. (2018). Estimates of grassland biomass and turnover time on the Tibetan Plateau. *Environ. Res. Lett.*, *13*(1), 014020.
- Xie, X., He, B., Guo, L., Miao, C., & Zhang, Y. (2019). Detecting hotspots of interactions between vegetation greenness and terrestrial water storage using satellite observations. *Remote Sens. Environ.*, *231*, 111259.
- Xu, D., Chen, B., Shen, B., Wang, X., Yan, Y., Xu, L., & Xin, X. (2019). The classification of grassland types based on object-based image analysis with multisource data. *Rangeland Ecol. Manage.*, *72*(2), 318–326.
- Xu, D., Wang, C., Chen, J., Shen, M., Shen, B., Yan, R., Li, Z., Karnieli, A., Chen, J., Yan, Y., et al. (2021). The superiority of the normalized difference phenology index (NDPI) for estimating grassland aboveground fresh biomass. *Remote Sens. Environ.*, *264*, 112578.

- Yang, S., Feng, Q., Liang, T., Liu, B., Zhang, W., & Xie, H. (2018). Modeling grassland above-ground biomass based on artificial neural network and remote sensing in the three-river headwaters region. *Remote Sens. Environ.*, *204*, 448–455.
- Yu, J., Vandever, M., Volesky, J. D., & Harmoney, K. (2019). Estimating the basis risk of rainfall index insurance for pasture, rangeland, and forage. *J. Agril. Resour. Econ.*, *44*(1835-2019-069), 179–193.
- Zeng, N., Ren, X., He, H., Zhang, L., Zhao, D., Ge, R., Li, P., & Niu, Z. (2019). Estimating grassland aboveground biomass on the Tibetan Plateau using a random forest algorithm. *Ecol. Indic.*, *102*, 479–487.
- Zhang, B., Zhang, L., Xie, D., Yin, X., Liu, C., & Liu, G. (2016). Application of synthetic NDVI time series blended from Landsat and MODIS data for grassland biomass estimation. *Remote Sens.*, *8*(1), 10.
- Zhang, H., Fan, J., Wang, J., Cao, W., & Harris, W. (2018). Spatial and temporal variability of grassland yield and its response to climate change and anthropogenic activities on the Tibetan Plateau from 1988 to 2013. *Ecol. Indic.*, *95*, 141–151.
- Zhang, H., Tang, Z., Wang, B., Meng, B., Qin, Y., Sun, Y., Lv, Y., Zhang, J., & Yi, S. (2022). A non-destructive method for rapid acquisition of grassland aboveground biomass for satellite ground verification using UAV RGB images. *Global Ecol. Conserv.*, *33*, e01999.
- Zhang, X., Du, X., Hong, J., Du, Z., Lu, X., & Wang, X. (2020). Effects of climate change on the growing season of alpine grassland in Northern Tibet, China. *Global Ecol. Conserv.*, *23*, e01126.

- Zhao, Y., Zhu, W., Wei, P., Fang, P., Zhang, X., Yan, N., Liu, W., Zhao, H., & Wu, Q. (2022). Classification of Zambian grasslands using random forest feature importance selection during the optimal phenological period. *Ecol. Indic.*, *135*, 108529.
- Zheng, F., Hu, Y., Qibing, W., & Feng, Z. (2021). Changes and controls of aboveground net primary production in response to grassland policy in Inner Mongolian grasslands of China. *Remote Sens. Appl.: Soc. Environ.*, *22*, 100526.
- Zhou, W., Li, H., Xie, L., Nie, X., Wang, Z., Du, Z., & Yue, T. (2021). Remote sensing inversion of grassland aboveground biomass based on high accuracy surface modeling. *Ecol. Indic.*, *121*, 107215.

3. BIOMASS BALES INFIELD AGGREGATION LOGISTICS ENERGY FOR TRACTORS AND AUTOMATIC BALE PICKERS — A SIMULATION STUDY *

3.1. Abstract

Infield bale aggregation is essential for bale removal and for preparing the field for subsequent crops, which can be more efficiently performed using the modern automatic bale picker (ABP) that supports multiple bales/trip (BPT) than commonly used tractors. But the energy involved in the bale aggregation logistics using ABP has not been thoroughly evaluated. Therefore, the energy involved in the bale aggregation, in terms of fuel consumption, was studied for different logistic scenarios using a tractor (control) and ABP through a user-developed simulation program in ‘R.’ Different variables such as field areas (8 to 259 ha), biomass yields (3–40 Mg ha⁻¹), four outlet locations, and five equipment speeds (6.6–10.5 km h⁻¹) using realistic equipment turning paths were used in the simulation. The Nebraska Tractor Test general method and fuel efficiency method were considered for the fuel consumption calculations. Fuel consumption for the ABP (8–259 ha) with 8 BPT on an average decreased by 72 % and 53 % compared to a tractor with 1 and 2 BPT, respectively, based on logistics distance and equipment operation. Field area, biomass yield, and BPT were the most influential variables affecting logistics distance;

* This paper was already published with the citation: Srinivasagan N. Subhashree, C. Igathinathane, M. Liebig, J. Halvorso, D. Archer, J. Hendrickson, and S. Kronberg. (2021). Biomass bales infield aggregation logistics energy for tractors and automatic bale pickers — A simulation study. *Biomass and Bioenergy*, 144(2021) 105915. DOI: <https://doi.org/10.1016/j.biombioe.2020.105915>. Subhashree performed literature search, developed simulation, analyzed results, and wrote the manuscript. Dr. Igathinathane Cannayan is the major advisor, principal investigator, and the corresponding author who worked with Subhashree throughout the research and manuscript development. All the co-authors have assisted in the research direction and review of the manuscript.

while, field area, biomass yield, BPT, and equipment speed affecting the operation time and fuel quantity. Convenient prediction models (multi-variate nonlinear) for logistics distance, operation time, and fuel quantity, using the influential field variables, produced very good fits ($R^2 \geq 0.98$). Overall, an ABP with a capacity of 8 BPT, which can also handle 11 BPT, is recommended considering the logistics energy.

3.2. Introduction

Agricultural biomass is one of the most abundant renewable energy resources. The demand for biomass is increasing due to its versatility ranging from energy generation to livestock feed applications. Biofuel production at large-scale faces multiple issues and challenges associated with logistics, schedule of delivery, and inconsistent feedstock supply (Hess et al., 2007). Logistic operations for biomass including collection, handling, storage, and transport, contribute to the major cost of bio-energy. Supply chain modeling, involving five different types of biomass (Miscanthus [*Miscanthus giganteus*], forest fuel, short rotation coppice, and straw), concluded that 20%–50% of the costs associated with biomass logistics involve handling and transport (Allen et al., 1998).

Biomass logistics cost is one of the major barriers to biomass utilization. Hence several models of supply chain logistics have been developed to improve biomass logistics efficiency. These models studied supply chain for ethanol production (Ebadian et al., 2013; Lin et al., 2014), Miscanthus (Huisman et al., 1997; Shastri et al., 2010), biomass supply to biorefineries (Sokhansanj et al., 2006), forest residues (Gallis, 1996; Mobini et al., 2011), woody biomass (Svanberg et al., 2013; Umeki et al., 2010), GIS-based switchgrass logistics across 11 US states (Graham et al., 2000), and GIS-based biomass delivery to a specific location (Graham et al., 1997).

Previous logistics studies usually assume biomass is a “point source” available at the field location and moved to a distant processing facility. A review on biomass collection, storage, and handling techniques suggests loose biomass from fields be packed into small bundles (e.g., bales) and then transported to biomass stations for repackaging to the desired density and size before transporting to the biofuel plants (Zhou et al., 2016). Since the logistics cost accounts for 90% of the total costs (EkşiođLu et al., 2010), many studies have been conducted to model the logistics of biomass using predictive modeling approaches integrated with GIS-based methods (Frombo et al., 2009; Velázquez-Martí and Annevelink, 2009). These studies mainly focused on developing effective methods to achieve optimal on-road logistics and transport strategies in whole fields or larger areas considered as a single unit of biomass supply.

In reality, biomass is a “distributed source” and after harvest residues are left, throughout the field, to dry until they reach optimum moisture of 5%–20% wet basis and baled for collection (Rotz and Muck, 1994; Rotz and Shinnors, 2007). Infield biomass bale logistics of aggregation and transportation to a field outlet, which can then be considered a biomass point source, is an elaborate operation. Bales need to be collected to clear the field for the subsequent crops, avoid microbial degradation (Coblentz et al., 1996), spontaneous heating (Coblentz and Hoffman, 2009), dry matter loss (Scarborough et al., 2005), and nutritive value changes (Turner et al., 2002). Therefore, the infield logistics of bale collection should be efficiently performed and completed within a limited time frame.

Efficient infield biomass collection and handling not only reduce logistics costs but preserve the quality of the bales. Despite the importance of efficient biomass collection and handling, studies on infield logistics of bale collection are limited. A method for ef-

efficient aggregation of bales, based on the minimum distance between subsequent bales, was developed (Igathinathane et al., 2014). Increasing the number of bales/trip (BPT) using additional equipment was found to improve infield logistics efficiency. For temporarily stacking bales before moving to an outlet, comparing the middle edges and the corners of the field, the middle was found to be the best in terms of efficient logistics distance (Igathinathane et al., 2016). Another related study, comparing the field middle method to other mathematical grouping methods, such as centroid, middle data range, geometric median, medoid, and origin found that the geometric median was the best location for bale stacks (Subhashree et al., 2017), but recommended the field middle since it is practical and simple to locate on the field. Various field equipment such as harvester, baler, tractor, and automatic bale picker (ABP) generate equipment track impacted areas, and it was found that baler generated the least while ABP generated the most track impacted area (Subhashree and Igathinathane, 2019).

Many studies have been conducted for predicting tractor fuel consumption during various infield operations, such as tillage, fertilizer and chemical application, planting, cultivation, and forage harvesting (Grisso et al., 2014; Kheiralla et al., 2004; Naderloo et al., 2012; Voltarelli et al., 2013). Fuel efficiency is an important aspect of the tractor engine that directly influenced fuel consumption. Varying load characteristics, as applicable to the different number of bales handled in logistics, is one of the major parameters that affect fuel efficiency (Hansson et al., 2003; Pitla et al., 2016). Speed of equipment's ground operation also influences the quantity of fuel consumed. Fuel consumption rate increased by 105 % between slow (3.0 km h^{-1}) and fast (8.3 km h^{-1}) operation speed of the tractor (Kichler et al., 2011).

The variability in the field parameters (e.g., area, biomass yield, windrow variation) and operating parameters (e.g., type of equipment, BPT, equipment speed) that the producers encounter should be accounted for to make the results robust. But studies on the energy involved (or fuel consumption) in the infield biomass bale aggregation logistics, a high effort field operation (Subhashree and Igathinathane, 2019), are not available. Therefore, a robust study utilizing a novel approach of predicting the fuel consumption during infield bale aggregation, with varying load and equipment speed scenarios, using the fuel efficiency and operation time will be beneficial for producers to make efficient management decisions.

In the proposed study, a mathematical simulation was employed to mimic the infield bale aggregation process, as closely as possible, involving the influential field and operating parameters, for determining the energy involved using two methods as a function of field parameters. Specific objectives included (i) comparison of logistic distances and energy involved in infield bale aggregation, in terms of fuel consumption, by the tractor and ABP using general and fuel efficiency methods, (ii) determination of the effect of field parameters, such as field area, outlet location, BPT, biomass yield, equipment speed, and windrow variation on logistics distances and fuel usage, and (iii) development of convenient models to evaluate the logistics distances, operation time, and fuel requirements from the field area, BPT, biomass yield, and equipment speed.

3.3. Materials and Methods

The conventional method for infield aggregation is using a tractor and was considered the “control” method in this study (fig. 3.1A). This was compared to the ABP, also known as “self-loading bale carrier,” which aggregates and transports bales to the stack

location or outlet in a single trip (fig. 3.1B). The ABP is a trailer attached to the tractor with a bale picking arm on its side. Unlike the tractor, which can usually handle only 1 or 2 BPT, the ABP can handle 8–23 BPT.



Figure 3.1. Examples of common and modern bale aggregation equipment: (A) Tractor equipped with bale spears at the front and rear (capacity = 1–2 bales); and (B) An automatic bale picker (ABP) with loading arm (capacity up to 23) — Image sources: <https://www.himac.com.au> and <https://www.farm-king.com>.

All infield bale logistics operations in the study were performed through mathematical simulation using the statistical software environment R (R Core Team, 2017). The program codes were developed to simulate the layout of bales in the field, mimic the equipment actions, generate logistic distances, estimate energy involved in the operations through fuel consumption, perform statistical analysis, generate prediction models, and visualize the results. Both R ‘base’ graphics and package ‘ggplot2’ (Wickham, 2016) were used to generate high-quality vector-based graphics for visualization. Bale aggregation by a tractor (1 and 2 BPT) and ABP (8–23 BPT) gave rise to several turning cases (instances where the tractor would need to turn) based on the location of adjacent bales (Subhashree and Igathinathane, 2019), and these realistic turning distances were incorporated in the analysis. This study only considered a few capacities for specific prediction model devel-

opment to address the range (1 BPT for tractor; and 8 and 23 BPT for ABP), while the simulation can accommodate any reasonable BPT (e.g., 1–23). Various aspects involved in this study are represented in the form of a flow diagram (fig. 3.2).

3.3.1. Mathematical Simulation of Infield Bales Aggregation

The number of bales made by the baler from the windrow was a function of the mass of the material along the windrow as influenced by the random yield variation (10% assumed) and the target bale mass considered. The baler followed the path of the windrows, made by the harvester in the field, and generated the layout of bales in a pattern based on the windrow biomass availability. The layout of bales in the field, represented by x_i and y_i coordinates indicating bale locations used in the logistics analysis, influenced the path generated by the equipment. The randomness in this bale layout depends on biomass availability along the windrows as described earlier. Detailed simulation methodology of bale formation and the field layout is reported elsewhere (Igathinathane et al., 2014), and was used in this study.

Aggregation logistics involving minimum path distance and realistic equipment turning paths were simulated to trace the path generated by the tractor and ABP. The minimum path distance was simulated to achieve the minimum cumulative distance; for each aggregation trip, the equipment starts (no bales) and ends (full BPT unloaded) at the field outlet location. A realistic curvilinear turning path was generated based on the turning radius of the equipment and bales layout. Kinematics and geometrical principles were used to derive various equipment turning scenarios during bale aggregation (Subhashree and Igathinathane, 2019).

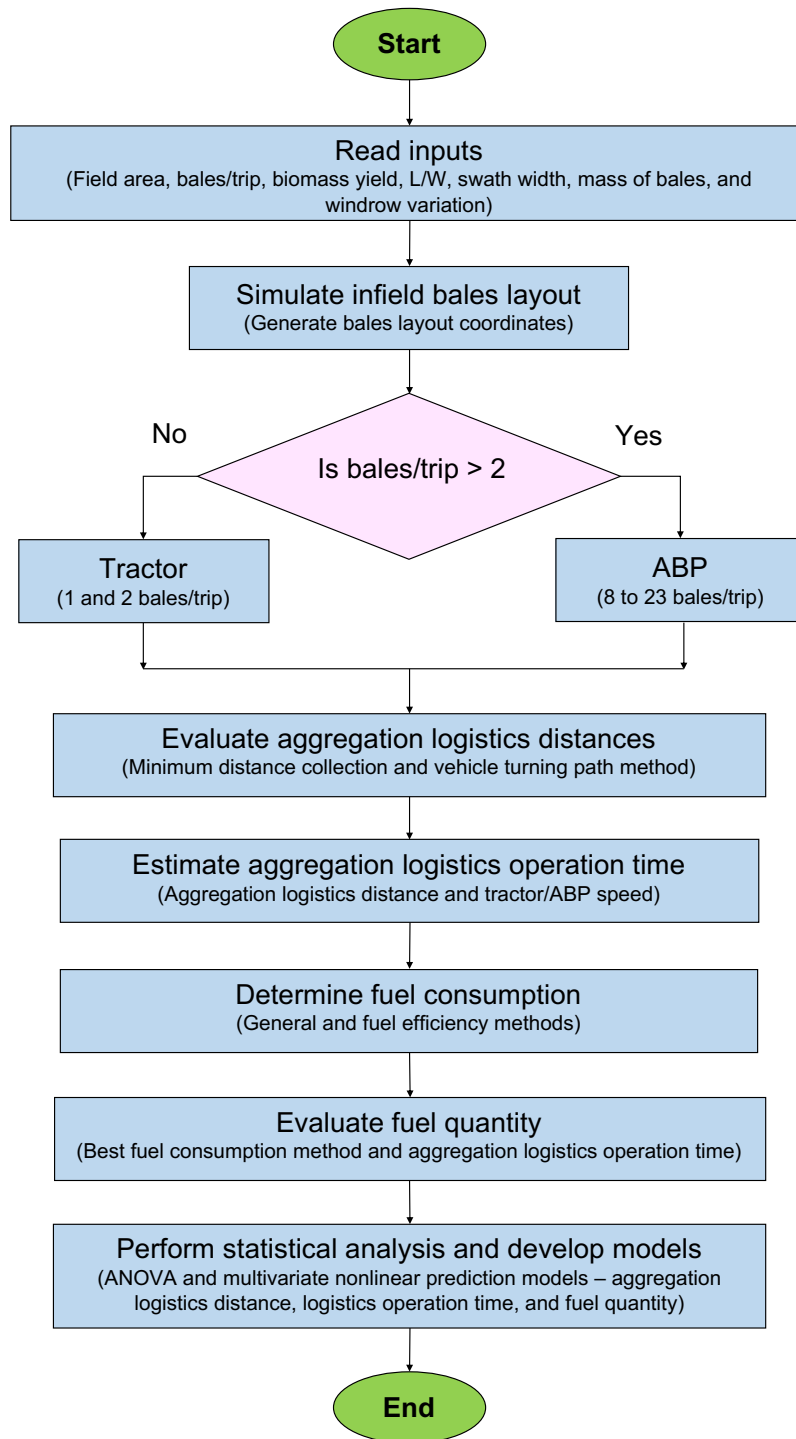


Figure 3.2. Flowchart showing the details of the developed algorithm for the R program simulation to compare the tractor and ABP (automatic bale picker) performances based on the generated logistics distances and fuel consumption.

3.3.2. Parameters Considered in the Simulation

Various inputs to the simulation program were selected to represent different conditions in the field and generate appropriate scenarios of infield bale aggregation. The input parameters considered were: (i) field areas, expressed as fractions of a “section” (1 square mile = 640 acres = 259 ha) as a standard U.S. land unit as 8, 16, 24, 32, 40, 65, 129, and 259 ha; (ii) BPT 1 and 2 for tractor bale aggregation, while 8, 11, 14, 17, and 23 BPT were considered based on the commonly available commercial carrying capacity of ABP; (iii) biomass yields, accommodating variation in the yield range of the potential forages and bioenergy feedstocks, of 3, 4, 5, 6, 7, 8, 10, 15, 20, 30, and 40 Mg ha⁻¹; (iv) different outlet locations, where the bales are stacked, such as field origin (corner), field middle, along the field mid-width edge, and along the field mid-length edge; (v) percentage of windrow variation, reflecting the spatial variation of yield, as 5 %, 10 %, 15 %, and 20 %; and (vi) equipment operation speeds at 6.4, 7.4, 8.5, 9.5, and 10.5 km h⁻¹ (4–6.5 mph). Simulation program with various levels considered for the field parameters, such as area (8), BPT (7), windrow variation (3), biomass yield (11), outlet locations (4), and equipment operation speed (5) generated 36 960 scenarios. Several other field parameters that can affect the simulation, such as (i) length by width (L/W) ratio values representing the field shape, (ii) harvester swath width (9 m considered); and (iii) random number generation seed value (2016 considered) were assumed as constant based on the findings of previous studies (Igathinathane et al., 2014; Subhashree et al., 2017).

3.3.3. Bale Aggregation Energy Through Fuel Consumption

The energy involved in the infield bale aggregation is based on the size of the equipment (tractor directly handling the bales and tractor with ABP) and the logistics distance of

the bales in the field to the outlet (mass \times distance). Possible changes in elevation across the field and the soil type and conditions are known to influence the fuel consumption, but were beyond the scope of this study. Energy ultimately comes from the fuel used in the equipment after meeting various efficiencies. Fuel consumption of a tractor, defined as the estimation of fuel quantity utilized over a period of time (Grisso et al., 2014), is dependent on the tractor engine power.

Various methods are available to calculate the fuel consumption for different types of equipment and levels of loading. Two established methods, namely general and fuel efficiency, were considered for fuel consumption calculations. The general method was developed using the Nebraska Tractor Test results data obtained between 1980 and 2005 from more than 500 tractors (Grisso et al., 2014), which considered compression ignition operating at or below maximum load conditions. While the fuel efficiency method was built using the data obtained from diesel tractors (Hunt, 2008; Khalilian et al., 1985). These two methods estimated fuel consumption based on the relationship of varying engine loads, which in turn relied on the total tractor load (tractor total weight).

3.3.4. Total Tractor Load of Fuel Consumption Methods

Two different tractors with engine power capacities of 60 and 93 kW (80 and 125 hp) were considered based on the handling capacity of 1 and 2 BPT for control and 8–23 BPT for ABP. The mass of each bale was considered \approx 500 kg. A 60 kW (80 hp) tractor was capable of lifting 1200–2600 kg or 2–5 bales (JD, 2006), however, only 2 BPT was considered maximum due to the limitation of commercially available lifting attachments and maneuverability of the tractor. The tractor used in the control method was assumed to aggregate bales by lifting them using bale spears attached to the front and rear of the tractor

(fig. 3.1A). The ABP, however, is essentially a trailer equipped with a picking arm attached to a tractor, hence it can handle a large number of bales. The selected engine power of 125 hp was enough to pull the weight of the trailer loaded with 23 bales (Anderson, 2008; Pronovost, 2017), which is also the maximum capacity considered of ABP in the study.

The total tractor load was calculated based on the empty tractor weight and the bale load lifted (control) or pulled using a trailer (ABP). A common assumption for both these methods is that the empty tractor load and maximum allowable bale load (control = 5 BPT and ABP = 23 BPT) constituted about 30 % and 70 % of the maximum total tractor load, respectively (JD, 2006; Pronovost, 2017). The unitary method was employed to determine the percentage of bale load of every additional bale aggregated for BPT less than 5 and 23, respectively, for control and ABP. Therefore the total tractor load differs based on the BPT considered.

$$L_T = L_E + L_B \quad (3.1)$$

where, L_T = total tractor load (%), L_E = empty tractor load (%), and L_B = bale load (%).

Even though hauling bales by the tractor is related to the drawbar (pulling) power, the simple fuel consumption methods using drawbar power were not available; therefore, the documented power take-off (PTO, (ASABE, 2011)) and tractor engine (Khalilian et al., 1985) power-based fuel consumption methods were employed. Also, in the case of ABP, the PTO power is used by a self-contained hydraulic system and the ABP's picking arm utilizes this hydraulic system for the automatic collection (lifting and loading operations) of round bales from the field. It is, therefore, logical to use PTO power for ABP bale aggregation fuel consumption. Further, the rated PTO power was always less than the

engine power, as it accounted for losses in the powertrain, and using this will be a better representation of the usable power and fuel consumption.

3.3.4.1. General method

The general method utilized the ASABE Standards (ASABE, 2011) equation developed for compression ignition engines. This simple method is based on the rated and available PTO. The rated PTO power was assumed as 75 % of engine power for both tractors (80 and 125 hp) based on the existing sources (JD, 2012; Mahindra, 2018). The rated PTO power remained constant while the available PTO power varied based on the partial or full tractor load. Fuel consumption, given in imperial units (original source units presented here), was calculated using the following relationships (ASABE, 2011):

$$C_{F1} = (a'X + 0.019) \times P_R \quad (3.2)$$

while,

$$X = \frac{P_A}{P_R} \quad \text{and} \quad P_A = P_R \times \frac{L_T}{100} \quad (3.3)$$

where, C_{F1} = fuel consumption at partial and full tractor load for general method (gal h^{-1}), $a' = 0.0434$ ($\text{gal hp}^{-1} \text{h}^{-1}$), P_R = rated PTO power (hp), X = ratio of equivalent available PTO power based on tractor load to the rated PTO power, P_A = available PTO power based on the part and full tractor load (hp), and L_T is substituted from eq. (5.1). The resulting fuel consumption (gal h^{-1}) can be easily converted to metric units (L h^{-1}) by appropriate conversion factor.

3.3.4.2. Fuel efficiency method

In addition to the tractor load, the fuel efficiency method (Khalilian et al., 1985) utilized the fuel efficiency to estimate the fuel consumption. The fuel efficiency was ex-

pressed in kWh L^{-1} which denotes the amount of energy in kW generated by the tractor's engine in one hour while consuming one liter of fuel. The fuel consumption was determined using the following equation:

$$C_{F2} = \frac{C_T}{E_F} \quad (3.4)$$

where, C_{F2} = fuel consumption (L h^{-1}) using energy efficiency method, C_T = tractor capacity (kW), and E_F = fuel efficiency (kWh L^{-1}). Estimation of tractor capacity and fuel efficiency will be presented subsequently.

3.3.4.2.1. Tractor capacity

Tractor capacity or operational engine power is the amount of power utilized from the maximum engine power to lift or pull the tractor load and thus can vary with the varying tractor load. The tractor capacity is estimated using the engine power and tractor load. The following equation was used to determine the tractor capacity.

$$C_T = P_E \times \frac{L_T}{100} \quad (3.5)$$

where, P_E = engine power (kW; corresponding to 80 and 125 hp). The tractor load (L_T) was substituted from eq. (5.1).

3.3.4.2.2. Fuel efficiency

Fuel efficiency is the effectiveness of the tractor in utilizing the fuel for a specific time, which is influenced by the tractor load. Diesel tractor data were documented by the Agricultural Engineering Department, Oklahoma State University, which was used in developing a fuel efficiency table (table 3.1) for part (20 %, 40 %, 60 %, and 80 %) and full (100 %) tractor loads (Hunt, 2008).

Table 3.1. Fuel efficiency of different tractor loads (part and full) and different diesel types engines in kW h L⁻¹ (hp h gal⁻¹) (Hunt, 2008).

Tractor load (%)	Types of diesel engine		
	Natural aspirated	Turbo	Turbo and cooled
100	2.90 (14.72)	3.07 (15.58)	3.09 (15.68)
80	2.84 (14.41)	2.82 (14.31)	2.86 (14.52)
60	2.60 (13.19)	2.55 (12.94)	2.59 (13.15)
40	2.13 (10.81)	2.10 (10.66)	2.15 (10.91)
20	1.38 (7.00)	1.36 (6.90)	1.42 (7.21)

The type of diesel engine assumed for this study was the turbo and cooled (turbocharger and intercooled) considering the modern tractors used for bale aggregation. The values of the total tractor load (L_T) and fuel efficiency (E_F) for turbo-charged and inter-cooled diesel type engine (table 3.1) when plotted produced a logarithmic trend (fig. 3.3).

The developed nonlinear prediction model (eq. (4.11)), describing the logarithmic trend, produced a good fit performance.

$$E_F = 1.047 \times \ln(L_T) - 1.711 \quad (R^2 \geq 0.99) \quad (3.6)$$

The tractor load (%) for each bale, ranging from 1–23, was calculated using this logarithmic model (eq. (5.1)) and used to predict respective fuel efficiency (E_F). The fuel consumption (L/h) for 80 and 125 hp tractor engine power using the fuel efficiency method was determined by substituting eqs. (4.5) and (4.11) in eq. (4.4).

3.3.5. Fuel Quantity Calculation

Fuel quantity utilized by both 80 (direct) and 125 hp tractors (ABP) was determined as a product of the fuel consumption (eq. (5.2) or eq. (4.4)) and the aggregation operation time for different levels of field area, BPT, and biomass yield as follows. The estimated

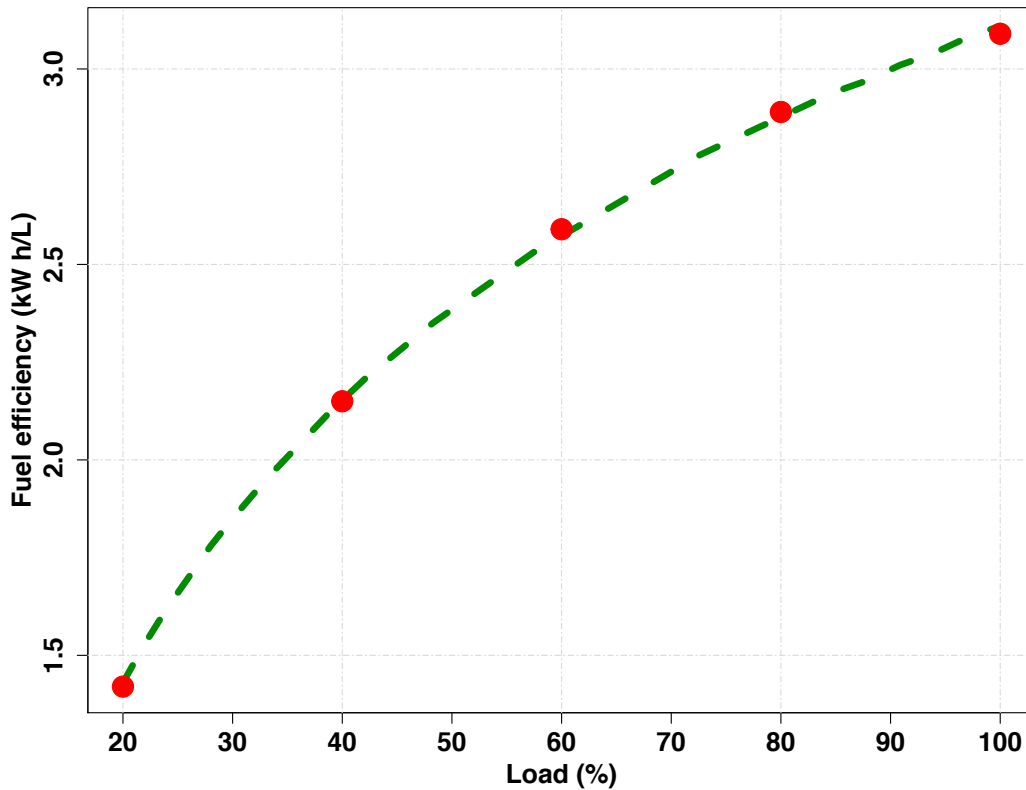


Figure 3.3. Logarithmic model ($R^2 > 0.99$) to predict the fuel efficiency (kW h/L) using the predictor variable of tractor load (%).

fuel quantity was used to study the effect of different field parameters, conduct statistical analysis, and develop appropriate prediction models.

$$Q_F = C_F \times T_L \quad (3.7)$$

where, Q_F is the fuel quantity (L), C_F is the fuel consumption (kW h/L) based on the evaluation method (eq. (5.2) or eq. (4.4)), and T_L is the bale aggregation logistics time (h) evaluated based on developed models.

3.3.6. Statistical Analysis

The results of logistics distance and fuel consumption one-way ANOVA was dependent on the normality spread and equal variances of the data. The normality of data was determined using the Shapiro-Wilk normality test by employing the R function

`shapiro.test()`. Though the results of the Shapiro-Wilk normality test demonstrated non-normality for both logistics distance and fuel consumption ($p < 0.001$), one-way ANOVA was still conducted assuming normality since the simulated data were balanced (Bathke, 2004). The one-way ANOVA was performed to evaluate the variation among these dependent variables as influenced by the aggregation equipment on different areas, BPT, and biomass yield. The statistical analysis was conducted with 5% level of significance ($\alpha = 0.05$). In addition, Tukey's HSD was used to determine the specific field area, BPT, and biomass yield that contributed significantly by comparing within all possible pairs of groups. Functions `aov()` and `TukeyHSD()` in R `stats` package were used to conduct these analyses.

3.3.7. Development of Prediction Models

Prediction models to evaluate the logistics distances, time involved, and fuel consumption were developed from common input variables. The most influential predictor variables among field area, BPT, biomass yield, outlet location, and windrow variation were determined using the R function `relweights()` (Johnson, 2000; Kabacoff, 2015). The variables with highest weights were considered for developing logistics and fuel consumption models.

In infield bale aggregation logistics modeling with specific BPT simplified models nonlinear models were used and with all the three significant inputs of field area (ha), biomass yield (Mg ha^{-1}), and BPT. A "Biomass Infield Bale Logistics Multivariate Model" (BIBLMM) similar to the isotherms based on the Modified Handerson equation (ASABE, 2003; Igathinathane et al., 2005) were developed (Subhashree and Igathinathane, 2019). For developing these models, R `stats` package and `nls()` function were employed.

$$\text{Specific BPT model: } y = a A_F^b Y_B^c \quad (3.8)$$

$$\text{BIBLMM3: } y = \left[\frac{A_F Y_B}{a'(B_T + b')} \right]^{c'} \quad (3.9)$$

$$\text{BIBLMM4: } y = \left[\frac{A_F Y_B}{a'' + b'' B_T + c'' S_P} \right]^{d''} \quad (3.10)$$

where, BIBLMM3 and BIBLMM4 are the respective 3 and 4 parameters models, y is the dependent variable which might include aggregation logistics distance, aggregation time, and fuel quantity in appropriate units; A_F is the field area (ha); Y_B is biomass yield (Mg ha^{-1}); B_T is the BPT; S_P is the equipment speed (km h^{-1}); a, a', b'', c'' are the coefficients; b' and a'' are the constants; b, c, c', d'' are the exponents of the models (eqs. (3.8) to (3.10)).

3.4. Results and Discussion

3.4.1. Bale Collection Using Tractor and ABP

The simulation of the tractor and ABP using the curvilinear path method for a field area of 2 ha with windrow variation of 15 % and other parameters are illustrated in fig. 3.4. The outlet location for bale aggregation was selected as the field middle. For the 2 ha field area, with other input parameters, 30 bales were generated. The number of trips generated by a tractor with 1 BPT (fig. 3.4A) is equal to the number of bales in the bale field layout. The number of whole and fractional trips generated by a tractor (2 BPT, fig. 3.4B) ABP (8 BPT, fig. 3.4C) were 15 and 0, and 3 and 1, respectively. The bold brown box along the borders of the field (fig. 3.4) represents the two-pass headland that was simulated to allow vehicle turning within the field at the edge. The black dots in the layout indicate the bale points within the field. The bale radius circle was color-coded with

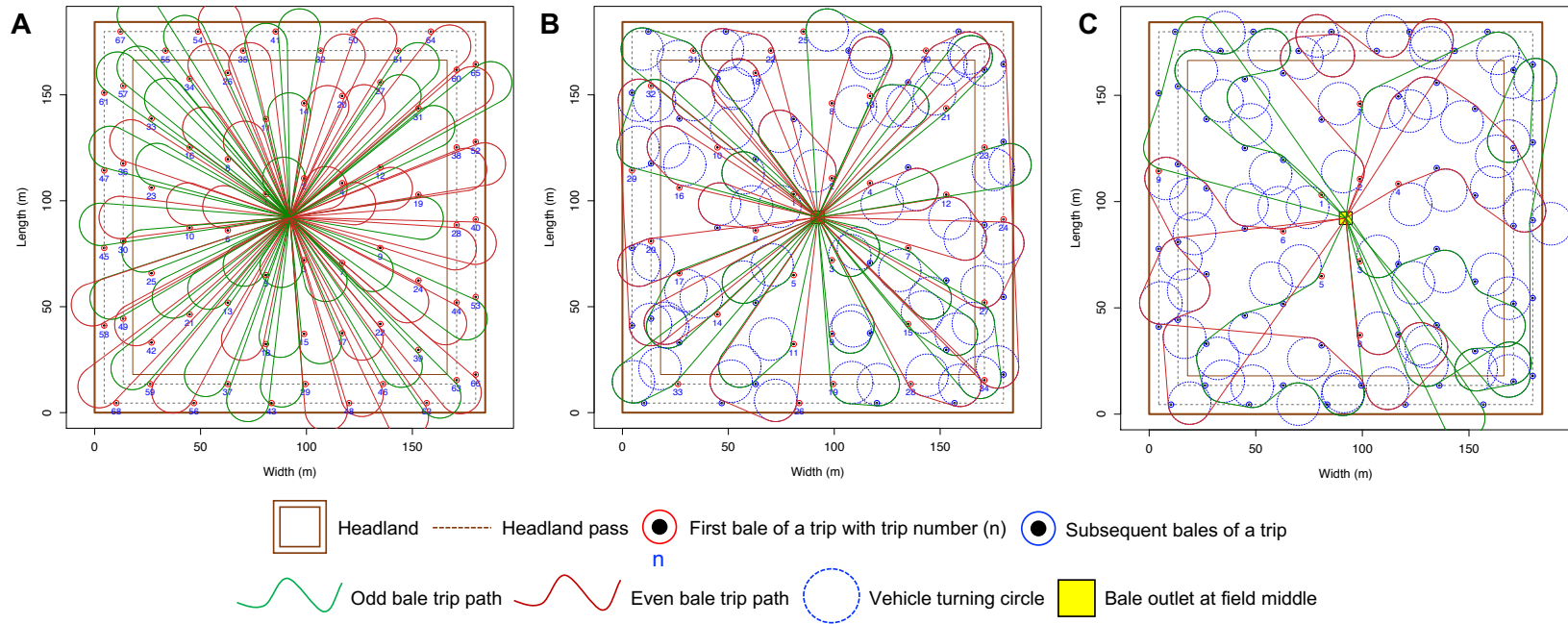


Figure 3.4. Bale aggregation equipment simulation results: (A) Tractor, BPT (bales/trip) = 1; (B) Tractor, BPT = 2; and (C) Automatic bale picker, BPT = 8; Simulation data: area = 2 ha; turning radius, $r_t = 10$ m; biomass yield/ha = 10 Mg; bale mass = 500 kg; harvester swath = 9 m; field aspect ratio = 1.0 ; random variation in biomass yield = 15 %; and random number seed used = 2016.

red for every first bale of the trip and blue for the rest of the bales of the trip. The trip number was also marked next to the first bale of the trip. Also, the odd and even bale trip paths were color-coded in green and red, respectively, for better visualization. The larger dashed blue circles, tangential to the bales, represent the turning circle which allowed for better visualization of the vehicle turning path during bale collection.

This bale layout with the generated vehicle path represented the actual collection of bales in the field. The bale collection started from the center, for the field middle outlet, and radially expanded to outer bales after collecting the bales near the outlet. It can also be seen that the logistics distance was greater with the tractor, and it reduced with ABP. The traffic near the outlet was also reduced with the increase in the number of BPT.

3.4.2. Field Parameters Influence on Bale Aggregation Logistics Distances

The effect of various field parameters on bale aggregation logistics distances, such as field area, BPT, biomass yield, and outlet locations was similar to the equipment track impacted areas reported elsewhere (Subhashree and Igathinathane, 2019), for logistics distances and track impacted areas are proportional. Therefore, brief results are presented in a tabular form (table 3.2) and detailed descriptions were included in Appendix A.

3.4.3. Statistical Model Development for Logistics Distance and Time

3.4.3.1. Relative weights analysis results for models

Among the independent variables, such as BPT, field area, biomass yield, outlet location, and windrow variation, the variables with the highest relative weights were selected for developing the logistics distance prediction models. In addition to the above independent variables, the equipment speed was also accounted for in the analysis in developing operation time prediction models.

Table 3.2. Effect of field parameters on bale aggregation logistics distance.

Effect	Results in brief	Details
Field area	<ul style="list-style-type: none">• Increased field size increased the logistics distances;• Logistics distance generated for field areas were highly significantly different*;• Overall, field areas were significant when the number of BPT <17	Appendix A.1.1.
Bales/trip	<ul style="list-style-type: none">• Increased BPT decreased the logistics distances;• A drastic reduction of distances between tractor (1 and 2 BPT) and ABP (8 and 23 BPT);• ABP with 8 BPT (capable of handling 11 BPT) was considered optimum as the equipment would have a smaller footprint and a lower subsoil compaction	Appendix A.1.2
Biomass yield	<ul style="list-style-type: none">• Increased biomass yield gradually increased the logistics distance;• One-way ANOVA showed highly significant* difference among biomass yields affecting logistics distance;• Overall, logistics distances were highly significant* with biomass yield (>20 Mg ha⁻¹)	Appendix A.1.3
Outlet location	<ul style="list-style-type: none">• Field middle outlet produced the least logistics distance, followed by the mid-edge, and the origin the least;• Logistics distance reduction of field middle was 44 % and for mid-edges was 30 % (8–259 ha areas);• Differences among the outlet locations diminished with BPT >8.	Appendix A.1.4

Note: SM - Supplementary material. * - Statistically significant ($p < 0.001$) at $\alpha = 0.05$.

Logistics distance relative weight analysis revealed that the field area, biomass yield, and BPT accounted for 43 %, 39 %, and 18 %, respectively, while outlet and windrow variations made insignificant contributions with their weights of 0.74 % and <0.1 %. Operation time analysis showed that field area, biomass yield, BPT, and equipment speed accounted for 41.66 %, 36.31 %, 20.89 %, and 0.82 %, of weights respectively, while the outlet (0.31 %) and windrow variation (<0.1 %) were insignificant. Therefore, only the significant variables were used in models development.

The most influential parameters were based on relative weights analysis, namely the field area, biomass yield, and BPT affecting the bale aggregation distances. Equip-

ment speed included for operation time (section 3.4.3.1) was used in the specific BPT and combined prediction models.

3.4.3.2. Simple specific BPT prediction models

The effects of field area, BPT, and biomass yields on the aggregation logistic distances showed a nonlinear pattern (Appendix A). Specific BPT prediction models developed, following eq. (3.8), for the aggregation distances (km) from field areas and biomass yield produced a very good fit ($R^2 > 0.99$). With the increase in BPT, both the coefficient and exponents of field area and biomass yield decreased from 0.004 to 0.002, from 1.527 to 1.313, and from 1.345 to 1.135 (a , b and c of eq. (3.8)), respectively, indicating the logistics distance reduction effect with increased BPT. The nonlinear models predicting aggregation logistics distance for different BPT (1 minimum, 8 recommended, and 23 maximum) are given as:

$$\text{Tractor (1 bale):} \quad D_L = 3.943 \times 10^{-3} \times A_F^{1.527} Y_B^{1.345} \quad (R^2 = 0.99) \quad (3.11)$$

$$\text{ABP (8 bales):} \quad D_L = 1.621 \times 10^{-3} \times A_F^{1.439} Y_B^{1.179} \quad (R^2 = 0.99) \quad (3.12)$$

$$\text{ABP (23 bales):} \quad D_L = 1.701 \times 10^{-3} \times A_F^{1.313} Y_B^{1.135} \quad (R^2 = 0.99) \quad (3.13)$$

where, D_L = total bale aggregation logistics distance (km); A_F = field area (ha); and Y_B = biomass yield (Mg ha^{-1}).

3.4.3.3. Combined multivariate prediction model

Rather than specific BPT prediction models, the combined multivariate model (BIBLMM3; eq. (3.9)) proved more convenient for modeling overall systems. The data considered for development included field areas (8, 16, 24, 32, 40, 65, and 129 ha), biomass yield (3, 4, 5, 6, 7, 8, 10, 15, 20, 30, and 40 Mg ha^{-1}), BPT (1, 2, 8, 11, 14, 17, and 23) values with fixed windrow variation of 5% and outlet location at field middle (M:M). The

developed BIBLMM3 predicted the aggregation logistics distance (eq. (C.3)) with a good fit ($R^2 = 0.98$).

$$D_L = \left[\frac{A_F Y_B}{17.879 \times (B_T + 0.895)} \right]^{1.377} \quad (R^2 = 0.98) \quad (3.14)$$

where, D_L = total bale aggregation logistics distance (km); A_F = field area (ha); Y_B = biomass yield (Mg ha^{-1}); and B_T = bales/trip.

3.4.3.4. Aggregation logistics operation time

The operation time for the tractor and ABP is directly dependent on the bale aggregation logistics distance and the operational speed of the respective equipment. The speed of equipment during bale aggregation ranges from $6.4\text{--}10.5 \text{ km h}^{-1}$ ($4\text{--}6.5 \text{ mph}$) (Taylor et al., 1991).

Since the equipment operation speed is typically slow, the tractor and ABP drawn by the tractor have similar speeds, and the difference in the operational times came from the bale aggregation logistics distances. The operation time of the tractor, for the studied areas ($8\text{--}259 \text{ ha}$), with 1 and 2 BPT on an average was 7 and 2 times that of ABP with 8 BPT, respectively. Reduction in operation time of ABP with capacity 8 BPT while operating on a quarter section of the field ($\approx 65 \text{ ha}$) was 84% and 49%, respectively, compared to the tractor with 1 and 2 BPT.

Furthermore, an increase in the number of bales and equipment speed will reduce the operation time of ABP. The prediction BIBLMM4 developed for aggregation logistics operation time (eq. (C.4)), which gave the best fit of $R^2 = 0.98$, was used in the fuel consumption calculations.

$$T_L = \left[\frac{A_F Y_B}{-46.003 + 80.230 B_T + 15.052 S_p} \right]^{1.381} \quad (R^2 = 0.98) \quad (3.15)$$

where, T_L = total bale aggregation logistics operation time (h); A_F = field area (ha); Y_B = biomass yield (Mg ha^{-1}); B_T = bales/trip; and S_p = equipment speed (km h^{-1}).

3.4.4. Comparison of Fuel Consumption Methods - General vs Fuel Efficiency

The tractor and ABP fuel consumption calculation results using the general (PTO) and fuel efficiency methods for BPT ranging from 0 to 23 are presented in table 3.3. Except for empty tractor load (%), all quantities increased with BPT which is an expected association as the loads and fuel consumption through both methods would increase with increased BPT (table 3.3).

A plot of these methods against engine powers demonstrated linear increasing trend fuel consumption with the load represented by BPT (fig. 3.5). The slopes of the trend were steeper for lower power (80 hp) and gradual for higher power (125 hp), which is indicative of better handling of the high power engines of the increasing load. Even though the fuel consumption started lower for 80 hp tractor compared to 125 hp, the advantage vanished after 4 BPT as indicated by the intersection of the two trends. Thus hauling more BPT using ABP with high-power tractor, while reducing the logistics distances (fig. 3.5), results in lower fuel consumption.

The fuel efficiency method was about 1.35 times the general method. The lower estimation of the fuel consumption using the general method was due to calculated fuel consumption being based only on varying PTO power, while the fuel efficiency method included fuel efficiency values of diesel in addition to the varying tractor loads. Therefore, the fuel consumption values estimated from the fuel efficiency method (C_{F2}) were more realistic and were used further for fuel quantity calculations for various field areas, BPT, and biomass yield levels.

Table 3.3. Fuel consumption calculation for tractor and ABP using two methods.

P_E (hp)	B_T	L_B (%)	L_E (%)	L_T (%)	P_A (hp)	C_T (kW)	X	E_F (kWhL ⁻¹)	C_{F1} (Lh ⁻¹ (galh ⁻¹))	C_{F2} (Lh ⁻¹)
80	0	0.00	30.00	30.00	18.00	17.90	0.30	1.85	7.27 (1.92)	9.67
	1	14.00	30.00	44.00	26.40	26.25	0.44	2.25	8.65 (2.29)	11.66
	2	28.00	30.00	58.00	34.80	34.60	0.58	2.54	10.03 (2.65)	13.62
125	0	0.00	30.00	30.00	28.13	27.96	0.30	1.85	11.36 (3.00)	15.11
	1	3.04	30.00	33.04	30.98	30.80	0.33	1.95	11.83 (3.13)	15.78
	2	6.09	30.00	36.09	33.83	33.64	0.36	2.04	12.30 (3.25)	16.46
	3	9.13	30.00	39.13	36.68	36.47	0.39	2.13	12.77 (3.37)	17.14
	4	12.17	30.00	42.17	39.54	39.31	0.42	2.21	13.24 (3.50)	17.81
	5	15.22	30.00	45.22	42.39	42.15	0.45	2.28	13.71 (3.62)	18.49
	6	18.26	30.00	48.26	45.24	44.98	0.48	2.35	14.18 (3.74)	19.16
	7	21.30	30.00	51.30	48.10	47.82	0.51	2.41	14.64 (3.87)	19.83
	8	24.35	30.00	54.35	50.95	50.66	0.54	2.47	15.11 (3.99)	20.49
	9	27.39	30.00	57.39	53.80	53.49	0.57	2.53	15.58 (4.12)	21.15
	10	30.43	30.00	60.43	56.66	56.33	0.60	2.58	16.05 (4.24)	21.80
	11	33.48	30.00	63.48	59.51	59.17	0.63	2.63	16.52 (4.36)	22.46
	12	36.52	30.00	66.52	62.36	62.00	0.67	2.68	16.99 (4.49)	23.10
	13	39.57	30.00	69.57	65.22	64.84	0.70	2.73	17.46 (4.61)	23.75
	14	42.61	30.00	72.61	68.07	67.68	0.73	2.78	17.93 (4.74)	24.38
	15	45.65	30.00	75.65	70.92	70.52	0.76	2.82	18.39 (4.86)	25.02
	16	48.70	30.00	78.70	73.78	73.35	0.79	2.86	18.86 (4.98)	25.65
	17	51.74	30.00	81.74	76.63	76.19	0.82	2.90	19.33 (5.11)	26.28
	18	54.78	30.00	84.78	79.48	79.03	0.85	2.94	19.80 (5.23)	26.90
	19	57.83	30.00	87.83	82.34	81.86	0.88	2.97	20.27 (5.35)	27.52
	20	60.87	30.00	90.87	85.19	84.70	0.91	3.01	20.74 (5.48)	28.14
	21	63.91	30.00	93.91	88.04	87.54	0.94	3.04	21.21 (5.60)	28.75
	22	66.96	30.00	96.96	90.90	90.37	0.97	3.08	21.68 (5.73)	29.36
23	70.00	30.00	100.00	93.75	93.21	1.00	3.11	22.14 (5.85)	29.96	

Note: APB - automatic bale picker, P_E - engine power (hp), B_T - BPT, L_B - bale load (%), L_E - empty tractor load (%), L_T - tractor load (%), P_A - available PTO power based on the part and full tractor load (hp), C_T - tractor capacity (kW), X - ratio of equivalent available PTO power based on the tractor load to the rated PTO power, E_F - fuel efficiency (kWhL⁻¹), C_{F1} - fuel consumption calculated using the general method (Lh⁻¹), and C_{F2} - fuel consumption calculated using the fuel efficiency method (Lh⁻¹).

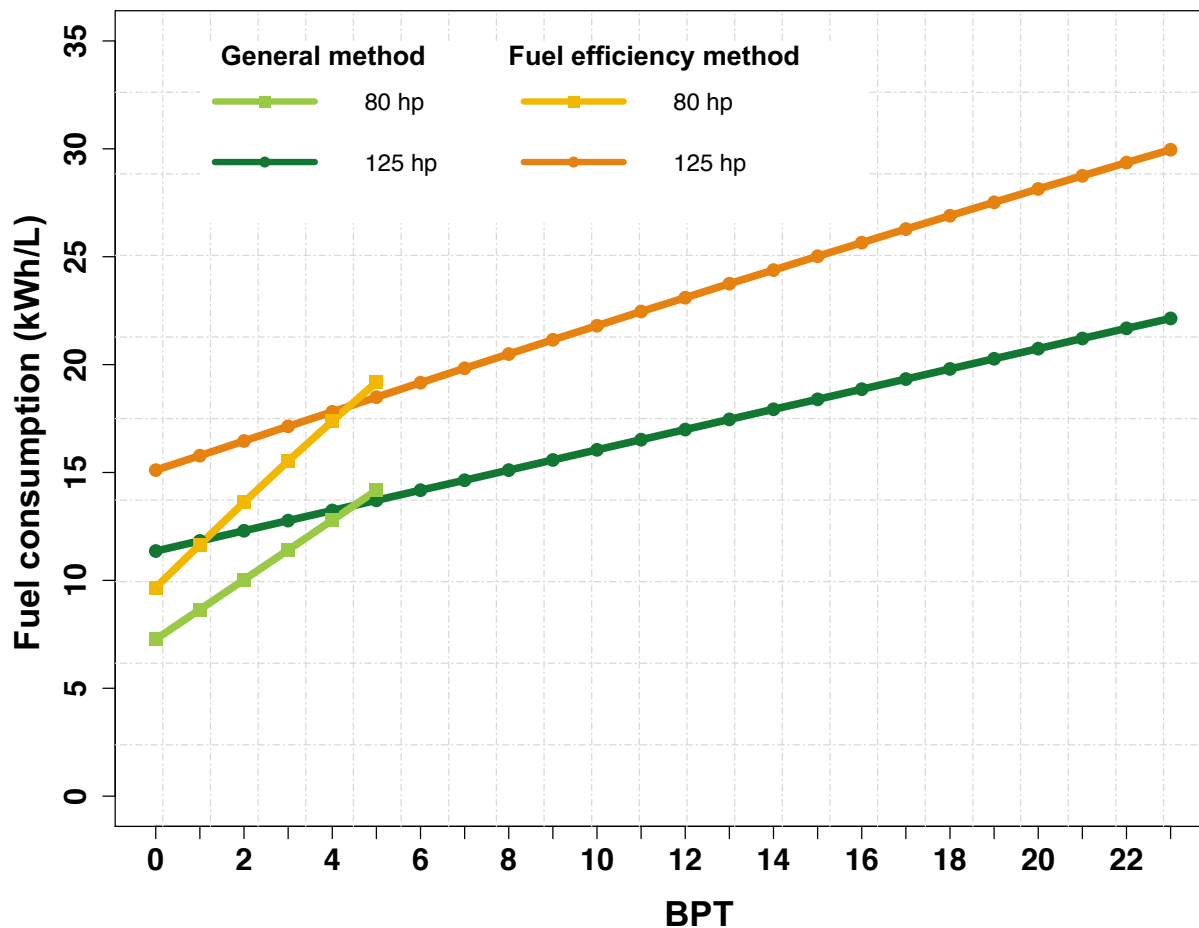


Figure 3.5. Fuel consumption methods comparison at two engine powers.

3.4.5. Effect of Field Parameters on Fuel Quantity

3.4.5.1. Relative weights analysis for fuel quantity models

Based on relative weights analysis the order of influential parameters was field area (47.14%), biomass yield (40.58%), BPT (10.98%), equipment speed (0.94%), outlet location (0.35%), and windrow variation (<0.1%) for the fuel quantity. From these results, the predictor variables such as field area, biomass yield, BPT, and equipment speed emerged as the first four influential parameters with the cumulative relative weights ac-

counting for 99.99 %, therefore only these four predictor variables were used for modeling the fuel quantity.

3.4.5.2. Effect of field area on fuel quantity

Specific levels of field area and BPT for biomass yield at 10 Mg ha^{-1} were selected to represent their respective range of 8–259 ha and 1–23 BPT (fig. 3.6).

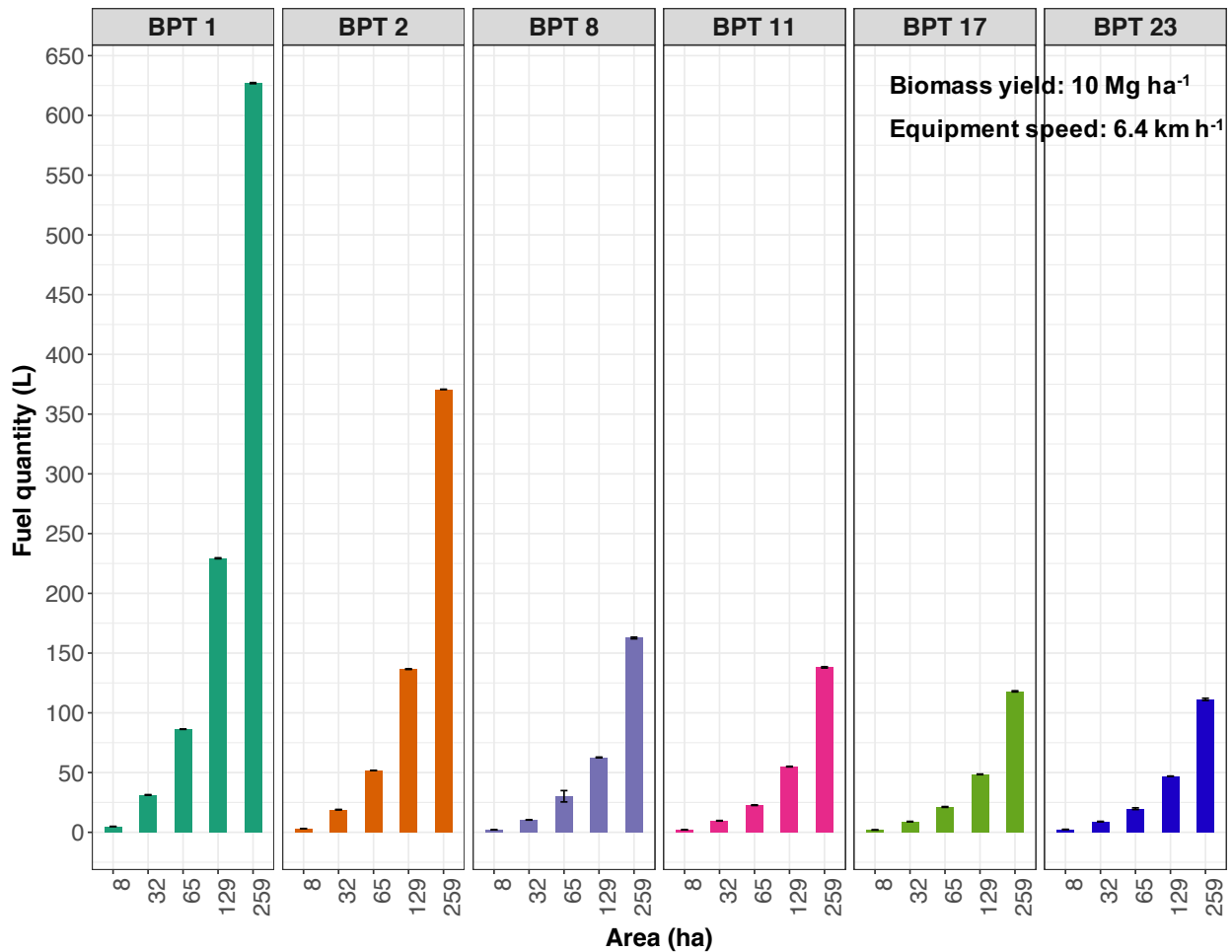


Figure 3.6. Effect of field area on the fuel quantity required for selected BPT (bales/trip) for tractor (1 and 2 BPT) and automatic bale picker (8, 11, 17, and 23 BPT), and field areas (8, 32, 65, 129, and 259 ha) with 10 Mg ha^{-1} biomass yield.

A general decreasing trend in fuel quantity was observed with the increase in BPT. However, with the increase in field areas within individual BPT an obvious increasing trend

(nonlinear) in fuel quantity was observed across the selected BPT levels as more field areas resulted in more distance traveled by tractor for bale aggregation.

Consolidated data of field area and their calculated fuel quantity with replications derived from the windrow variation of 5 %, 10 %, and 15 % was used to conduct one-way ANOVA which demonstrated a high significance ($p < 0.001$; table 3.4). Results indicate that an increase in field area significantly influenced the quantity of fuel utilized in bales aggregation.

Table 3.4. ANOVA of field area, BPT, biomass yield, and equipment speed on the bale aggregation fuel quantity.

Parameter	<i>df</i>	Sum Sq	Mean Sq	F value	Pr(>F)
Field area	7	1 740 747	248 678	24.28	$<2.00 \times 10^{-16}$ ***
BPT (bales/trip)	6	638 933	106 489	6.897	$<1.06 \times 10^{-6}$ ***
Biomass yield	10	1.475×10^7	1 475 479	5.726	$<5.19 \times 10^{-8}$ ***
Equipment speed	4	8.136×10^5	203 399	1.828	0.121

Combined data with field areas of 8, 16, 24, 32, 40, 65, 129, and 259 ha; BPT of 1, 2, 8, 11, 14, 17, and 23; biomass yield ha^{-1} of 3, 4, 5, 6, 7, 8, 10, 15, 20, 30, and 40; equipment speeds of 6.4, 7.4, 8.4, 9.5, and 10.5 km h^{-1} ; *df* is the degrees of freedom; level of significance used is $\alpha = 0.05$; *** is the significance level of $p < 0.001$.

Results derived from further analysis using Tukey’s HSD showed some significant difference scenarios in fuel quantity across all the possible field area groups in 1–23 BPT (Appendix: table A3). Across all possible pairs of field area groups, the tractor capacity of 1 and 2 BPT displayed a significant difference in fuel consumed. Interestingly, for ABP, a significant difference in fuel quantity across pairs of field area groups was more prominent with the increase in BPT. Field area ≥ 32 ha displayed a significant difference in fuel quantity for a higher ABP capacity of 17 and 23 BPT. A significant difference in fuel quantity was observed for field areas ≥ 65 ha across BPT of the tractor and ABP ranging from 1–23 (data not shown).

3.4.5.3. Effect of BPT on fuel quantity

A steep drop in the fuel quantity was observed with the tractor (1 and 2 BPT) and ABP (8–23 BPT) with the increase in BPT (fig. 3.7).

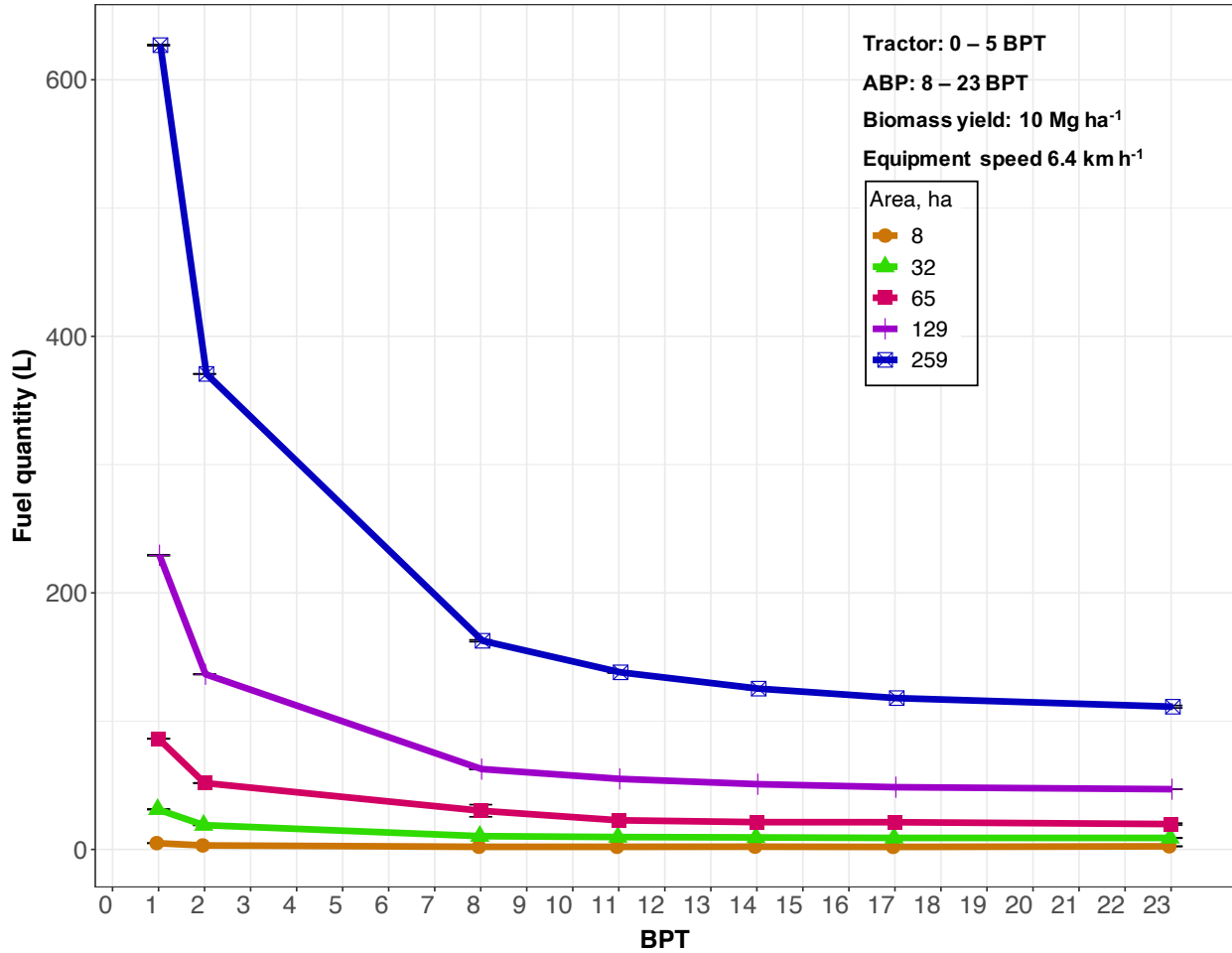


Figure 3.7. Effect of BPT (bales/trip) on the fuel quantity required by tractor and ABP (automatic bale picker) for aggregating 1–23 BPT for selected field areas of 8, 32, 65, 129, and 259 ha with 10 Mg ha⁻¹ biomass yield.

This trend was similar across all the field areas considered but more pronounced with increased field areas. Reduction in fuel quantity on an average for ABP 8 bales/trip when compared with tractor capacity of 1 and 2 bales/trip was observed at 72.22% and 53.29%, respectively.

The ANOVA with combined data showed that BPT of the tractor and ABP had a highly significant influence on the fuel quantity ($p < 0.001$; table 3.4). The fuel consumed by the tractor with 1 and 2 BPT was found to be significant across the whole 8–259 ha field area (data not shown) based on Tukey’s HSD. Similarly, the ABP minimum and maximum capacities, 8 and 23 BPT group pairs, produced a significant difference for all the field areas considered ($p < 0.05$). The ABP group pair 8 and 11 BPT did not produce any significant difference in fuel quantity for the field areas suggesting that ABP of capacity 8 BPT can be used effectively to aggregate 11 BPT (“Appendix” table A4). A significant difference in fuel consumption for aggregating >14 BPT was not significant for field areas >32 ha, indicating no advantage in the quantity of fuel consumed at higher BPT and field areas — however, the time saved cannot be discounted.

3.4.5.4. Effect of biomass yield on fuel quantity

The impact of biomass yield on fuel quantity across field area range 8–259 ha with 8 BPT (optimum) showed an increase in fuel quantity with the increase in the biomass yield across all the field areas ranging from 8–259 ha (fig. 3.8). However, this trend was significant only between 8 and 40 Mg ha⁻¹. In general, the increase in fuel quantity was linear beyond 20 Mg ha⁻¹ across all field areas.

From the combined data using one-way ANOVA, overall the biomass yield had a highly significant effect on the fuel quantity ($p < 0.001$; table 3.4). The Tukey’s HSD analysis showed that biomass yield <10 Mg ha⁻¹ did not affect the fuel consumption for the field area range of 8–259 ha (Appendix: table A4). Biomass yields ≥ 30 Mg ha⁻¹, produced a significant difference in fuel quantity for field areas ≥ 32 ha. As the field area increased, the significance of fuel quantity impacted by the biomass yield decreased.

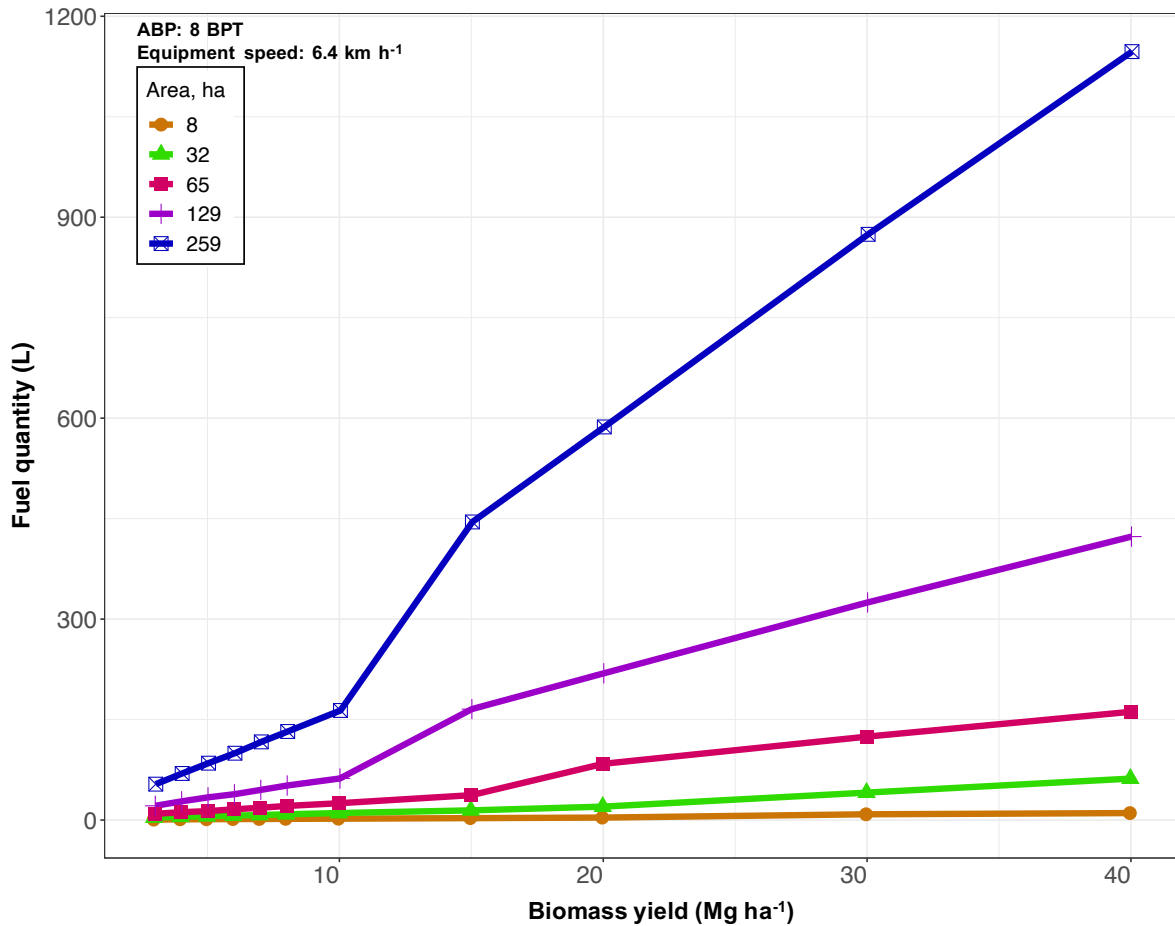


Figure 3.8. Effect of biomass yield on the fuel quantity required by ABP (automatic bale picker) for aggregating 8 BPT (bales/trip) for selected field areas of 8, 32, 65, 129, and 259 ha.

3.4.5.5. Effect of equipment speed on fuel quantity

The effect of increase in equipment speed from 6.4 km h⁻¹ to 10.5 km h⁻¹ on the fuel quantity for the field area 8–259 ha with 8 BPT (optimum) and biomass yield at 10 Mg ha⁻¹ displayed a decreasing trend (fig. 3.9). The decreasing trend however was more pronounced with areas greater than 32 ha.

The ANOVA results from the combined data showed that overall the equipment speed did not have any significant effect on the fuel quantity ($p > 0.1$; table 3.4). Though a significant decreasing trend was observed with the increase in equipment speed for field

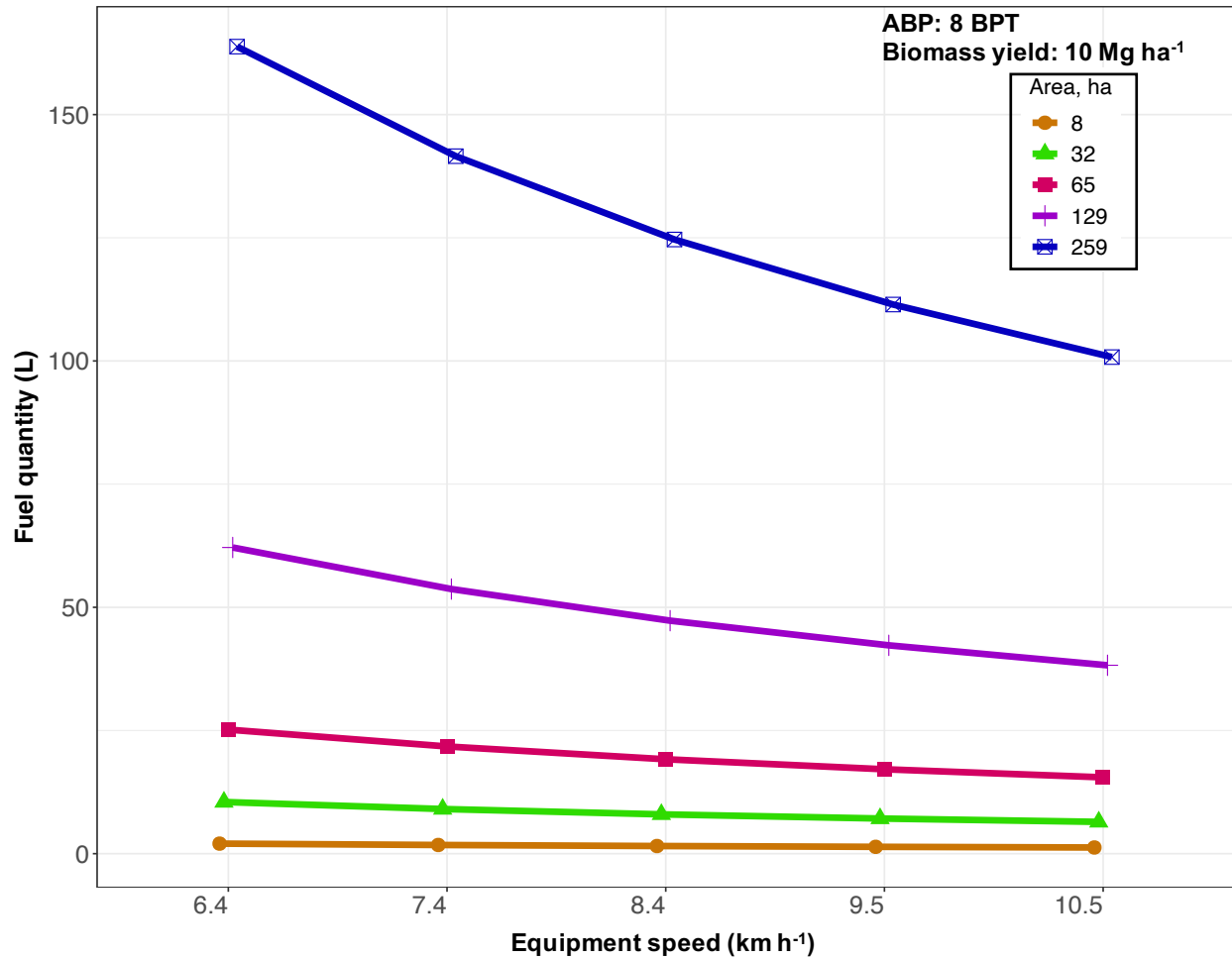


Figure 3.9. Effect of equipment speed on the fuel quantity required to aggregate 8 BPT (bales/trip) for selected field areas of 8, 32, 65, 129, and 259 ha.

areas (>32 ha), the Tukey’s HSD analysis (data not shown) revealed that equipment speed did not affect the fuel consumption for all the field areas in the range of 8–259 ha.

3.4.6. Statistical Model Development for Fuel Quantity

Following the relative weights analysis, the most significant variables such as field area, biomass yield, BPT, and equipment speed affecting the fuel consumption were used in the specific BPT and combined fuel quantity prediction models (section 3.4.5.1).

3.4.6.1. Specific fuel consumption prediction models

Simple specific fuel quantity models for tractor and ABP (1–23 BPT), following eq. (3.8) with area of field and biomass yield, developed gave very good fit ($R^2 > 0.99$). The coefficients/exponents (eq. (3.8)) for the entire range of BPT were: $a = 0.071$ – 0.079 ; $b = 1.527$ – 1.313 ; and $c = 1.345$ – 1.347 . Increased coefficients/exponents indicated increased fuel use as BPT increased from 1 to 23.

The specific models predicting the fuel quantity utilized in bale aggregation for different BPT (1 and 2 for tractor, 8 recommended, and 23 maximum) are given as a function of field area and biomass yield as:

$$\text{Tractor (1 bale):} \quad Q_F = 0.046 \times A_F^{1.527} Y_B^{1.345} S_P^{-1.000} \quad (R^2 = 0.99) \quad (3.16)$$

$$\text{Tractor (2 bales):} \quad Q_F = 0.028 \times A_F^{1.523} Y_B^{1.338} S_P^{-1.000} \quad (R^2 = 0.99) \quad (3.17)$$

$$\text{ABP (8 bales):} \quad Q_F = 0.034 \times A_F^{1.435} Y_B^{1.179} S_P^{-1.001} \quad (R^2 = 0.99) \quad (3.18)$$

$$\text{ABP (23 bales):} \quad Q_F = 0.051 \times A_F^{1.313} Y_B^{1.135} S_P^{-1.000} \quad (R^2 = 0.99) \quad (3.19)$$

where, Q_F is the fuel quantity utilized in bale aggregation (L); A_F = field area (ha); Y_B = biomass yield (Mg ha^{-1}); and S_P = equipment speed (km h^{-1}).

The variation of the fuel quantity utilized as a function of field area and biomass yield was visualized through a 3D plot developed from fuel consumption models (fig. 3.10). Increased field area and biomass yield exponentially increased the fuel quantity for 1 BPT (fig. 3.10A) and reduced almost half as BPT increased to 2 BPT (fig. 3.10B) for the tractor. However, with the use of ABP with the optimum 8 BPT (fig. 3.10C) and the maximum 23 BPT (fig. 3.10D) the fuel quantity was reduced and the response surface was flatter with an obvious increase towards higher field area and biomass yield. A similar trend was

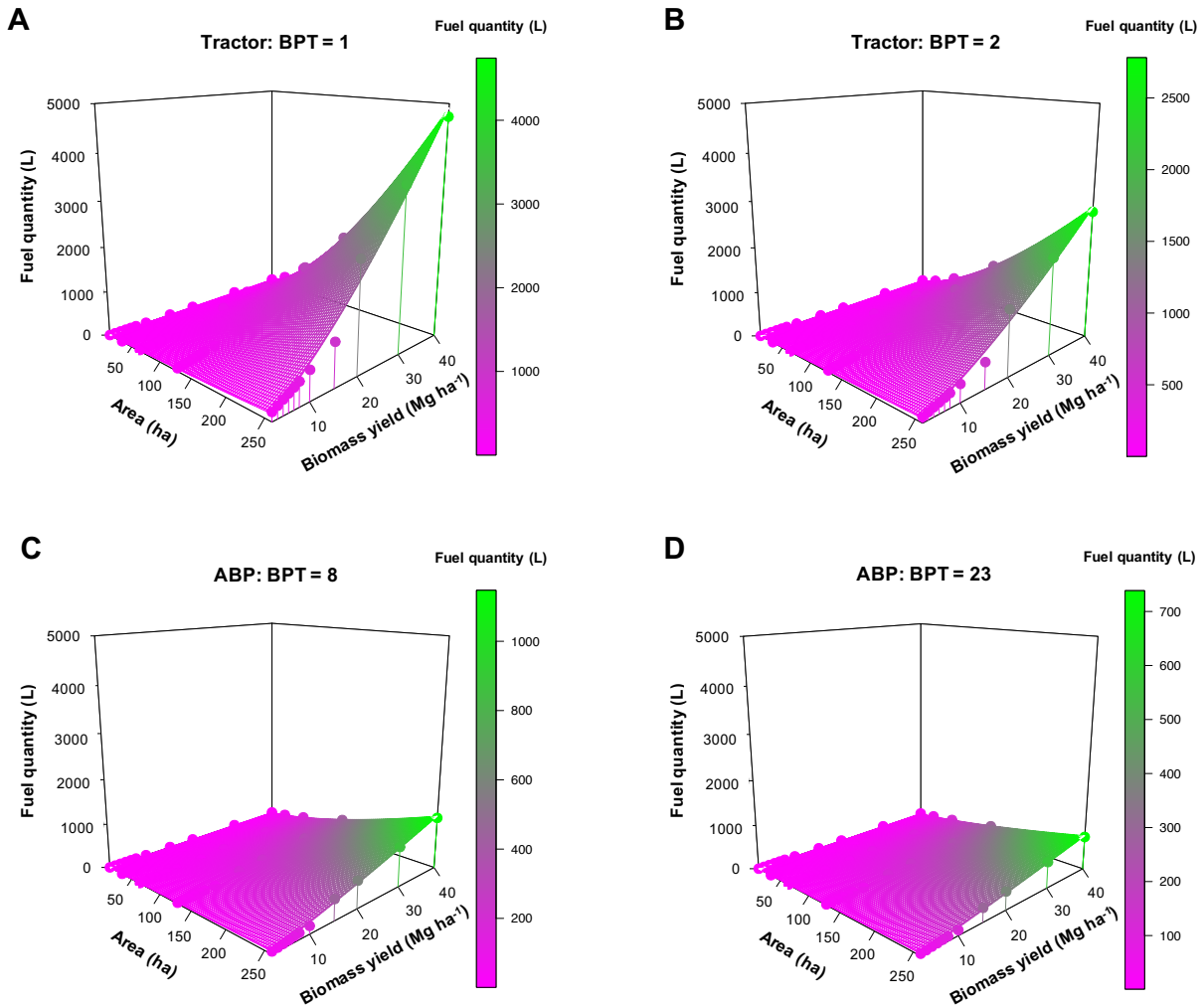


Figure 3.10. Fuel quantity utilized in bale aggregation as affected by field area and biomass yield at a selected equipment speed of 6.4 km h^{-1} . (A) Tractor with 1 BPT (bales/trip; tractor minimum); (B) Tractor with 2 BPT (tractor maximum); (C) ABP with 8 BPT (recommended); and (D) ABP (automatic bale picker) with 23 BPT (maximum).

observed for the other ABP capacity of 11, 14, and 17 BPT (data not shown). Thus, the nonlinear trend of the fuel quantity became less significant with the increase in the BPT.

3.4.6.2. Combined fuel quantity prediction models

Combined multivariate nonlinear models, developed with parameters such as field area, biomass yield, and equipment speed, based on the BIBLMM4 for prediction of fuel

quantity exclusively for tractor and ABP for any BPT, were presented with usual notations. These models fit performance ($R^2 = 0.98$) was nearly as good as specific BPT models ($R^2 = 0.99$).

$$\text{Tractor (1 to 2 bales):} \quad Q_F = \left[\frac{A_F Y_B}{-5.913 + 13.164 B_T + 2.777 S_P} \right]^{1.414} \quad (R^2 = 0.98) \quad (3.20)$$

$$\text{ABP (8 to 23 bales):} \quad Q_F = \left[\frac{A_F Y_B}{-4.991 + 1.165 B_T + 4.827 S_P} \right]^{1.242} \quad (R^2 = 0.98) \quad (3.21)$$

where, Q_F is the fuel quantity utilized in bale aggregation (L); A_F = field area (ha); Y_B = biomass yield (Mg ha^{-1}); B_T = bales/trip; and S_P = equipment speed (km h^{-1}).

The advantage of using combined models (eqs. (C.3) to (C.6)) over specific BPT models (eqs. (3.11) to (3.13) and (3.16) to (3.19)) is the interaction effect of all four parameters considered. These combined models could be applied as a component in building higher-level models for applications in various fields like agriculture, supply chain logistics, economics, and environmental science to predict the overall impact in conventional practices.

3.5. Model Validation and Future Recommendation

As the models were made robust involving the most influential variables with cumulative relative weights $>99\%$, the models will have self-validation properties. The simulation is robust and the variables considered will accommodate the possible variations that occur in the field. The delays in the logistics operations, however, were not considered in the study. However, it would be desirable to perform field measurements with tractor and ABP, at least for some scenarios, to compare the model with field observations, and should

be considered in the future. Future work should also explore bale stack formation in the bale aggregation, and rigorous economic analysis, using standard calculation procedures, of infield logistics using ABP.

3.6. Conclusions

From the infield bale aggregation logistics energy simulation study, field area (43 %), biomass yield (39 %), and bales/trip (BPT) (18 %) were found to be the most influential variables in modeling the bale aggregation logistics distance, while field area (41.66 % & 47.14 %), biomass yield (36.31 % & 40.58 %), BPT (20.89 % & 10.98 %), and equipment speed (0.82 % & 0.94 %) emerged as the most influential variables in modeling operation time and fuel quantity, respectively. Windrow variation and outlet location variables were insignificant in modeling logistics distance, operation time, and fuel quantity. The effects of field area, BPT, and biomass yield were highly significant ($p \leq 0.001$) with logistics distance and fuel quantity; however, the equipment speed considered for fuel quantity indicated no significance. Simple non-linear specific BPT prediction models for logistics distance (used only field area and biomass yield) and fuel quantity (used equipment speed with field area and biomass yield) produced good fits ($R^2 > 0.99$). Combined multivariate non-linear prediction models (BIBLMM) developed for (i) logistics distance that used BPT as a third variable (BIBLMM3), and (ii) operation time and fuel quantity that used equipment speed as the fourth variable (BIBLMM4) performed equally well ($R^2 > 0.98$).

The fuel efficiency method was the best since it included the fuel efficiency of the diesel in addition to considering the part and full tractor loads, and was therefore used in fuel quantity calculations in this study. The fuel quantity between tractor (1 and 2 BPT) and automatic bale picker (ABP) (8–23 BPT) demonstrated significant difference

($p \leq 0.05$), across the tested field areas. Fuel consumption for the ABP (8–259 ha) with 8 BPT on an average decreased by 72 % and 53 % compared to a tractor with 1 and 2 BPT, respectively. The fuel quantity was not significantly different for ABP with 8 and 11 BPT which suggested that ABP of capacity 8 BPT can be effectively used to aggregate 11 BPT. Biomass yield $\leq 10 \text{ Mg ha}^{-1}$ did not influence the fuel quantity across the field areas considered. Similarly, equipment speed $6.4\text{--}10.5 \text{ km h}^{-1}$ did not have any effect on the fuel quantity across the field areas. Application of bale stacks, rigorous economic analysis, and field measurements of bale aggregation should be addressed in the future.

This novel study successfully generated logistics distance, operation time, and fuel consumption prediction models developed from 36 960 bale aggregation scenarios. Hence, this study will serve as a tool for farmers/producers to decide between the traditional tractor and ABP, based on fuel consumption for efficient infield bale aggregation logistics. Besides, the developed multivariate models can serve as a basis to build more complex models in various fields, such as agriculture, supply chain logistics, economics, and the environment that could potentially impact conventional practices and influence policy decisions.

3.7. References

- Allen, J., Browne, M., Hunter, A., Boyd, J., & Palmer, H. (1998). Logistics management and costs of biomass fuel supply. *Int. J. Phys. Distrib. Logist. Manage.*, 28(6), 463–477.
- Anderson. (2008). *Anderson group: World's first self-loading bale carrier capable of handling round bales efficiently*. Retrieved March 14, 2022, from <https://grpanderson.com/en/comparator/?c=round-bales/>.

- ASABE. (2003). ASABE. Standard D245.5: Moisture relationship of plant-based agricultural products. *ASABE, St. Joseph, MI, USA*, 508–524.
- ASABE. (2011). ASABE. Standard D497.7: Agricultural machinery management data. *ASABE, St. Joseph, MI, USA*, 9–10.
- Bathke, A. (2004). The ANOVA F test can still be used in some balanced designs with unequal variances and nonnormal data. *J. Stat. Plan. Infer.*, 126(2), 413–422.
- Coblentz, W. K., Fritz, J. O., Bolsen, K. K., & Cochran, R. C. (1996). Quality changes in alfalfa hay during storage in bales. *J. Dairy Sci.*, 79(5), 873–885.
- Coblentz, W. K., & Hoffman, P. C. (2009). Effects of spontaneous heating on fiber composition, fiber digestibility, and in situ disappearance kinetics of neutral detergent fiber for alfalfa-orchardgrass hays. *J. Dairy Sci.*, 92(6), 2875–2895.
- Ebadian, M., Sowlati, T., Sokhansanj, S., Townley-Smith, L., & Stumborg, M. (2013). Modeling and analysing storage systems in agricultural biomass supply chain for cellulosic ethanol production. *Appl. Energ.*, 102, 840–849.
- Ekşioğlu, S. D., Li, S., Zhang, S., Sokhansanj, S., & Petrolia, D. (2010). Analyzing impact of intermodal facilities on design and management of biofuel supply chain. *Transp. Res. Rec.*, 2191(1), 144–151.
- Frombo, F., Minciardi, R., Robba, M., Rosso, F., & Sacile, R. (2009). Planning woody biomass logistics for energy production: A strategic decision model. *Biomass Bioenerg.*, 33(3), 372–383.
- Gallis, C. T. (1996). Activity oriented stochastic computer simulation of forest biomass logistics in Greece. *Biomass Bioenerg.*, 10(5), 377–382.

- Graham, R. L., English, B. C., & Noon, C. E. (2000). A geographic information system-based modeling system for evaluating the cost of delivered energy crop feedstock. *Biomass Bioenerg.*, 18(4), 309–329.
- Graham, R. L., Liu, W., Downing, M., Noon, C. E., Daly, M., & Moore, A. (1997). The effect of location and facility demand on the marginal cost of delivered wood chips from energy crops: A case study of the state of Tennessee. *Biomass Bioenerg.*, 13(3), 117–123.
- Grisso, R. D., Perumpral, J. V., Vaughan, D. H., Roberson, G. T., & Pitman, R. M. (2014). Predicting tractor diesel fuel consumption, College of Agriculture and Life Science, Virginia Cooperative Extension, Virginia Polytechnic and State University, Virginia; Publication 442-073.
- Hansson, P., Lindgren, M., Nordin, M., & Pettersson, O. (2003). A methodology for measuring the effects of transient loads on the fuel efficiency of agricultural tractors. *Appl. Eng. Agric.*, 19(3), 251–257.
- Hess, J. R., Wright, C. T., & Kenney, K. L. (2007). Cellulosic biomass feedstocks and logistics for ethanol production. *Biofuels, Bioprod. Biorefin.*, 1(3), 181–190.
- Huisman, W., Venturi, P., & Molenaar, J. (1997). Costs of supply chains of *Miscanthus giganteus*. *Ind. Crops Prod.*, 6(3), 353–366.
- Hunt, D. (2008). Economic performance. *Farm power and machinery management* (pp. 55–56). Waveland Press, 4180 IL Route 83 Long Grove, IL, USA.
- Igathinathane, C., Archer, D., Gustafson, C., Schmer, M., Hendrickson, J., Kronberg, S., Keshwani, D., Backer, L., Hellevang, K., & Faller, T. (2014). Biomass round bales infield aggregation logistics scenarios. *Biomass Bioenerg.*, 66, 12–26.

- Igathinathane, C., Tumuluru, J. S., Keshwani, D., Schmer, M., Archer, D., Liebig, M., Halvorson, J., Hendrickson, J., & Kronberg, S. (2016). Biomass bale stack and field outlet locations assessment for efficient infield logistics. *Biomass Bioenerg.*, *91*, 217–226.
- Igathinathane, C., Womac, A. R., Sokhansanj, S., & Pordesimo, L. O. (2005). Sorption equilibrium moisture characteristics of selected corn stover components. *Trans. ASAE*, *48*(4), 1449–1460.
- JD. (2006). *John Deere: Mid-size tractors 5015 series with 41 kW (55 hp) to 59 kW (80 hp)*. Retrieved March 14, 2022, from <https://tinyurl.com/yhv7yn6p/>.
- JD. (2012). *John Deere: 5E 50 - 100 horsepower utility 3 and 4 cylinder tractors with easy-to-use controls and loader compatibility*. Retrieved March 14, 2022, from <https://www.trigreenequipment.com/new-equipment/utility-tractors/5e-series-50-100-hp-/>.
- Johnson, J. W. (2000). A heuristic method for estimating the relative weight of predictor variables in multiple regression. *Multivar. Behav. Res.*, *35*(1), 1–19.
- Kabacoff, R. I. (2015). *R in Action: Data analysis and graphics with R*. 1230 Avenue of the Americas, New York, NY, USA.
- Khalilian, A., Batchelder, D., Self, K., & Summers, J. (1985). Revision of fuel consumption equations for diesel tractors. *ASAE Tech. Pap.*, 1522(CONF 841278).
- Kheiralla, A. F., Yahya, A., Zohadie, M., & Ishak, W. (2004). Modelling of power and energy requirements for tillage implements operating in Serdang sandy clay loam, Malaysia. *Soil Tillage Res.*, *78*(1), 21–34.
- Kichler, C., Fulton, J., Raper, R., McDonald, T., & Zech, W. (2011). Effects of transmission gear selection on tractor performance and fuel costs during deep tillage operations. *Soil Tillage Res.*, *113*(2), 105–111.

- Lin, T., Rodríguez, L. F., Shastri, Y. N., Hansen, A. C., & Ting, K. (2014). Integrated strategic and tactical biomass–biofuel supply chain optimization. *Bioresource Technol.*, *156*, 256–266.
- Mahindra. (2018). *Mahindra USA: 110 and 120 hp tractor with more performance, power, and value*. Retrieved March 14, 2022, from <https://www.mahindrausa.com/--series-tractor-9000/>.
- Mobini, M., Sowlati, T., & Sokhansanj, S. (2011). Forest biomass supply logistics for a power plant using the discrete-event simulation approach. *Appl. Energ.*, *88*(4), 1241–1250.
- Naderloo, L., Alimardani, R., Omid, M., Sarmadian, F., Javadikia, P., Torabi, M. Y., & Alimardani, F. (2012). Application of anfis to predict crop yield based on different energy inputs. *Measurement*, *45*(6), 1406–1413.
- Pitla, S. K., Luck, J. D., Werner, J., Lin, N., & Shearer, S. A. (2016). In-field fuel use and load states of agricultural field machinery. *Comput. Electron. Agric.*, *121*, 290–300.
- Pronovost. (2017). *Pronovost: Auto-load round bale handlers with maximum capacity up to 23 bales*. Retrieved March 14, 2022, from <https://pronovost.qc.ca/en/brochures/agricultural-products/>.
- R Core Team. (2017). *R: A Language and Environment for Statistical Computing*. R Foundation for Statistical Computing. Vienna, Austria. <https://www.R-project.org/>.
- Rotz, C. A., & Muck, R. E. (1994). Changes in forage quality during harvest and storage. *Forage Qual. Eval. Util.*, *20*, 828–868.

- Rotz, C. A., & Shinnars, K. J. (2007). *Hay harvest and storage* (Vol. 2). Forages, The Science of Grassland Agriculture. Sixth Edition. Blackwell Publishing, 2121 State Ave, Ames, IA, USA.
- Scarborough, D. A., Coblenz, W. K., Humphry, J. B., Coffey, K. P., Daniel, T. C., Sauer, T. J., Jennings, J. A., Turner, J. E., & Kellogg, D. W. (2005). Evaluation of dry matter loss, nutritive value, and in situ dry matter disappearance for wilting orchardgrass and bermudagrass forages damaged by simulated rainfall. *Agron. J.*, 97(2), 604–614.
- Shastri, Y. N., Hansen, A. C., Rodriguez, L. F., & Ting, K. C. (2010). Optimization of miscanthus harvesting and handling as an energy crop: BioFeed model application. *Biol. Eng. Trans.*, 3(1), 37–69.
- Sokhansanj, S., Kumar, A., & Turhollow, A. F. (2006). Development and implementation of integrated biomass supply analysis and logistics model (IBSAL). *Biomass Bioenerg.*, 30(10), 838–847.
- Subhashree, S. N., & Igathinathane, C. (2019). Tracks impacted field area simulation using kinematics and geometry for different equipment and operation scenarios. *Biosyst. Eng.*, 187, 185–200.
- Subhashree, S. N., Igathinathane, C., Bora, G. C., Ripplinger, D., & Backer, L. (2017). Optimized location of biomass bales stack for efficient logistics. *Biomass Bioenerg.*, 96, 130–141.
- Svanberg, M., Olofsson, I., Flodén, J., & Nordin, A. (2013). Analysing biomass torrefaction supply chain costs. *Bioresource Technol.*, 142, 287–296.
- Taylor, R., Shrock, M., & Wertz, K. (1991). Getting the most from your tractor. *Department of Agric. Eng. Cooperative Extension Service, Kansas State Univ., Manhattan, KS, USA.*

- Turner, J. E., Coblenz, W. K., Scarbrough, D. A., Coffey, K. P., Kellogg, D. W., McBeth, L. J., & Rhein, R. T. (2002). Changes in nutritive value of bermudagrass hay during storage. *Agron. J.*, 94(1), 109–117.
- Umeki, K., Yamamoto, K., Namioka, T., & Yoshikawa, K. (2010). High temperature steam-only gasification of woody biomass. *Appl. Energ.*, 87(3), 791–798.
- Velázquez-Martí, B., & Annevelink, E. (2009). GIS application to define biomass collection points as sources for linear programming of delivery networks. *Trans. ASABE*, 52(4), 1069–1078.
- Voltarelli, M. A., da Silva, R. P., Rosalen, D. L., Zerbato, C., Cassia, M. T., et al. (2013). Quality of performance of the operation of sugarcane mechanized planting in day and night shifts. *Aust. J. Crop Sci.*, 7(9), 1396.
- Wickham, H. (2016). *ggplot2: Elegant Graphics for Data Analysis*. Springer-Verlag New York, USA. <http://ggplot2.org>.
- Zhou, Y., Zhang, Z., Zhang, Y., Wang, Y., Yu, Y., Ji, F., Ahmad, R., & Dong, R. (2016). A comprehensive review on densified solid biofuel industry in China. *Renew. Sust. Energ. Rev.*, 54, 1412–1428.

4. DEVELOPMENT OF FORAGE ECONOMICS CALCULATOR WEB TOOL*

4.1. Abstract

Economic analysis of forage production and handling is vital for maintaining the agricultural enterprise and evaluating the associated risks. Economic analysis aids in making an educated decision related to growing or buying forage, setting forage prices, and purchasing additional equipment. Manual calculation of the economics is highly complex, tedious, and time-consuming. Therefore, a multi-device web-based tool, called the “forage economics calculator web tool” (FECWT) was developed using HTML, CSS, and JavaScript. The tool’s interface was designed for a user-friendly experience with easy access to commands set in an easy-to-follow layout. The FECWT uses 29 input variables to generate results “dynamically” for 37 output variables, based either on the supplied default data or with user-provided inputs (imperial or metric units). The tool emphasizes the cost of the bale collection activity, while cost of other activities (planting, fertilizer & chemical application, harvesting, and baling) are provided as direct inputs. Bale collection is performed using either a tractor; or a tractor pulling an “automatic bale picker” (ABP), which collects and transports multiple bales in a trip. The economic analysis outputs include net return, break-even ratio, payback period, and return on investment. Features of FECWT include the sensitivity of profit to changes in input values, and downloadable reports and charts for

* This paper is submitted to the *Computers and Electronics in Agriculture* journal. Authors: Subhashree N. Srinivasagan, C. Igathinathane, et al. 2021. Title: Forage Economics Calculator Web Tool. Subhashree performed the literature survey and wrote the manuscript. Dr. Igathinathane Cannayen is the major advisor, principal investigator, and the corresponding author who worked with Subhashree throughout the research and manuscript development. All the co-authors have assisted in the research direction and review of the manuscript.

record-keeping. Two case studies using farmers' actual field data inputs demonstrated the FECWTT's effectiveness, with its generated results corroborating well with farmers' records. The tool allows "what-if" scenario analysis of several practical situations and the results of equipment purchase decision, effect of forage crop types on net return, and low-inputs scenarios against different field areas are presented. The scenario analysis suggests that an ABP purchase for field areas greater than ≥ 65 ha (≥ 160 ac) could be profitable; alfalfa and corn were the most profitable forage and grain-forage crops, where the grain revenue stream of grain-forage crops easily covers the costs and makes a profit; and a low-inputs scenario (no fertilizers, chemicals, and/or seeds) for forages (alfalfa and grass) decreased the net returns on average by 8.1 times at 50% forage yield potential suggesting the use of all inputs and increased field areas (≥ 65 ha) make a better profit in this low-inputs scenario. Potential users of this web tool include farmers, hay producers, custom hay operators, educators, agricultural extension and financial personnel, and others interested in the economics of handling bales.

4.2. Introduction

Nearly 90% of the land area of North Dakota (ND) is in farms and ranches and cattle (*Bos taurus*) outnumber the human population by a ratio of 3 to 1 (NDG, 2020b). In North Dakota and other states with extensive agriculture, forages play a crucial role in livestock production because they provide the necessary nutrients required for maintaining livestock. Sufficient and year-round supply of forage is vital in maintaining herd size and animal health; therefore farmers and ranchers grow forage crops specifically to address seasonal shortfalls. Producing, harvesting, baling, and storing forage crops represents a large proportion of annual livestock production costs (Horrocks and Valentine, 1999;

Nayigihugu et al., 2007). Making effective decisions on the selection of crops, setting forage prices, and efficient management activities can increase profit and/or reduce the risk involved in an agricultural enterprise. Performing economic analysis helps forage growers make educated decisions regarding forage purchases, equipment purchases, and forage sale prices.

Various parameters and complex calculations, difficult to perform manually, are involved in executing an economic analysis of forage production, such as the revenue and costs (e.g., labor and fuel) of growing, harvesting, collecting, labor, fuel, and transporting forage. A few spreadsheet tools are available to replace the manual method of analyzing forage economics. One example spreadsheet tool was developed to evaluate the hay price for producers wanting to compare the net return between hay and corn (Barnett, 2009). Another spreadsheet tool allowed producers to use equipment and equipment information to determine the ownership and operating cost of specific types of haying systems (Brence and Griffith, 2012). Other decision support spreadsheet tools developed for alfalfa and grass enterprises helped producers determine the profitability of producing versus purchasing hay (Kirwan, 2020).

Although these tools are available online, the following caveats should be taken into account: (i) the tools require forage growers to use multiple spreadsheets to arrive at a decision; (ii) the available tools are in the format of spreadsheets and the user needs to download and most likely enable macros in order to run the calculations; and (iii) all of these tools mainly focus on activities such as forage harvest that might include, mowing, conditioning, tedding, raking, combining, etc., and baling, while forage (bale) collection is often ignored. Bale collection is an intensive field operation, wherein the cost associated

with equipment, fuel, and labor of bale collection plays a significant role in economic outcomes.

Therefore, we developed a user-friendly web-based tool namely “Forage Economics Calculator Web Tool” (FECWT) using technologies such as HTML (Hypertext Markup Language) (Hickson and Hyatt, 2011), CSS (Cascading Style Sheets) (Powell, 2010), and JavaScript (Mikkonen and Taivalaari, 2007) to perform an economic analysis of forage production, including bale collection. Some of the features guiding our development of the FECWT are: (i) serving as “one-stop” tool to aid decision making on major aspects such as growing versus buying forage, purchasing equipment, and setting forage prices based on net-return estimation; (ii) allowing hassle-free access to the tool from any internet-enabled device (computer, tablet/iPad or smartphone) with no download or installation of software required; (iii) compatible with different operating systems and browser applications; (iv) considering relevant hay production field activities and costs, with emphasis on round bale collection using a conventional tractor (collects maximum 2 BPT, BPT), or a tractor with an automatic bale picker (ABP) (collects multiple (up to 23) BPT); (v) easy operation of the tool through the availability of relevant research-based default input values, yet flexibility for altering data to suit user scenarios; (vi) capability of handling different forage crops and grain-forage crops and their associated revenue streams; and (vii) performing “what-if” scenario analysis to assess the sensitivity to different inputs of the bottom line for forage production.

The objective of this study is to develop a forage economics decision support web tool using open source software with the proposed features. The resulting FECWT is user-friendly, and allows for scenario analysis to user’s decisions regarding hay production eco-

nomics. Farmers, hay producers, custom hay operators, educators, and agricultural extension and financial personnel, and others interested in the economics of handling bales are prospective users of the FECWT.

4.3. Overview of the Web Tool

The FECWT was developed to perform standard economic analysis, with 29 user-inputs and 37 outputs (fig. 4.1). Some of the outputs are costs associated with harvest, baling, bale collection, bale transportation from field to storage, labor, and fuel as well as revenue generated from selling the bales and grain, net returns, break-even ratio, and payback period. The tool employs logistics models for the bale collection process and the cost associated with it as a function of distance and fuel consumption; whereas harvesting, baling, and bale transportation are processed as direct inputs. Bale collection in the field is commonly performed using a tractor with a spear or grapple attachment, or less commonly using an ABP which collects and transports multiple bales (≤ 23) in a single trip. Both of these bale collection equipment (tractor and ABP) are included in the tool for comparison. The cost associated with bale collection is based on simulations (36,960 scenarios) performed to estimate the logistics distance and fuel consumption of a tractor involved in the activities (Subhashree et al., 2021).

In addition to standard economic analysis, the tool is designed to perform input sensitivity analyses for profit as well as insights into equipment (ABP) purchase and forage harvest with collection decisions. The tool generates dynamic/real-time results based on default or user-input values and generates a downloadable report and chart containing selected inputs and estimated results for comparison, analysis, and record-keeping (fig. 4.1). Though the tool was developed based on data (common crop type, bale sale price, and

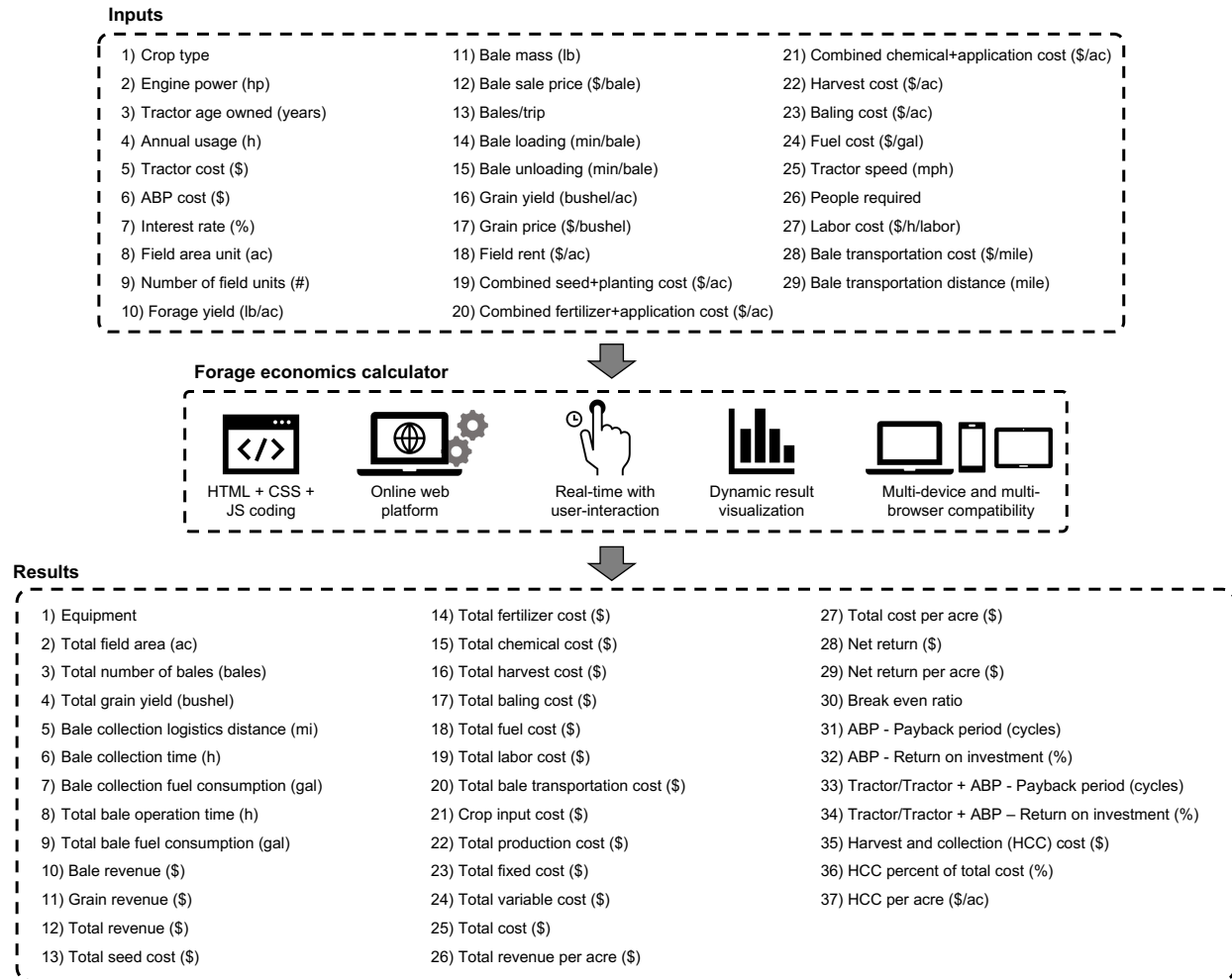


Figure 4.1. Information flow and overall features of forage economics calculator web tool (FECWT) showing the user-inputs, FECWT processes and features, and the generated results using imperial units. The \$ represents US dollars (USD).

other costs inputs) collected from ND, the tool can be extended to other locations by altering the user-input values

4.4. Web Tool Development

The FECWT was developed using the basic open source technologies, HTML, CSS, and JavaScript (Appendix D). The HTML was used to create the web tool’s content structure, while CSS was used to design the web tool, including layout, visual effect, and background color. In the FECWT, JavaScript forms the basis of front-end web development;

it creates interactive elements that engage the user with the web tool, and performs all analysis calculations. In addition to the basic web development technologies framework, a popular front-end open-source toolkit called *bootstrap* was used to create a responsive and mobile-first web tool (Spurlock, 2013). Data visualization of the results was achieved using SVG elements from the basic HTML, supplemented by an open-source JavaScript library *Chart.js* that produces responsive, customizable, and downloadable charts (Da Rocha, 2019). Visual Studio Code (*VS Code*) text editor was used to write programming languages (HTML, CSS, and JavaScript) to develop the web tool. The VS Code is an open-source free integrated development environment (IDE) that features language-specific syntax highlighting, code indentation, plug-in, and add-on to capture code errors. Code errors were additionally tested and captured by hosting the developed website onto the local server using Mac terminal commands.

The FECWT's functionality was built to work as seamlessly as possible with a similar feel in major web browsers such as Google Chrome, Firefox, and Safari. The tool was also made to accommodate smartphones, tablets (iOS and Android), and desktop media screen sizes consistently providing a good visual and responsive web tool experience.

4.4.1. Web Tool Sections

The FECWT consists of three main sections: (i) home page, (ii) user instructions and manual, and (iii) the actual calculator (fig. 4.2). Each section consists of a collapsible navigation sidebar at the top-left corner that enables a smooth transition between the sections. The first section is the home page that welcomes the user to the forage economics web tool (fig. 4.2A). A visitor counter was added to the home page to track the number of times the web tool has been accessed and used.



Figure 4.2. Overview of the forage economics calculator web tool (FECWT): A. home page of FECWT with web tool user-count feature; B. user instructions and manual section with downloadable 6-step instructions and detailed manual; C. calculator section of FECWT with 29 inputs, 37 output results, and a dynamic graph.

The second section consists of a simple and short 6-step user instructions (Appendix B) and a detailed manual (fig. 4.2B). The user instructions include a friendly *step-by-step guide* for the user, while the detailed manual contains comprehensive information about the various inputs, region-specific forage and economics data, forage bale collection logistics models, standard economics calculations that run in the background of the web tool, and the generated outputs. The 6-step user instructions and detailed manual are downloadable and printable PDF documents. The third section is the actual forage economics calculator section, which functions as a user interface with the calculator (fig. 4.2C). The calculator consists of editable inputs, read-only outputs, and a dynamic graph. Details on the FECWT user interface and application features are presented next.

4.4.2. User Interface and Web Tool Features

The FECWT's calculator section is presented in a two-column panel with “inputs” (29 input items) on the left and “results” (37 output items) on the right (fig. 4.3). Users interact with the calculator by choosing relevant inputs and input values with which to perform the analysis. The calculator is dynamic — automatically generating results with any change in the input values, without any specific button actions needed. Input values are provided as default, based on current/published research data, or can be modified by the user, while the results are read-only. A tooltip feature is provided for the input and result items to display a brief informative message when the user hovers the mouse cursor over the icon (fig. 4.3A).

Default research-derived values, are provided for all the input items and can be changed by the user through three different input options: drop-down boxes, checkbox sliders, and input text boxes. Among the 29 input items (fig. 4.1), four are fixed inputs in

A Tooltip info: Basic inputs with appropriate units necessary for calculation are only considered. The most common values were shown as defaults. Selection of the crop, aggregation machinery power, machine age owned, and annual usage can be performed through choice boxes. Slider position creates desired input. User can also change the limits by updating values on both input boxes around the sliders. The sliders will use the updated limits and inputs value for processing. "What-if" scenario analysis can be performed by modifying the various inputs.

B Toggle switch: Imperial units / Metric units

C Drop-down box: Crop type: Alfalfa (Perennial, 5 years), Alfalfa mix (Perennial, 5 years), Barley (Annual), Corn (Annual), Grain mix (Annual), Grass (Perennial), Grass (Annual), Grass mix (Annual), Millet (Annual), Oats (Annual), Wheat (Annual), (Others)

D Check-box option: Include ABP? ABP cost: (\$) 20000

E Slider with editable range values: Seed and seeding cost: 145 (SC, \$/ac)

F Read-only textbox: Equipment: Tractor

G Dynamic plot: Bar chart showing costs for FC, TR, TC, NR, BE, PB.

H Profit-based color output: Net return (NR): \$9,477 (NR = TR - TC)

I Equipment based output: Equipment: Tractor

J View chart: Bar chart showing Forage production calculator results.

K Download report: Forage Economics Calculator report showing detailed financial breakdown.

Figure 4.3. Forage economics calculator web tool (FECWT) user interface and features showing the inputs column and results column: A. tooltip info, B. drop-down box, C. checkbox option, D. input slider, E. read-only text box, F. dynamic plot, G. profit-based color output, H. equipment-based output (tractor or automatic bale picker), I. view chart, J. download report.

the form of a drop-down containing pre-defined lists and one is a check-box, while the remaining are variable inputs in the form of sliders or text boxes. The toggle switch helps the user toggle between the imperial and metric units, allowing the FECWT to be used globally (fig. 4.3B). Drop-down options display a specific list of items from which the user can choose one item (fig. 4.3C), selection of crop, engine power, tractor age, and annual usage. A checkbox is used to include ABP in the calculation (fig. 4.3D), while tractor alone is the default. This checkbox option, when activated, triggers a case scenario of equipment purchase that includes ABP along with a tractor for bale collection. Most of the inputs to the web tool are entered through sliders, which are versatile design tools to select a value between a range (fig. 4.3E). The slider consists of a minimum, maximum, and a selected value which are provided by default. However, the minimum and maximum values for each slider item can be changed, based on user-entered text box inputs.

Sliders are convenient tools to perform “what-if” scenario analyses. Dynamic arrow markers under each slider are coded to help the user quickly see a snapshot of sensitivity to each particular input. More specifically the position of these arrow markers informs the critical value of the input at which a loss or profit would result. The “Reset” button option at the bottom of the interface resets all input items to their default values for fresh calculations.

The results column consists of read-only text boxes displaying the determined outputs, which are updated automatically (fig. 4.3F). The dynamic graph in the results column displays various results in the form of a bar chart for quick visualization (fig. 4.3G). The chart automatically updates with the changing results based on the user inputs. Hovering over the bars in the graph displays a tooltip with their respective result values. For

the most common output of interest “Net return”, a colored text box was coded for ready visualization of the outcome; wherein a background color of green indicates profit and red indicates the loss (fig. 4.3H). The equipment-based outputs estimate the payback and return on investment (fig. 4.3I) for whichever set of equipment is selected (in fig. 4.3D): “tractor” only, “tractor and ABP,” or “ABP” only (fig. 4.3I). The payback period represents the number of cycles (harvests or years) required to cover the cost of equipment (tractor with or without ABP) and all other input costs captured in the net returns from forage (with or without grain revenue).

The “View Chart” button at the bottom of the interface allows users to visualize economic results such as total cost, total revenue, and net return in the form of a high-quality responsive bar chart that is suitable for printing (fig. 4.3J). The “Download report” button generates a printable document in PDF format, which contains selected user inputs and associated results, for record-keeping purposes (fig. 4.3K). The “Clear results” button clears all the generated results and resets the input panel to the default values for a new session.

4.4.3. Web Tool Inputs

Among the 29 inputs, 12 are cost-based inputs, while the remaining are related to the forage crop, equipment, and operation. Detailed description of each input item is presented in table 4.1. Most forage crop types prevalent in ND have been listed under the “Crop type” drop-down input. However, if the desired forage crop is not listed, the user can select “Others” from the list and provide relevant range values in the editable minimum and maximum input boxes for the sliders. The crop type belongs to two categories: (i) forage crops (e.g., alfalfa, grass, and grass mix), which produce one revenue stream

Table 4.1. Brief description of the forage economics calculator web tool (FECWT) input options.

Inputs	Description
1. Crop type	Forage crops available for sale as bales in commercial markets of North Dakota (ND), such as on the NDSU feedlist (NDSU, 2020) and BisManonline (BisManonline, 2020). Crop types include perennial and annual forage crop types (exclusive forage and grain+forage, which result in one or two revenue streams).
2. Engine power (hp)	Engine power ranges of commercially available tractors. The engine power requirement should match the bale load-carrying capacity (Anderson, 2008; JD, 2006; Mahindra, 2018).
3. Tractor age owned (years)	Number of years the tractor is owned by the user.
4. Annual usage (h)	Average annual operation of the tractor for bale collection in hours.
5. Tractor cost (\$)	The listed cost of the tractor during the purchase. The tractor cost is based on the engine power.
6. ABP cost (\$)	The listed cost of the ABP during the purchase, which depends on its capacity. The commercial capacity usually ranges from 8 to 23 bales assuming 5 ft wide bales.
7. Interest rate (%)	Interest rate at which tractor was purchased.
8. Field area unit (ac)	Expressed as fractions of a "section" (1 mile ² = 640 ac = 259 ha) as a standard US land unit. Range includes from the smallest (SI8ha) to the largest (259 ha) derived as fractions of the field area unit.
9. Number of field units (#)	Number of field area units in the farm where forage is cultivated.
10. Forage yield (lb/ac)	Forage production/ac from the specified field. The range accommodates possible yield variation of the potential forages.
11. Bale mass (lb)	The weight of a single large round bale (dimension 5 × 5 or 5 × 6 ft) in pounds (lb). The range limits are fixed based on the bale mass sold at the commercial markets of ND.
12. Bale sale price (\$/bale)	Specific to the crop types; price range changes based on the selected crop (BisManonline, 2020; NDSU, 2020).
13. Bales/trip	Bales/trip ≤ 2 was considered for conventional tractor bale collection, while bales/trip ≥ 3 were considered based on the available commercial carrying capacity of ABP.
14. Bale loading time (min/bale)	Time required to pick up a bale and load it onto a truck for transport.
15. Bale unloading time (min/bale)	Time required to unload a bale from the truck or ABP and place it in a stack.

continued . . .

Table 4.1 Brief description of the forage economics calculator web tool (FECWT) input options — (continued)

Inputs	Description
16. Grain yield (bushel/ac)	Grain yield from the specified field. The range of grain yield values provided as default are based on the National Agricultural Statistics Service (NASS) database for ND in 2020 (Jantzi et al., 2020).
17. Grain price (\$/bushel)	Grain sale price is specific to the grain-forage crops considered; the default values provided are based on the NASS database for ND in 2020 (Jantzi et al., 2020).
18. Field rent (\$/ac)	The per-acre cost of the average rent for a field. The provided range limits are based on the data from the 2020 ND Department of Trust Lands survey (NDG, 2020a).
19. Combined seed and planting cost (\$/ac)	Seed cost/ac was direct or annualized, depending on the selected forage crop type. Typical planting cost is \$18/ac for ND (Jantzi et al., 2020). The planting cost should be added to the input.
20. Combined fertilizer and application cost (\$/ac)	Fertilizer cost/ac, which is the total cost of fertilizers such as nitrogen, phosphorous, potassium, sulfur, limestone, and others. Typical application cost is \$7/ac for ND (Jantzi et al., 2020). The application cost should be added to the input.
21. Combined chemical and application cost (\$/ac)	Chemical cost/ac is the cost of herbicide, fungicide, and insecticide used. Typical application cost is \$7/ac for ND (Jantzi et al., 2020). The application cost should be added to the input.
22. Harvest cost (\$/ac)	Involves equipment, fuel and labor cost for harvesting the forages/ac and is provided as an overall direct input. Harvesting forage crops might include activities such as mowing, conditioning, tedding, raking, etc. For grain + forage crops harvesting might include activities such as combining, raking, etc.
23. Baling cost (\$/ac)	Involves equipment, fuel and labor cost for baling the forages/ac and is provided as an overall direct input.
24. Fuel cost (\$/gal)	Cost/gal of fuel (diesel) used in the tractor was fixed based on a 10-year average, and can be changed to reflect the current price.
25. Tractor speed (mph)	Operating speed of the tractor (with or without ABP) in the field during bale collection.
26. People required	Number of people involved during bale collection to operate the equipment.
27. Labor cost (\$/h/labor)	Labor cost per hour is the cost of labor operating the equipment during bale collection.
28. Bale transportation cost (\$/mile)	Fuel and labor cost of transporting the bale/mile from field to storage facility.
29. Bale transportation distance (mile)	Distance between the field and the storage facility.

Note: Inputs #1 – #4 are drop-down options, #6 is a checkbox and slider option, #9 is an input box, and the rest are slider options showing the research data based default values that can be edited by users to fit their situation. All \$ represents US dollars (USD).

from the sale of forage bales; and (ii) grain-forage (e.g., corn, wheat, barley, oats, and millets), which produce two revenue streams from the sale of both grain and forage. A grain crop that was grown exclusively for forage (e.g., forage oats) can be readily handled by setting either “Grain yield” or “Grain sale price” or both inputs to zero. Furthermore, with cultivated perennial forage crops such as alfalfa, which yields forage during four to five years after planting, the cost of cultivation was annualized to spread the cost across the productive period. However, for annual forage crops, the cost calculations are straightforward and applicable for the year of planting.

In the event of zero inputs (“low-inputs” scenario), which is prevalent in the case of naturally grown forages (e.g., prairie grass) or others that perennial grasses that require less management, the user can change the value in the minimum input box to zero and set the slider to the left-most position to select the zero value. The low-inputs scenario makes sense with perennial forage crops as some of the inputs like seed, fertilizer, and chemical cost will be zero in some situations, while the other costs like field rent and labor will be factored into the analysis.

However, without the seed, fertilizer, and chemical, the forage yield is expected to decrease between 40% and 60% of the total yield potential (Angima, 2007). This scenario of low-inputs was analyzed and presented for different yields and field areas (section 4.6.3). However, while running this low-inputs scenario, the users are expected to input their actual forage yield, which represents the reduction based on low-inputs to obtain the correct outputs.

4.4.4. Web Tool Generated Results

The results panel is located on the right-hand side of the FECWT with a total of 37 generated outputs (fig. 4.2C). All the outputs are displayed in read-only uneditable text box. Among the outputs, 14 are cost-based and the rest are standard economic results, such as net return, revenue, break-even ratio, payback period, return on investment, and so on. Three non-linear regression models ($R^2 = 0.98$) were developed in our previous study (Subhashree et al., 2021) to estimate the total logistics distance, operation time, and fuel quantity consumed during bale collection runs in the background of the calculator. Eight standard economic analysis equations were included to generate all other results. For ease of use by the US farmers and ranchers the results presented are in imperial units, but the models were developed in SI units and therefore conversion factors were employed in calculations and codes behind the units toggle switch (fig. 4.3B).

It will be always useful to the producers to evaluate whether it will make sense to harvest and collect the forage or leave it standing in the field based on the costs involved exclusively for these activities. To address this scenario, the “harvest and collection” cost (HCC), which was already a part of the total cost (section 4.4.4.12), was also presented default as an output. This cost involves that associated with the harvest, baling, collection, and transportation; so that these collective activities leave the field ready for the next crop. Observing this cost, its proportion with the total cost, and its cost/ac along with net return values, the users can make an informed decision on this scenario.

4.4.4.1. Equipment type

The equipment type result displays “tractor” or “tractor and ABP” combined depending on which was selected in the checkbox. (table 4.1, #6). The conditions for equipment type is as follows:

$$\text{Equipment} = \begin{cases} \text{Tractor,} & \text{bales/trip} \leq 2 \\ \text{Tractor with ABP,} & \text{bales/trip} \geq 3 \end{cases}$$

4.4.4.2. Total field area

Total field area is estimated as a product of the two following inputs: (i) field area unit and (ii) number of units (table 4.1: #8 and #9).

4.4.4.3. Total number of bales

The total number of bales generated depended on the input values, such as forage yield, bale mass, field area unit, and number of field units table 4.1: #8 – #11). A random variation of 10% in the crop stand uniformity was assumed (Subhashree et al., 2017). Any change in these inputs is reflected in the resulting total number of bales.

$$N_B = \frac{A_F \times N_F \times Y_B}{M_B} \quad (4.1)$$

where, N_B = number of bales, A_F = field area (ha), N_F = number of field units, Y_B = biomass yield (Mg/ha), and M_B = bale mass (Mg).

4.4.4.4. Bale collection logistics distance

Logistics distance during bale collection is estimated using the prediction model developed (Subhashree et al., 2021) with the input values of total field area, BPT, and biomass yield (table 4.1: #8, #10, and #13).

$$D_L = \left[\frac{A_F Y_B}{17.879 \times (B_T + 0.895)} \right]^{1.377} \quad (R^2 = 0.98) \quad (4.2)$$

where, D_L = total bale collection logistics distance (km), and B_T = bales/trip.

4.4.4.5. Bale collection time

The bale collection operational time is estimated using the developed multivariate model (Subhashree et al., 2021) with the user input values of total field area, BPT, biomass yield, and equipment speed (table 4.1: #8, #10, #13, and #25).

$$T_C = \left[\frac{A_F Y_B}{-46.003 + 80.230B_T + 15.052S_p} \right]^{1.381} \quad (R^2 = 0.98) \quad (4.3)$$

where, T_C = bale collection time (h) and S_p = equipment operation speed (km/h).

4.4.4.6. Bale collection fuel consumption

The fuel (diesel) consumption (gallons) is estimated using the multivariate prediction model developed (Subhashree et al., 2021) with the input values of total field area, BPT, biomass yield, and equipment speed (table 4.1: #8, #10, #13, and #25). Different prediction models based on standard fuel consumption methods (ASABE Standards (ASABE, 2011) and fuel efficiency (Khalilian et al., 1985)) were used to estimate the fuel consumption of the equipment (tractor and ABP). These methods estimated fuel consumption based on the horsepower of the engine and bale load.

$$\text{Tractor (1 to 2 bales):} \quad F_C = \left[\frac{A_F Y_B}{-5.913 + 13.164B_T + 2.777S_p} \right]^{1.414} \quad (R^2 = 0.98) \quad (4.4)$$

$$\text{ABP (8 to 23 bales):} \quad F_C = \left[\frac{A_F Y_B}{-4.991 + 1.165B_T + 4.827S_p} \right]^{1.242} \quad (R^2 = 0.98) \quad (4.5)$$

where, F_C = fuel quantity (L) consumed during bale collection operation.

4.4.4.7. Total bale movement time

The total bale movement time is estimated using bale collection (eq. (5.3)) time plus the time required for loading bales onto a truck and then unloading the bales into a stack or other storage location. The loading and unloading time can be determined using the number of bales generated (eq. (5.1)) and the loading and unloading time (min) per bale inputs (table 4.1, #14 and #15).

$$T_{LU} = N_B \times (T_L + T_U)/60 \quad (4.6)$$

$$T_{OT} = (T_{LU} + T_C)/60 \quad (4.7)$$

where, T_{LU} = total bale loading and unloading time (h), T_L = loading time per bale (min), T_U = unloading time per bale (min), T_{OT} = total bale movement time (h).

4.4.4.8. Total bale fuel consumption

Total bale fuel consumption is determined using the fuel consumed during bale collection (eqs. (4.4) and (4.5)) and during loading and unloading bales. The fuel consumption for loading and unloading of bales is calculated using tractor capacity and fuel efficiency (Khalilian et al., 1985). The estimated fuel consumption is 15.7L/h assuming a tractor capacity of 150 hp and a load of 1 bale (680 kg) for both loading and unloading operations.

$$F_{LU} = 15.7 \times T_{LU} \quad (4.8)$$

where, F_{LU} = fuel quantity (L) for loading and unloading operation.

$$T_{FQ} = F_C + F_{LU} \quad (4.9)$$

where, T_{FQ} = total fuel quantity (L).

4.4.4.9. Total revenue

The total revenue depends on the number of revenue streams (i.e., revenue from just bales, or from bales and grain), which is based on the crop type (forage and forage+grain). The revenues and costs (\$) presented in this study are based on US dollars (USD). The bale revenue (\$) is based on the input values for crop type and price per bale (table 4.1: #1 and #13), and the number of bales generated (eq. (5.1)). In ND, the forage crop alfalfa has the highest price per bale while grain residue bales (e.g. straw or stover) have the lowest price per bale assuming equal bale size (e.g. 5 × 5 ft). However, this price structure may vary with other geographic locations. Similarly, the grain revenue depends on the total field area, grain yield, and grain price (table 4.1: #8, #16, and #17).

$$\text{Total revenue (\$)} = \begin{cases} \text{Bale revenue,} & \text{Forage crop} \\ \text{Bale+grain revenues,} & \text{Grain crop} \end{cases} \quad (4.10)$$

4.4.4.10. Crop input cost

Crop input cost is the sum of total seed cost, fertilizer cost, and chemical cost including their application costs. This cost is influenced by the selected crop type. Total seed, fertilizer, and chemical costs are estimated based on the inputs, field area unit (ac), number of units, and seed, fertilizer, and chemical cost (\$/ac) with their application, respectively (table 4.1: #8, #9, and #19 – #21).

$$\text{CIC (\$)} = \text{TSC} + \text{TFRC} + \text{TCC} \quad (4.11)$$

where, CIC = crop input cost (\$), TSC = total combined seed+application cost (\$), TFRC = total combined fertilizer+application cost (\$), and TCC = total combined chemical +

applicaiton cost (\$).

4.4.4.11. Total bale production cost

Total bale production cost is the sum of crop input cost (eq. (4.11)), harvest cost, and baling cost but the cost of collecting and transporting the bales. Total harvest and baling costs are estimated using harvest cost (\$/ac), baling cost (\$/ac), field area unit, and number of field units (table 4.1: #9, #10, #18, #19).

$$\text{TPC (\$)} = \text{CIC} + \text{THC} + \text{TBC} \quad (4.12)$$

where, TPC = total bale production cost (\$), THC = total harvest cost (\$), and TBC = total baling cost (\$).

4.4.4.12. Total cost

The standard economic analysis used in determining the total costs with total fixed cost components, such as depreciation, taxing, housing, insurance, and interest for the bale collection equipment and total field area rent (Appendix C.1) and total variable cost components, such as repair and maintenance, total fuel and labor for bale collection and total bale transportation cost (Appendix C.2) are presented in Appendix C. Total cost is the sum of total production (eq. (4.12)), total fixed (Appendix C.1), and total variable costs (Appendix C.2).

$$\text{TC (\$)} = \text{TPC} + \text{TFC} + \text{TVC} \quad (4.13)$$

where, TC = total cost (\$), TFC = total fixed cost (\$), and TVC = total variable cost (\$).

Transportation activity of collected bales from the field to the storage unit and the cost associated is accounted as a component in the variable cost (Appendix C.2.4).

4.4.4.13. Net return

Net return refers to the amount of revenue that remains after all the costs are deducted, within a particular year (otherwise, if revenue and costs spill across multiple years, discounting would be needed before values in different years are added or subtracted). Then the net return can be calculated using the total revenue (eq. (4.10)) and the total cost (eq. (4.13)).

$$\text{Net return (\$)} = \text{Total revenue} - \text{Total cost} \quad (4.14)$$

A net return value greater than zero indicates profit and a value less than zero indicates a loss.

4.4.4.14. Break-even ratio

Break-even ratio is the ratio of total revenue (eq. (4.10)) to total cost (eq. (4.13)).

$$\text{Break even ratio} = \frac{\text{Total revenue}}{\text{Total cost}} \quad (4.15)$$

A break-even ratio value greater than 1 indicates profit and a value less than 1 indicates a loss.

4.4.4.15. Payback period and return on investment

Payback period is the length of time required to recover the initial investment on the equipment (tractor with or without ABP) through profit. The payback period is estimated in cycles; a year can have one or more cycles depending on the frequency of forage crop harvest and resulting revenue streams.

$$\text{Payback period (cycles)} = \frac{\text{Equipment cost}}{\text{Net return (profit per year)}} \quad (4.16)$$

The return on investment (ROI) is expressed as a percentage and is the ratio of annual profit to the equipment cost (eq. (4.17)).

$$\text{Return on investment (\%)} = \frac{\text{Net return (profit per year)}}{\text{Equipment cost}} \times 100 \quad (4.17)$$

The payback period and return on investment are only calculated if the outcome of net return is positive. These results were calculated only for a tractor (major piece of equipment) as well as for the combined tractor and ABP (minor piece of equipment; but only if ABP was included in the operation), to help with the equipment purchase decision. More specifically, a farmer might consider investing in an ABP if it meets the following criteria: (i) generates positive net return; (ii) generates more net return than using a tractor only; (iii) saves time substantially and has a shorter payback period, and (iv) generates more net return than any other alternative use of funds being considered for investment.

4.5. Case Studies With Actual Farmers

Case studies were carried out to demonstrate the functionality and applicability of FECWT in actual field scenarios. Two farmers were contacted to apply real-field input values and compare the estimated results with their existing records. The farms of 80 ac (case study 1) and 40 ac (case study 2) were located in Sioux and Morton County, ND, USA, respectively. Farmer-1 produced alfalfa, perennial forage variety, and farmer-2 produced bromegrass (“Grass (Perennial)” - option to be used in FECWT; perennial forage variety). The tool was temporarily hosted on a local server for the farmer. Input values for field parameters, bale collection operation, and crop input costs were entered in the FECWT. Some of the default input options were left as such, while the farmer appropriately modi-

fied others according to their fields and activities. Selected inputs and the tool-generated results are presented in table 4.2.

4.5.1. Case Study Inputs

Appropriate data were input into the FECWT using drop-down options, sliders, and input boxes. The case studies focused on estimating the economics of alfalfa and bromegrass (5-year crops) using a tractor that can handle only two bales at a time (2 BPT). For farmer-1 and farmer-2, with alfalfa and bromegrass stands producing forage for five years, the original combined seed and planting cost (\approx \$145/ac and \$84/ac, respectively) was annualized at \$29/ac and \$17/ac, respectively. The combined cost of fertilizer and application for farmer-1 and farmer-2 was set at \$0 and \$15, respectively. Similarly, the combined chemical and application cost incurred for farmer-1 and farmer-2 was \$22/ac. Harvesting, baling, equipment, field rent, fuel, and labor costs are provided as direct inputs based on their operation.

4.5.2. Case Study Results

Selected results of the two case studies are shown in table 4.2 and the “View chart” in Figure 4.4. The FECWT evaluated net return per acre for the inputs from case studies 1 and 2 as \$92 and $-\$38$ for 2 BPT, respectively, corroborated well with the farmer’s own estimates of about \$100/ac and $-\$35$ /ac, respectively.

The sensitivity analysis inputs from farmers 1 and 2 revealed a break-even forage yield of 2834 and 4686 lb/ac, respectively. That is, if the farmers’ respective yields fall below these values, they will experience an economic loss. Conversely, any yields above these will generate positive profit. Similarly, the break-even price per bale is \$44 and \$81

Table 4.2. Field case studies using forage economics calculator web tool (FECWT) analyzing a perennial and annual forage crop.

Inputs			Results		
Parameter	Farmer-1	Farmer-2	Parameter	Farmer-1	Farmer-2
Crop type	Alfalfa (Perennial, 5 years)	Brome grass (Perennial, 5 years)	Equipment	Tractor	Tractor
Engine power (hp)	80-149	80-149	Total field area (ac)	80	40
Tractor age owned (years)	10	20	Total number of bales	234	77
Annual usage (h)	200	200	Bale collection distance (mi)	35.0	8.2
Tractor cost (\$)	50,000	20,000	Bale collection time (h)	7.0	1.6
ABP cost (\$)	NA	NA	Bale collection fuel consumption (gal)	20.4	4.6
Interest rate (%)	5	6	Total bale movement time (h)	10.9	2.9
Field area unit (ac)	80	40	Total bale fuel consumption (gal)	36.6	9.9
Number of field units (#)	1	1	Total revenue (\$)	17,550	4620
Forage yield (lb/ac)	5000	3500	Total seed cost (\$)	2320	672
Bale mass (lb)	1500	1500	Total fertilizer cost (\$)	0	1280
Bale sale price (\$/bale)	75	60	Total chemical cost (\$)	1760	880
Bales/trip	2	2	Total harvest cost (\$)	1600	800
Bale loading time (min/bale)	0.5	0.5	Total baling cost (\$)	1200	800
Bale unloading time (min/bale)	0.5	0.5	Total fuel cost (\$)	73.1	29.8
Field rent (\$/ac)	35	40	Total labor cost (\$)	217.4	58.4
Combined seed+planting cost (\$/ac)	145*	84*	Total bale transportation cost (\$)	15	40
Combined fertilizer+application cost (\$/ac)	0	32	Crop input cost (\$)	4080	2832
Combined chemical+application cost (\$/ac)	22	22	Total production cost (\$)	6880	4432
Harvest cost (\$/ac)	20	20	Total fixed cost (\$)	2952	1617
Baling cost (\$/ac)	15	20	Total variable cost (\$)	309	129
Fuel cost (\$/gal)	2	3	Total cost (\$)	10141	6178
Tractor speed (mph)	5	5	Total net revenue/acre (\$)	219	116
People required	1	1	Total cost/acre (\$)	127	154
Labor cost (\$/h/labor)	20	20	Net return (\$)	7409	-1558
Bale transportation cost (\$/mile)	3	4	Net return/acre (\$)	92	-38
Bale transportation distance (mile)	5	10	Break even ratio	1.7	0.8
			Payback period (cycle; tractor only)	7	NA
			Return on investment (%)	15	NA
			Harvest and collection cost (HCC, \$)	3106	1728
			HCC to total cost (%)	31	28
			HCC/ac (\$)	39	43

Note: The units used are: hp - horsepower, h - hour, lb - pound, ac - acre, \$ - US Dollars, mph - miles per hour, and gal - US gallon.

* Farmer-1 and Farmer-2 — total seed cost and planting investment for alfalfa and grass crop (perennial, \$145/ac/5 years and \$84/ac/5 years) is annualized (\$29/ac/year and \$17ac/year) in the results, respectively.

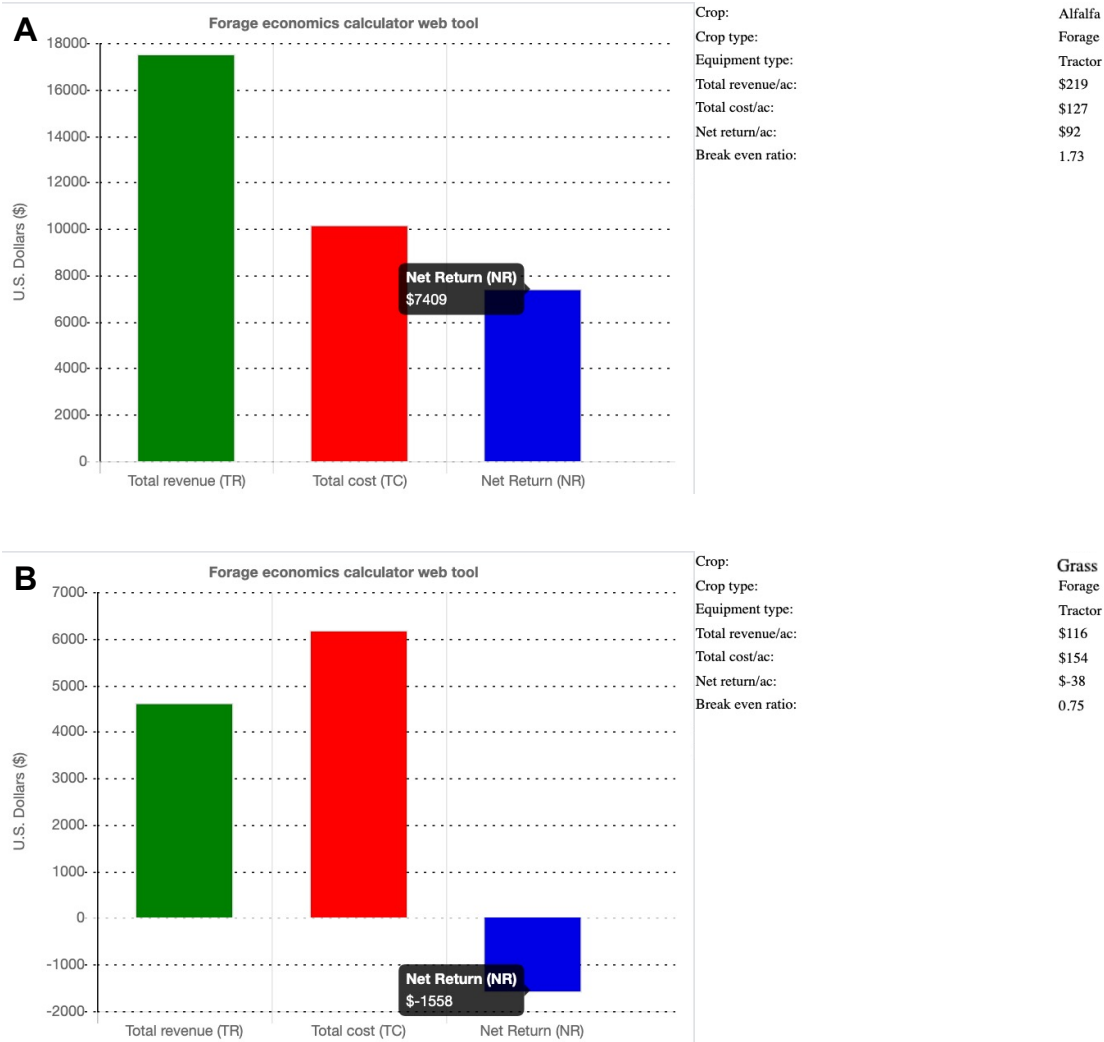


Figure 4.4. Downloadable graphical visualization chart comparing total revenue, total cost, and net return. Other prominent economics outputs are presented in text.

for farmers 1 and 2, respectively. If the farmers sell their bales for anything less than these break-even prices, respectively, they will experience an economic loss. Farmer-1, with self-reported forage yield of 5000 lb/ac and bale sale price of \$75, make a profit. Farmer-2, with a self-reported forage yield of 3500 lb/ac and bale price of \$60, incurs a loss. Further sensitivity analysis revealed that an increase in the bromegrass forage yield from 3500 lb/ac to 4686 lb/ac (break-even), holding all else constant, would increase the net return from -\$1557 (loss) to \$18 (profit) for the field area of 40 ac.

The results of the low-inputs scenario were obtained assuming the combined cost of seed + application, fertilizer+application, and chemical+application at \$0 and reduced forage yields (2500 lb/ac and 1750 lb/ac), which is 50% of the total yield potential (5000 lb/ac and 3500 lb/ac) for case studies 1 and 2, respectively. Farmer-1 decreases net return by 60%, payback increases by 10 cycles, and the return on investment was decreased by 9%. While for farmer-2 the low-inputs net return increases by 39%, and payback cycle and ROI were not available for farmer-2 since the net return was negative.

The HCC was \$3106 for the 80 ac field with a cost of \$39/ac and contributed to 31% of the total cost for farmer-1. While for farmer-2, the HCC was \$1728 for the 40 ac with a cost of \$43/ac and contributed to 28% of the total cost, respectively. The values of HCC/ac of 34% and 29%, which are not substantial (say >50%) makes sense to harvest and collect the forage bales, otherwise leaving the crop in the field would reduce the profit or further increase the loss. Overall, based on these two case studies the accuracy of the developed tool was highly satisfactory, and more case studies further establish the accuracy of the analysis.

4.5.3. ABP Inclusion in Case Studies

As both farmers have not used the ABP in their enterprise, a scenario analysis was conducted to study this additional equipment purchase decision. In this analysis, the ABP collected 8 BPT while the tractor collected 2 BPT, with all other inputs remaining the same. Changing the BPT from 2 to 8 alone affected bale collection logistics distance, operation time, fuel consumption, net return, break-even ratio, and payback period (table 4.3).

Results of ABP inclusion in the two farmers' case studies indicated that, on average, the total logistics distance for bale collection decreased by 4.7 times, and the operation

Table 4.3. Effect of including automatic bale picker (ABP) in case studies.

Case studies	Logistics and economics	Tractor (2 bales/trip)	ABP (8 bales/trip)
Farmer-1 (80 ac, Sioux County, ND; Alfalfa, perennial 5-years)	Logistics distance (mi)	35.0	7.4
	Operation time (h)	7.0	1.5
	Fuel consumption (gal)	20.4	15.7
	Net return (\$/ac)	92	94
	Payback period (cycle)	7	2.6*
Farmer-2 (40 ac, Morton County, ND; Bromegrass, annual 1-year)	Logistics distance (mi)	8.2	1.8
	Operation time (h)	1.6	0.4
	Fuel consumption (gal)	4.6	4.3
	Net return (\$/ac)	-38	-38
	Payback period (cycle)	NA	NA

Note: * Payback period (cycle) for ABP equipment only.

time decreased by 78 % using 8 BPT in comparison to the traditional 2 BPT. Since total labor cost is influenced by the time required to collect and transport bales, a considerable reduction in cost by using ABP was observed as well. The fuel consumption is proportional to the bale load, so for case studies 1 and 2, the fuel consumption decreased by 23 % and 8 %, respectively. The net return increased on average by 1.5 % from using ABP instead of a traditional tractor in the field areas of 40 ac (16.2 ha) and 80 ac (32.4 ha). However, the equipment purchase scenario analysis results showed (section 4.6.1) that the net return using ABP increased significantly over a traditional tractor for field areas above 160 ac (65 ha) prominently.

4.6. Scenario Analysis

The FECWT allows users to perform many kinds of scenario analyses by simply adjusting the input values, either by choosing a different input value within the provided default range or by altering the range itself to suit the user's requirement. Scenario analysis using the FECWT, with its useful defaults and well-defined set of assumptions, will help users gain insight into different cases (practical or hypothetical). To further illustrate the

FECWT's scenario analysis capabilities, next we explore and provide answers to questions such as: 1. "Should I purchase an ABP for bale collection?," 2. "Which major forage crop type is more profitable, or how do the forage crops rank on economic standpoint?," and 3. "How much net return to land and management will be possible for farm operators (typical drylands agriculture of perennial forages) who do not use fertilizer, chemical and/or seed based on the type of forage grown?"

4.6.1. Equipment Purchase Decision Scenario

Bale collection activity is conventionally performed using a tractor where a spear or grappler attachment is fixed to the tractor. A maximum of 2 bales can be collected during a single trip using the tractor. Conversely, the ABP's bale capacity ranges from 8 to 23 in a single trip, thus reducing the bale collection time and fuel consumption which is reflected in the cost savings of labor and fuel. Based on commercial market rates, the cost of an ABP machine with 8 BPT capacity for 5×6 feet bale size was fixed at \$20 000.

The scenario analysis used the payback period as the measure to help farmers with the equipment tractor (2 bales) and ABP (8 bales) purchase decision. Payback period is estimated using profit and the equipment cost. The effect of field area (8, 32, 65, 129, and 259 ha) on the payback period (i.e., number of cycles) was studied for the following equipment scenarios: (i) combined tractor and ABP, (ii) tractor only, and (iii) ABP only (fig. 4.5). Tractor being the major piece of equipment, its contribution to the payback period is obviously much greater than the ABP (minor equipment).

Other inputs in calculating the payback period were considered from the case study of farmer-1 (table 4.2). The scenario, which considered only the ABP purchase as an additional piece of equipment, assumed that the farmer already has a tractor — a common

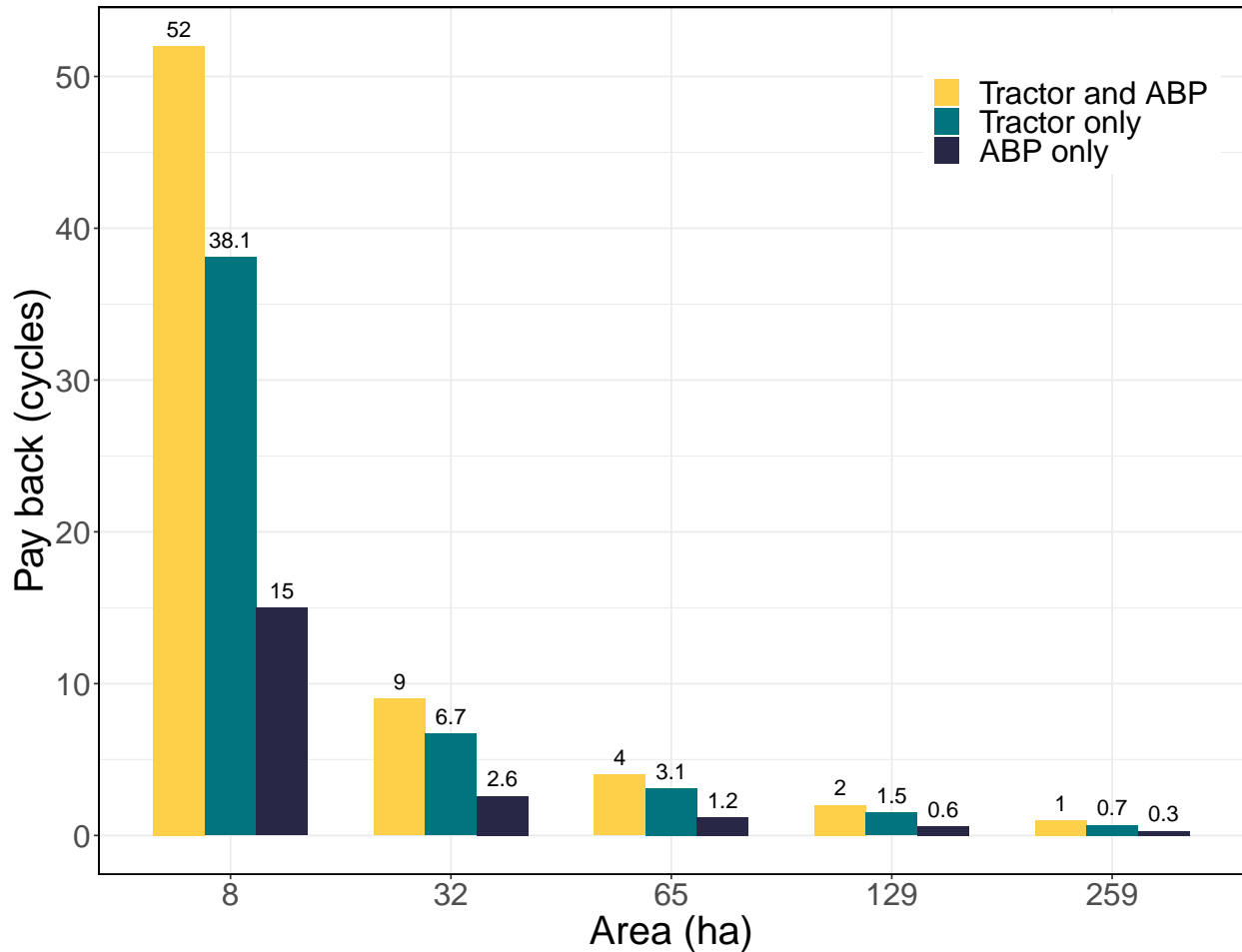


Figure 4.5. Equipment purchase scenario analysis for alfalfa forage crop: Effect of field area sections (8, 32, 65, 129, and 259 ha) on payback period (cycles) for equipment: tractor and ABP, tractor only, and ABP only. Tractor only = 2 BPT; ABP only and tractor and ABP = 8 BPT.

scenario among traditional farmers and ranchers. The payback period in cycles for the ABP equipment only was <2.6 for 32 ha (80 ac) and was <1.2 for field areas ≥ 65 ha (≥ 160 ac; fig. 4.5). If tractor alone (new model for example) should be purchased, the payback period will be 6.7 cycles for 32 ha and ≤ 3 for ≥ 65 ha. The payback period for the combined tractor and ABP also decreased with an increase in the field areas. The recommendation for the equipment purchase decision is to purchase the ABP if the field area is ≥ 32 ha, and a new tractor (independent of the ABP decision) if the area is ≥ 65 ha (≥ 160 ac).

4.6.2. Forage Crop Type Scenario

Comparison among the selected forage crops (grass and alfalfa) and grain-forage (millet, oats, wheat, barley, and corn) was performed based on the revenue streams/ac, total revenue/ac, total cost/ac, and net return/ac (fig. 4.6). The grain yields and prices (year 2020) we used were based on average values reported in the 2020 National Agricultural Statistics Service database for North Dakota (Jantzi et al., 2020). The lower and upper bounds of forage yield (defaults in the input panel) for grain crops were determined using the established harvest index (ratio of grain to straw yield; McCartney et al. (2006)). The cost values for seed, chemical, and fertilizer for forage and grain crops were obtained from the farm financial management database for ND in 2020 (FINBIN, 2020). Other inputs for the development of the scenario were obtained from the case study for farmer-1 (table 4.2).

The net return/ac for grain crops (millet, oats, wheat, barley, and corn) was always higher for the forage crops (grass and alfalfa), because it includes revenue streams from both grain and forage (i.e., what some refer to as crop aftermath). Revenue from the grain stream for grain-forage crops is substantial, so it easily covers the production cost of grain and forage; revenue from the forage then generates additional income. The grain revenue stream ranged between 80.4% to 89.7% of the total revenue, and the ratio of grain revenue to the total cost ranged between 1.3 to 2.0 indicating cost recovery. When ratios of net return to total cost were compared (again assuming 2020 prices and data from the case study farmer-1), the best crop was corn (1.44) followed by barley (0.98), oats (0.90), alfalfa (0.89), wheat (0.88), millet (0.43) and grass (0.35). It should also be noted that all the crops studied made a profit but to varying degrees (fig. 4.6).

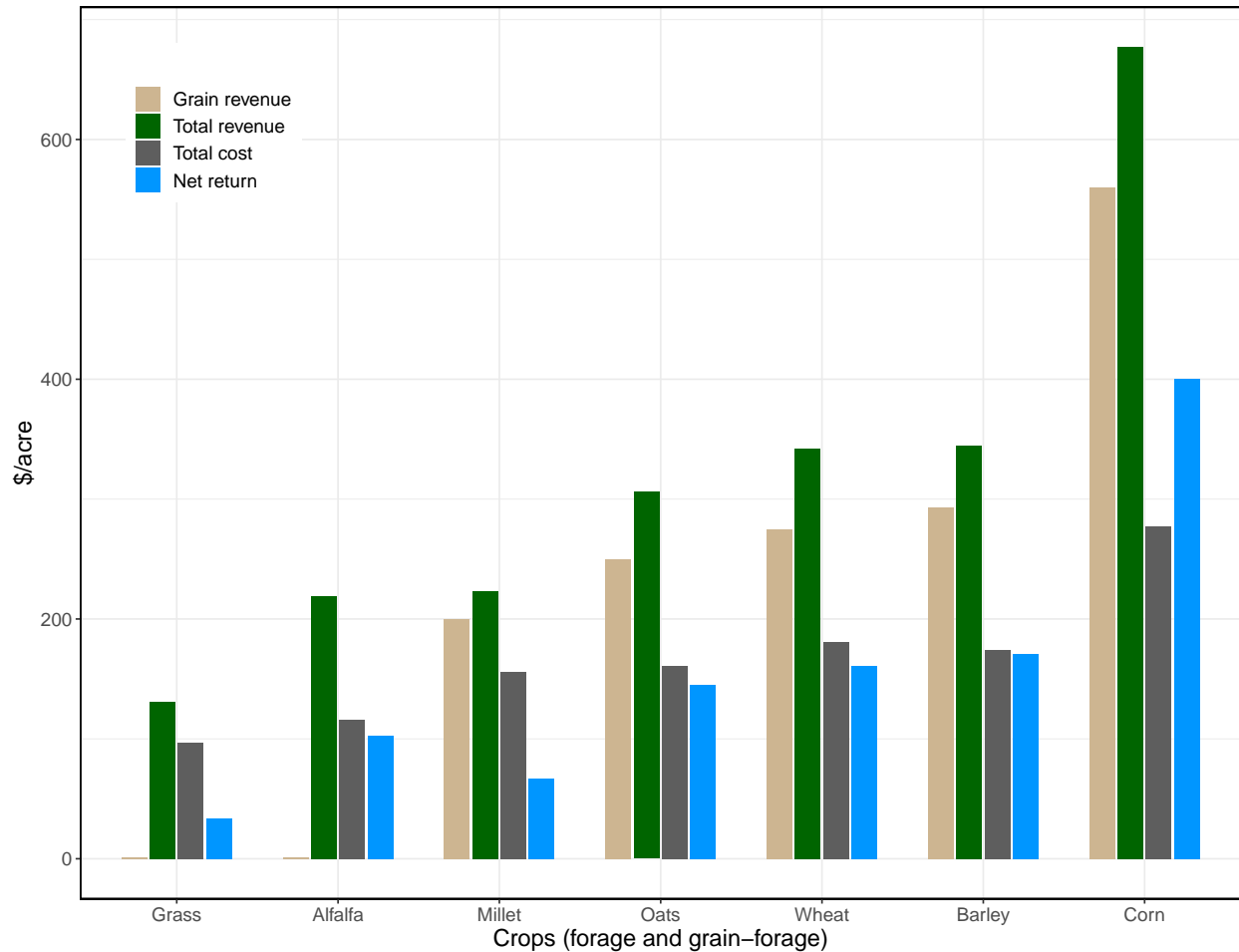


Figure 4.6. Forage crop type net return scenario: Effect of forage crop types (exclusive forage and grain-forage crops) economics showing grain revenue, total (grain + forage) revenue, total cost, and net return.

Alfalfa is a dominant perennial forage crop with high yield potential and value; therefore, the average net return per acre for alfalfa forage is 3 times that of grasses and grass mix varieties. Furthermore, comparable net return was observed for alfalfa and certain grain crops (millet, oats, wheat, and barley) considering the net return was only from the forage; that is, if a grain-forage crop is being grown strictly for forage, then its net return would be similar to that for alfalfa. While alfalfa is the most profitable forage

for this case study, corn is the yields most profit with forage among the grain-forage crops; however, the choice of crop is based on the field conditions and investment availability.

4.6.3. Low-Inputs Scenario

4.6.3.1. High- and low-yielding forage crops comparison

Low-inputs scenarios for the two forage crops: (i) alfalfa — a high-yielding forage crop wherein seed+seeding cost was included (required after every 5-year cycle) while the combined fertilizer and chemical applications costs were set to \$0; and (ii) grass — a low-yielding and low-maintenance perennial forage crop wherein all the associated costs of seed+seeding (naturally grown grasses do not require seeding), and combined fertilizer and chemical applications were set to \$0, were analyzed. It should also be noted that some of the high-value grasses need seeding at necessary intervals. The analysis results of these forage crops for a minimum and maximum field area (8 and 259 ha) with various percents of potential yield are presented in Figure 4.7. The highest forage potential yield for alfalfa and grass were assumed to be 5000 lb/ac and 3000 lb/ac, respectively, while utilizing the other inputs from case study 1 for the analysis (table 4.2). Linear trends of low-input net return increase with percent potential yield were observed at both minimum (8 ha) and maximum (259 ha) field areas for both crops considered. The shaded area between the limiting linear trends represents the net return for the other field areas with the corresponding linear trends.

For alfalfa the positive net returns occur around 53 % and 43 % (fig. 4.7A), and for grass around 64 % and 51 % (fig. 4.7B) with 8 ha and 259 ha, respectively. Overall, it can be observed that alfalfa generates positive net returns with the low-inputs scenario from about 45 % yield potential and for grass from about 51 %. It was also observed that the

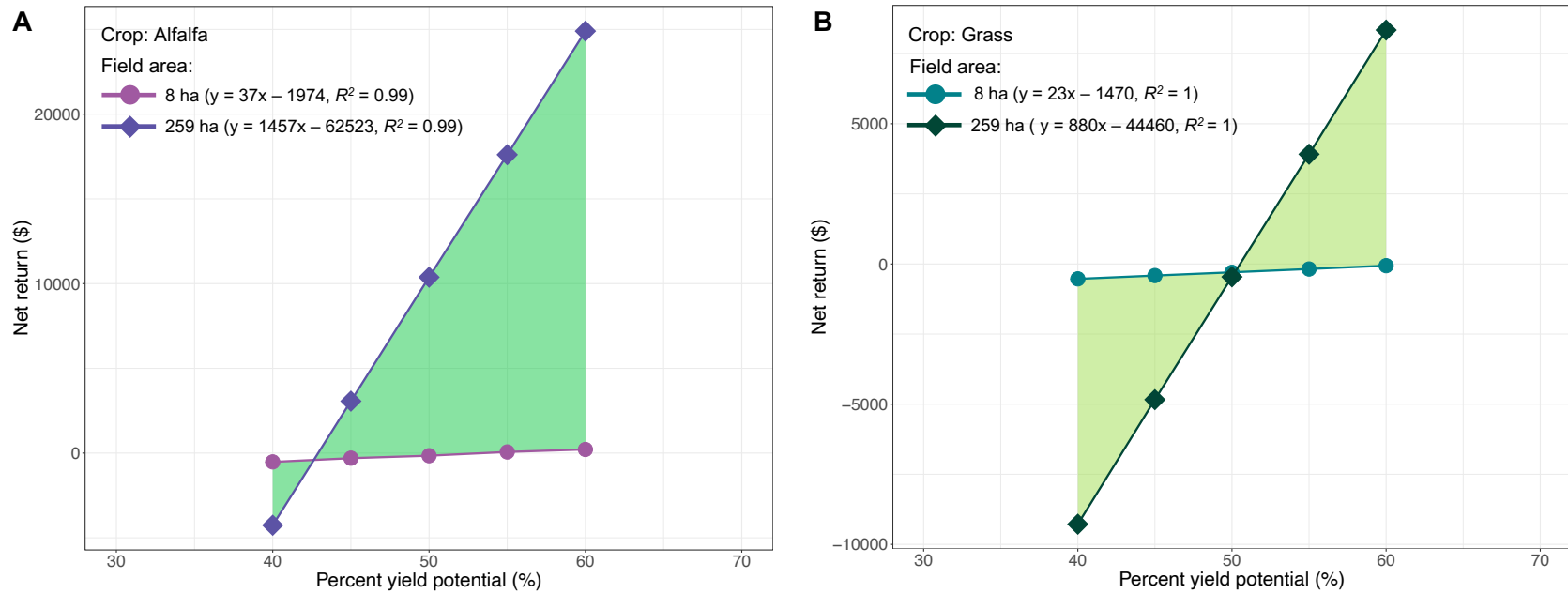


Figure 4.7. Low-inputs scenario analysis for alfalfa and grass on the effect of forage percent yield potential (alfalfa: 5000 lb/ac; grass: 3000 lb/ac) on net return for tractor only (bales/trip = 2) for field areas between 8 and 259 ha.

slopes for smaller field areas are smaller with \$23 and \$37 per percent yield potential than the larger areas with \$880 and \$1457 per percent yield potential, respectively for grass and alfalfa, indicating better net returns at larger field areas with an increase in percent potential yield.

4.6.3.2. Normal and low-inputs net return comparison for alfalfa

To determine how the low-inputs net returns compare with normal use of inputs (includes fertilizers, and chemicals cost), alfalfa crop was analyzed for different field areas ranging from 8 to 259 ha (20 to 640 ac) with highest forage potential (5000 lb/ac), while other input values were considered from case study 1 (table 4.2). The normal net return was on average 8.4 ± 2.2 and 7.9 ± 2.0 times higher than the low-inputs net return, indicating that application of fertilizer and chemical contributes to $88 \% \pm 3 \%$ and $87 \% \pm 3 \%$ of the net return for tractor (BPT = 2) and ABP (BPT = 8) (ignoring negative net return values), respectively, by increasing the forage yield (fig. 4.8). The low-inputs net return and normal net return for ABP were always slightly higher than tractor as expected; however, a noticeable difference between in low-inputs and normal net return values was observed only for field areas ≥ 65 ha (≥ 160 ac).

The recommendation based on the low-inputs scenario is to cultivate forage on larger field areas and by applying fertilizers and chemicals in addition to the naturally available forage to increase the forage yield. Although there are costs involved with fertilized and plant protection controlled forages, the net return from the increased forage yield is significant when compared to the net return from naturally grown forage with fewer inputs.

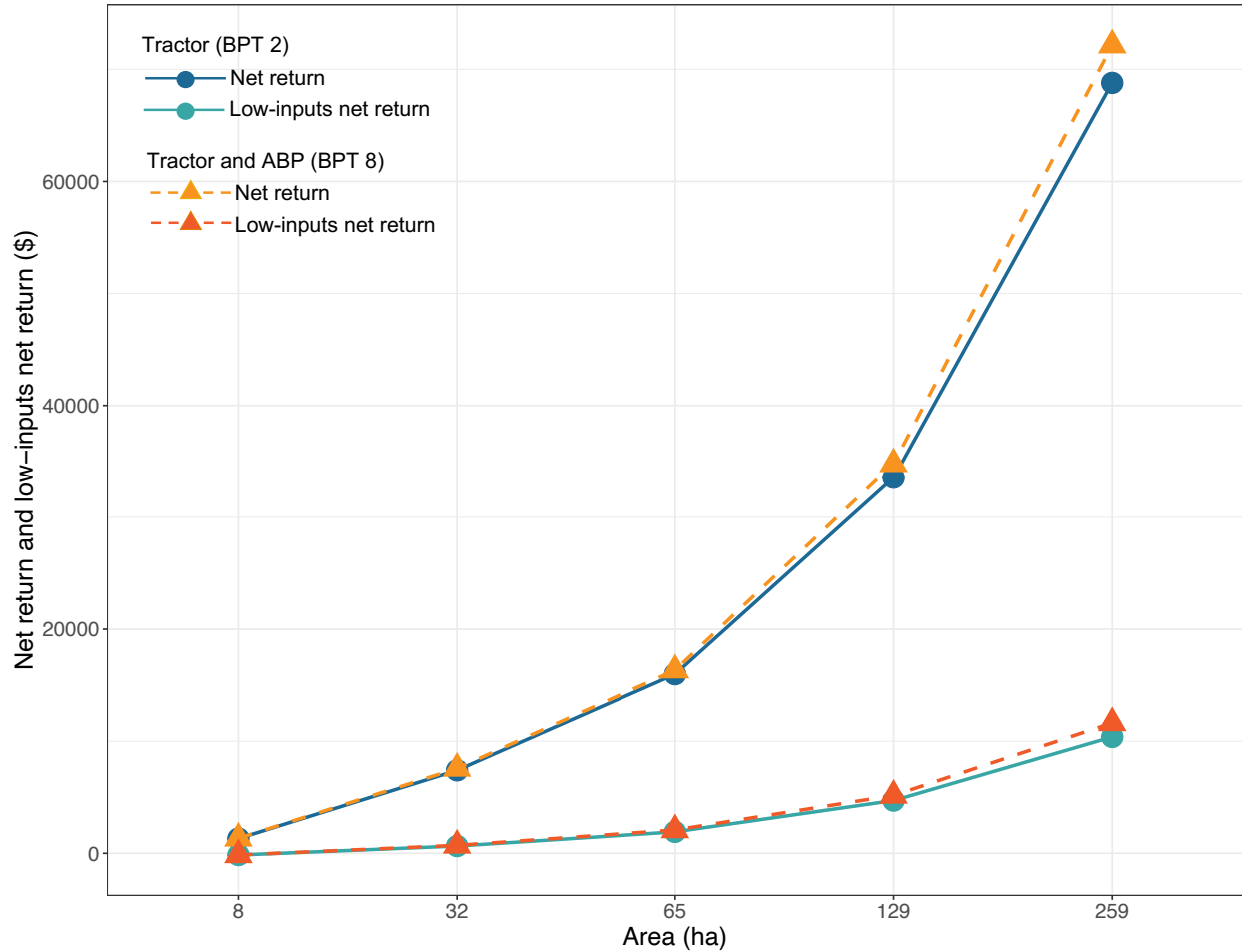


Figure 4.8. Low-inputs scenario analysis with 50 % forage yield potential (2500 lb/ac) for alfalfa crop: Effect of field area sections (8 ha–259 ha) on normal net return and low-inputs net return for tractor only (bales/trip = 2) and tractor and automatic bale picker (ABP) combined (bales/trip = 8).

4.7. Conclusions

In this study, we developed a forage economics calculator web tool (FECWT) to analyze the economics of various scenarios for forage and grain-forage crop decisions, requiring minimal user interaction guided by complete user instructions and user-manual. The tool interface was designed with user-friendly input features (drop-down choices, text input, and slider) to suit the target users, such as farmers, hay producers, custom hay

operators, agricultural extension, financial personnel, and anyone else interested in the economics of handling bales. The inputs included biophysical production parameters along with costs and prices associated with the forage enterprise. Economic results calculated by the tool were net return, break-even ratio, payback period, and return on investment. The tool allowed for various decision analyses, such as equipment purchase (tractor vs automatic bale picker, ABP), the sensitivity of profit to what-if scenarios. The FECWT presents results onscreen as values and dynamic charts, which were also made available as downloadable report and chart.

Case studies involving farmers with actual field inputs were used to test the applicability of FECWT. Case study results from two farms conformed well with the farmer's own field records and the tool's performance was highly satisfactory. Additional scenario analysis was conducted on the inclusion of ABP in the two case studies. This revealed that larger field areas (≥ 65 ha or ≥ 160 ac) or higher-yielding and higher-value crops (e.g., alfalfa, grain-forage crops) could help increase the case-study farmers' profits.

Some findings of the scenario analysis from practical case studies and hypothetical situations were: (i) ABP equipment purchase for field areas ≥ 65 ha (≥ 160 ac) was profitable; (ii) among the crop types, alfalfa and corn was the most profitable forage and grain-forage options; (iii) low-inputs (no fertilizers, chemicals, and/or seeds) net return for alfalfa and grass decreased by 8.4 and 7.9 times, respectively at 50% yield potential suggesting the use of all inputs; however, the low-inputs scenario produces positive net returns with increased field areas ≥ 65 ha.

The FECWT can be further developed to include other forage types with relevant data and other regions. More sophisticated web tool features, such as individual pro-

file creation with username and password security, data archiving, and data management should also be considered. Further testing with more case studies using different forage crops will help in determining the accuracy of the tool.

4.8. References

- Anderson. (2008). *Anderson group: World's first self-loading bale carrier capable of handling round bales efficiently*. Retrieved March 14, 2022, from <https://grpanderson.com/en/comparator/?c=round-bales/>.
- Angima, S. (2007). *Fertilizing For Hay Production*. Retrieved March 14, 2022, from <https://extension.oregonstate.edu/crop-production/pastures-forages/fertilizing-hay-production/>.
- ASABE. (2011). ASABE. Standard D497.7: Agricultural machinery management data. *ASABE, St. Joseph, MI, USA, 9–10*.
- Barnett, K. (2009). *Hay Price Calculator - University of Wisconsin-Madison: Team Forage, Division of Extension*. Retrieved March 14, 2022, from <https://fyi.extension.wisc.edu/forage/economics/>.
- Bismanonline. (2020). *Bismanonline: Hay/Feed/Seed sale price*. Retrieved March 14, 2022, from https://www.bismanonline.com/hay_feed_seed?/.
- Brence, L., & Griffith, D. (2012). *Montana State University Extension Economics*. Retrieved March 14, 2022, from <https://tinyurl.com/4naemjn7/>.
- Da Rocha, H. (2019). *Learn chart.js: Create interactive visualizations for the web with chart.js 2*. Packt Publishing Ltd, 35 Livery Street Birmingham B3 2PB, UK.
- FINBIN. (2020). *Farm Financial Management Database*. Retrieved March 14, 2022, from <https://finbin.umn.edu/>.

- Hickson, I., & Hyatt, D. (2011). HTML 5. Apple Computer, Inc., Mozilla Foundation, and Opera Software ASA.
- Horrocks, R. D., & Valentine, J. F. (1999). *Harvested Forages*. Academic Press, Cambridge, MA, USA.
- Jantzi, D., Hagemeister, K., & Krupich, B. (2020). *North Dakota Agricultural Statistics 2020*. Retrieved March 14, 2022, from <https://tinyurl.com/2p8njx3r/>.
- JD. (2006). *John Deere: Mid-size tractors 5015 series with 41 kW (55 hp) to 59 kW (80 hp)*. Retrieved March 14, 2022, from <https://tinyurl.com/yhv7yn6p/>.
- Khalilian, A., Batchelder, D., Self, K., & Summers, J. (1985). Revision of fuel consumption equations for diesel tractors. *ASAE Tech. Pap.*, 1522(CONF 841278).
- Kirwan, B. (2020). *NRCS - Hay Production vs. Buying*. Retrieved March 14, 2022, from <https://www.nrcs.usda.gov/wps/portal/nrcs/main/national/technical/econ/tools/>.
- Mahindra. (2018). *Mahindra USA: 110 and 120 hp tractor with more performance, power, and value*. Retrieved March 14, 2022, from <https://www.mahindrausa.com/--series-tractor-9000/>.
- McCartney, D., Block, H., Dubeski, P., & Ohama, A. (2006). The composition and availability of straw and chaff from small grain cereals for beef cattle in western Canada. *Can. J. Anim. Sci.*, 86(4), 443–455.
- Mikkonen, T., & Taivalaari, A. (2007). Using javascript as a real programming language. Sun Microsystems, 16 Network Circle Menlo Park, CA, USA.

- Nayigihugu, V., Schleicher, A., Koch, D., Held, L., Flake, J., & Hess, B. (2007). Beef cattle production, nutritional quality, and economics of windrowed forage vs. baled hay during winter. *Agron. J.*, *99*(4), 944–951.
- NDG. (2020a). *2020 County Rents and Prices North Dakota*. Retrieved March 14, 2022, from <https://www.land.nd.gov/resources/north-dakota-county-rents-prices-annual-survey/>.
- NDG. (2020b). *North Dakota Agriculture by the Numbers*. Retrieved March 14, 2022, from <https://tinyurl.com/2p963fcf/>.
- NDSU. (2020). *NDSU Feedlist: Feed For Sale/Donation*. Retrieved March 14, 2022, from <https://www.ag.ndsu.edu/info/feedlist/>.
- Powell, T. A. (2010). *HTML & CSS - The Complete Reference Fifth Edition*. McGraw-Hill, 1325 Avenue of the Americas, New York City, NY, USA.
- Spurlock, J. (2013). *Bootstrap: Responsive Web Development*. “O’Reilly Media, Inc.”, Sebastopol, CA, USA.
- Subhashree, S. N., Igathinathane, C., Bora, G. C., Ripplinger, D., & Backer, L. (2017). Optimized location of biomass bales stack for efficient logistics. *Biomass Bioenerg.*, *96*, 130–141.
- Subhashree, S. N., Igathinathane, C., Liebig, M., Halvorson, J., Archer, D., Hendrickson, J., & Kronberg, S. (2021). Biomass bales infield aggregation logistics energy for tractors and automatic bale pickers – A simulation study. *Biomass Bioenerg.*, *144*, 105915.

5. BIOMASS YIELD PREDICTION FOR PASTURES USING REMOTELY SENSED VEGETATION INDEX AND CLIMATE DATA THROUGH MACHINE LEARNING *

5.1. Abstract

Uncertain climate conditions such as extreme drought in native rangeland, pastures, and hay land reduce production up to 80 %, which leads to forage shortages for livestock producers. Predicting forage biomass yield is critical in managing livestock since it impacts livestock stocking rates, the amount of hay purchased, and livestock marketing strategies. Only a few biomass yield prediction studies on pasture and rangeland exist despite this need. Therefore, this study focused on developing a biomass yield prediction methodology through remote sensing satellite image (multispectral bands) and climate data using open-source software technologies. Biomass ground truth data were obtained from local pastures. Remote sensing data included spatial bands (6 predictors) and vegetation indices (VI, 30 predictors) estimated from the Landsat, Sentinel, and CubeSat satellites (3–30 m resolution). The climate data (NDAWN) included precipitation, turf soil temperature, mean temperature, mean dew point temperature, and others (16 predictors). To model the complex non-linear relationship between the biomass and the spatial and data, a potential approach of machine learning (ML) was followed for feature selection and prediction modeling. Recursive feature elimination (RFE) emerged as the best ML

* This paper will be submitted to the *Biomass and Bioenergy* journal in 2022. Authors: Srinivasagan N. Subhashree, C. Igathinathane, A. Akyuz, J. Hendrickson, D. Archer, M. Liebig, J. Halvorson, S. Kronberg, D. Toledo, K. Sedevic, and D. Peck. Subhashree performed the systematic literature review and wrote the manuscript. Dr. Igathinathane Cannayen is the major advisor, principal investigator, and the corresponding author who worked with Subhashree throughout the research and manuscript development. All the co-authors have assisted in the research direction and review of the manuscript.

feature selection method among others tested (Boruta and backward elimination). The top-ranked features (52 tested) from RFE were short wave infrared 2, normalized difference moisture index, and average turf soil temperature. The random forest ML model produced the highest accuracy ($R^2 = 0.83$) among others tested (support vector machine, k-Nearest neighbor, and multiple linear regression) for biomass yield prediction. Applications of the selected methodology (RFE and RF) revealed that (i) the methodology is equally applicable to other unseen pastures ($R^2 = 0.79$), (ii) finer satellite spatial resolution (e.g., CubeSat; 3 m) was better in predicting pasture biomass, (iii) the methodology extended successfully to high-value alfalfa hay crop with good yield prediction accuracy ($R^2 = 0.96$). Future research scopes include the application of the proposed methodology on a large scale, other species, use of hyperspectral images and unmanned aerial vehicles, and development of an interactive tool. Thus it can be recommended that the developed methodology of using remotely sensed images with climate data and using RFE for feature selection and RF for biomass yield modeling for biomass and hay forage yield prediction.

5.2. Introduction

In Northern Great Plains (NGP), rangeland forage productivity is greatly influenced by climatic factors such as precipitation and temperature (Lupo et al., 2013). North Dakota, located northeast of NGP, has a continental climate and experiences naturally occurring drought and significantly varying temperatures. Local ranchers and livestock producers deal with the challenge of forage availability under these typical varying climatic conditions. Therefore, timely forage biomass production estimation during the growing season in rangeland and pastures can aid in making efficient management decisions for livestock production.

Despite this need, only a few studies on biomass yield monitoring and prediction for pasture and rangeland exist. These studies relied on a traditional destructive method of recording biomass production, which involved hand clipping and drying the biomass from the randomly placed quadrats across a large landscape (Catchpole and Wheeler, 1992; Ma et al., 2019). This traditional method is highly time-consuming, therefore, not performed frequently during the growing season. However, continuous monitoring of the biomass production data aids the ranchers in making and adapting real-time management decisions.

Remote sensing (RS), an alternative methodology, has proved effective in nondestructive, extensive, and repetitive coverage of land areas, making it the perfect technology for continuous monitoring of growth in rangeland and pastures. The RS data includes imagery from satellite and UAV platforms. Visible, thermal, multispectral, and hyperspectral bands captured by the RS sensors were used to validate the clipped biomass (Aparicio et al., 2000; Lussem et al., 2018). Over the last few years, the high spatial and temporal resolution satellites, such as Landsat, Sentinel, and CubeSat satellite platforms having respective 30, 10, and 3 m spatial resolution, are freely available and increasingly accessible, which makes periodic yield monitoring achievable. Some of the free imagery sources for these satellites are Google Earth Engine, PlanetScope Inc., and U.S. Geological Survey.

Satellites record multispectral bands, including visible, near-infrared (NIR), short-wave infrared imagery (SWIR), and were used to estimate vegetation indices (VIs). These indices provided indications to the vegetation characteristics such as greenness, photosynthetic activity, and moisture content (Gómez et al., 2021; Ji and Fan, 2019; Safi et al., 2022). Some of the most commonly used VIs are normalized difference vegetation index

(NDVI), enhanced vegetation index (EVI), and atmospherically resistant vegetation index (ARVI), among many others (Xue and Su, 2017). The effect of climate variables on crop growth has been extensively documented, and long-term studies showed a strong relationship between climate and plant growth (Zhihui et al., 2016). In addition to climate, soil plays an imperative role in affecting the growth of plants; warm soil temperature induces better water and nutrient uptake and contributes to the overall plant growth (Onwuka and Mang, 2018).

Biomass yield is a combination of spatial and temporal changes, and the variability can be captured by satellite, climate, and soil data (Meng et al., 2021). The data (satellite, climate, and soil) are strongly linked and present themselves as nonlinear and complex interaction in predicting crop yield. Complex interactions among the dependent and independent variables, in recent times, have been widely analyzed using machine learning (ML) therefore ideal for agricultural applications. The ML models have been suitable for applications such as crop yield predictions, nutrient management, species identification, weed detection, and many others (Subhashree et al., 2020; Timsina et al., 2021; Van Klompenburg et al., 2020).

In general, a better performance by ML models was reported than by traditional linear regression models (Belayneh et al., 2014; Cai et al., 2019; Guzmán et al., 2018). The essential factors of yield estimation using ML were: (i) identification of the most important independent variables using feature selection methods (ii) development of suitable prediction models, and (iii) calibration and validation of the developed ML models.

Selection of important climate, soil, and VI (satellite) features for crop yield prediction was performed using feature selection methods such as Boruta, recursive feature

elimination, information gain, sequential feed-forward selection, Relief, and many others (Gopal and Bhargavi, 2018; Prasad et al., 2021; PS, 2019). Among the developed ML models, random forest (RF) has been widely used in predicting crop and forage biomass yield predictions (López-Calderón et al., 2020; Ramoelo et al., 2015; Zimmer et al., 2021). Many studies involving soil, climate, and VIs have reported good performance using support vector regression (SVR) in predicting yield (Kamir et al., 2020; Kuwata and Shibasaki, 2016). For instance, for predicting winter wheat yield in China using climate, soil, and remote sensing data, SVR emerged as one of the best ML models (Han et al., 2020). Several studies have also tested the performance of k-nearest neighbor (kNN) methods for yield prediction (Ahamed et al., 2015).

With this background and research opportunity, a study was designed to develop yield prediction models for the pasture biomass using climate and satellite-based multispectral images that help the forage producers and ranchers. The specific objectives for pasture biomass prediction included (i) determining the potential use of using climate variables and multispectral images (non-destructive method) for biomass prediction; (ii) identifying and recommending an overall methodology of the best features selected and ML model based on the prediction accuracy, (iii) investigating the effect of satellite spatial resolution among Landsat, Sentinel, and CubeSat for biomass prediction; and (iv) evaluating the adaptability of the recommended methodology (features + trained ML model) for additional unseen pastures and alfalfa forage hay crop.

5.3. Materials and Methods

5.3.1. Study Site Description

The study sites were located at the Northern Great Plains Research Laboratory (NGPRL; USDA-ARS), Mandan, North Dakota 46°46'12"N 100°55'59"W; fig. 5.1). North Dakota receives peak precipitation occurring during June–July (3–4 inch). The average high temperature was recorded in July (28 °C), and the average low temperature recorded was January (−2 °C).

The NGPRL site included three pastures, out of which two were native vegetation pastures and the rest was seeded forage pasture (Liebig et al., 2013). The former two are historical pastures: (i) heavily grazed pasture (HGP; 2.8 ha) and (ii) moderately grazed pasture (MGP; 15.4 ha), were initiated in 1916 and maintained without applying fire, fertilizer, or herbicides. The crested wheatgrass pasture (CWP; 2.6 ha) once native was seeded in 1932. Vegetation in MGP was dominated by Kentucky bluegrass (*Poa pratensis* L.), an invasive cool-season grass. Blue grama [*Bouteloua gracilis* (Willd. ex Kunth) Lag. ex Griffiths], a warm-season native grass, dominated the HGP pasture until 2010 and was too dominated by the Kentucky bluegrass. A mix of crested wheatgrass [*Agropyron desertorum* (Fisch. ex Link) J.A. Schultes] and Kentucky bluegrass can be found in CWP. Among the pastures, the data from the MGP pasture was used to train the prediction models, while CWP and HGP data were used for model testing.

5.3.2. Data Acquisition

The whole process methodology followed in the study that includes data extraction, data preprocessing, and model development is depicted in Figure 5.2. Various details of the processes involved are described subsequently.

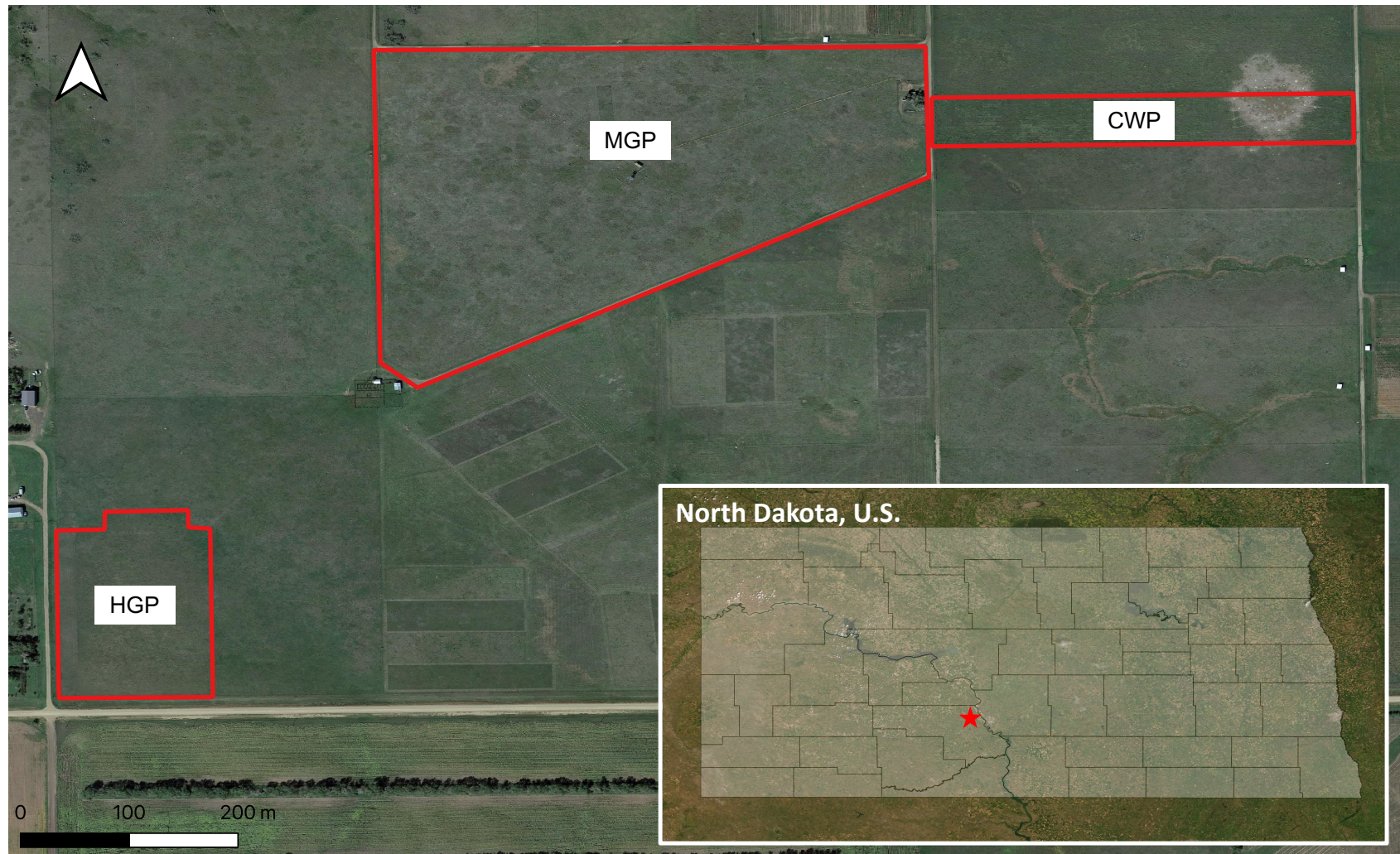


Figure 5.1. Study site pastures located at Northern Great Plains Research Laboratory (NGPRL; USDA-ARS), Mandan, ND. Polygonal shapefiles of the study pastures are overlaid on the map. CWP: crested wheat pasture, HGP: highly grazed pasture, MGP: moderately grazed pasture. Inset: Mandan, ND, USA.

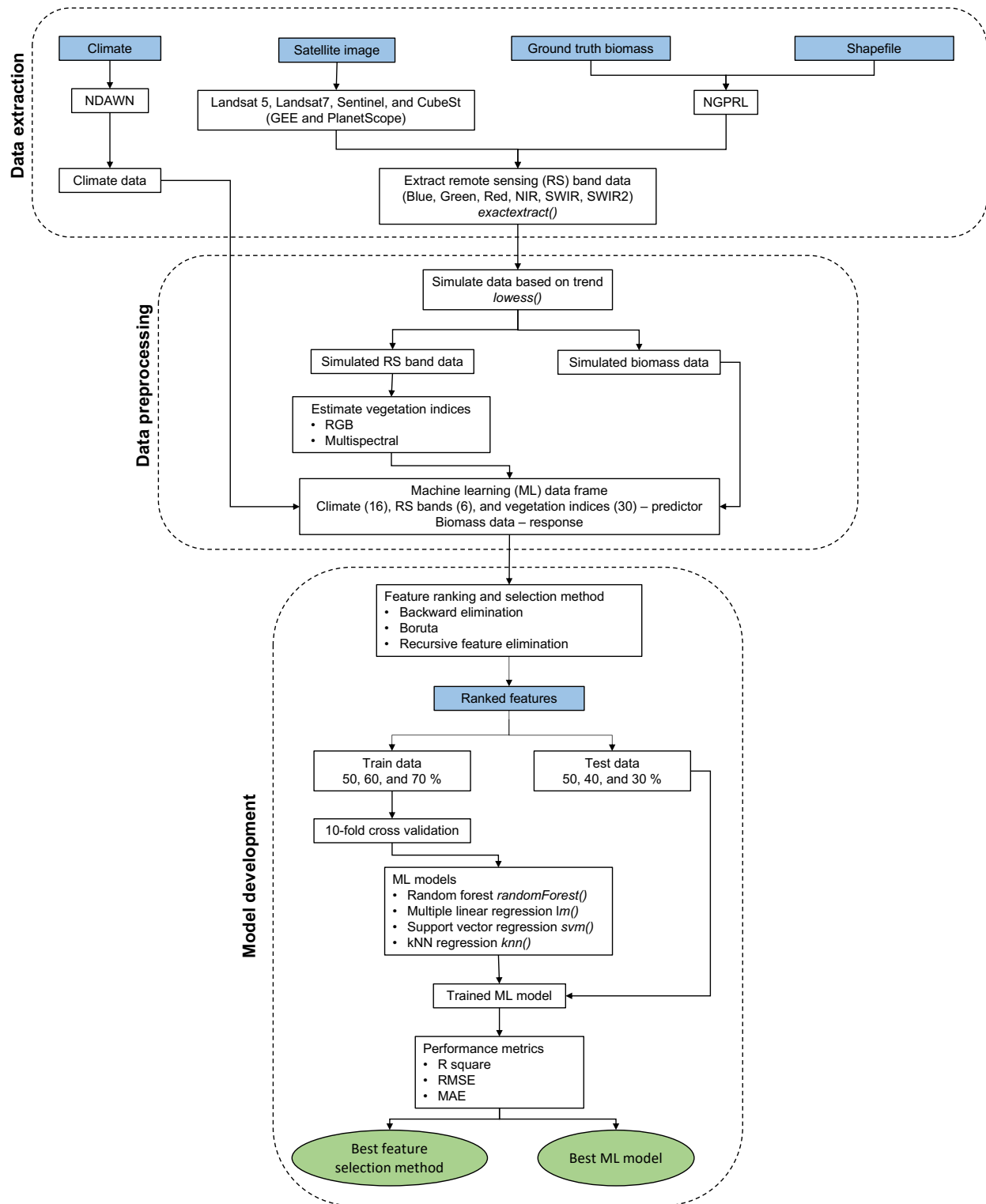


Figure 5.2. Overall process methodology including data extraction, processing, and developing biomass prediction models using climate and remote sensing data. NDAWN - North Dakota Agricultural Weather Network and NGPRL - Northern Great Plains Research Laboratory.

5.3.2.1. Ground truth biomass data

The forage data at NGPRL was collected as aboveground live biomass every 2-3 weeks from mid-April to late September or mid-October (growing season) in the CWP, HGP, and MGP pastures for the years 2004–2006 and 2017–2018. The biomass was clipped from four representative samples using 0.25 m² quadrats. The collected biomass was dried at 60–80 °C and weighed for moisture content measurements.

5.3.2.2. Climate and soil data

The pastures' local weather data were obtained from North Dakota Agricultural Weather Network (NDAWN). The weather station located at NGPRL, Mandan, ND, in this network was selected, where the data were available from 1999 to the present. Since the pastures were not far from each other, the same weather data was used. Monthly data were obtained for nine climate and soil variables: average air temperature, bare soil temperature, turf soil temperature, wind speed, dew point, and chill and total values of solar radiation, potential evapotranspiration (PET), and rainfall (table 5.1). This monthly weather data was exported as a CSV file, a format suitable for reading and processing.

5.3.2.3. Satellite image data

The remote sensing data for 2004–2006 (NGPRL study site) was retrieved from the Landsat archive of the Google Earth Engine (GEE) using JavaScript (Appendix E.2). The Landsat images were available once every two weeks from 1972 to the present day and provide satellite images of the earth's surface using seven spectral bands at 30 m spatial resolution. Satellite data for the pastures was obtained by creating a rectangular extent (as JSON) including all three pasture areas (CWP, HGP, and MGP) for the three years from

Table 5.1. Climate and remote sensing data considered for the study.

Remote sensing data (Satellite platforms)					Climate data (NDAWN)			
No.	Parameter	Abbreviation	Availability			No.	Parameter	Abbreviation
			Landsat	Sentinel	CubeSat			
<u>Surface reflectance bands</u>					<u>Weather variables</u>			
1	Blue (0.45–0.52 μm)	B	✓	✓	✓	37	Air temperature (minimum, °C)	Min_T
2	Green (0.52–0.60 μm)	G	✓	✓	✓	38	Air temperature (average, °C)	Avg_T
3	Red (0.63–0.69 μm)	R	✓	✓	✓	39	Air temperature (maximum, °C)	Max_T
4	Near infrared (0.77–0.90 μm)	NIR	✓	✓	–	40	Air temperature (diurnal range, °C)	Di_TR
5	Short-wave infrared 1 (1.57–1.75 μm)	SWIR1	✓	✓	–	41	Bare soil temperature (°C)	AvgB_Soil
6	Short-wave infrared 2 (2.09–2.35 μm)	SWIR2	✓	✓	–	42	Turf soil temperature (°C)	AvgT_Soil
<u>Color vegetation Indices</u>					<u>Wind variables</u>			
7	Red chromatic coordinate	RCC	✓	✓	✓	43	Wind speed (average, km/h)	Avg_WindS
8	Green chromatic coordinate	GCC	✓	✓	✓	44	Wind speed (maximum, km/h)	Max_WS
9	Blue chromatic coordinate	BCC	✓	✓	✓	45	Wind direction (average, °)	Avg_WD
10	Excess green	ExG	✓	✓	✓	46	Total solar radiation (Ly)	Tot_Sol_R
11	Normalized excess green	ExG2	✓	✓	✓	47	Potential evapotranspiration (Penman, mm)	Pen_PT
12	Excess red	ExR	✓	✓	✓	48	Potential evapotranspiration (Jensen-Haise, mm)	JH_PET
13	Excess green minus excess red	ExGR	✓	✓	✓	49	Total rainfall (mm)	Rainfall
14	Green red vegetation index (VI)	GRVI	✓	✓	✓	50	Dew point (average, °C)	Dew_P
15	Green blue VI	GBVI	✓	✓	✓	51	Wind chill (minimum, °C)	Min_Wind_Chill
16	Blue red VI	BRVI	✓	✓	✓	52	Wind chill (average, °C)	Wind_Chill
17	Green-red ratio	G/R	✓	✓	✓			
18	Green-red difference	G–R	✓	✓	✓			
19	Blue-green difference	B–G	✓	✓	✓			
20	Visible-band difference VI	VDVI	✓	✓	✓			
21	Visible atmospherically resistant index	VARI	✓	✓	✓			
22	Modified green red VI	MGRVI	✓	✓	✓			
23	Colour index of vegetation	CIVE	✓	✓	✓			
24	Woebbecke index	WI	✓	✓	✓			
25	Coloration index	CI	✓	✓	✓			
<u>Multispectral vegetation indices</u>								
26	Normalized difference VI	NDVI	✓	✓	✓			
27	Green normalized VI	GNDVI	✓	✓	✓			
28	Soil adjusted VI	SAVI	✓	✓	✓			
29	Modified soil adjusted VI	MSAVI	✓	✓	✓			
30	Enhanced VI	EVI	✓	✓	✓			
31	Normalized difference moisture index	NDMI	✓	✓	–			
32	Green atmospherically resistance VI	GARI	✓	✓	✓			
33	Simple ratio index	SR	✓	✓	✓			
34	Atmospherically resistant VI	ARVI	✓	✓	✓			
35	Green chlorophyll index	GCI	✓	✓	✓			
36	Structure intensive pigment index	(SIPI)	✓	✓	✓			

Note: VI - Vegetation index, Spatial resolution of Landsat - 30 m, Sentinel - 30 m, CubeSat - 3 m; NDAWN - North Dakota Agricultural Weather Network.

Landsat 5 (Thematic Mapper, TM) and Landsat 7 (Enhanced thematic mapper, ETM) (Gorelick et al., 2017). The TM images were mostly used for data collection, while ETM images were only used in case of missing or no cloud-free TM image available. The Landsat images were considered from the ‘Tier 1’ category of the GEE datasets for their higher data quality and level of processing. Atmospheric aspects such as aerosols and thin clouds are accounted for by using the atmospherically corrected datasets using surface reflectance from the TM and ETM sensors. Additionally, these Tier 1 and surface reflectance data were further screened for clouds, snow, and shadows using the CFMask() function (Zhu and Woodcock, 2012).

Remotely sensed data for the years 2017–2018 for the NGPRL study sites was collected from Sentinel-2. The Sentinel-2 images were available since 2015 once every ten days with a spatial resolution ranging from 10–30 m. Multi-spectral instrument (MSI) sensor in the Sentinel-2 platforms generates an image with 13 spectral bands ranging from visible to short-wave infrared. PlanetScope imagery from Planet Labs Inc. was used to download raw Sentinel-2 images. The satellite image tile covering the study site pastures was selected with cloud cover condition less than 20%. These obtained raw Sentinel images were preprocessed for atmospheric correction. The semi-automatic classification plugin available in the QGIS (version 3.16) software was used for performing atmospheric correction for the Sentinel images using the provided metadata (Congedo, 2016).

5.3.3. Data Processing

The approach of obtaining various VIs, representing the forage growth, specific to the study pastures is to overlay the pasture’s shapefiles on the satellite images and extract relevant spatial and band information for data processing. The satellite image data

processing was performed in open-source QGIS and R (version 4.1.1) software. Shapefiles were generated using the New Shapefile Layer (polygon) option in QGIS (Appendix E.1). A shapefile vector layer with three polygons was created for the NGPRL pastures to perform image processing analysis. The downloaded Landsat satellite images were a single raster layer consisting of multiple bands (eight) as stacks. In contrast, the images from Sentinel-2 were a single raster layer consisting of multiple bands (11 in total). These multiple bands from Sentinel-2 were stacked using the R function `stack()` to form a multi-band raster layer.

The five major bands, commonly used in estimating the plant characteristics are: blue (B), green (G), red (R), near-infrared (NIR), short-wave infrared (SWIR), and short-wave infrared 2 (SWIR2) was stripped from the stacked raster layers for estimating VIs (table 5.1). A stripped band (raster layer) was overlaid onto the pasture shapefile (vector layer) for extracting band value for the pastures' shapefiles. The extraction was performed through zonal statistics using the `exact_extract()` R function. The zonal statistics result presented the mean value of the pixels (band data) available in the polygon created for each pasture. This satellite image processing was repeated for all the satellite images downloaded. Therefore, a user-coded function in R was created to automate the process of stacking, stripping, and applying zonal statistics for the bands (Appendix F.1 – F.3).

5.3.4. Estimation of Vegetation Indices

The VIs derived by combining spectral bands can be attributed to various plant characteristics, including growth, water content, pigments, protein content, among others (Foley et al., 1998). The VIs were estimated from the selected spectral bands (B, G, R, NIR, SWIR, and SWIR2) from the Landsat and Sentinel-2 images. The list of RGB mul-

tispectral based vegetation indices commonly used in various applications is presented in Table 5.2. Estimating VIs had to be repeated multiple times over different dates for the satellite images. To automate this process, a user-coded R function was created (Appendix F.4) to execute the estimation of VI (table 5.1).

5.3.4.1. Common RGB bands

The RGB color system is the most used for digital image processing. As RGB bands correspond to the visible range of the electromagnetic spectrum, true-color composites can be generated using these spectral bands. In addition to viewing, the three bands can be mathematically combined (VIs) to extract further information. Most of the RGB-based VIs were developed to highlight the greenness and spectral variation within the vegetation. Among the RGB-based VIs, excess green index (ExG) produced using the R, G, and B bands were the most commonly used to estimate greenness (Woebbecke et al., 1995). Based on the derived spectral bands from the Landsat and Sentinel-2 platforms, 19 RGB-based vegetation indices were computed for biomass prediction in the pastures (table 5.2).

5.3.4.2. Multispectral

The sensors in the Landsat and Sentinel-2 were equipped to capture information in the electromagnetic spectrum that was not visible to the human eye. These multispectral bands were NIR and SWIR bands. Multispectral VIs were calculated mathematically by combining multispectral bands and or RGB bands. The normalized VI is the most widely used multispectral VI and is estimated using the NIR and R band (Rouse et al., 1974). The NDVI values ranged between -1 and $+1$, where -1 and $+1$ relate to poor and healthy vegetation, respectively. NDVI proved successful in estimating canopy cover and

Table 5.2. List of RGB and multispectral based vegetation indices.

Vegetation index	Equation	Reference
Red chromatic coordinate (RCC)	$\frac{R}{R+G+B}$	(Woebbecke et al., 1995)
Green chromatic coordinate (GCC)	$\frac{G}{R+G+B}$	(Woebbecke et al., 1995)
Blue chromatic coordinate (BCC)	$\frac{B}{R+G+B}$	(Woebbecke et al., 1995)
Excess green (ExG)	$2G - B - R$	(Woebbecke et al., 1995)
Normalized excess green (ExG2)	$\frac{B}{R+G+B}$	(Woebbecke et al., 1995)
Excess red (ExR)	$\frac{1.4R-G}{R+G+B}$	(Meyer et al., 1999)
Excess green minus excess red (ExGR)	ExG2 - ExR	(Meyer et al., 2004)
Green red vegetation index (GRVI)	$\frac{G-R}{G+R}$	(Hunt et al., 2005)
Green blue vegetation index (GBVI)	$\frac{G-B}{G+B}$	
Blue red vegetation index (BRVI)	$\frac{B-R}{B+R}$	
Greed-red ration (G/R)	$\frac{G}{R}$	(Steele et al., 2009)
Green-red difference ($G-R$)	$G - R$	
Blue-green difference ($B-G$)	$B - G$	
Visible-band difference vegetation index (VDVI)	$\frac{2G-R-B}{2G+R+B}$	(Xiaoqin et al., 2015)
Visible atmospherically resistant index (VARI)	$\frac{G-R}{G+R-B}$	(Gitelson et al., 2002)
Modified green red vegetation index (MGRVI)	$\frac{G^2-R^2}{G^2+R^2}$	(Bendig et al., 2015)
Colour index of vegetation (CIVE)	$0.441R - 0.881G + 0.385B + 18.787$	(Kataoka et al., 2003)
Woebbecke index (WI)	$\frac{G-B}{R-G}$	(Woebbecke et al., 1995)
Coloration index (CI)	$\frac{R-B}{R}$	
Normalized difference vegetation index (NDVI)	$\frac{NIR-R}{NIR+R}$	(Rouse et al., 1974)
Green normalized vegetation index (GNDVI)	$\frac{NIR-G}{NIR+G}$	(Gitelson et al., 1996)
Soil adjusted vegetation index (SAVI)	$\frac{1.5(NIR-R)}{NIR+G+0.5}$	(A. R. Huete, 1988)
Modified soil adjusted vegetation index (MSAVI)	$\frac{2NIR+1-\sqrt{(2(NIR)+1)^2-8(NIR-R)}}{2}$	(Qi et al., 1994)
Enhanced vegetation index (EVI)	$2.5 \times \frac{NIR-R}{1+NIR+6R-7.5B}$	(A. Huete et al., 1997)
Normalized difference moisture index (NDMI)	$\frac{NIR-SWIR}{NIR+SWIR}$	(Wilson and Sader, 2002)
Green atmospherically resistant vegetation index (GARI)	$\frac{NIR-(G-(B-R))}{NIR+(G-(B-R))}$	(Gitelson et al., 1996)
Simple ratio index (SR)	$\frac{NIR}{R}$	(Birth and McVey, 1968)
Atmospherically resistant vegetation index (ARVI)	$\frac{NIR-2R-B}{NIR+2R-B}$	(Kaufman and Tanre, 1992)
Green chlorophyll index (GCI)	$\frac{NIR}{G-1}$	(Gitelson, Gritz, et al., 2003)
Structure intensive pigment index (SIPI)	$\frac{NIR-B}{NIR+B}$	(Penuelas et al., 1995)

Note: R - red, B - blue, and G - green bands recorded from the satellite platforms

vigor; however, it was sensitive to the effects of soil, atmosphere, and cloud. Therefore 10 multispectral VIs were utilized to validate the pasture biomass (table 5.2).

5.3.5. Modeling Approaches

The ML modeling techniques were used to predict the pasture biomass through selected features. Different wrapper-based feature selection methods were employed to compare and choose the best features representing the pasture biomass. Using the best features, various ML models were considered to predict the biomass and were compared within the selected ML models and against the simple multiple linear regression (MLR) models. The feature selection and prediction models considered are presented in detail subsequently.

5.3.6. Feature Selection

Features for this study included the extracted satellite band values (6), estimated VIs (RGB: 19, multispectral: 10), and climate variables (16), a total of 51 variables (table 5.1). Among these features, understandably, some were highly relevant in predicting pasture biomass than others. Feeding all the variables into machine learning models (including the irrelevant features) would impact the accuracy and increase the computation load and time. To address this a wrapper-based feature selection method was employed.

In the wrapper-based feature selection process, a subset of the most relevant features was selected from a dataset, and features are either removed or added based on training a model and the inference obtained. In this study, three wrapper feature selection algorithms such as Boruta, recursive feature elimination, and stepwise regression were used to estimate the relevant features. Correlation and mutual information were used to validate the results of the selected feature selection algorithms.

5.3.6.1. Backward elimination

Backward elimination was one of the three popular simple filter-based feature selection methods, and others are forward selection and stepwise regression. It was a wrapper-based feature selection algorithm that initially considered all the features to build MLR models. The R function `step()` was used to perform the backward elimination algorithm (Venables and Ripley, 2002). The MLR model was used to estimate the features with less relevance based on the calculated Akaike information criterion (AIC). Like adjusted R -squared, the AIC also penalizes the model performance while using an increased number of unnecessary variables. In this process, some features considered significant at an early stage may be eliminated later. In general, backward elimination produced a better subset of features since it was evaluated for significance by comparing with the other features (Xu and Zhang, 2001). Therefore, only backward elimination feature selection was considered for this study.

5.3.6.2. Boruta

Boruta was a wrapper-based method built using a random forest (RF) algorithm that determined variable importance measures by default (Chen et al., 2022; Luo et al., 2022). The Boruta feature selection method was implemented by using the `Boruta()` R package (Kursa, Rudnicki, et al., 2010). In the Boruta algorithm, for each feature, a shadow feature was created, and the values were obtained by randomly shuffling the values of the original feature. This extended dataset was subjected to the RF to evaluate the important features. The number of RF iterations performed on the extended dataset containing the original and shadow features was 120. At every iteration, the maximum Z -score of the shadow features (maximal importance of the random features, MIRA) were

calculated to compare with the Z -score of the individual original feature. The algorithm hypothesizes that the importance of the original feature is equal to or higher than the estimated MIRA and when the hypothesis holds true, the number of hits (N) were recorded from the total iteration. An original feature was considered significant if the value of the hits is at least $0.5N$.

5.3.6.3. Recursive feature elimination

Recursive feature elimination (RFE) was a wrapper-based algorithm built around the random forest (RF, section 5.3.7.3) model (ML) to yield the optimum features (Prasad et al., 2021; Pullanagari et al., 2018). In R, the RFE feature selection was performed using the `rfe()` function in the `caret` package (Kuhn, 2008). The RFE method initially employed all the features and eliminated the feature with the least RMSE calculated from the out-of-bag (OOB) data. A new RF model was developed using the remaining features. The process was recursively applied by employing 10-fold cross-validation (repeated 5 times) to optimize the variable selection process and select the most important features. At every run of this recursive process, the RF model with the selected subset of features yielding the least RMSE was considered optimum. However, the rank of the features was updated when another model with a different subset of features yielded the minimum RMSE. The RFE estimated the best subset of features yielding a minimum RMSE value through this repeated process (Appendix F.5).

5.3.7. Linear and Machine Learning Prediction Models

The features were ranked based on the feature importance results from the backward elimination, Boruta, and RFE. Then, the ranked features were fed to selected the linear and ML models, MLR, RF, support vector regression (SVR), and k-nearest neighbor-

hood (kNN) (fig. 5.2). The number of the feature data fed into the ML models increased successively by one feature; the ML models were analyzed using the highest-ranked feature, and the process was repeated by including the second-highest feature and so on.

5.3.7.1. Train, validation, and test dataset

The original dataset containing selected features from the feature selection methods (predictors) and pasture biomass (response) were subjected to random splitting with a replacement for obtaining train and test data. The R function `sample()` was used perform the data splitting operation. The partition ratio considered for the train and test datasets was 50, 60, 70, and 50, 40, and 30, respectively (fig. 5.2). The 10-fold cross-validation method was used to validate the performance of the developed ML model. The train and validate dataset was used to train the prediction models, while the test dataset was used to estimate the accuracy of the trained models. The models developed using the train dataset were run ten times to record the accuracy from the test dataset; the partition ratio yielding consistent accuracy was considered optimum.

5.3.7.2. Multiple linear regression

The MLR statistical models are simpler compared to the ML counterparts but have the advantage of being easy to calculate and comprehend and can be considered as “control” model to compare ML models. These models used two or more predictor variables to explain the outcome of one response variable by fitting a linear equation (Jiang et al., 2019; Shastry et al., 2015). In R, the MLR was performed using the `lm()` function (Chambers and Hastie, 1992). The model assumes a linear relationship between the predictor and response variables, and the predictor variables are not highly correlated. Each value

of the predictor variables was associated with the response variable, and the model determined a regression coefficient that had the least overall model error.

5.3.7.3. *Random forest*

The RF was an ensemble learning algorithm (ML) with a collection of several decision trees (Filippi et al., 2019; Li et al., 2020). The function `ranger()` in R was used to perform RF analysis (Appendix F.5). In RF, random samples were drawn from the train data with replacement using the bootstrap aggregating (bagging) method to avoid overfitting (Fawagreh et al., 2014). The random samples selected from the train data were called in-bag data and constituted for 64% of the train data. At the same time, the remaining 36% of the samples were called the out-of-bag (OOB) data. Decision trees in RF are built independently using in-bag data and a random subset of features selected at each node where the feature importance was assigned based on the prediction accuracy. The OOB data was used to validate the built decision trees and the resulting mean square error determined the prediction accuracy and variable importance. The final predictions for regression-based RF were obtained by averaging the prediction results from all the trees (bagging).

5.3.7.4. *Support vector regression*

The SVR was a supervised ML algorithm developed to predict discrete values (Shafiee et al., 2021; Were et al., 2015). The SVR algorithm in R was performed using the function `svm()` from the library “e1071”. The SVR principles were similar to the support vector machine and used kernel functions to project the data onto a hyperspace to represent complex nonlinear patterns (Gunn et al., 1998). Kernel functions of SVR include sigmoid, polynomial, nonlinear, and radial basis (RBF); however, only RBF was used for this study

for its proven performance (Zhang et al., 2020). The SVR provides flexibility by defining the amount of error acceptable by the model and determining the best fit line within that allowed threshold value. The threshold value was the distance between the hyperplane (best-fit line) and the boundary called the maximum error ϵ (epsilon). The value of epsilon can be tuned to obtain the desired SVR model accuracy.

5.3.7.5. *k*-nearest neighbors

The kNN was an instance-based learner where for the test data instance, the model finds the k samples nearest in the train data based on the distance value and averages their responses (Gonzalez-Sanchez et al., 2014; Subhashree et al., 2020). The “caret” package in R with the method option selected as “kNN” was used to implement the algorithm. The k value was always an odd number and played a significant role in determining the model’s accuracy. A small k value might lead to poor accuracy if the noise were present in the data, while a large k value might ignore the noise in the data but would significantly increase the computation load. An optimum k value can be estimated based on the model’s accuracy obtained from a selected range of k values.

5.3.8. High-Performance Computing Resources Used

Selecting features and training ML models, especially with RFE, were computationally intensive involving a lot of number crunching in a repeated manner. Such computational loads cannot be efficiently handled by local computers (common laptop or desktop), specifically during the developmental stage where several iterations are involved. Therefore, we used the North Dakota State University’s Center for Computationally Assisted Science and Technology (CCAST) high-performance computer clusters. An example of performance comparison with a single run using OnDemand RStudio Server IDE is:

the runtime for RFE feature selection method on CCAST (system time: 719 s; 1 node and 4 cores with a 16 GB RAM configuration at basic service level) was on an average 1.5 times faster (other calculations up to 2.5 times) than the local system (system time: 1127 s). The performance of the CCAST basic service level can be improved further by requesting more resources. It was observed that the use of systems like CCAST or similar is necessary while developing ML models involving several variables (multispectral image bands and climate data).

5.3.9. Model Performance Assessment

5.3.9.1. Hypertuning parameters

The best performance of the ML models was not guaranteed with the default hyperparameter settings; therefore, the hyperparameters need to be tuned to achieve the best predictions (Schratz et al., 2019). The ML models considered for this study were all subjected to hyperparameter tuning to determine the robust estimates. The tuning can be performed by manually selecting the parameters; however, automatic selection was recommended to estimate the optimum parameter.

The RF models involved several hyperparameters such as the number of trees involved (`num.trees`), the number of variables randomly selected at each split (`mtry`), and minimum observation at each node (`min.node.size`). The number of trees tested was 500, 1000, and 1500, while the `mtry` value was set to $p/3$ (default value for regression) where p is the total number of features, and `min.node.size` was selected as 5 (default value for regression). All these RF hyperparameters were used in the grid search operation.

With SVR, the essential parameters were kernel, epsilon (ϵ), cost, and gamma. Kernels were crucial in SVR since they used the data for transitioning into higher dimensional

space. The ϵ determined the width of the tube around the hyperplane (decision boundary) developed using the RBF function. The cost function in SVR determines the softness of the margin, and the gamma determines the shape of the decision boundary; a high gamma value results in more curvature. The values considered for ϵ were between the range 0 and 1, while the cost values ranged between 2^2 and 2^9 , and the gamma values considered were 0.001, 0.1, 1, and 3.

The kNN model used a range of k values between 5 and 9 with an increment of 1 for determining the optimum based on the accuracy.

5.3.9.2. Performance metrics

The robustness of the models was determined using 10-fold cross-validation repeated ten times. The performance of the models was recorded using the metrics, such as coefficient of determination (R^2), root mean square error (RMSE), and mean absolute error (MAE) for the predictions from ML regression models, which were represented in the following equations. A higher value of R^2 and a smaller value of RMSE and MAE represent a better prediction performance of the model tested.

$$R^2 = 1 - \frac{\sum_{i=1}^n (y_i - \hat{y}_i)^2}{\sum_{i=1}^n (y_i - \bar{y}_i)^2} \quad (5.1)$$

$$\text{RMSE} = \sqrt{\frac{1}{n} \sum_{i=1}^n (y_i - \hat{y}_i)^2} \quad (5.2)$$

$$\text{MAE} = \frac{1}{n} \sum_{i=1}^n |y_i - \hat{y}_i| \quad (5.3)$$

where, y_i = observed value, \hat{y}_i = predicted value, \bar{y}_i = mean of observed values, and n = number of observations.

5.4. Results and Discussion

5.4.1. Feature Ranking Results

The 51 predictor features including climate, remote sensing bands, and VIs (table 5.1) were ranked using the feature selection strategy described in section 5.3.6. The ranking results from one pasture site (CWP) for the year 2006 are shown in Figure 5.3. Among the feature selection methods considered, the ranking differed which reflected the unique techniques of the feature selection. However, the similarity between the top-ranking features for the random forest-based feature selection algorithms, Boruta, and RFE methods was observed.

The best feature in predicting biomass in all three methods was the SWIR2, a reflectance band captured by the satellite sensors. The band SWIR2 was reported as one of the best wavelengths to estimate the fractional cover of the vegetation and the bare soil (Sagan et al., 2021). In addition to SWIR2, the red band ranked among the top 6 features in the feature selection methods and has been used in predicting yield in agricultural applications (Yang and Anderson, 2000). Several studies have reported the successful prediction of biomass yield using the NDMI also known as the drought index (El-Hendawy et al., 2017; Jin et al., 2016). The important climate variables were average wind speed (Avg_WindS) and average turf soil temperature (AvgT_Soil).

Among the vegetation indices, the normalized difference moisture index (NDMI) ranks one of the top 4 features in all the feature selection methods. The NDMI was generated using the RS bands NIR and SWIR; it can be observed that the band SWIR ranked as the second most important variable in Boruta and RFE feature selection methods.

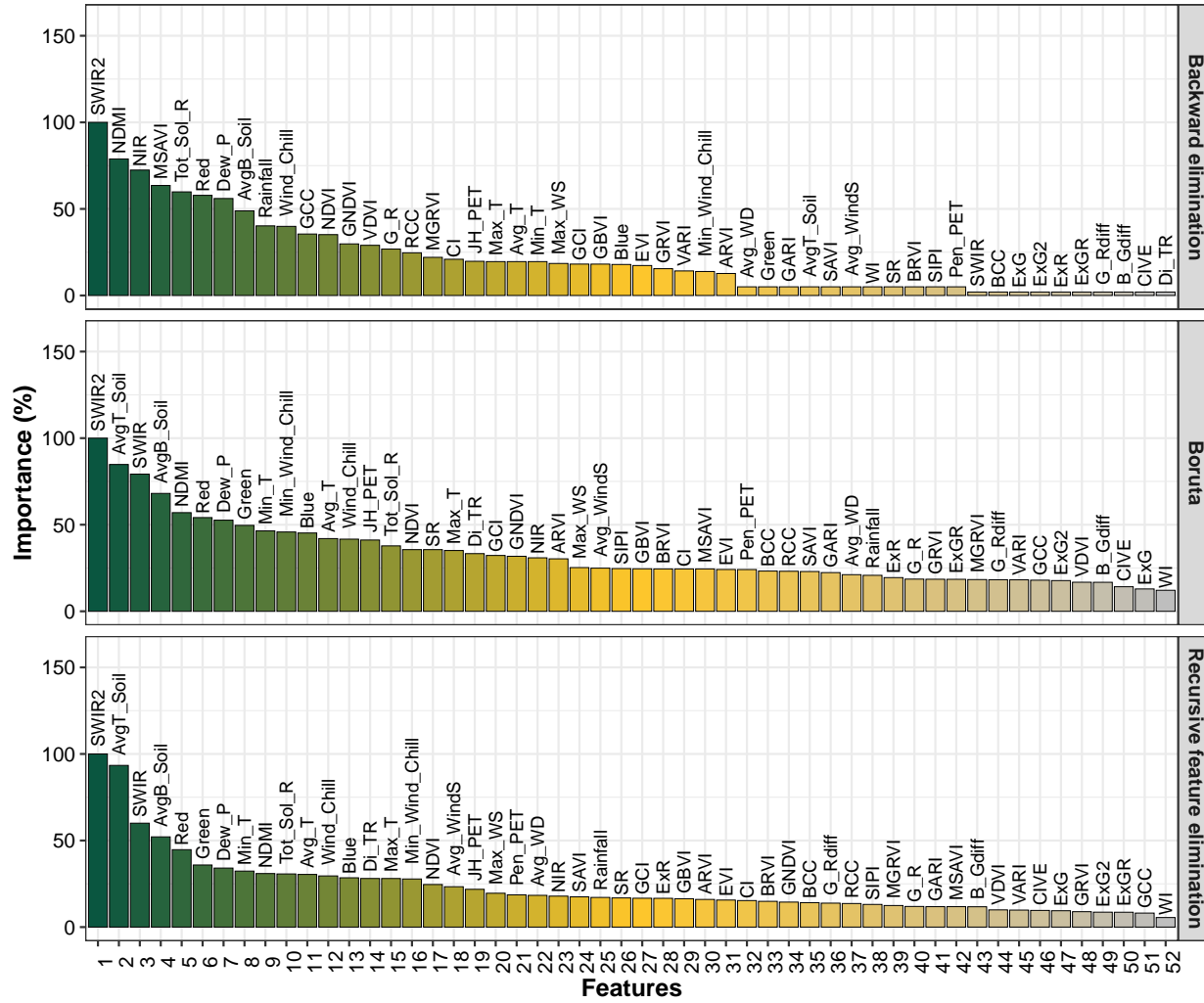


Figure 5.3. Feature (52 total) ranking results from backward elimination, Boruta, and recursive feature elimination feature selection methods.

It is interesting to note that wind speed, which is not an obvious variable to explain the biomass yield, is ranked higher than several obvious variables such as rainfall, ExG, and so on. However, the wind speed was a crucial parameter in impacting the evapotranspiration and soil erosion and thereby affecting the crop yield. Wind speed also increases the crop water requirements by increasing potential evapotranspiration as the accumulated humid air near the leaves is removed (Dong et al., 2020). Furthermore, the turf soil temperature for grasses was essential for the growth of crops since the warm temperature provides a favorable condition for water and nutrient uptake and has been used in various agricultural studies (Kahimba et al., 2008; Kaspar and Bland, 1992).

The vegetation indices VARI and MGRVI which commonly used combined band values of green and red was ranked the least in predicting biomass yield. The climate variable rainfall did not contribute to predicting biomass yield data; therefore, ranked as one of the least important features. Interestingly, the 6 RS bands obtained ranked in the top 15 features for at least 2 feature selection methods. Though the feature ranking is available for all the features, the optimum number of features required can be determined by sequentially feeding to the ML models and observing the prediction accuracy.

5.4.2. Feature Selection and Model Performance Comparison

The ranked features from the selected feature selection models for MGP pasture were fed sequentially and the responses of the ML models were compared using RMSE metrics, the lower RMSE value implies higher model performance in predicting biomass. Based on the observed model responses, the best-performing feature selection method, the number of features, and ML models were determined.

5.4.2.1. Feature selection methods comparison

Overall, a decrease in RMSE was observed with an increase in the number of features across all the feature selection methods (fig. 5.4). However, a steep decrease in the RMSE trend was observed for features less than 10. Among the feature selection methods, RFE recorded the lowest RMSE value across all the ML methods except MLR indicating a better selection of important features.

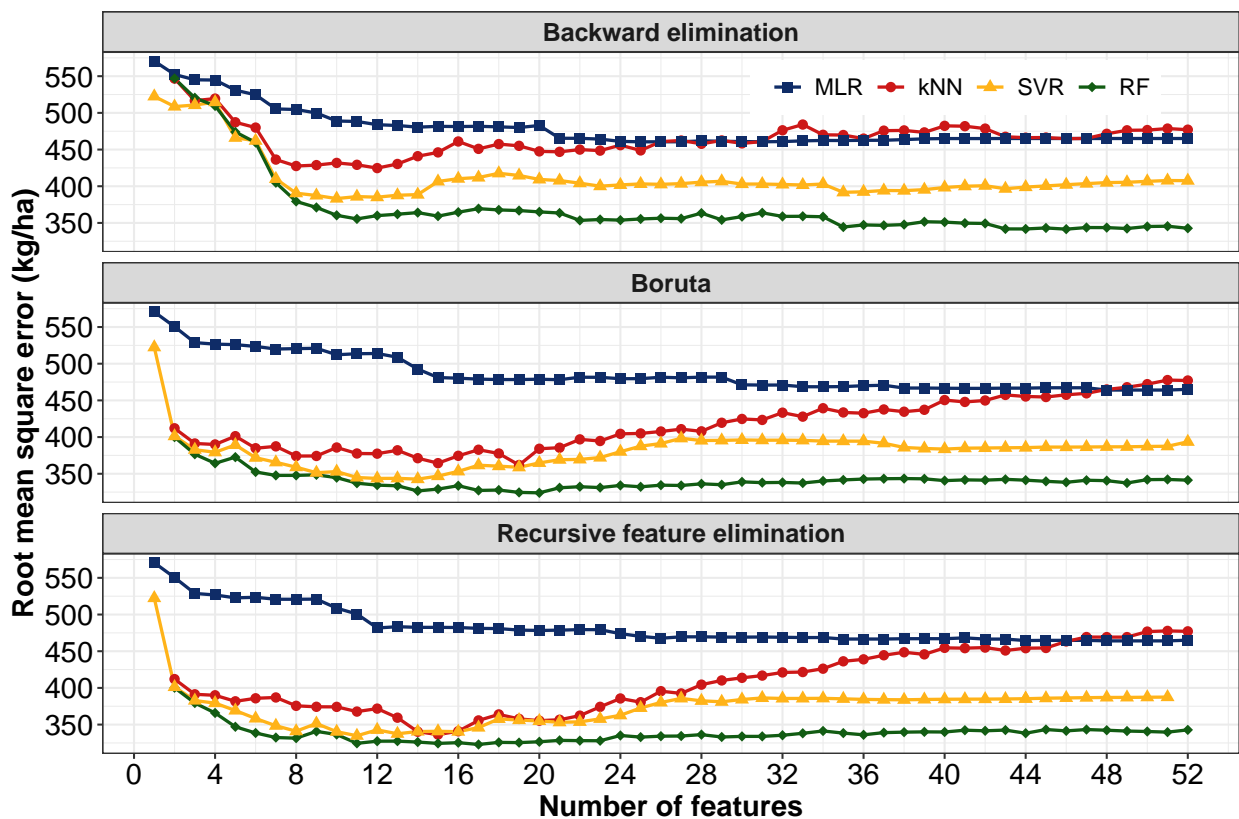


Figure 5.4. Feature ranking from backward elimination, Boruta, and recursive feature elimination feature selection methods. MLR - multiple linear regression, kNN - k-nearest neighbor, SVR - support vector regression, and RF - random forest.

For MLR, the backward elimination feature selection method performed the best because the wrapper-based backward elimination feature selection algorithm internally uses the MLR model to estimate the best features (Mao, 2004).

A comparable RMSE trend was observed for the feature selection methods Boruta and RFE because of the similar feature rank as discussed in the previous section (section 5.4.1). The average percentage decrease for RMSE value for RFE compared to MLR and Boruta was 11 % and 2 %, respectively (fig. 5.5).

5.4.2.2. Machine learning models comparison - ranking

Among the ML models, the RMSE was the lowest for RF followed by SVM, kNN, and MLR across all the feature selection methods (fig. 5.4). As expected, the MLR model was the least accurate in biomass prediction since it assumes a linear relationship between the predictor and response variables. Previous studies also report similar dominance of ML models in yield prediction over the linear regression models (Belayneh et al., 2014; Cai et al., 2019; Guzmán et al., 2018). With the increase in the number of features, a steady decrease in RMSE was observed for the MLR model for all the feature selection methods. While for other ML models (kNN, RF, and SVM), the lowest RMSE was observed for features less than 10 and the addition of more features increased the RMSE values indicating a reduced performance of the ML models. This trend was strongly observed with the kNN model. The average reduction in RMSE of the ML models, kNN, SVM, and RF compared to MLR was 13, 19, and 29 % (fig. 5.5A).

Overall, RFE performed well in the selected most influential predictors for estimating the biomass yield. The RFE methodology has been widely followed for evaluating remote sensing variables and climate in estimating pasture and forage yield prediction

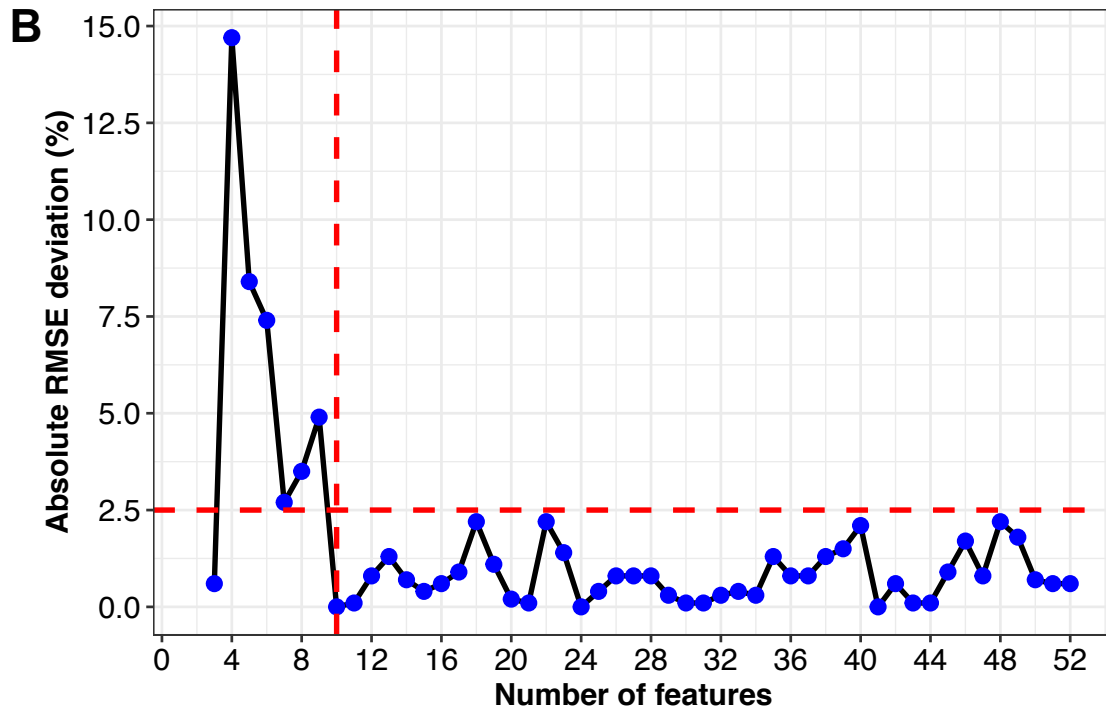
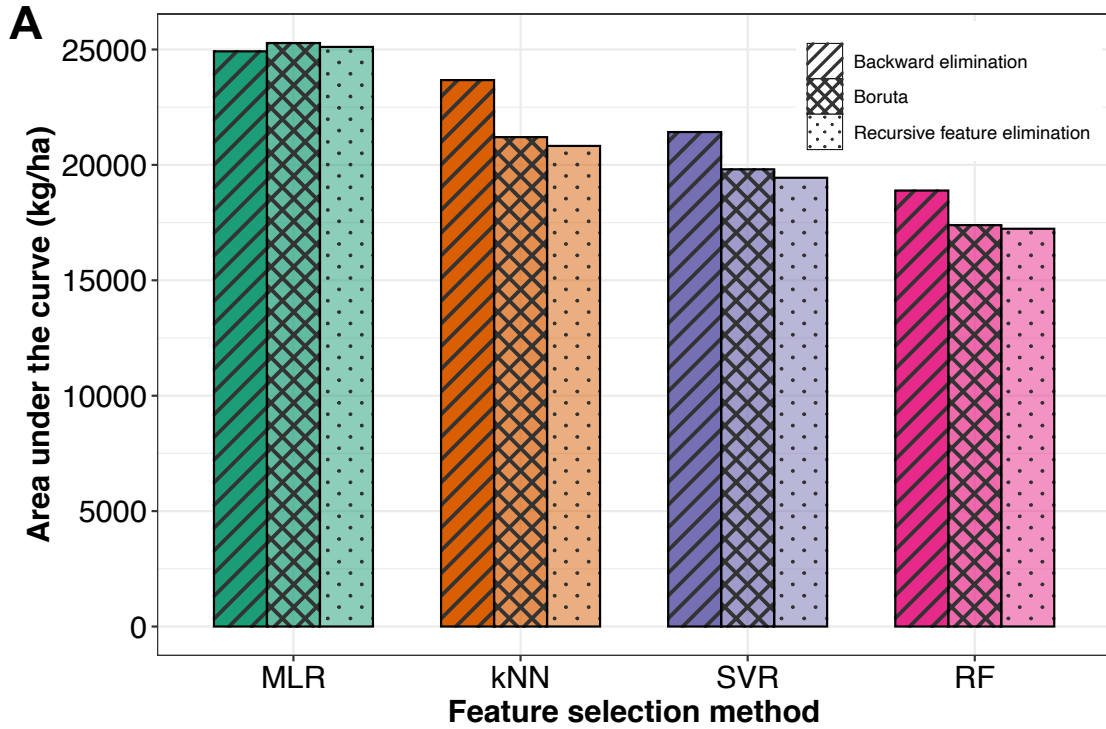


Figure 5.5. A. Area under the curve for feature selection methods and ML models (kNN: k-Nearest Neighbor, MLR = multiple linear regression, RF - random forest, SVR - support vector regression; B. absolute RMSE deviation for recursive feature elimination feature selection method and random forest model).

(Feng et al., 2020; Pullanagari et al., 2018). Among the ML models, RF performed better in biomass prediction. Previous ML comparison studies show that RF has proven to be efficient in agricultural applications for predicting crop yield and above-ground biomass (Filippi et al., 2019; Li et al., 2020). Using the selected RFE and RF methodology, the absolute RMSE deviation percentage was estimated for each additional feature (fig. 5.5B). The cut-off value for selecting the features was fixed at 2.5 % of absolute RMSE deviation.

Results revealed that for every additional feature after 10 the deviation of absolute RMSE value was less than 2.5 %. Therefore, the top 10 ranked features from RFE recommended for training the RF model were: SWIR2, AvgT_Soil, SWIR, AvgB_soil, Red, Green, Dew_P, Min_T, NDMI, and Tot_Sol_R (table 5.1). Based on these results, for studies that used combined climate and remote sensing data to predict pasture and forage biomass, the methodology RFE for feature selection and RF for building ML prediction model was recommended.

5.4.3. Application of the Developed Methodology and Model

The validity of the developed methodology (section 5.4.2) of RFE (features selection) and RF (prediction model) was further explored by using it for the three different applications by addressing questions such as: (i) What is the predictive performance of the methodology, developed based on one pasture, for estimating biomass in other pastures? (ii) How does the spatial resolution of satellite images (Landsat, Sentinel, and CubeSat) influence the accuracy of predicting pasture biomass? (iii) How capable is the developed methodology in predicting cultivated hay crops such as alfalfa?

5.4.3.1. Application 1 - Performance of the developed methodology in other pastures

The performance of the selected methodology based on the results from MGP pasture was tested using the unseen biomass data from the pastures CWP and HGP. Feature selection using RFE and building RF models were individually performed for the pastures CWP and HGP. Based on the feature selection results, the essential common features that emerged important in all the pastures are SWIR2, SWIR, Red, NDMI, AvgT_Soil, and AvgB_Soil (table 5.1). A linear trend was more pronounced in HGP and MGP than CWP (fig. 5.6). The trend produced by the developed RF models in HGP ($R^2 = 0.84$) and MGP ($R^2 = 0.83$) was linear for 2004, 2005, and 2006, indicating a good correlation between the observed and predicted data. For CWP, a good correlation was observed for biomass <1500 kg/ha ($R^2 = 0.79$); however, with increasing biomass, the trend showed a reduced correlation. It is vital to note that the ground truth data (observed) was already not producing a clear growth trend for the CWP pasture.

For prediction model assessment, the pasture biomass data from the CWP and HGP pastures were provided as test data to the trained RF model using MGP pasture data. The results showed that better predictions were obtained for the HGP pasture ($R^2 = 0.65$) followed by CWP pasture ($R^2 = 0.37$). Comparable predictions were obtained for pastures MGP, and HGP since both the pastures were dominated by Kentucky bluegrass. Even though CWP pasture contained Kentucky bluegrass, however, it was dominated by crested wheatgrass, which resulted in a lesser performance of the trained ML model. The selected methodology RFE and RF was recommended for predicting biomass in other pastures as it produced good accuracy.

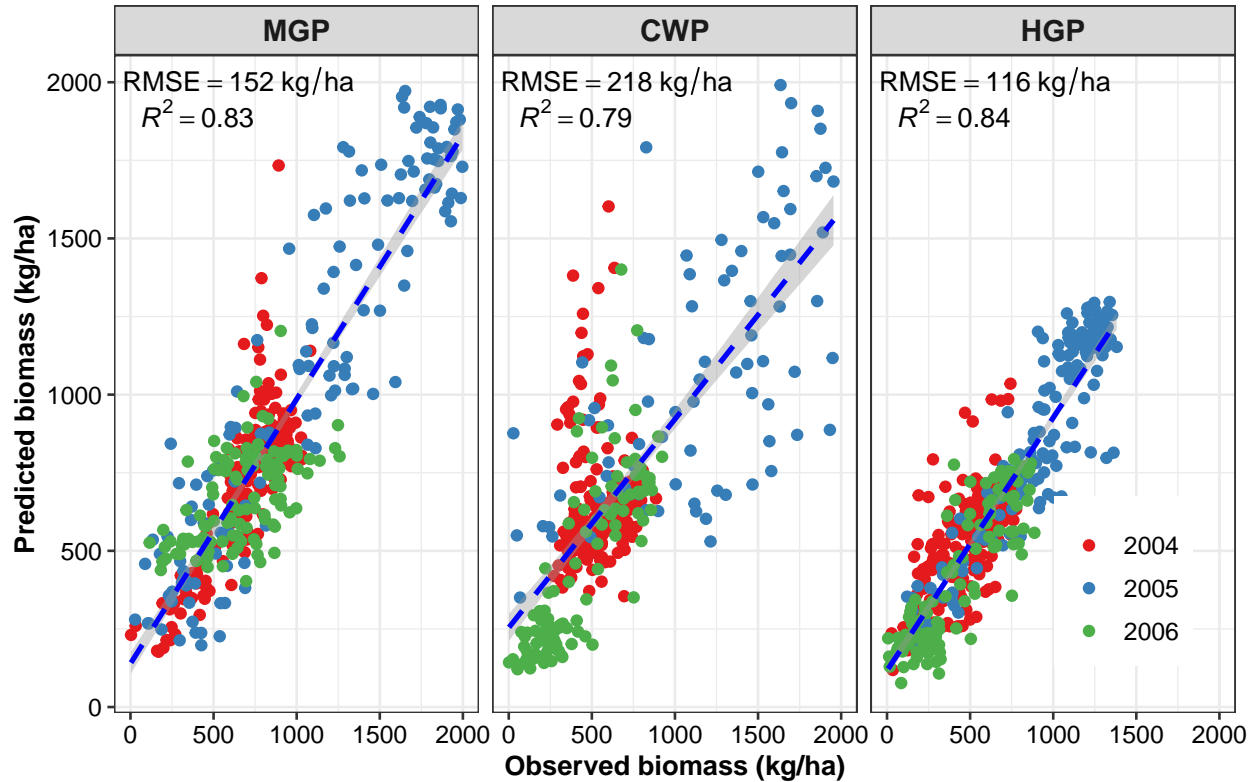


Figure 5.6. Observed versus predicted biomass for the developed machine learning model for the pastures mildly grazed pasture (MGP), highly grazed pasture (HGP), and crested wheat pasture (CWP).

Furthermore, the results revealed that the direct trained ML model (opposed to methodology RFE and RF) developed using the MGP pasture data can be used for predicting biomass for other pastures dominated by Kentucky bluegrass. The application of trained ML models directly to pastures with similar soil and plant characteristics will be simpler, and the development of such trained ML models for specific pastures or fields will prove to be practical and useful.

5.4.3.2. Application 2 - Effect of remote sensing platforms resolution in forage prediction

To evaluate the effect of satellite images resolutions, the developed methodology (RFE & RF) was used to build models to validate MGP pasture biomass using bands and VI features sourced from three different satellite platforms with varying resolutions, such as Landsat, Sentinel, and CubeSat along with climate features obtained from NDAWN for the years 2017 and 2018 (fig. 5.7). The ranked top 10 features from the RFE for MGP with different satellites are presented in Table 5.3.

It was observed that the band values SWIR and SWIR2 were influential in predicting biomass in the pasture for Landsat and Sentinel platforms. However, in CubeSat with the absence of SWIR or SWIR2 bands, the NIR band emerged as the best predictor band feature.

Studies have reported that CubeSat NIR with fine resolution showed good performance in determining green leaf biomass and phenology (Gitelson, Viña, et al., 2003; John et al., 2020). The prominence of SWIR, SWIR2, and NIR bands indicates that the wavelength range of 0.77–2.35 μm was best for estimating biomass growth in pastures. More vegetation indices such as GARI, GCI, GNDVI, and BCC (4 out of 10) emerged as important features for CubeSat compared to Landsat and Sentinel platforms. Blue and GCC remote sensing data commonly appeared as influential bands and VI for Landsat and CubeSat satellite platforms.

Based on the predictions on the trained RF model using the ranked features from RFE and data from the satellite platforms, it can be observed that CubeSat has the highest

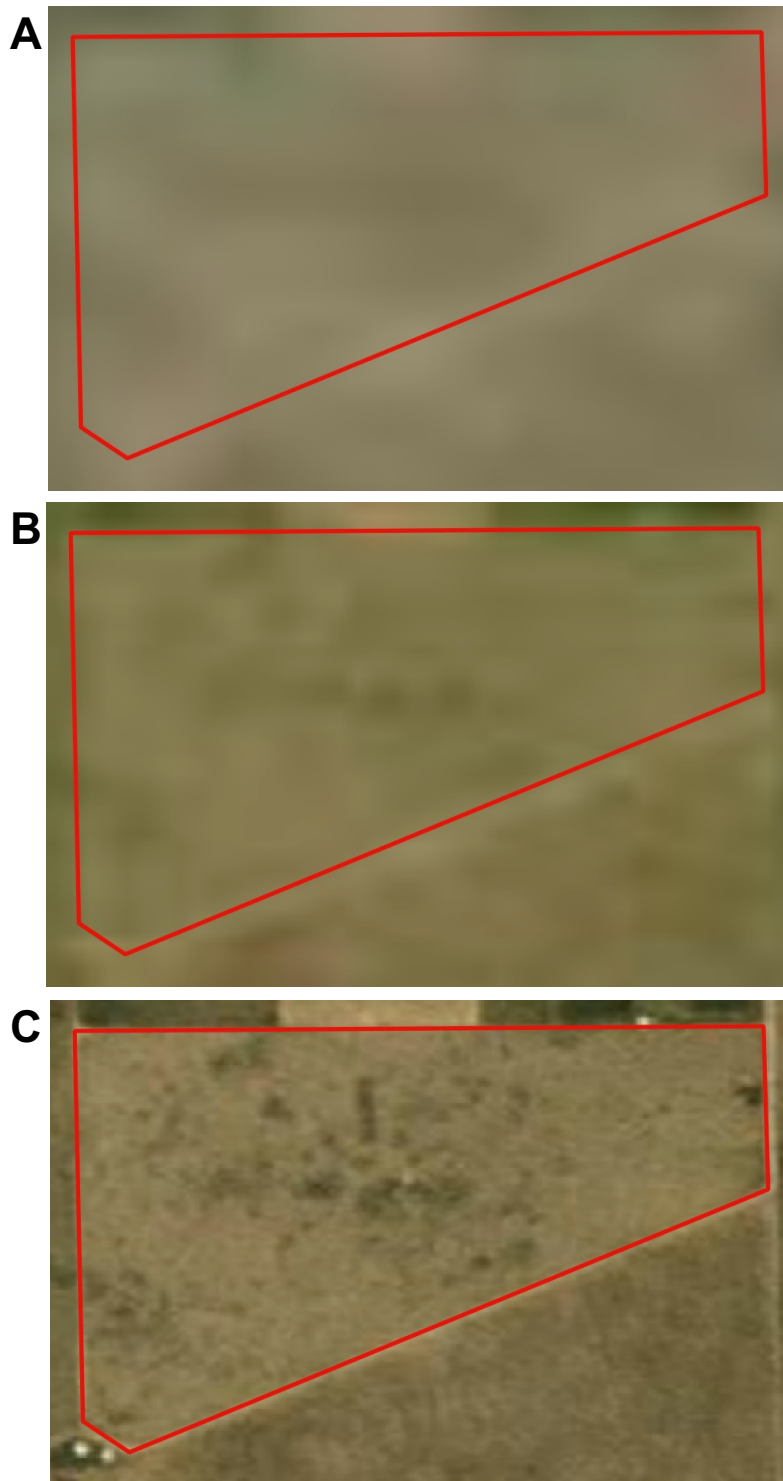


Figure 5.7. Satellite imagery with spatial resolution for moderately grazed pasture at Northern Great Plains Research Laboratory; A. Landsat 30 m (July 31, 2018); B. Sentinel 10 m (July 13, 2018); C: PlanetScope's CubSat 3 m (July 14, 2018).

Table 5.3. Feature rank from recursive feature elimination for satellite platforms.

Rank	Landsat	Sentinel	CubeSat
1	AvgT_Soil	AvgT_Soil	AvgT_Soil
2	Green	Di_TR	NIR
3	G_Rdiff	SWIR2	GCI
4	SWIR2	Tot_Sol_R	MSAVI
5	SWIR	Avg_WindS	GNDVI
6	AvgB_Soil	AvgB_Soil	SAVI
7	Blue	SWIR	AvgB_Soil
8	SIPI	Avg_WD	Blue
9	BCC	NDMI	RCC
10	Di_TR	JH_PET	NDVI

Note: Please refer to Table 5.1 for more information on the features.

R^2 and the lowest RMSE and MAE followed by Sentinel and Landsat (fig. 5.8).

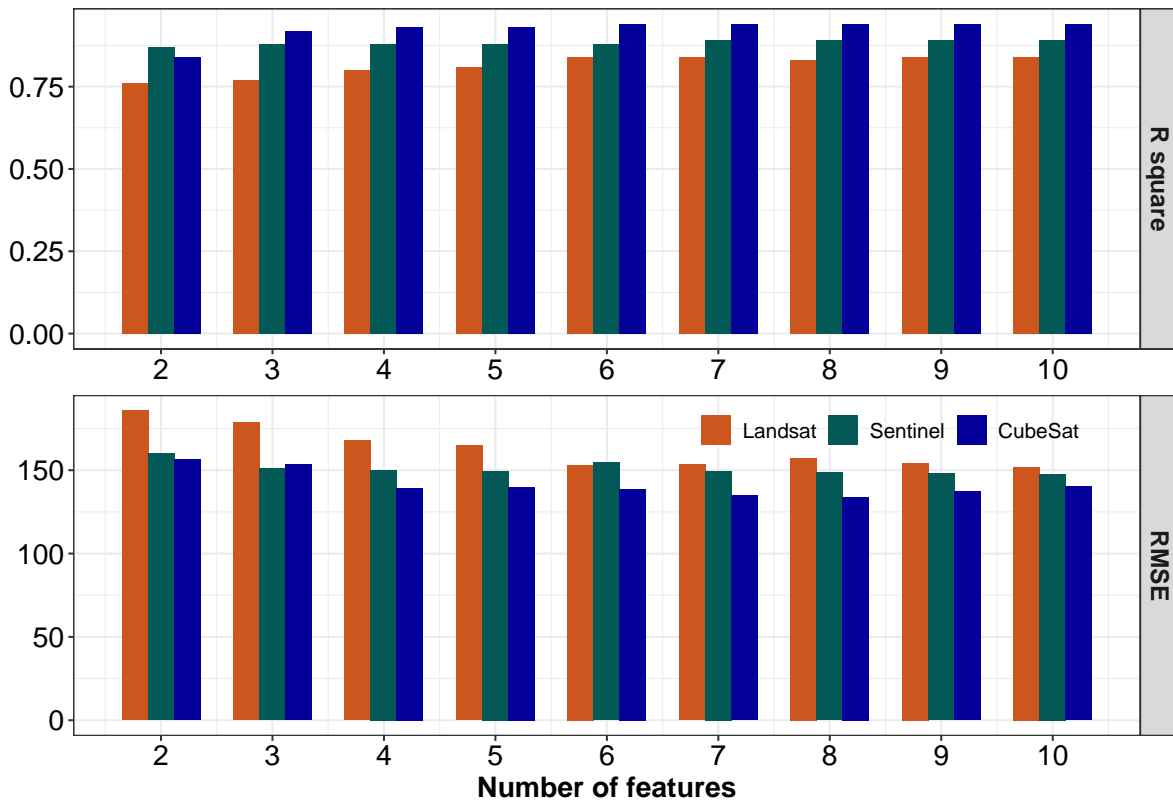


Figure 5.8. Landsat, Sentinel, and CubeSat satellite comparison using performance metrics coefficient of determination (R^2) and root mean square error (RMSE).

In most instances, the performance of Sentinel was more close to CubeSat than to Landsat. The RMSE and MAE followed a similar trend because of the nature of estimation. A more stabilized trend of the metrics was observed for the CubeSat satellite with finer resolution. Therefore, satellite images with higher resolution, such as CubeSat that is available from 2014, were recommended in predicting pasture biomass. Based on the availability of the satellite imagery, the recommended order of preference was CubeSat, Sentinel, and Landsat platforms for better biomass prediction accuracy.

5.4.3.3. Application 3 - Cultivated hay crop alfalfa yield prediction with developed methodology using CubeSat

The selected methodology and CubeSat satellite imagery were used to evaluate the prediction of the cultivated alfalfa hay crop. Forage from the alfalfa fields (H1 and G1; fig. 5.9) were harvested mechanically and fed to livestock. The alfalfa crops were seeded in 2015 for H1 and in 2019 for G1 and were harvested three times every year between June and August for the years 2017, 2018, and 2020. The amount of biomass harvested during the first harvest was on an average 2.4 times higher than the second and the third harvest. The dry matter alfalfa yield (ground truth) was used for the analysis.

The results from the RFE feature selection methodology revealed that climate features such as average turf soil temperature and potential evapotranspiration, all three visible bands (*R*, *G*, and *B*), and MSAVI vegetation index as influential in predicting alfalfa forage. Previous yield prediction study on Italian ryegrass (*Lolium multi-florum* Lam.) has reported that MSAVI was a significant feature in predicting forage biomass (Lim et al., 2015).

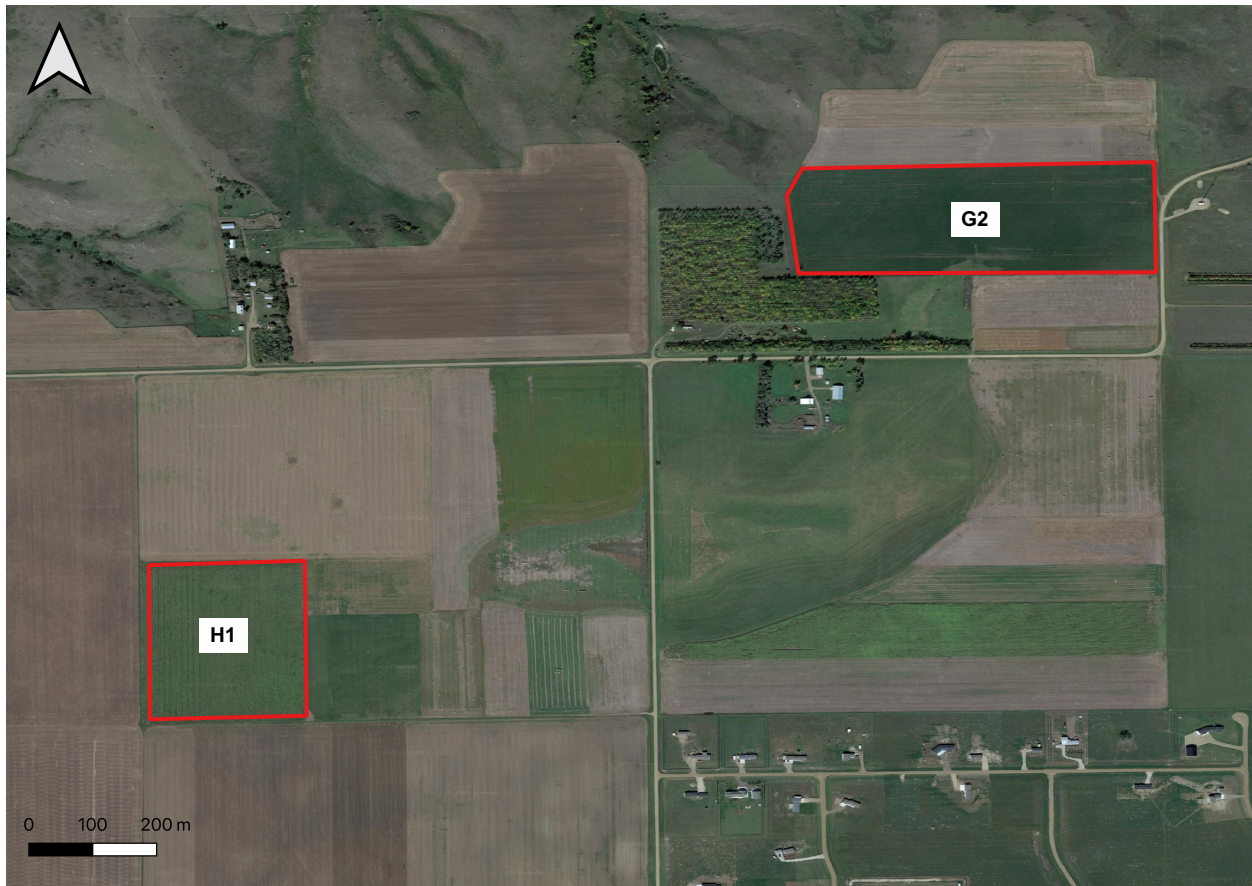


Figure 5.9. Alfalfa forage fields H1 and G2 represented as polygon shapefiles located at Northern Great Plains Research Laboratory, (NGPRL; USDA-ARS), Mandan, ND, USA.

The prediction results (different years and cuts) reveal that the methodology, developed using perennial pastures, can be applied to hay crops and was successful in predicting the alfalfa forage yield for all the years with an accuracy of $R^2 = 0.95$ (fig. 5.10). The methodology of RFE and RF used only the three years limited data for three years; however, more data and different fields should be tested in the future to validate the methodology to be applied for hay forage prediction.

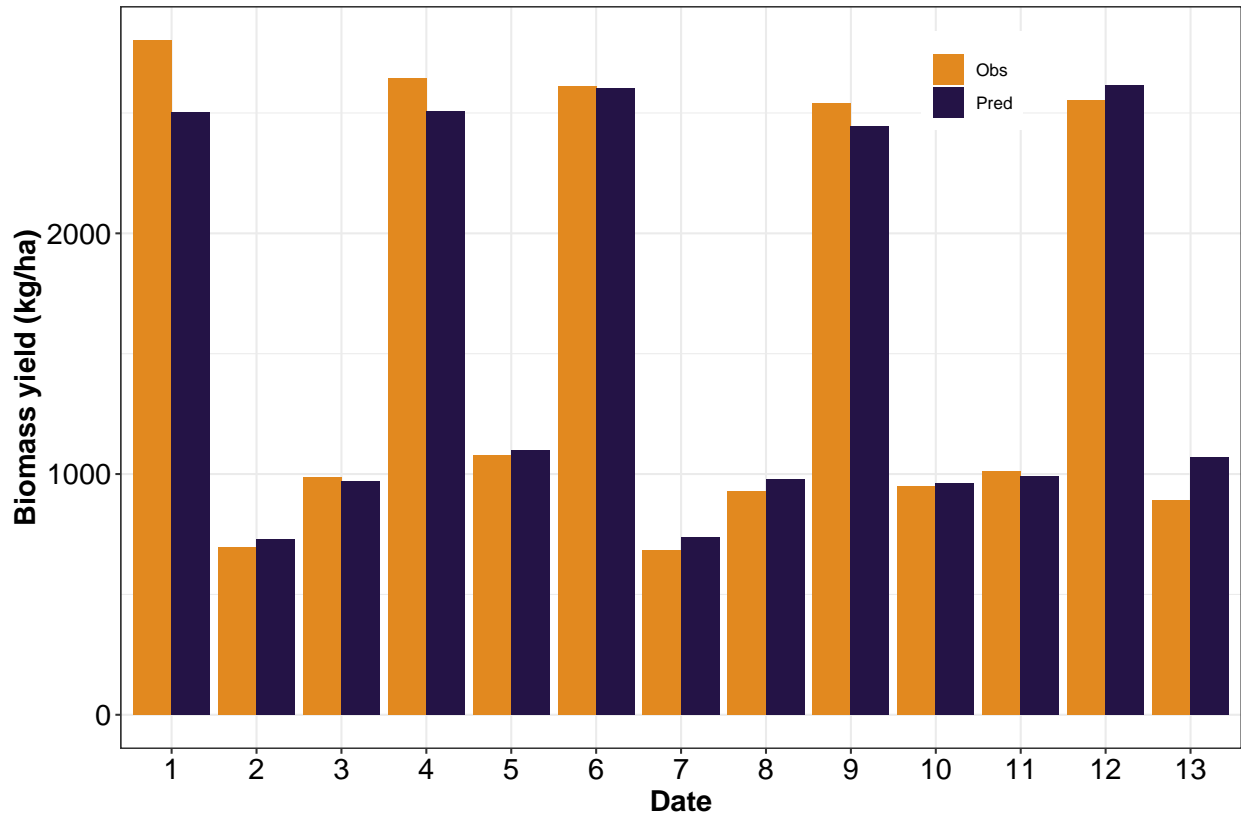


Figure 5.10. Observed versus predicted yields for alfalfa forage (hay crop) for different years (2017, 2018, and 2020), cuts (1–3), and fields (H1 and G2; fig. 5.9).

5.5. Conclusions

Multispectral satellite images and climate features were found to be the potential indicator for predicting pasture biomass in a non-destructive, more frequent, and large-scale method. The machine learning (ML) approach was useful in building prediction models for evaluating pasture biomass. Among the feature selection methods considered, recursive feature elimination (RFE) emerged as the best, followed by Boruta and backward elimination to identify the most significant features in predicting biomass.

Highly influential remote sensing bands, vegetation index, and climate features predicting pasture biomass were SWIR2, normalized moisture index, and turf soil temper-

ature for Landsat and NIR, green chlorophyll index, and average turf soil temperature for CubeSat, respectively. The top-ranking most common features with Landsat and CubeSat satellites are infra-red bands (NIR and SWIR), blue band, turf soil temperature, and bare soil temperature.

Among prediction models including multiple linear regression and three ML regression algorithms (random forest (RF), support vector regression, and k-nearest neighbor), the RF was the most satisfactory based on the prediction performance. The developed overall methodology of “RFE” for feature selection and “RF” for prediction was found to be successful and recommended in predicting pasture biomass.

Some of the conclusions based on the use of the developed methodology to different applications are (i) the methodology (RFE and RF) accurately predicted biomass yields in other unseen pastures; (ii) finer satellite spatial resolution was better in predicting pasture biomass, and based on the availability of satellite imagery the order of preference was CubeSat (3 m), Sentinel (10 m), and Landsat (30 m); and (iii) the methodology can be extended successfully to high-value hay crop like alfalfa for accurate forage yield prediction.

In the future, the proposed methodology should be investigated on a large scale and on more diverse pasture grass/forage and variable soil types. The use of hyperspectral imagery from unmanned aerial vehicles should be explored to evaluate the biomass/forage prediction potential and accuracy, individually and combined with high-resolution satellite imagery. An interactive tool built using the trained model and/or methodology to predict forage and deliver real-time forage monitoring for the farmers and ranchers will be a natural progression of this research outcome.

5.6. References

- Ahamed, A. M. S., Mahmood, N. T., Hossain, N., Kabir, M. T., Das, K., Rahman, F., & Rahman, R. M. (2015). Applying data mining techniques to predict annual yield of major crops and recommend planting different crops in different districts in Bangladesh. *2015 IEEE/ACIS 16th International Conference on Software Engineering, Artificial Intelligence, Networking and Parallel/Distributed Computing (SNPD)*, 1–6.
- Aparicio, N., Villegas, D., Casadesus, J., Araus, J. L., & Royo, C. (2000). Spectral vegetation indices as nondestructive tools for determining durum wheat yield. *Agron. J.*, *92*(1), 83–91.
- Belayneh, A., Adamowski, J., Khalil, B., & Ozga-Zielinski, B. (2014). Long-term SPI drought forecasting in the Awash River Basin in Ethiopia using wavelet neural network and wavelet support vector regression models. *J. Hydrol.*, *508*, 418–429.
- Bendig, J., Yu, K., Aasen, H., Bolten, A., Bennertz, S., Broscheit, J., Gnyp, M. L., & Bareth, G. (2015). Combining UAV-based plant height from crop surface models, visible, and near infrared vegetation indices for biomass monitoring in barley. *Int. J. Appl. Earth Obs. Geoinf.*, *39*, 79–87.
- Birth, G. S., & McVey, G. R. (1968). Measuring the color of growing turf with a reflectance spectrophotometer. *Agron. J.*, *60*(6), 640–643.
- Cai, Y., Guan, K., Lobell, D., Potgieter, A. B., Wang, S., Peng, J., Xu, T., Asseng, S., Zhang, Y., You, L., et al. (2019). Integrating satellite and climate data to predict wheat yield in australia using machine learning approaches. *Agric. For. Meteorol.*, *274*, 144–159.

- Catchpole, W., & Wheeler, C. (1992). Estimating plant biomass: A review of techniques. *Aust. J. Ecol.*, 17(2), 121–131.
- Chambers, J., & Hastie, T. (1992). Linear models. Chapter 4 of statistical models in S. *Wadsworth & Brooks/Cole*.
- Chen, Z., Cheng, Q., Duan, F., Huang, X., Xu, H., Sui, R., & Li, Z. (2022). UAV-based hyperspectral and ensemble machine learning for predicting yield in winter wheat. *Agronomy*, 12(1), 202.
- Congedo, L. (2016). Semi-Automatic Classification Plugin: A Python tool for the download and processing of remote sensing images in QGIS. *J. Open Source Softw.*, 6(64), 3172.
- Dong, W., Li, C., Hu, Q., Pan, F., Bhandari, J., & Sun, Z. (2020). Potential evapotranspiration reduction and its influence on crop yield in the North China Plain in 1961–2014. *Adv. Meteorol.*, 2020.
- El-Hendawy, S. E., Hassan, W. M., Al-Suhaibani, N. A., & Schmidhalter, U. (2017). Spectral assessment of drought tolerance indices and grain yield in advanced spring wheat lines grown under full and limited water irrigation. *Agric. Water Manage.*, 182, 1–12.
- Fawagreh, K., Gaber, M. M., & Elyan, E. (2014). Random forests: From early developments to recent advancements. *Syst. Sci. Control Eng.*, 2(1), 602–609.
- Feng, L., Zhang, Z., Ma, Y., Du, Q., Williams, P., Drewry, J., & Luck, B. (2020). Alfalfa yield prediction using UAV-based hyperspectral imagery and ensemble learning. *Remote Sens.*, 12(12), 2028.

- Filippi, P., Jones, E. J., Wimalathunge, N. S., Somarathna, P. D., Pozza, L. E., Ugbaje, S. U., Jephcott, T. G., Paterson, S. E., Whelan, B. M., & Bishop, T. F. (2019). An approach to forecast grain crop yield using multi-layered, multi-farm data sets and machine learning. *Precis. Agric.*, *20*(5), 1015–1029.
- Foley, W. J., McIlwee, A., Lawler, I., Aragones, L., Woolnough, A. P., & Berding, N. (1998). Ecological applications of near infrared reflectance spectroscopy—a tool for rapid, cost-effective prediction of the composition of plant and animal tissues and aspects of animal performance. *Oecologia*, *116*(3), 293–305.
- Gitelson, A. A., Gritz, Y., & Merzlyak, M. N. (2003). Relationships between leaf chlorophyll content and spectral reflectance and algorithms for non-destructive chlorophyll assessment in higher plant leaves. *J. Plant Physiol.*, *160*(3), 271–282.
- Gitelson, A. A., Kaufman, Y. J., & Merzlyak, M. N. (1996). Use of a green channel in remote sensing of global vegetation from EOS-MODIS. *Remote Sens. Environ.*, *58*(3), 289–298.
- Gitelson, A. A., Kaufman, Y. J., Stark, R., & Rundquist, D. (2002). Novel algorithms for remote estimation of vegetation fraction. *Remote Sens. Environ.*, *80*(1), 76–87.
- Gitelson, A. A., Viña, A., Arkebauer, T. J., Rundquist, D. C., Keydan, G., & Leavitt, B. (2003). Remote estimation of leaf area index and green leaf biomass in maize canopies. *Geophys. Res. Lett.*, *30*(5).
- Gómez, D., Salvador, P., Sanz, J., & Casanova, J. L. (2021). New spectral indicator potato productivity index based on Sentinel-2 data to improve potato yield prediction: A machine learning approach. *Int. J. Remote Sens.*, *42*(9), 3426–3444.

- Gonzalez-Sanchez, A., Frausto-Solis, J., & Ojeda-Bustamante, W. (2014). Predictive ability of machine learning methods for massive crop yield prediction. *Span. J. Agric. Res.*, *12*(2), 313–328.
- Gopal, P. M., & Bhargavi, R. (2018). Feature selection for yield prediction in Boruta algorithm. *Int. J. Pure Appl. Math.*, *118*, 139–144.
- Gorelick, N., Hancher, M., Dixon, M., Ilyushchenko, S., Thau, D., & Moore, R. (2017). Google Earth Engine: Planetary-scale geospatial analysis for everyone. *Remote Sensing of Environment*, *202*, 18–27.
- Gunn, S. R. et al. (1998). Support vector machines for classification and regression. *ISIS Tehc. Rep.*, *14*(1), 5–16.
- Guzmán, S. M., Paz, J. O., Tagert, M. L. M., Mercer, A. E., & Pote, J. W. (2018). An integrated SVR and crop model to estimate the impacts of irrigation on daily groundwater levels. *Agric. Syst.*, *159*, 248–259.
- Han, J., Zhang, Z., Cao, J., Luo, Y., Zhang, L., Li, Z., & Zhang, J. (2020). Prediction of winter wheat yield based on multi-source data and machine learning in China. *Remote Sens.*, *12*(2), 236.
- Huete, A. R. (1988). A soil-adjusted vegetation index (SAVI). *Remote Sens. Environ.*, *25*(3), 295–309.
- Huete, A., Liu, H., Batchily, K., & Van Leeuwen, W. (1997). A comparison of vegetation indices over a global set of TM images for EOS-MODIS. *Remote Sens. Environ.*, *59*(3), 440–451.

- Hunt, E. R., Cavigelli, M., Daughtry, C. S., McMurtrey, J. E., & Walthall, C. L. (2005). Evaluation of digital photography from model aircraft for remote sensing of crop biomass and nitrogen status. *Precis. Agric.*, 6(4), 359–378.
- Ji, L., & Fan, K. (2019). Climate prediction of satellite-based spring Eurasian vegetation index (NDVI) using coupled singular value decomposition (SVD) patterns. *Remote Sens.*, 11(18), 2123.
- Jiang, X., Zou, B., Feng, H., Tang, J., Tu, Y., & Zhao, X. (2019). Spatial distribution mapping of Hg contamination in subclass agricultural soils using GIS enhanced multiple linear regression. *J. Geochem. Explor.*, 196, 1–7.
- Jin, X., Kumar, L., Li, Z., Xu, X., Yang, G., & Wang, J. (2016). Estimation of winter wheat biomass and yield by combining the aquacrop model and field hyperspectral data. *Remote Sens.*, 8(12), 972.
- John, A., Ong, J., Theobald, E. J., Olden, J. D., Tan, A., & HilleRisLambers, J. (2020). Detecting montane flowering phenology with CubeSat imagery. *Remote Sens.*, 12(18), 2894.
- Kahimba, F. C., Ranjan, R. S., Froese, J., Entz, M., & Nason, R. (2008). Cover crop effects on infiltration, soil temperature, and soil moisture distribution in the Canadian Prairies. *Appl. Eng. Agric.*, 24(3), 321–333.
- Kamir, E., Waldner, F., & Hochman, Z. (2020). Estimating wheat yields in Australia using climate records, satellite image time series and machine learning methods. *SPRS J. Photogramm. Remote Sens.*, 160, 124–135.
- Kaspar, T., & Bland, W. L. (1992). Soil temperature and root growth. *Soil Sci.*, 154, 290–290.

- Kataoka, T., Kaneko, T., Okamoto, H., & Hata, S. (2003). Crop growth estimation system using machine vision. *Proceedings 2003 IEEE/ASME International Conference on Advanced Intelligent Mechatronics (AIM 2003)*, 2, b1079–b1083.
- Kaufman, Y. J., & Tanre, D. (1992). Atmospherically resistant vegetation index (ARVI) for EOS-MODIS. *IEEE Trans. Geosci. Remote Sens.*, 30(2), 261–270.
- Kuhn, M. (2008). Building predictive models in R using the caret package. *J. Stat. Softw.*, 28(1), 1–26.
- Kursa, M. B., Rudnicki, W. R. et al. (2010). Feature selection with the Boruta package. *J Stat Softw*, 36(11), 1–13.
- Kuwata, K., & Shibasaki, R. (2016). Estimating corn yield in the United States with MODIS EVI and machine learning methods. *ISPRS Ann. Photogramm. Remote Sens. Spat. Inf. Sci*, 3(8), 131–136.
- Li, B., Xu, X., Zhang, L., Han, J., Bian, C., Li, G., Liu, J., & Jin, L. (2020). Above-ground biomass estimation and yield prediction in potato by using UAV-based RGB and hyperspectral imaging. *SPRS J. Photogramm. Remote Sens.*, 162, 161–172.
- Liebig, M., Kronberg, S., Hendrickson, J., Dong, X., & Gross, J. (2013). Carbon dioxide efflux from long-term grazing management systems in a semiarid region. *Agric. Ecosyst. Environ.*, 164, 137–144.
- Lim, J., Kawamura, K., Lee, H.-J., Yoshitoshi, R., Kurokawa, Y., Tsumiyama, Y., & Watanabe, N. (2015). Evaluating a hand-held crop-measuring device for estimating the herbage biomass, leaf area index and crude protein content in an Italian ryegrass field. *Grassland Sci.*, 61(2), 101–108.

- López-Calderón, M. J., Estrada-Ávalos, J., Rodríguez-Moreno, V. M., Mauricio-Ruvalcaba, J. E., Martínez-Sifuentes, A. R., Delgado-Ramírez, G., & Miguel-Valle, E. (2020). Estimation of total nitrogen content in forage maize (*Zea mays* L.) using spectral indices: Analysis by random forest. *Agriculture*, *10*(10), 451.
- Luo, C., Zhang, X., Wang, Y., Men, Z., & Liu, H. (2022). Regional soil organic matter mapping models based on the optimal time window, feature selection algorithm and Google Earth Engine. *Soil Til. Res.*, *219*, 105325.
- Lupo, C. D., Clay, D. E., Benning, J. L., & Stone, J. J. (2013). Life-cycle assessment of the beef cattle production system for the Northern Great Plains, USA. *J. Environ. Qual.*, *42*(5), 1386–1394.
- Lussem, U., Bolten, A., Gnyp, M., Jasper, J., & Bareth, G. (2018). Evaluation of RGB-based vegetation indices from UAV imagery to estimate forage yield in grassland. *Int. Arch. Photogramm. Remote Sens Spatial Inf Sci*, *42*, 1215–1219.
- Ma, Y., Kang, Y., Ozdogan, M., & Zhang, Z. (2019). County-level corn yield prediction using deep transfer learning. *AGU Fall Meeting Abstracts, 2019*, B54D–02.
- Mao, K. Z. (2004). Orthogonal forward selection and backward elimination algorithms for feature subset selection. *IEEE Transactions on Systems, Man, and Cybernetics, Part B (Cybernetics)*, *34*(1), 629–634.
- Meng, L., Liu, H., L Ustin, S., & Zhang, X. (2021). Predicting maize yield at the plot scale of different fertilizer systems by multi-source data and machine learning methods. *Remote Sens.*, *13*(18), 3760.
- Meyer, G. E., Hindman, T. W., & Laksmi, K. (1999). Machine vision detection parameters for plant species identification. *Precis. Agric. Biol. Qual.*, *3543*, 327–335.

- Meyer, G. E., Neto, J. C., Jones, D. D., & Hindman, T. W. (2004). Intensified fuzzy clusters for classifying plant, soil, and residue regions of interest from color images. *Comput. Electron. Agric.*, 42(3), 161–180.
- Onwuka, B., & Mang, B. (2018). Effects of soil temperature on some soil properties and plant growth. *Adv. Plants Agric. Res*, 8(1), 34.
- Penuelas, J., Filella, I., & Gamon, J. A. (1995). Assessment of photosynthetic radiation-use efficiency with spectral reflectance. *New Phytol.*, 131(3), 291–296.
- Prasad, N., Patel, N., & Danodia, A. (2021). Crop yield prediction in cotton for regional level using random forest approach. *Spatial Inf. Res.*, 29(2), 195–206.
- PS, M. G. (2019). Performance evaluation of best feature subsets for crop yield prediction using machine learning algorithms. *Appl. Artif. Intell.*, 33(7), 621–642.
- Pullanagari, R. R., Kereszturi, G., & Yule, I. (2018). Integrating airborne hyperspectral, topographic, and soil data for estimating pasture quality using recursive feature elimination with random forest regression. *Remote Sens.*, 10(7), 1117.
- Qi, J., Chehbouni, A., Huete, A. R., Kerr, Y. H., & Sorooshian, S. (1994). A modified soil adjusted vegetation index. *Remote Sens. Environ.*, 48(2), 119–126.
- Ramoelo, A., Cho, M. A., Mathieu, R., Madonsela, S., Van De Kerchove, R., Kaszta, Z., & Wolff, E. (2015). Monitoring grass nutrients and biomass as indicators of rangeland quality and quantity using random forest modelling and WorldView-2 data. *Int. J. Appl. Earth Obs. Geoinf.*, 43, 43–54.
- Rouse, J. W., Haas, R. H., Schell, J. A., Deering, D. W., et al. (1974). Monitoring vegetation systems in the Great Plains with ERTS. *NASA Spec. Publ.*, 351(1974), 309.

- Safi, A. R., Karimi, P., Mul, M., Chukalla, A., & de Fraiture, C. (2022). Translating open-source remote sensing data to crop water productivity improvement actions. *Agric. Water Manage.*, *261*, 107373.
- Sagan, V., Maimaitijiang, M., Bhadra, S., Maimaitiyiming, M., Brown, D. R., Sidike, P., & Fritschi, F. B. (2021). Field-scale crop yield prediction using multi-temporal WorldView-3 and PlanetScope satellite data and deep learning. *SPRS J. Photogramm. Remote Sens.*, *174*, 265–281.
- Schratz, P., Muenchow, J., Iturritxa, E., Richter, J., & Brenning, A. (2019). Hyperparameter tuning and performance assessment of statistical and machine-learning algorithms using spatial data. *Ecol. Modell.*, *406*, 109–120.
- Shafiee, S., Lied, L. M., Burud, I., Dieseth, J. A., Alsheikh, M., & Lillemo, M. (2021). Sequential forward selection and support vector regression in comparison to LASSO regression for spring wheat yield prediction based on UAV imagery. *Comput. Electron. Agric.*, *183*, 106036.
- Shastri, A., Sanjay, H., & Hegde, M. (2015). A parameter based ANFIS model for crop yield prediction. *2015 IEEE International Advance Computing Conference (IACC)*, 253–257.
- Steele, M. R., Gitelson, A. A., Rundquist, D. C., & Merzlyak, M. N. (2009). Nondestructive estimation of anthocyanin content in grapevine leaves. *Am. J. Enol. Vitic.*, *60*(1), 87–92.
- Subhashree, S. N., Sunoj, S., Hassanijalilian, O., & Igathinathane, C. (2020). Decoding common machine learning methods: Agricultural application case studies using

- open source software. *Applied intelligent decision making in machine learning* (pp. 21–52). CRC Press, Boca Raton, FL, USA.
- Timsina, J., Dutta, S., Devkota, K. P., Chakraborty, S., Neupane, R. K., Bishta, S., Amgain, L. P., Singh, V. K., Islam, S., & Majumdar, K. (2021). Improved nutrient management in cereals using Nutrient Expert and machine learning tools: Productivity, profitability and nutrient use efficiency. *Agric. Syst.*, *192*, 103181.
- Van Klompenburg, T., Kassahun, A., & Catal, C. (2020). Crop yield prediction using machine learning: A systematic literature review. *Comput. Electron. Agric.*, *177*, 105709.
- Venables, W., & Ripley, B. (2002). *Modern applied statistics with S-PLUS*. Springer Science & Business Media, NY, USA.
- Were, K., Bui, D. T., Dick, Ø. B., & Singh, B. R. (2015). A comparative assessment of support vector regression, artificial neural networks, and random forests for predicting and mapping soil organic carbon stocks across an Afromontane landscape. *Ecol. Indic.*, *52*, 394–403.
- Wilson, E. H., & Sader, S. A. (2002). Detection of forest harvest type using multiple dates of Landsat TM imagery. *Remote Sens. Environ.*, *80*(3), 385–396.
- Woebbecke, D. M., Meyer, G. E., Von Bargen, K., & Mortensen, D. A. (1995). Color indices for weed identification under various soil, residue, and lighting conditions. *Trans. ASAE*, *38*(1), 259–269.
- Xiaoqin, W., Miaomiao, W., Shaoqiang, W., & Yundong, W. (2015). Extraction of vegetation information from visible unmanned aerial vehicle images. *Trans. Chin. Soc. Agric. Eng.*, *31*(5).

- Xu, L., & Zhang, W.-J. (2001). Comparison of different methods for variable selection. *Anal. Chim. Acta*, 446(1-2), 475–481.
- Xue, J., & Su, B. (2017). Significant remote sensing vegetation indices: A review of developments and applications. *J. Sens.*, 2017.
- Yang, C., & Anderson, G. L. (2000). Mapping grain sorghum yield variability using airborne digital videography. *Precis. Agric.*, 2(1), 7–23.
- Zhang, Z., Flores, P., Igathinathane, C., L Naik, D., Kiran, R., & Ransom, J. K. (2020). Wheat lodging detection from UAS imagery using machine learning algorithms. *Remote Sens.*, 12(11), 1838.
- Zhihui, W., Jianbo, S., Blackwell, M., Haigang, L., Bingqiang, Z., & Huimin, Y. (2016). Combined applications of nitrogen and phosphorus fertilizers with manure increase maize yield and nutrient uptake via stimulating root growth in a long-term experiment. *Pedosphere*, 26(1), 62–73.
- Zhu, Z., & Woodcock, C. E. (2012). Object-based cloud and cloud shadow detection in Landsat imagery. *Remote Sens. Environ.*, 118, 83–94.
- Zimmer, S. N., Schupp, E. W., Boettinger, J. L., Reeves, M. C., & Thacker, E. T. (2021). Considering spatiotemporal forage variability in rangeland inventory and monitoring. *Rangeland Ecol. Manage.*, 79, 53–63.

6. DEVELOPMENT OF A USER-FRIENDLY RANGELAND FORAGE YIELD PREDICTION WEB TOOL *

6.1. Abstract

Frequently occurring droughts in North Dakota significantly reduce forage production in the rangelands and pastures and affect the livelihood of the ranchers and other forage producers. In addition, overgrazing, during these extreme conditions due to inefficient cattle stocking rates, impacts the rangeland environment. A decision support tool for the ranchers in the Northern Great Plains area monitoring and predicting the forage potential would be valuable, especially during adverse drought conditions, for resource allocation and stocking rate planning. The existing tool (North Dakota Drought Calculator) was a simple and useful spreadsheet-based program that uses only precipitation as input and generates forage yield potential. However, other parameters that affect the forage yield prediction could be used following the recent advances in remote sensing satellite technology, local weather data, soil, plant species, and field-specific inputs modeled using advanced analysis such as machine learning (ML) will be beneficial but have not been reported so far. Therefore, an exclusive web-based interactive tool was developed using open-source ShinyR software with an ML model operating at the background trained based on the satellite and climate data. The tool was designed to accommodate user inputs specific to their pasture. The tool's simple inputs include rangeland/pasture shapefile, climate

* This paper will be submitted to the *Computers and Electronics in Agriculture* journal in 2022. Authors: Srinivasagan N. Subhashree, C. Igathinathane, S. Ludwig, A. Akyuz, J. Hendrickson, D. Archer, M. Liebig, D. Toledo, K. Sedevic, and D. Peck. Subhashree performed the systematic search, collected the data, developed the necessary code, and wrote the manuscript. Dr. Igathinathane Cannayen is the major advisor, principal investigator, and the corresponding author who worked with Subhashree throughout the research and manuscript development. All the co-authors have assisted in the research direction and review of the manuscript.

data, and satellite imagery using the freely available PlanetScope Inc. platform. The tool extracts spatial data from the supplied satellite images, estimates vegetation indices (VIs), collects climate data, and inputs to the already trained random forest model (best among tested ML models). The tool's output includes biomass production and maps to visualize estimated vegetation indices. This developed user-friendly web-based tool will work as a decision-support tool that places ranchers, forage producers, natural resource planners, and researchers in the driver's seat in making forage production, stocking rates, and rangeland health management decisions.

6.2. Introduction

The rangeland ecosystem in the United States, spanning millions of hectares, is primarily managed by livestock operations. Climatic factors such as rainfall and temperature greatly influence rangeland productivity. A study successfully linked the rangeland production to the growing season precipitation, which is a highly variable parameter (Knapp and Smith, 2001). Therefore, extreme conditions such as droughts, like the one recently experienced by vast areas of the Northern Great Plains (NGP) from 2020–2021 can trigger undesirable changes in the rangelands which reduced forage production and endangered the ranching livelihoods (Godde et al., 2020).

The livestock operations were vulnerable to the reduced rangeland production since it reduces the number of livestock supported by the rangelands, which reduces the value of cattle and calf. In addition, excessive rangeland grazing during drought conditions was more prone to ecological degradation, including increased soil erosion due to the lost plant cover (Thurow and Taylor, 1999).

Increasing variability in climate factors and its effect on the rangeland ecosystem heightens the need for ranchers and farmers to monitor rangelands and devise management plans to adapt to the oncoming drought, such as reserve forage to balance demand and supply and varying animal stocking rate based on the forage availability.

In this context, few interactive tools for rangeland monitoring were developed. The existing tool, exclusively meant for North Dakota, was the “Drought Calculator” developed by NRCS and USDA–ARS, a spreadsheet-based tool that predicted the forage yield potential based only on the precipitation data and generic forage growth curves. The drought calculator was used precipitation data to provide regression-based predictions for above-ground forage biomass. And, the drought calculator was recommended as a decision-support tool for cattle production (Reeves et al., 2015).

Another web-based map tool known as the United States Drought Monitor (USDM) tool was available, which categorized drought into five zones based on the temperature, soil moisture, snow cover, and drought indices such as Palmer drought severity index and standard precipitation index. The USDM tool was recommended for ranchers for adopting a management framework based on the existing drought conditions (Derner and Augustine, 2016).

The Grass-Cast was a recent tool developed for forecasting grassland production in the Great Plains and Southwest areas. The tool used normalized difference vegetation index (NDVI) and evapotranspiration data as inputs for the ecological DayCent model for predicting forage at a spatial grid of $10\text{ km} \times 10\text{ km}$, or $\sim 6\text{ miles} \times 6\text{ miles}$ (Peck et al., 2019). The rangeland analysis platform tool enabled users to access geospatial data and visualize annual biomass growth trends from 1984 to current (Allred et al., 2021).

The existing tools were very few in numbers and were predominantly focused on forage prediction at a larger scale. Recent advances in remote sensing (satellite) technology have made existing forage (e.g., Red, Green, Blue, NIR, and SWIR bands) and automatic recording of climate variables (weather station) related information access more affordable and provided continuous data for forage production analysis. However, the field-specific (field-scale) predictions using local weather, soil, and plant species will be beneficial but have not been reported so far.

In this research, described in the previous chapter, the developed machine learning (ML) random forest (RF) model using 10 significant features, such as blue band, near-infrared band, NDVI, soil adjusted vegetation index (SAVI), modified soil adjusted vegetation index, green chlorophyll index, green normalized difference vegetation index, and red chromatic coordinates from the CubeSat satellite (3 m spatial resolution) along with bare soil temperature and turf soil temperature emerged as the best in predicting forage yield. Therefore, the objective of this study was to extend the developed RF prediction model, while the significant features might vary based on the field-specific conditions during feature extraction, as a user-friendly web tool for farmers and ranchers.

6.3. Application Methodology

The open-source programming language R (R Core Team, 2017) is globally popular for its robust statistical and computing and analysis and was commonly used software in the data science community (Lai et al., 2019). This benefit combined with the highly active community providing help and contributing to the development of a large variety of R packages has rendered R an ideal tool for creating applications. Therefore, the tool “Range-Forage” was developed and implemented using the Shiny package (Chang et al., 2019),

which can be used to create intuitive web applications in R software without JavaScript, HTML, or CSS. Shiny is based on the reactive-programming approach which automatically renders the results when the inputs are provided/modified. The tool used packages such as `sf` (Hijmans and van Etten, 2011) and `raster` (Pebesma et al., 2018), which were equipped with handling and processing geospatial data and was efficiently combined with ML analysis. The package `leaflet()` was applied to the tool to produce interactive map visualization. The basic Shiny functionality and appearance can be enhanced using advanced HTML, CSS, and JavaScript-based features since “shinyR” is capable of working cross-platform. The shinyR is an R package to build dynamic R shiny-based dashboards to analyze CSV files, and it provides a simple dashboard design and performs data analysis and ML (supervised and unsupervised).

In general, shiny applications are categorized into two sections: client-side user interface (UI.R) script and cloud-based server (server.R) script. The UI was responsible for the appearance including the type and arrangement of components in the web applications. The components mostly were widgets designed to accept inputs from the user such as text, numbers, tables, and many others. The UI was also sometimes presented with multiple tabs based on the need of the application. The Server defines and controls the output data generated based on the inputs from the UI which were combined with the operations.

In RangeForage app, these operations include: (i) data (raster and shapefile) loading and parsing; (ii) estimating and visualizing band values and vegetation indices (VI); and (iii) predicting forage yield based on the trained ML model. The Shiny framework of the RangeForage application is presented in Figure 6.1.

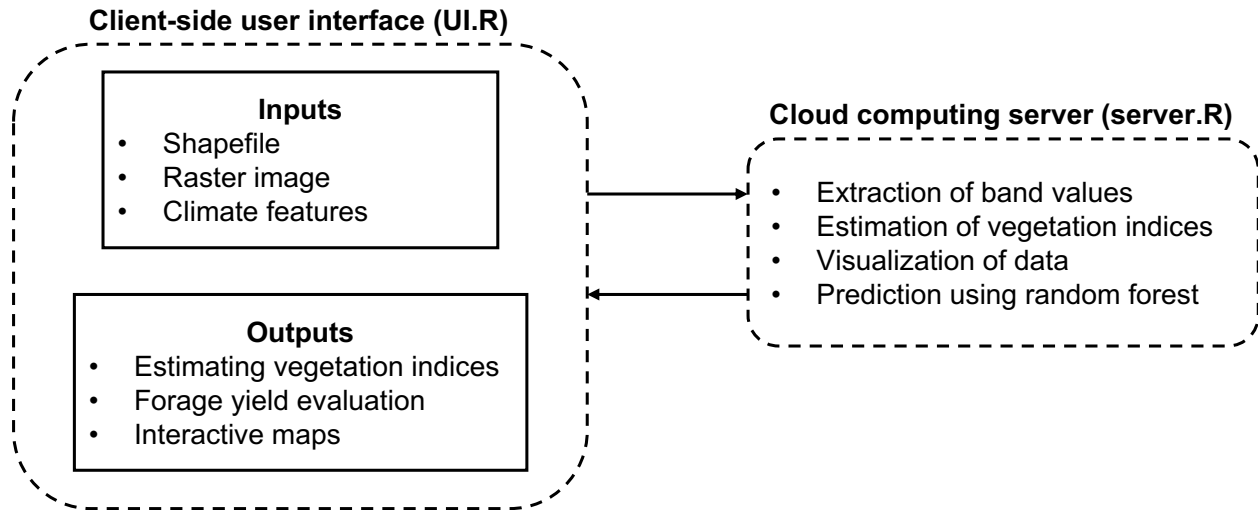


Figure 6.1. Shiny R framework of RangeForage tool consisting on user interface and server components.

6.4. RangeForage Prediction Tool

The tool consists of the main calculator tab “RangeForage” with inputs in the side layout panel and results were presented in the main panel (fig. 6.2). Map visualization of the estimated VI is presented in the “Data visualization” tab and the general information and user instructions were presented in the “About” tab. The user can navigate between the tabs by clicking on the navigation bar at the top. The subsequent sections focus on the data collection and processing of input data such as shapefile and raster dataset and detailed presentation of the user interface and server components.

6.4.1. Data Collection and Processing

The inputs shapefile and raster file were required as user inputs. The input data needs to be procured and processed before it can be used in the tool. The following sections presented the approaches followed to obtain input data from freely available resources and open-source software.

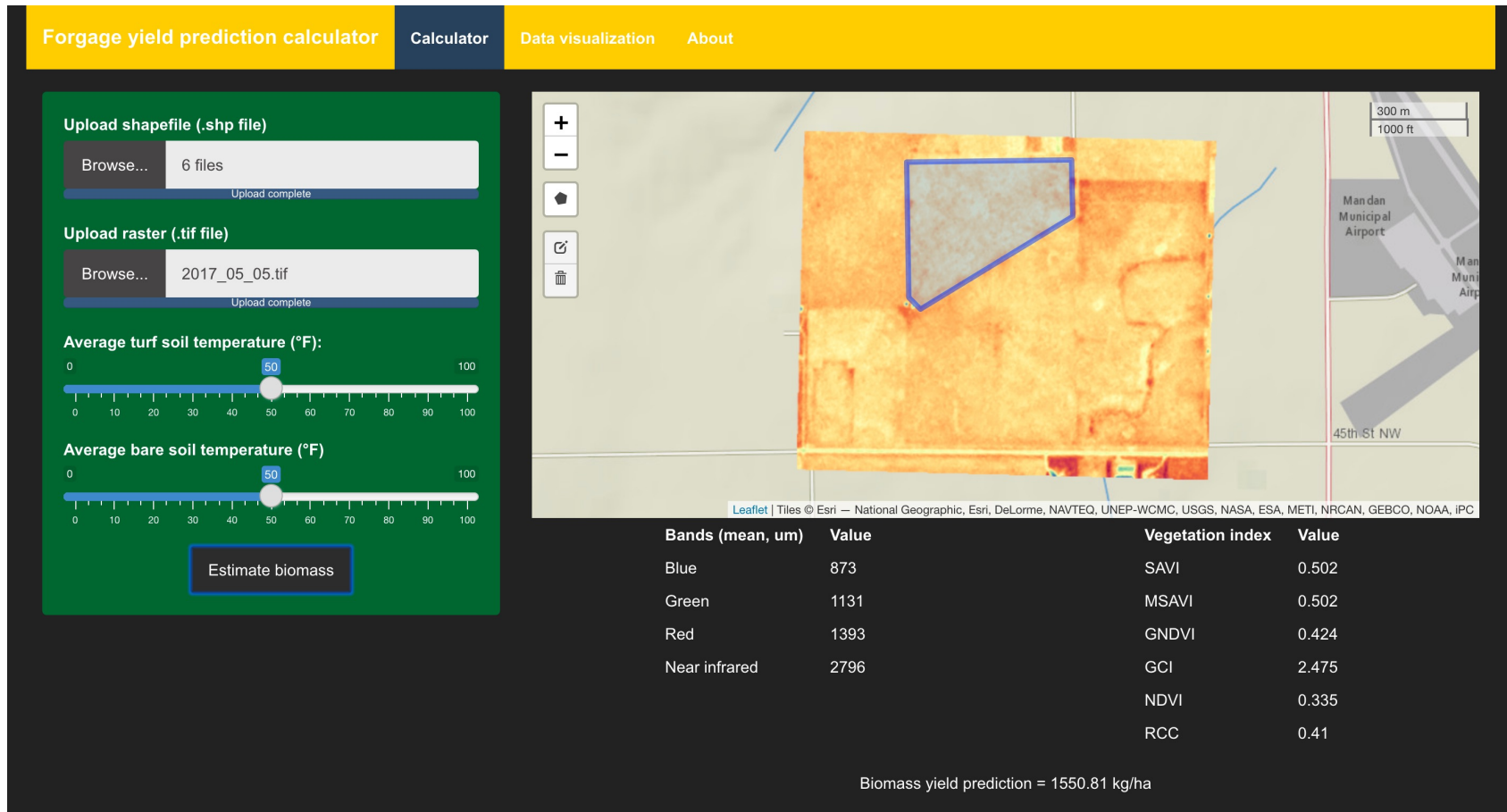


Figure 6.2. User interface of RangeForage web tool showing inputs (left) and results panel (right).

6.4.1.1. Creating shapefile

Shapefile defined the geometry of a feature comprising a set of geographical coordinates. The shapefile for rangeland was created using the open-source software QGIS (QGIS Development Team, 2022). An empty shapefile layer (.shp format) was created using Layer → New → New Shapefile Layer. In the dialog box, the file name, geometry type (polygon), and projection for the shapefile need to be selected (fig. 6.3).

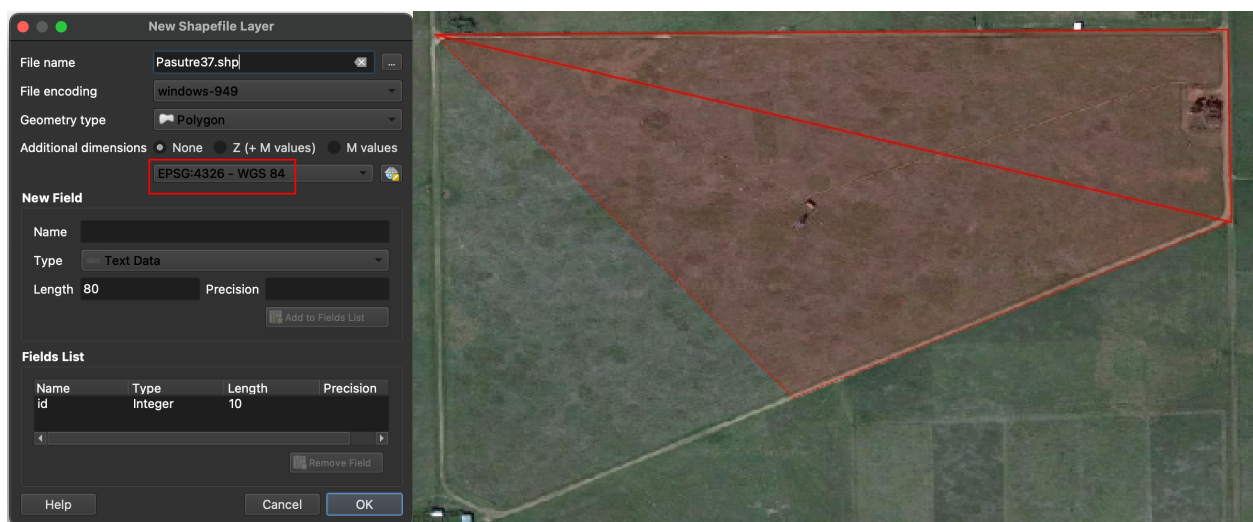


Figure 6.3. Creating a new polygon shapefile layer using QGIS software.

For the geometry type, the option polygon should be selected and the projection should be set to EPSG:4326-WGS 84. Vector features can be digitized using the toggle editing feature by right-clicking on the shapefile. Once the polygon shapefile is digitized, the toggle editing feature is clicked again to generate a new shapefile product.

6.4.1.2. Downloading raster image

The raster images were captured using different band wavelengths by the satellite sensors which can be used for crop health monitoring, weed detection, and many other agricultural applications. PlanetScope was one of the easily accessible resources to procure

raster images as TIFF files from satellites such as Landsat 8, Sentinel 2, and CubeSat (fig. 6.4).

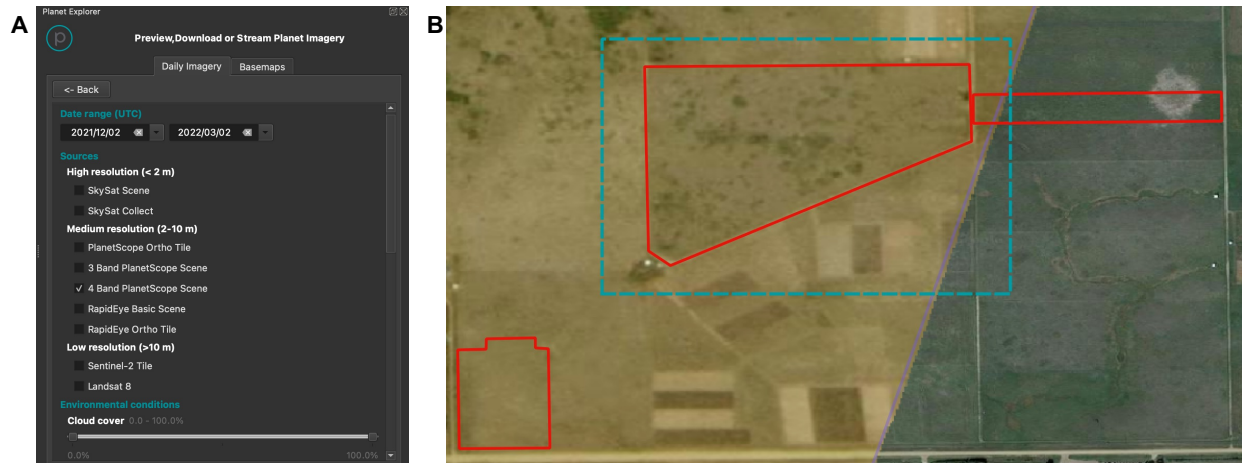


Figure 6.4. Downloading raster images; A. PlanetScope’s filter search dialog box; B. raster image tile (captured by the satellite) available for the selected extent (shown in blue).

The source contained atmospherically corrected surface reflectance raster images that were available for ready use. An extent was drawn to download the tile images from satellite for the selected area. The PlanetScope dialog box was used to edit inputs such as time range, cloud cover (0 and 20%), satellite platform (CubeSat), to filter search results. The resulting raster images were further screened by overlaying onto the extent created and selecting the best images for the time range selected. The screened raster images from CubeSat contained four bands, blue, green, red, and near-infrared (NIR).

6.4.1.3. Obtaining weather data

Local weather data was obtained from North Dakota Agricultural Weather Network (NDAWN). Among the list of stations available, a station near the rangeland location (Mandan, ND) was selected (fig. 6.5). Most weather data at this resource was available from

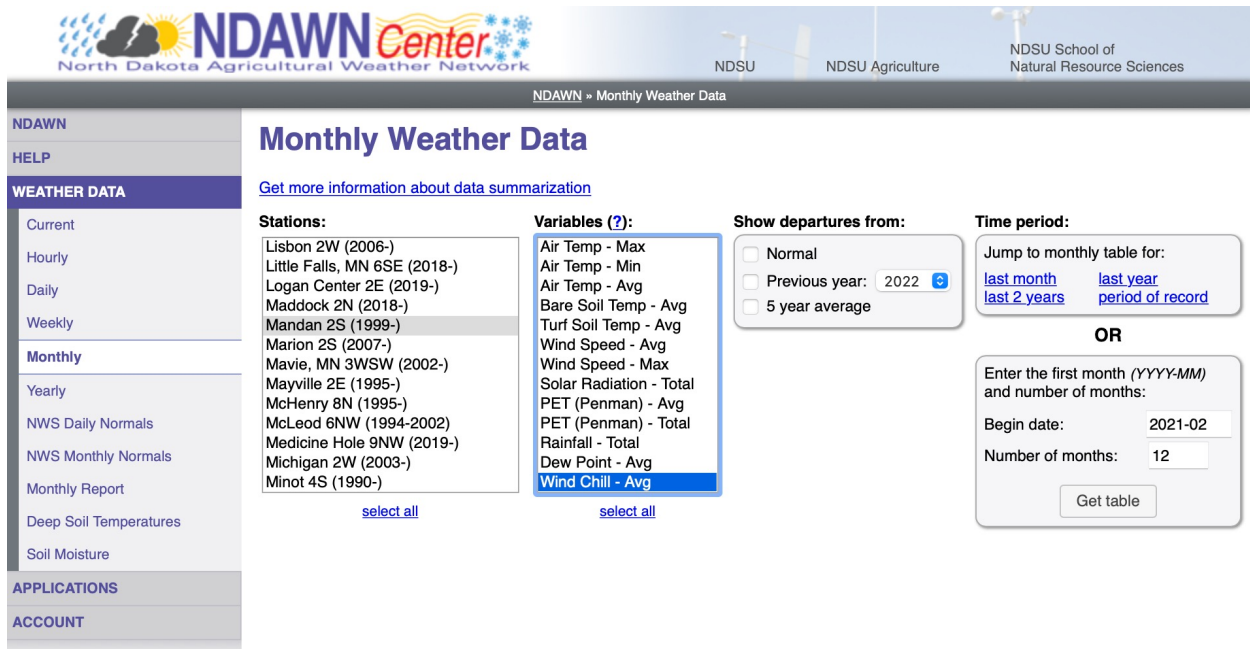


Figure 6.5. Weather variables selected using North Dakota agricultural weather network (NDAWN).

the year 1999 to the present. The weather variables of interest were selected among the 13 available and the time period range was fed to create a table based on the selection. The generated table was exported from NDAWN as a CSV file.

6.4.2. Shiny User Interface

The user-interface of the tool was designed using Shiny widgets (fig. 6.6) such as file upload box (`fileInput()`), slider (`sliderInput()`), action button (`actionButton()`), and checkbox (`checkboxInput()`). The file upload box was used to upload shapefile and raster image into the tool (fig. 6.6A). One or more files can be uploaded using this option, however, the tool allowed for multiple upload at a time (Appendix G.1).

The slider input was used to feed the weather variable inputs into the tool. A minimum and maximum value were provided for the slider range and the user can select the value between the range by dragging the slider position (fig. 6.6B). Unlike other widgets,

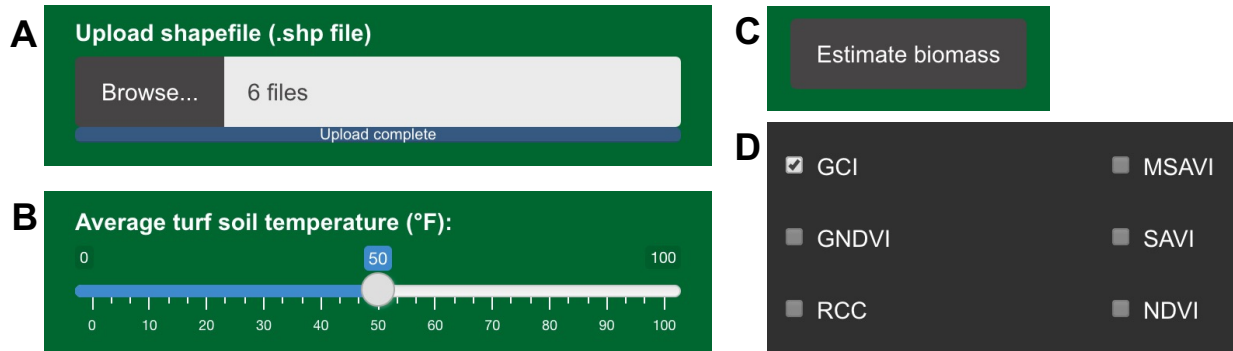


Figure 6.6. Shiny widgets used in the RangeForage prediction tool; A. file upload, B. slider, C. action button, and D. checkbox.

the action button named “Estimate biomass” was used to observe the events from the user interface and then activates a block of code from the server-side to present forage yield prediction results (fig. 6.6C). The checkboxes were used to visualize different estimated VIs as raster files overlaid onto a map (fig. 6.6D). The conditions for the checkboxes were designed in a way that if one checkbox was checked, the other checkboxes were disabled to avoid overlaying of multiple raster files. When the selected checkbox was unchecked, all checkboxes were made available for visualization.

6.4.3. Shiny Server

The server side of shiny consists of `reactEvent()` and `observeEvent()` functions which triggers block of code or user-defined functions when the inputs are entered or modified (Appendix G.2). This tool used several user-defined functions to perform various operations such as loading input data (raster, shapefile, and weather variables), performing analysis, transforming the projections of the shapefile to a raster image, cropping the raster image based on the shapefile extent, extracting individual band values from the raster image, estimate the VI, predicted forage yield and create interactive maps. The trained RF model is available as an RDS file and was read using `readRDS()` function by the

tool for prediction analysis. The base map from the ESRI (Environmental Systems Research Institute) was added to the tool as the default layer. The outputs of the functions were rendered to the user interface using `renderTable()`, `renderText()`, and `renderLeaflet()` pre-defined functions.

6.5. RangeForage Tool Application - A Demonstration

The application of the RangeForage tool was demonstrated using mildly grazed pasture (MGP) located in Northern Great Plains Research Laboratory (NGPRL) located in Mandan, ND. The date of the pasture satellite image selected for the tool demonstration was June 18, 2017.

6.5.1. Loading Tool Inputs

A shapefile for the pasture was created using the method presented in Section 6.4.1.1. The shapefile was uploaded from the local system into the user interface using the file input “Upload shapefile” option (fig. 6.7). The tool reads the shapefile and renders it as an overlaid feature on ESRI “Leaflet” as the base map. Once the file is uploaded, the interactive map zooms to the geographic location showing the shapefile extent.

After the shapefile was rendered, the “Upload raster” input file option was clicked to browse the raster file from the local system. The raster file from CubeSat satellite obtained from PlanetScope was uploaded to the tool (section 6.4.1.2). The entire raster file tile overlaid the leaflet base map and the map visualization panel showed the uploaded raster file and shapefile (fig. 6.8).

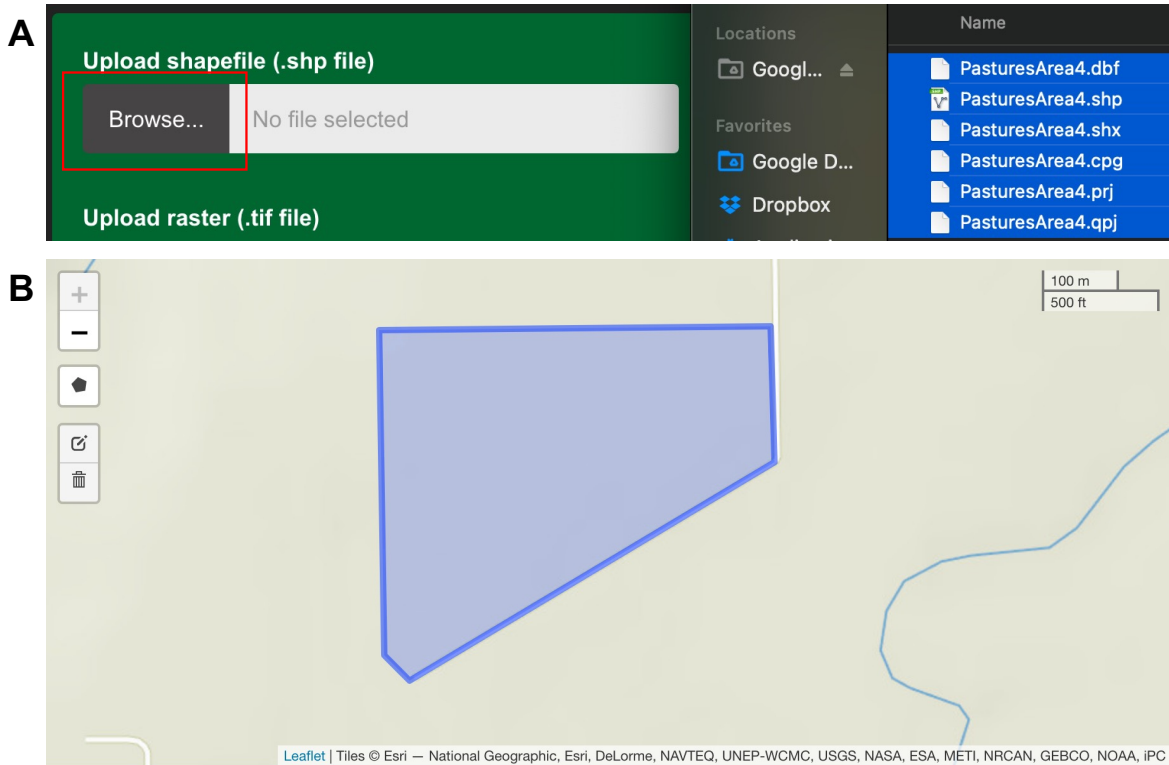


Figure 6.7. Loading shapefile; A. file upload from a local system, and B. extent of shapefile overlaid on the base map.

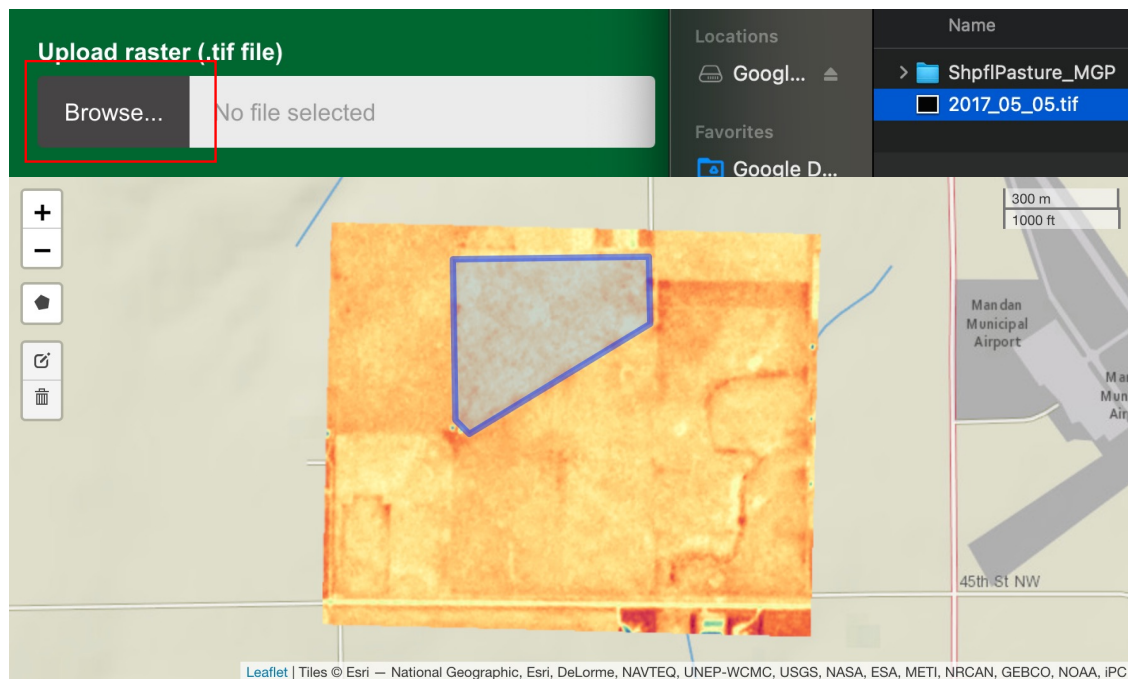


Figure 6.8. Loading raster file; A. file upload from a local system, and B. raster and shapefile overlaid on the base map.

The inputs for weather variables, turf soil temperature (75 °F) and bare soil temperature (65 °F) from NDAWN (section 6.4.1.3) are simply fed as inputs using the slider widget (fig. 6.9). The selected value is displayed on the top of the slider bar. The slider values can be changed for creating scenario analysis for extreme weather and soil conditions.

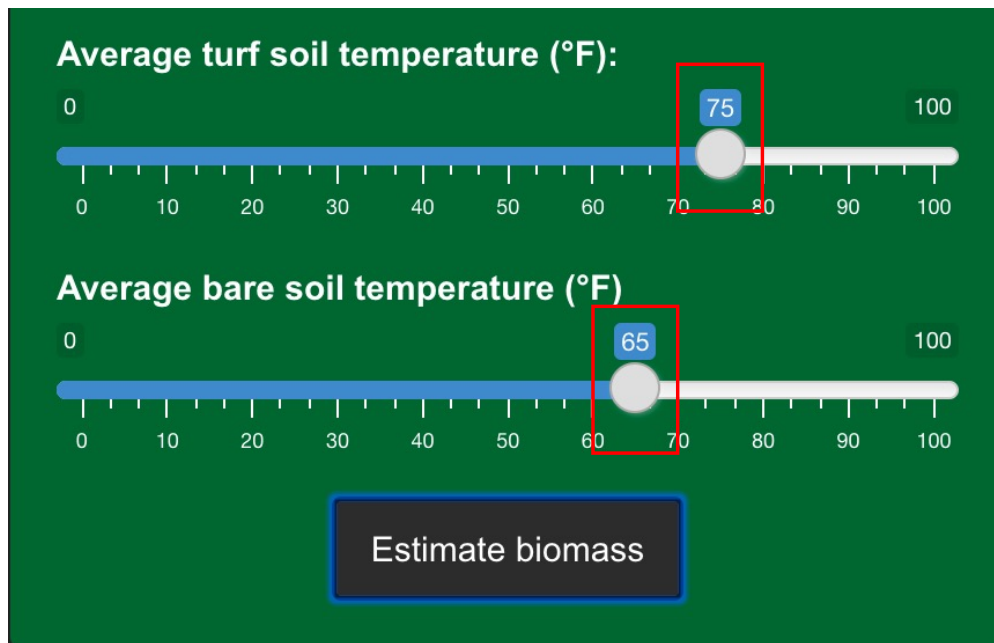


Figure 6.9. Weather variable input using slider shiny widget.

Upon receiving shapefile and raster inputs the tool automatically estimated the individual band values from the raster image. The bands' values of the raster images were averaged (mean) for the extent of the shapefile and were presented in the main panel as a table format (fig. 6.10). The estimated vegetation indices from the average band values were also presented. At this stage, all the required inputs such as weather variables, band values, and VI were available. The tool creates a data frame consisting of all the required inputs and feeds to the trained RF model for prediction. The action button “Estimate

biomass” (fig. 6.9) was clicked to trigger the results of the yield prediction to be displayed in the main panel (fig. 6.10) The predicted yield 1666.11 kg/ha was comparable to the observed yield was 1726.70 kg/ha.

Bands (mean, um)	Value	Vegetation index	Value
Blue	949	SAVI	0.562
Green	1168	MSAVI	0.545
Red	1357	GNDVI	0.437
Near infrared	2983	GCI	2.557
		NDVI	0.375
		RCC	0.391

Biomass yield prediction = 1665.11 kg/ha

Figure 6.10. Extracted band values, estimated vegetation indices, forage yield results presented in tool’s main panel.

The data visualization tab of RangeForage tool produced raster maps containing choropleth images for the 6 estimated vegetation indices, the checkbox option enabled the user to check the VI to be displayed in the main panel (fig. 6.11). A legend with the VI values and choropleth colors was created with the generation of every VI raster map. The map aids in visualizing the change in biomass yield at every geographical location.

This demonstration serves how a user can able to use the RangeForage tool using the strategy of inputs, cloud computing using a pre-trained model, and outputs (fig. 6.1). Therefore, the tool can be used by any stakeholder by properly specifying the inputs and deriving their desired “field-specific” outputs.

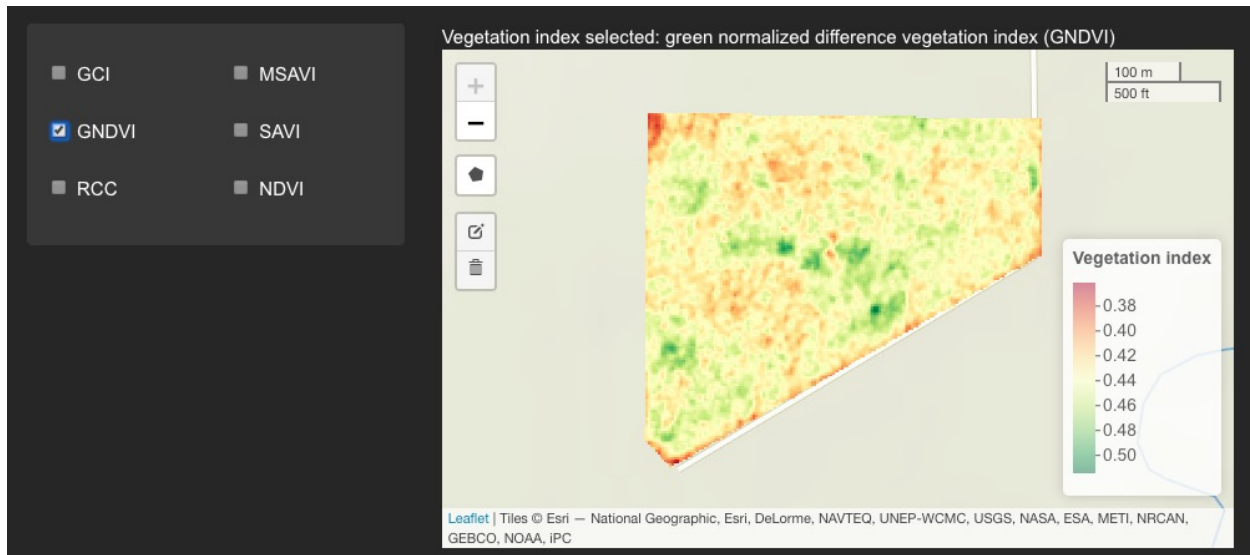


Figure 6.11. Extracted band values, estimated vegetation indices, forage yield results presented in tool’s main panel.

6.6. Conclusions

There is an increasing need for decision-support tools for predicting and monitoring rangeland forage. The developed user-friendly tool “RangeForage” predicted rangeland biomass and is expected to support farmers, ranchers, and other stakeholders in buying forage, planning livestock, and developing management plans. The R programming language has proved to be an ideal environment to combine spatial analysis, build ML models, generate visualization, and develop web applications.

The tool can be considered as a contribution to make “pasture-specific” yield predictions feasible and accessible. A further step in the context of this tool is to integrate more satellite-specific models (Landsat and Sentinel), currently only CubeSat-based model is present. The tool can be equipped to store the past years’ yield data and inclusion of more data visualization tools to produce a history of production yields that is specific to

the rangeland. Features to facilitate more scenario analysis that can be used to predict biomass at various conditions can be added in the future versions of this tool.

6.7. References

- Allred, B. W., Bestelmeyer, B. T., Boyd, C. S., Brown, C., Davies, K. W., Duniway, M. C., Ellsworth, L. M., Erickson, T. A., Fuhlendorf, S. D., Griffiths, T. V., et al. (2021). Improving Landsat predictions of rangeland fractional cover with multitask learning and uncertainty. *Methods Ecol. Evol.*, *12*(5), 841–849.
- Chang, W., Cheng, J., Allaire, J., Xie, Y., & McPherson, J. (2019). Shiny: Web application framework for R: R package version 1.3. 2; 2019. URL: <https://cran.r-project.org/web/packages/shiny/index.html>.
- Derner, J. D., & Augustine, D. J. (2016). Adaptive management for drought on rangelands. *Rangelands*, *38*(4), 211–215.
- Godde, C. M., Boone, R. B., Ash, A. J., Waha, K., Sloat, L. L., Thornton, P. K., & Herrero, M. (2020). Global rangeland production systems and livelihoods at threat under climate change and variability. *Environ. Res. Lett.*, *15*(4), 044021.
- Hijmans, R. J., & van Etten, J. (2011). Geographic analysis and modeling with raster data. <https://cran.r-project.org/web/packages/raster/index.html>.
- Knapp, A. K., & Smith, M. D. (2001). Variation among biomes in temporal dynamics of aboveground primary production. *Science*, *291*(5503), 481–484.
- Lai, J., Lortie, C. J., Muenchen, R. A., Yang, J., & Ma, K. (2019). Evaluating the popularity of R in ecology. *Ecosphere*, *10*(1), e02567.
- Pebesma, E. J. et al. (2018). Simple features for r: Standardized support for spatial vector data. *R Journal*, *10*(1), 439.

- Peck, D., Derner, J. D., Parton, W., Hartman, M., & Fuchs, B. (2019). Flexible stocking with grass-cast: A new grassland productivity forecast to translate climate outlooks for ranchers. *Western Economics Forum*, 17(1837-2019-973), 24–39.
- QGIS Development Team. (2022). *QGIS Geographic Information System*. QGIS Association. <https://www.qgis.org/>.
- R Core Team. (2017). *R: A Language and Environment for Statistical Computing*. R Foundation for Statistical Computing. Vienna, Austria. <https://www.R-project.org/>.
- Reeves, J. L., Derner, J. D., Sanderson, M. A., Kronberg, S. L., Hendrickson, J. R., Vermeire, L. T., Petersen, M. K., & Irisarri, J. G. (2015). Seasonal weather-related decision making for cattle production in the Northern Great Plains. *Rangelands*, 37(3), 119–124.
- Thurow, T. L., & Taylor, C. A. (1999). The role of drought in range management. *Rangeland Ecol. Manage.*, 52(5), 413–419.

7. GENERAL CONCLUSIONS AND SUGGESTIONS FOR FUTURE WORK

7.1. General Conclusions

Rangeland forage prediction is crucial for maintaining livestock production and sustenance of the ranching enterprise. Extreme climatic conditions such as drought reduce forage production and lost vegetation cover that leads to soil erosion. Frequently occurring droughts heightens the need for monitoring forage yield as well as predicting yields in rangelands. The study focuses on forage yield potential assessment through naturally grown on rangelands or cultivated forage and prediction model and tool development.

Objective 1: A systematic literature review was successfully performed by reviewing 85 qualified research manuscripts (2010 to 2022) to gain insights on forage yield prediction including input features, models, and economic analysis tools. A strong trend of remote monitoring of grasslands was observed as a large number of literature collected used remotely sensed vegetation index (VI, $n = 55$) than climate features ($n = 26$) as inputs. Only very few studies used both VI and climate to predict the forage yield. Among the satellite platform, MODIS ($n = 16$) was the most frequently used followed by Landsat and Sentinel. Normalized difference vegetation index (NDVI) was the most widely used VI (28 %) while precipitation (33 %) and soil moisture (15 %) was the most used climate and soil features. Existing tools such as Drought Calculator, U.S. Drought Monitor, Grass-Cast, and Rangeland Analysis Platform focused on large-scale grass and forage yield prediction and monitoring. Several spreadsheet-based calculators such as alfalfa production, haying system enterprise, enterprise budgeting for production of irrigated alfalfa, and price of standing hay crop were available for forage economic analysis and focused majorly on

the alfalfa forage crop. However, NDSU's forage economic calculator was web-based and included more than 10 forage crops. Based on the scenario analysis using the tool for different forage and forage-grain crops, where alfalfa and corn produced the highest profits.

Objective 2: Biomass/forage bale collection logistics distance and fuel consumption (energy) were studied and compared between the conventional tractor and advanced automatic bale picker (ABP; carrying capacity of 2 and 23). The most influential field parameters affecting the aggregation distance, fuel quantity, and operation time were field area, biomass yield, bales per trip (BPT), and equipment speed. Combined multivariate prediction models developed for logistics distance, fuel quantity, and operation time from the 36 960 bale aggregation scenarios performed equally well ($R^2 > 0.98$). Fuel consumption of ABP at 8 BPT for field areas between 8 and 259 ha on average decreased by 72% and 53% on comparison with a tractor with 1 and 2 BPT. No significant difference was observed for ABP with 8 and 11 BPT, therefore, ABP with 8 BPT was recommended for aggregation which can be effectively used to aggregate 11 BPT.

Objective 3: A user-friendly web tool named "Forage Economics Calculator Web Tool" (FECWT) was successfully developed using HTML, CSS, and JavaScript to perform forage economics analysis including the bale collection logistics operation. The tool's input included biophysical production parameters along with cost and price associated with forage enterprise. Major economic results obtained were net return, break-even ratio, payback period, and return on investment. In addition, the tool aided as a decision-support system for equipment purchase (tractor or ABP for bale collection), the sensitivity of profits in the form of "what-if scenario analysis." The outputs of the tools also include a dynamic chart and a generated report that were available as downloadable items. Case studies

performed with the farmers' actual field inputs and records compared to the tool's performance were found to be highly satisfactory. Scenario analysis results performed using practical case studies and hypothetical situations revealed that ABP equipment purchase was profitable for field areas ≥ 65 ha (≥ 160 ac) or for fields with high-yielding or high-value forage or grain crops.

Objective 4: The study successfully identified the best overall methodology of best features selected for predicting grass and forage yield. Multispectral satellite images along with climate features were successfully used to predict pasture biomass in a non-destructive manner. Literature in this subject area indicate that machine learning (ML) is a potential approach for forage yield monitoring and prediction. Among the feature selection methods, recursive feature elimination (RFE) was the best in identifying significant features for biomass prediction followed by Boruta and backward elimination. The top-ranking features were infra-red bands, blue band, turf soil temperature, and bare soil temperature. Among ML prediction models, the prediction performance of random forest (RF) was the best followed by support vector machine and k-nearest neighbor. The ML models produced better predictions than multiple linear regression models. The selected methodology of RFE for feature selection and RF for model development produced a good prediction performance on the unseen pasture data. Comparison between the satellite platforms using the selected methodology yielded that the satellite with finer spatial resolution and the methodology can be explored with high-value crops such as alfalfa.

Objective 5: A rangeland forage prediction tool was successfully developed using the Shiny package in R, an open-source platform for applications development. The tool predicted the rangeland forage based on the developed pre-trained ML model. The R

programming proved to be an ideal environment to integrate spatial analysis, build ML models, generate visualization, and develop web applications. The tool can be seen as a contribution to making “field-specific”, pasture level, yield prediction feasible and accessible. The tool is expected to aid ranchers and hay producers in aspects such as buying forage, planning livestock, and developing range management plans.

7.2. Suggestions for Future Work

- Inclusion of more robust ML models and comparison for rangeland forage prediction. Build more interactive and user-friendly forage related tools focusing on field-specific applications using local weather, soil, and plant inputs. Development of smartphone applications for forage prediction and economic analysis for increased visibility, usability, and awareness of farming and ranching outputs.
- Exploring more aggregation logistics methods scenario for identifying the methods that are most efficient in fuel consumption. Inclusion of more aggregation scenarios such as stacking locations of the collected bales before moving to the corner of the field for transportation. Extending the simulation study on evaluating the aggregation and fuel quantity consumption to real-field bale collection using aerial imagery with geolocation of the bales.
- The tool FECWT can be further developed to include more forage and crop types and relevant data (costs) for other regions. Conducting more case studies for understanding the performance of the calculator based on the input variability and geographic location. More features such as creating profiles using username and password for individuals for security, data archiving, and data management should be considered.

- The proposed methodology of forage yield monitoring and prediction should be further investigated with high-volume data and inclusion of more diverse soil, climate, and plant species community. The use of hyperspectral imagery using an unmanned aerial vehicle (UAV) should be explored to understand the potential and scope for predicting pasture biomass. Development of an interactive tool with minimal inputs can aid farmers to monitor forage prediction in real-time.
- The rangeland forage prediction tool to include more satellite data specific models and past years yield data for forage yield prediction and trend analysis. Past years' data can be made available for users and the developing trend plots for the users to visualize the history of the production yield that is specific to their field-/pasture/rangeland. Inclusion of features facilitating scenario analysis to predict biomass at various climatic and soil conditions will be useful.

APPENDIX A. BALE COLLECTION LOGISTICS ENERGY - EFFECT OF FIELD PARAMETERS ON AGGREGATION LOGISTICS DISTANCE

This appendix contains additional information for Chapter 3. Energy expended in biomass bale aggregation logistics using automatic bale picker (ABP) can be significantly influenced by the field parameters such as field area, biomass yield, and outlet location. Different levels of these parameters were simulated and the effect on the bale aggregation logistics distance, which directly affects the energy involved in the logistics that is also expressed in fuel quantity, is presented in this supplementary material. The results of Tukey's HSD conducted to determine the specific field area, bales/trip of ABP, and biomass yield that contributed significantly by comparing within all possible pairs of groups for aggregation logistics distance and fuel quantity consumed were also presented.

A.1. Effect of Field Parameters on Logistics Distance

A.1.1. Effect of Field Area on Logistics Distance

The distance required to aggregate bales increased as the field size increased (Subhashree and Igathinathane, 2019). A general increasing trend of bale aggregation logistics distance using automatic bale picker (ABP) with an increase in field area from 8 to 259 ha for biomass yield at 10 Mg ha^{-1} was observed (fig. A1). This trend was obvious as more field areas generated more bales and hence aggregation distances. With all bales/trip (BPT) tested (1–23 BPT), the increase in logistics distances showed a similar increasing trend across the field areas.

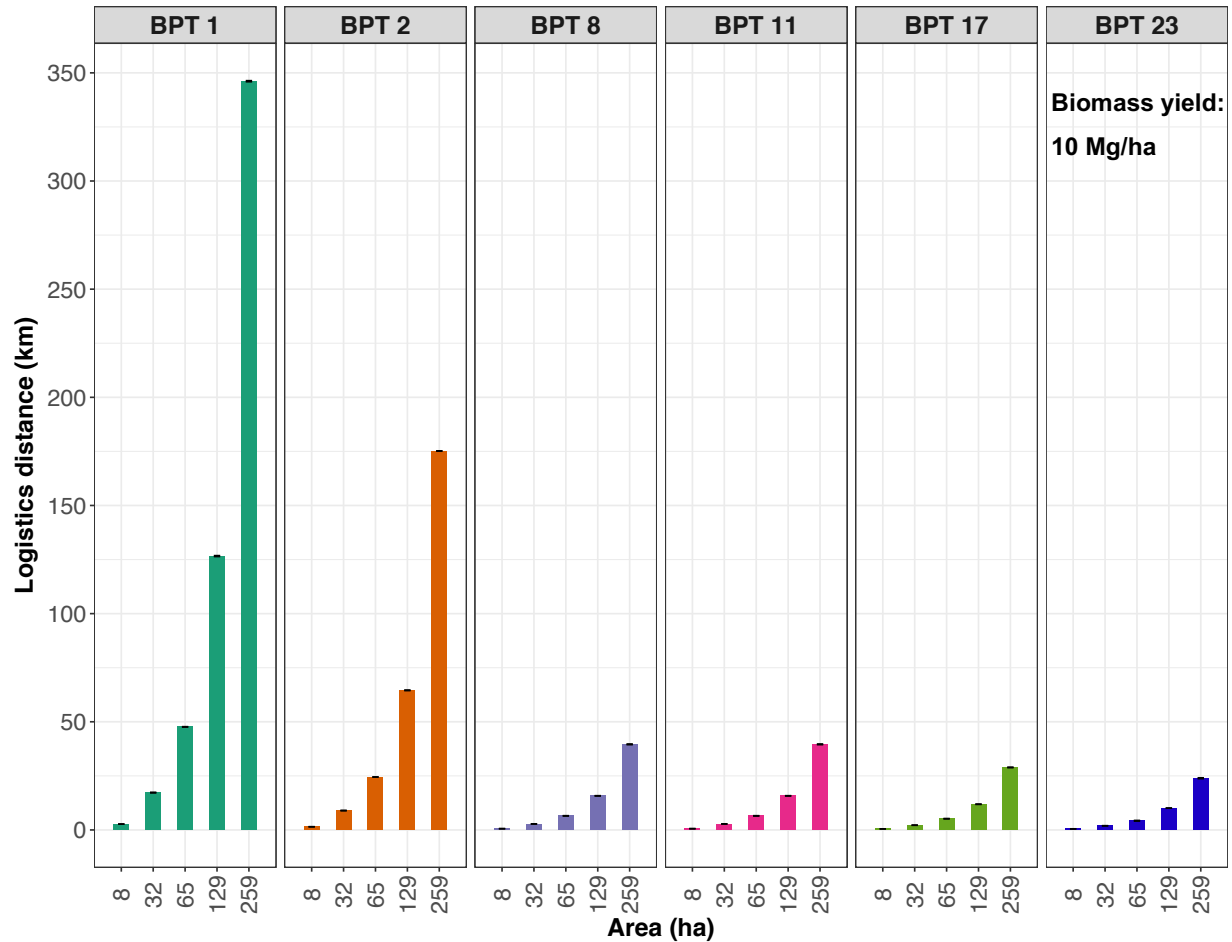


Figure A1. Effect of field area on the aggregation logistics distances generated for selected BPT (bales/trip) for tractor (1 and 2 BPT) and automatic bale picker (8, 11, 17, and 23 BPT), and field areas (8, 32, 65, 129, and 259 ha) with biomass yield at 10 Mg.ha⁻¹.

Table A1. ANOVA of field area, BPT, and biomass yield on bale aggregation logistics distances.

Parameter	<i>df</i>	Sum Sq	Mean Sq	F value	Pr(>F)
Field area	7	167 245	23 892	12.580	<8.43 × 10 ⁻¹³ ***
BPT (bales/trip)	6	90 895	15 149	6.414	<4.45 × 10 ⁻⁶ ***
Biomass yield	10	1 903 302	190 330	4.493	<5.22 × 10 ⁻⁶ ***

Combined data with field areas of 8, 16, 24, 32, 40, 65, 129, and 259 ha; BPT of 1, 2, 8, 11, 14, 17, and 23; biomass yield of 3, 4, 5, 6, 7, 8, 10, 15, 20, 30, and 40 Mg ha⁻¹; *df* is the degrees of freedom; and *** represents the significance at *p* < 0.001.

A.1.2. Effect of BPT on Logistics Distance

An obvious increase in aggregation distances, inversely proportional to the number of bales handled in a trip, was also observed (fig. A2).

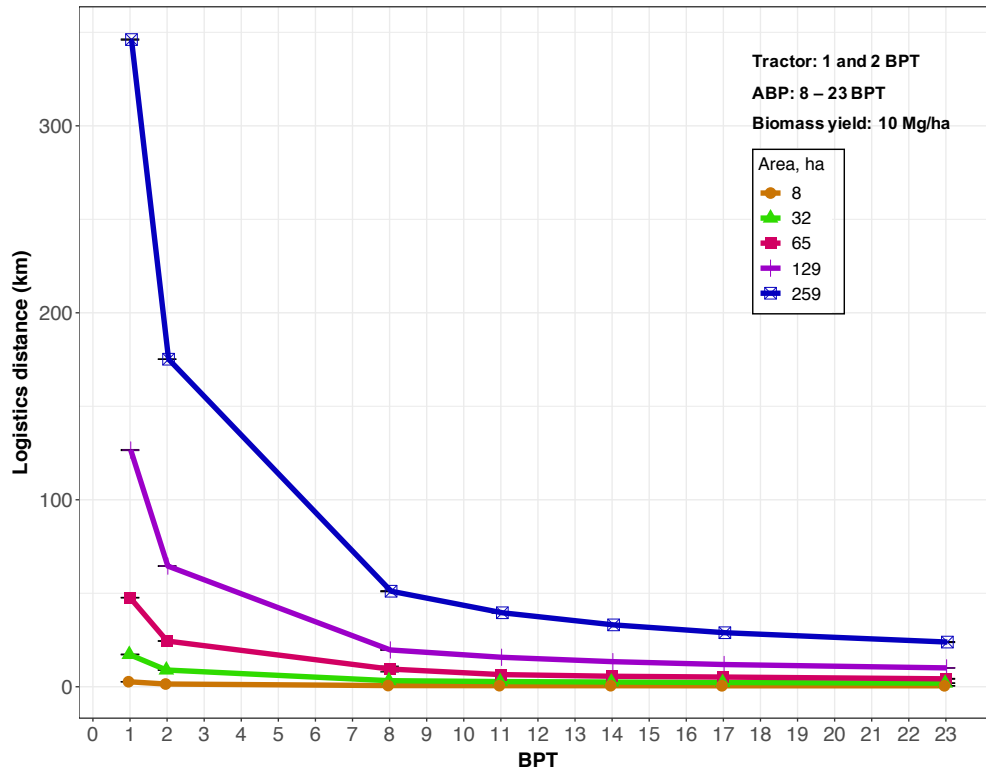


Figure A2. Effect of BPT (bales/trip) on the aggregation logistics distance generated for selected field areas (8, 32, 65, 129, and 259 ha) for tractor (0–5 BPT) and automatic bale picker (ABP; 8–23 BPT) with biomass yield at 10 Mg ha⁻¹.

A drastic reduction of aggregation distances was observed between tractor (1 and 2 BPT) and ABP (8 and 23 BPT). A similar reduction in logistics distances with increased BPT of tractor and ABP was also observed across all the field areas for 10 Mg ha⁻¹. Reduction in logistics distance, on an average 83 % and 67 %, was observed for ABP of 8 BPT when compared with tractor of 1 and 2 BPT respectively. This shows the clear advantage of using

the ABP in place of the tractor. However, the reduction in logistics distances especially ≥ 8 BPT was reduced across all the areas considered.

The one-way ANOVA with the combined data of all the areas and BPT with the replications derived from the windrow variations of 5 %, 10 %, and 15 % showed highly significant differences ($p < 0.001$) among the BPT (fig. A1). The Tukey's HSD analysis indicated that for smaller areas (≤ 24 ha), the studied BPT ranges were not significantly different ($p > 0.05$). For areas ≥ 32 ha, both the tractor and ABP the BPT ranges were significantly different. Based on these results, ABP is favored over a tractor for reduced bale aggregation logistics distances with large field areas. However, an ABP with 8 BPT, which is also capable of handling 11 bales, is recommended because the equipment would have a smaller footprint and a lower potential for creating subsoil compaction (Voorhees et al., 1986), especially for field areas ≤ 24 ha. With increased field areas, higher capacity ABPs are more efficient but the equipment size and the compaction due to load become important concerns.

A.1.3. Effect of Biomass Yield on Logistics Distance

The influence of biomass yield (3–40 Mg ha⁻¹) on logistic distance with 8 BPT (optimum) for different field areas (8–259 ha) showed a gradual increasing trend in logistics distance with the increasing biomass yield, however, this was more pronounced between the biomass yields 10–40 Mg ha⁻¹ and at increased field areas (> 32 ha) (fig. A3). A similar steady increasing trend across 8–129 ha but a steep increase at 259 ha were observed because of an increased number of bales generated in combination with the biomass productivity and field area.

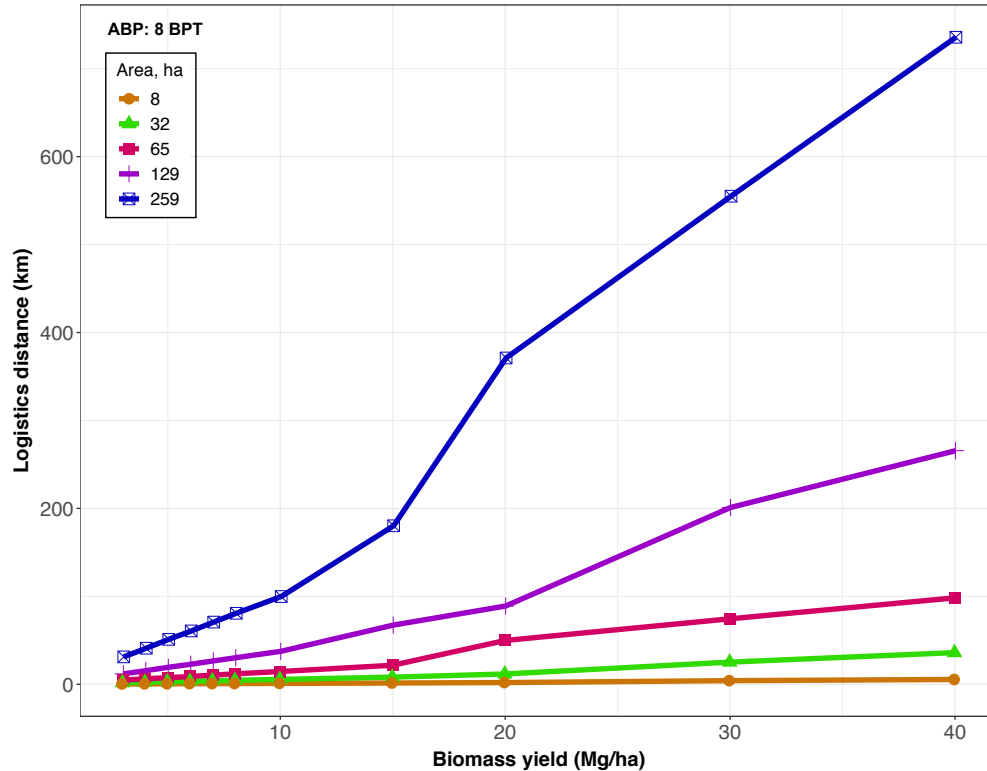


Figure A3. Effect of biomass yields (3–40 Mg ha⁻¹) on the aggregation logistics distance generated for selected field areas (8, 32, 65, 129, and 259 ha) using automatic bale picker (ABP) with 8 BPT (bales/trip).

The one-way ANOVA (table. A1) showed highly significant differences ($p < 0.001$) among the biomass yields affecting the bale logistics distance. The Tukey’s HSD analysis revealed significant differences for 40 Mg ha⁻¹ when compared with 3 to 10 Mg ha⁻¹ respectively, for the field areas <129 ha. However, for the area of 259 ha significant differences were observed between the highest level 40 Mg ha⁻¹ and the lower levels 3 to 5 Mg ha⁻¹ biomass yields. No significant differences were observed for biomass yields ≥ 15 Mg ha⁻¹ across all the field areas ≥ 32 ha. Overall, these results indicate that for reduced biomass yields (e.g., ≤ 20 Mg ha⁻¹) the differences in bale aggregation logistics distances will not be significant.

A.1.4 Effect of Outlet Location on Logistics Distance

An illustration of the effect of four outlet locations in a field area of 4 ha and 8 BPT depicts the variation in the bale aggregation paths and traffic near the outlet is shown in Figure A4. The outlet field middle (O:M; fig. A4A) is around the field center, mid-width (O:W; fig. A4B) is along the middle of the width-edge (x -axis), and mid-length (O:L; fig. A4C) is along the middle of the length-edge (y -axis), and the origin (O:O; fig. A4D) is the corner of the field.

The bale aggregation distances of the tractor and ABP followed a similar trend for all the outlet locations (fig. A5). When square fields were considered, the logistics distance of edge outlets (O:W and O:L) were identical. In the case of rectangular fields, the outlet at the longest edge should be the primary consideration (Igathinathane et al., 2016). The field middle outlet produced the least logistics distance, followed by the mid-edge, and the origin outlet the least. The logistics distance reduction of field middle was 44% and for mid-edges was 30% based on 8–259 ha field areas. With BPT >8 (ABP), the differences among the outlet locations diminished. However, when aggregating bales with tractors directly that handle only a couple of bales, the field middle emerged as the best choice for an outlet.

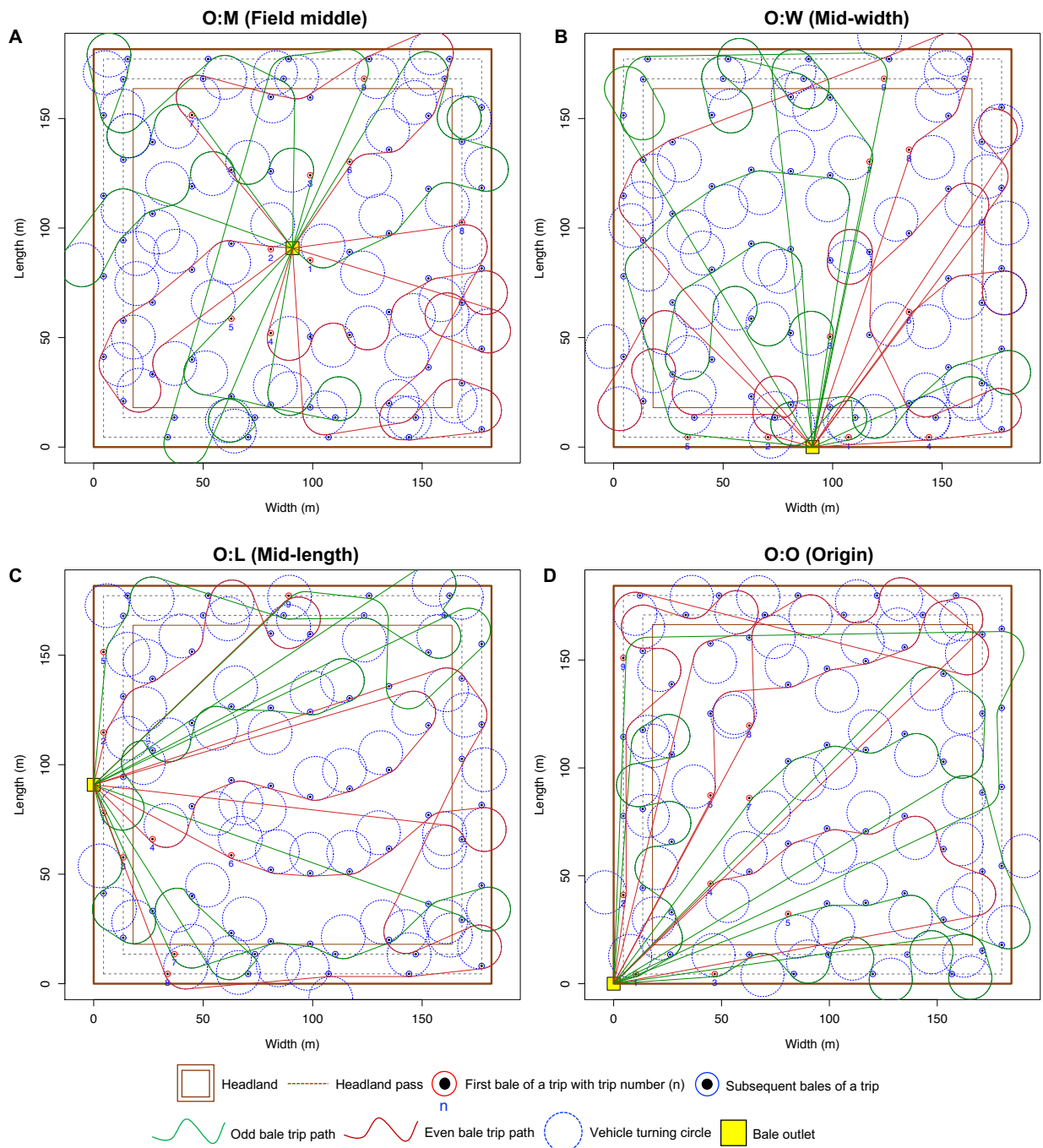


Figure A4. Effect of outlet location on bale aggregation; Simulation data: area = 4 ha; BPT = 8; turning radius, $r_t = 10$ m; biomass yield/ha = 10 Mg; bale mass = 500 kg; harvester swath = 9 m; field aspect ratio = 1.0 ; random variation in biomass yield = 15%; and random number seed used = 2016.

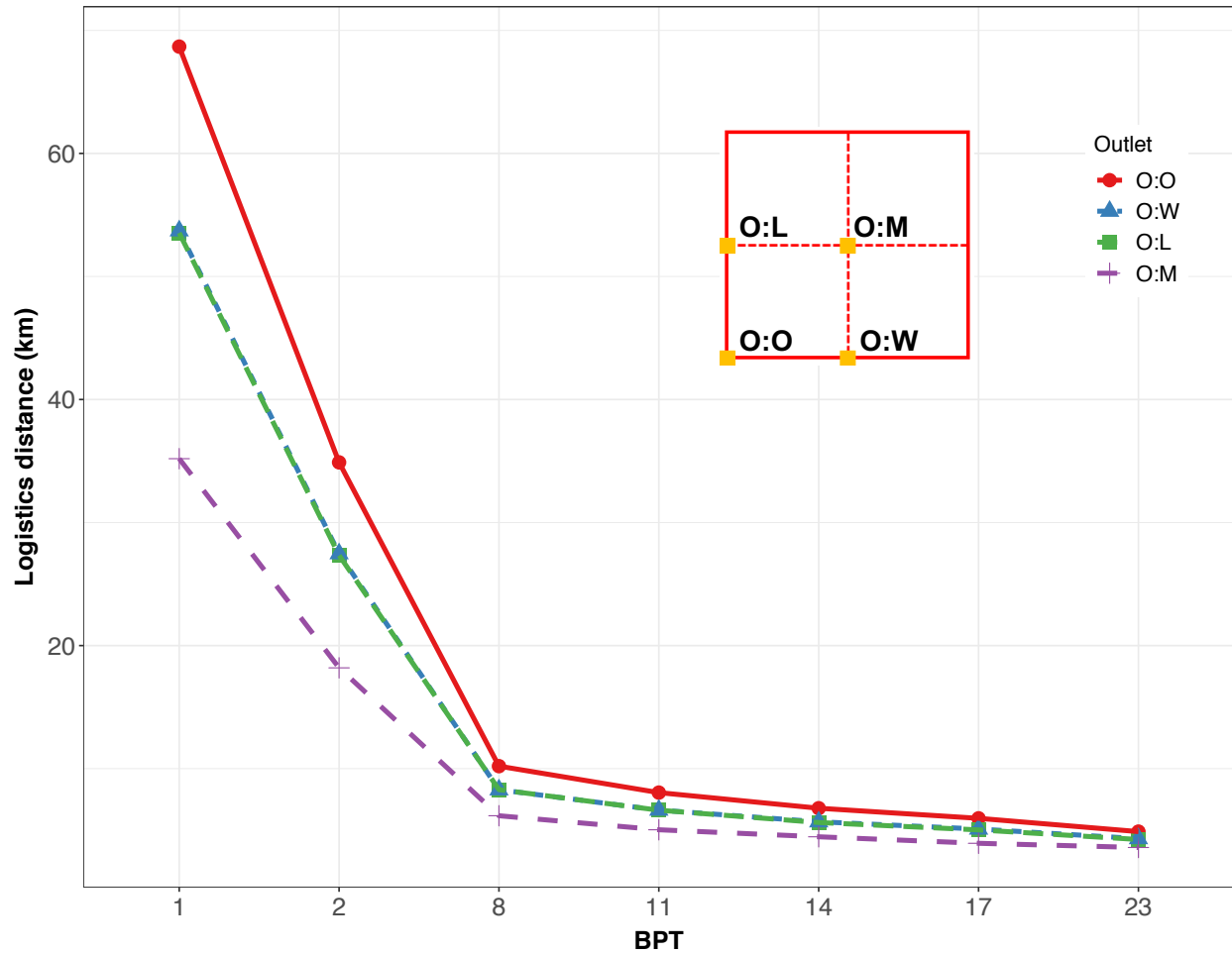


Figure A5. Outlet locations effect on logistics distance (km). O:M = field middle; O:W = along mid-width edge; O:L = along mid-length edge; O:O = field origin; Simulation data: field area = 65 ha, BPT = 8, biomass yield = 10 Mg ha⁻¹, and rest of the data were similar to fig. A4.

A.2. Tukey's HSD R Source Code

```

1 #***** ANOVA and Tukey's HSD R code and results *****#
2 # DV – Dependent variables (Logistics aggregation distance and fuel quantity consumed)
3 # IV – Independent variable (Field area, bales/trip, biomass yield)
4 #Importing data
5 dat <- read.table(header = T, text = '
6             Area BY BG LD Time FQ
7             8 3 1 0.75 1.17 18.467
8             8 3 2 0.46 0.71 11.686
9             8 3 8 0.21 0.33 6.762
10            8 3 11 0.23 0.35 7.860
11            8 3 14 0.22 0.34 8.290
12            8 3 17 0.19 0.3 7.883
13            8 3 23 0.19 0.29 8.690
14            ... ')
15
16 DV <- dat$LD; IV <- dat$BY
17 #-----
18
19 # Testing anova to determine significant difference in logistics
20 # distance influenced by biomass yield
21 anov <- aov(DV ~ as.factor(IV))
22 > anov
23 Call:
24 aov(formula = DV ~ as.factor(IV))
25
26 Terms:
27             as.factor(IV) Residuals
28 Sum of Squares      1903302  15841473
29 Deg. of Freedom         10      374
30
31 Residual standard error: 205.8079
32 Estimated effects may be unbalanced
33 #-----
34
35 # Further Tukey's HSD analysis from the anova results to determine the
36 # biomass yield pair contributing to the significant difference
37 # in logistics distance
38 # Output of the Tukey's HSD analysis is shown hereunder:
39
40 #*****
41 tuk <- TukeyHSD(anov)
42 > tuk
43 Tukey multiple comparisons of means
44 95% family-wise confidence level
45
46 Fit: aov(formula = DV ~ as.factor(IV))
47 $'as.factor(IV) '
48      diff      lwr      upr      p adj
49 4-3    3.133429 -156.2070285 162.4739 1.0000000
50 5-3    6.294571 -153.0458856 165.6350 1.0000000
51 6-3    9.320286 -150.0201713 168.6607 1.0000000
52 7-3   12.513143 -146.8273142 171.8536 1.0000000
53 8-3   15.666286 -143.6741713 175.0067 0.9999999
54 10-3  21.686000 -137.6544571 181.0265 0.9999974
55 15-3  45.765429 -113.5750285 205.1059 0.9976260
56 20-3  94.722000 -64.6184571 254.0625 0.7002749
57 30-3 162.009429   2.6689715 321.3499 0.0424590
58 40-3 218.254571  58.9141144 377.5950 0.0006138
59 5-4    3.161143 -156.1793142 162.5016 1.0000000
60 6-4    6.186857 -153.1535999 165.5273 1.0000000
61 7-4    9.379714 -149.9607428 168.7202 1.0000000
62 8-4   12.532857 -146.8075999 171.8733 1.0000000

```

63	10-4	18.552571	-140.7878856	177.8930	0.9999994
64	15-4	42.632000	-116.7084571	201.9725	0.9986972
65	20-4	91.588571	-67.7518856	250.9290	0.7418159
66	30-4	158.876000	-0.4644571	318.2165	0.0514229
67	40-4	215.121143	55.7806858	374.4616	0.0008057
68	6-5	3.025714	-156.3147428	162.3662	1.0000000
69	7-5	6.218571	-153.1218856	165.5590	1.0000000
70	8-5	9.371714	-149.9687428	168.7122	1.0000000
71	10-5	15.391429	-143.9490285	174.7319	0.9999999
72	15-5	39.470857	-119.8695999	198.8113	0.9993315
73	20-5	88.427429	-70.9130285	247.7679	0.7811803
74	30-5	155.714857	-3.6255999	315.0553	0.0620517
75	40-5	211.960000	52.6195429	371.3005	0.0010559
76	7-6	3.192857	-156.1475999	162.5333	1.0000000
77	8-6	6.346000	-152.9944571	165.6865	1.0000000
78	10-6	12.365714	-146.9747428	171.7062	1.0000000
79	15-6	36.445143	-122.8953142	195.7856	0.9996699
80	20-6	85.401714	-73.9387428	244.7422	0.8160245
81	30-6	152.689143	-6.6513142	312.0296	0.0738964
82	40-6	208.934286	49.5938287	368.2747	0.0013627
83	8-7	3.153143	-156.1873142	162.4936	1.0000000
84	10-7	9.172857	-150.1675999	168.5133	1.0000000
85	15-7	33.252286	-126.0881713	192.5927	0.9998557
86	20-7	82.208857	-77.1315999	241.5493	0.8494181
87	30-7	149.496286	-9.8441713	308.8367	0.0883630
88	40-7	205.741429	46.4009715	365.0819	0.0017764
89	10-8	6.019714	-153.3207428	165.3602	1.0000000
90	15-8	30.099143	-129.2413142	189.4396	0.9999422
91	20-8	79.055714	-80.2847428	238.3962	0.8787397
92	30-8	146.343143	-12.9973142	305.6836	0.1048264
93	40-8	202.588286	43.2478287	361.9287	0.0022985
94	15-10	24.079429	-135.2610285	183.4199	0.9999929
95	20-10	73.036000	-86.3044571	232.3765	0.9242692
96	30-10	140.323429	-19.0170285	299.6639	0.1429228
97	40-10	196.568571	37.2281144	355.9090	0.0037154
98	20-15	48.956571	-110.3838856	208.2970	0.9958609
99	30-15	116.244000	-43.0964571	275.5845	0.3936870
100	40-15	172.489143	13.1486858	331.8296	0.0215595
101	30-20	67.287429	-92.0530285	226.6279	0.9553874
102	40-20	123.532571	-35.8078856	282.8730	0.3014895
103	40-30	56.245143	-103.0953142	215.5856	0.9876523
104	#*****				

A.3. Tukey's HSD Results

A.3.1. Aggregation Logistics Distance Influenced by the Field Parameters BPT and Biomass Yield

This table consists of results of Tukey's HSD analysis conducted to determine the specific BPT and biomass yield (Mg ha^{-1}) pairs that contributed to a significant difference of aggregation logistics distance.

Table A2. Tukey's HSD analysis results of aggregation logistics distance influenced by the field parameters BPT and biomass yield.

Field parameter	Area (ha)				
	8	32	65	129	259
BPT (bales/trip)					
8-11	NS	*	*	*	*
11-14	NS	NS	*	*	*
11-23	NS	*	*	*	*
14-17	NS	NS	*	*	*
14-23	NS	*	*	*	*
17-23	NS	NS	*	*	*
Biomass yield (Mg ha^{-1})					
3-30	*	NS	NS	NS	NS
3-40	*	*	*	*	*
4-40	*	*	*	*	*
5-40	*	*	*	*	*
6-40	*	*	*	*	NS
7-40	*	*	*	*	NS
8-40	*	*	*	*	NS
10-40	*	*	NS	NS	NS
15-40	*	NS	NS	NS	NS

Note: * indicates bale aggregation logistics distance is significant and NS not significant at $p < 0.05$.

A.3.2. Fuel Quantity Influenced by Parameter Field Area

This table consists of the results of Tukey’s HSD analysis conducted to determine the specific field area pairs that contributed to a significant difference in fuel quantity consumed.

Table A3. Tukey’s HSD analysis results of fuel quantity influenced by the field area.

Field area (ha)	BPT (bales/trip)					
	1	2	8	11	17	23
8–16	*	*	NS	NS	NS	NS
8–24	*	*	NS	NS	NS	NS
8–32	*	*	NS	NS	*	*
8–40	*	*	NS	NS	*	*
16–24	*	*	NS	NS	NS	NS
16–32	*	*	NS	NS	NS	NS
16–40	*	*	NS	*	*	*
16–65	*	*	*	*	*	*
24–32	*	*	NS	NS	NS	NS
24–40	*	*	NS	NS	NS	NS
24–65	*	*	*	*	NS	*
32–40	*	*	NS	NS	*	*
32–65	*	*	NS	NS	*	*
40–65	*	*	NS	NS	*	*

Note: * indicates fuel quantity is significant and NS not significant at $p < 0.05$.

A.3.3. Fuel Quantity Influenced by Field Parameter BPT and Biomass Yield

This table consists of results of Tukey's HSD analysis conducted to determine the specific BPT and biomass yield (Mg ha^{-1}) pairs that contributed to a significant difference in fuel quantity consumed.

Table A4. Tukey's HSD analysis results of fuel quantity influenced by BPT and biomass yield.

Field parameters	Area (ha)				
	8	32	65	129	259
BPT (bales/trip)					
8-11	NS	NS	NS	NS	NS
8-14	NS	NS	*	*	*
8-17	NS	*	*	*	*
8-23	*	*	*	*	*
11-14	NS	NS	NS	NS	NS
11-17	NS	NS	NS	NS	NS
11-23	*	NS	NS	NS	NS
14-17	NS	NS	NS	NS	NS
14-23	*	NS	NS	NS	NS
17-23	*	NS	NS	NS	NS
Biomass yield (Mg ha^{-1})					
3-30	*	NS	*	*	*
3-40	*	*	*	*	NS
4-30	*	NS	NS	NS	NS
4-40	*	*	*	*	*
5-30	*	NS	NS	NS	NS
5-40	*	*	*	*	*
6-30	*	NS	NS	NS	NS
6-40	*	*	*	*	*
7-30	*	NS	NS	NS	NS
7-40	*	*	*	*	*
8-30	*	NS	NS	NS	NS
8-40	*	*	*	*	*
10-30	*	NS	NS	NS	NS
10-40	*	*	*	*	*
15-40	*	*	*	*	NS
20-40	*	*	NS	NS	NS

Note: * indicates the fuel quantity is significant and NS not significant at $p < 0.05$.

APPENDIX B. FORAGE ECONOMICS CALCULATOR - SIX-STEP USER INSTRUCTION

This appendix provides short six-step user instructions developed for the forage economics calculator (Chapter 4). The “Forage Economics Calculator” webtool can generate economic analysis outputs involving forage crop production, harvesting, baling, aggregation, labor, fuel cost, and the revenue generated from selling the bale forage or biomass. Emphasis is given to the bale aggregation operation, while the other operations are taken as direct inputs. The tool’s interface is designed to be user-friendly and dynamic that requires minimal inputs from the user.

The tool consists of inputs and results panel with buttons to perform relevant actions. The input values when fed through the input panel and their respective outcomes are dynamically generated and displayed in the results panel of the calculator. Default input values were already available as starters and dynamic arrow indicators, sensitive to the bottomline, show the optimum cutoff levels.

This document is the user-instructions, included in the subsequent pages, which describe how to use the “Forage Economics Calculator” web tool through its web-browser interface. It assumes that the user’s system is already directed to the tool’s web page.

B.1. Web Tool User Instructions

Step 1: Input drop-down option

Drop-down inputs are already loaded with default options, and however, can be changed using the instructions below:

1. **Open list:** Click on the drop-down list to view the options listed
2. **Scroll items:** Hover over the desired option on the list
3. **Select item:** Click to select

Inputs ⓘ	
Crop type:	✓ Alfalfa Alfalfa mix Barley Corn stover Grain mix Grass Grass mix Millet Oats Wheat (Others)
Machine age owned (years):	Engine power (hp): 80-149
Machine cost (\$): ⓘ	Annual usage (h): 200
Forage yield (lb/ac):	50000 ↑ ● 150000
Bale mass (lb): ⓘ	2500 ↑ ● 36000
Field area unit (ac):	800 ↑ ● 2000
Number of field units (#):	20 ↑ ● 640
	1

Repeat instructions under “Step 1” for all the drop-down options.

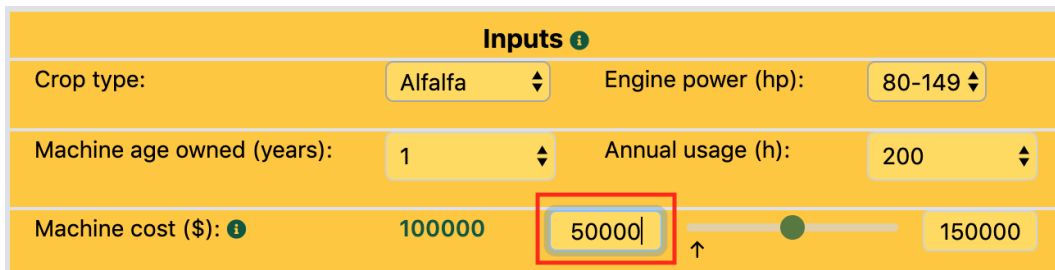
Using drop-down inputs, such as (1) Crop type, (2) Engine power, (3) Machine age owned, (4) Annual usage, and (5) Number of field units are fed.

Step 2: Slider inputs

Sliders are used to input values graphically by moving the slider between the lower and upper limits provided. A default is already selected and the value is shown on the left.

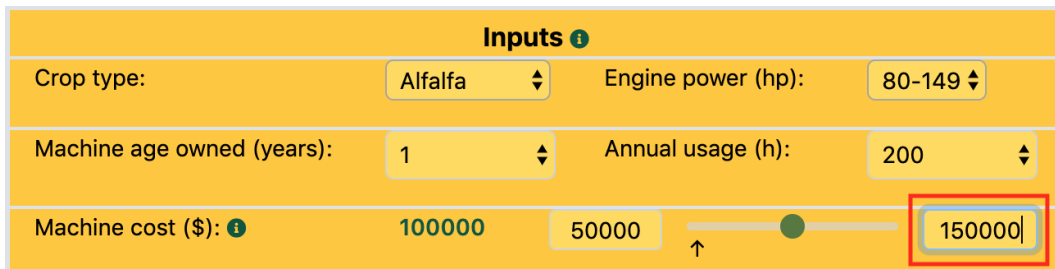
The minimum and maximum range values of the slider are given as a default, however can be changed following the instructions below. Actual values are input through the slider position.

1. **Edit minimum:** Click on editable text-box placed on the left of the slider bar to enter the minimum limit value for the range



The screenshot shows a yellow 'Inputs' form with three rows. The first row contains 'Crop type:' with a dropdown set to 'Alfalfa' and 'Engine power (hp):' with a dropdown set to '80-149'. The second row contains 'Machine age owned (years):' with a dropdown set to '1' and 'Annual usage (h):' with a dropdown set to '200'. The third row contains 'Machine cost (\$):' with an information icon, a default value of '100000', a slider bar, and a maximum value of '150000'. A red box highlights the text input field containing '50000' on the left side of the slider bar.

1. **Edit maximum:** Click on editable text-box placed on the right of the slider bar to enter the maximum limit value for the range



The screenshot shows the same 'Inputs' form as above. In this view, a red box highlights the text input field containing '150000' on the right side of the slider bar. The value in the left text box is now '50000'.

1. **Select slider:** Hover over the slider button to highlight.

Inputs ⓘ			
Crop type:	Alfalfa	Engine power (hp):	80-149
Machine age owned (years):	1	Annual usage (h):	200
Machine cost (\$): ⓘ	100000	50000	150000

1. **Slider input:** Click and drag the slider button over the bar to select a value between the set range
1. **Slider position - sensitivity:** A dynamic arrow indicates the cutoff value of the input the loss/profit, where the slider button on the left of the arrow gives loss while right gives profit. This dynamic arrow helps to eliminate the guesswork from the user to produce a positive bottomline.

Repeat instructions under “Step 2” for all the slider inputs.

Step 3: Number-box input

The editable number-box input only allows numbers to be entered. The number-box value can be changed to the desired value as follows:

1. **Select number-box:** Click on the editable number-box to select it.

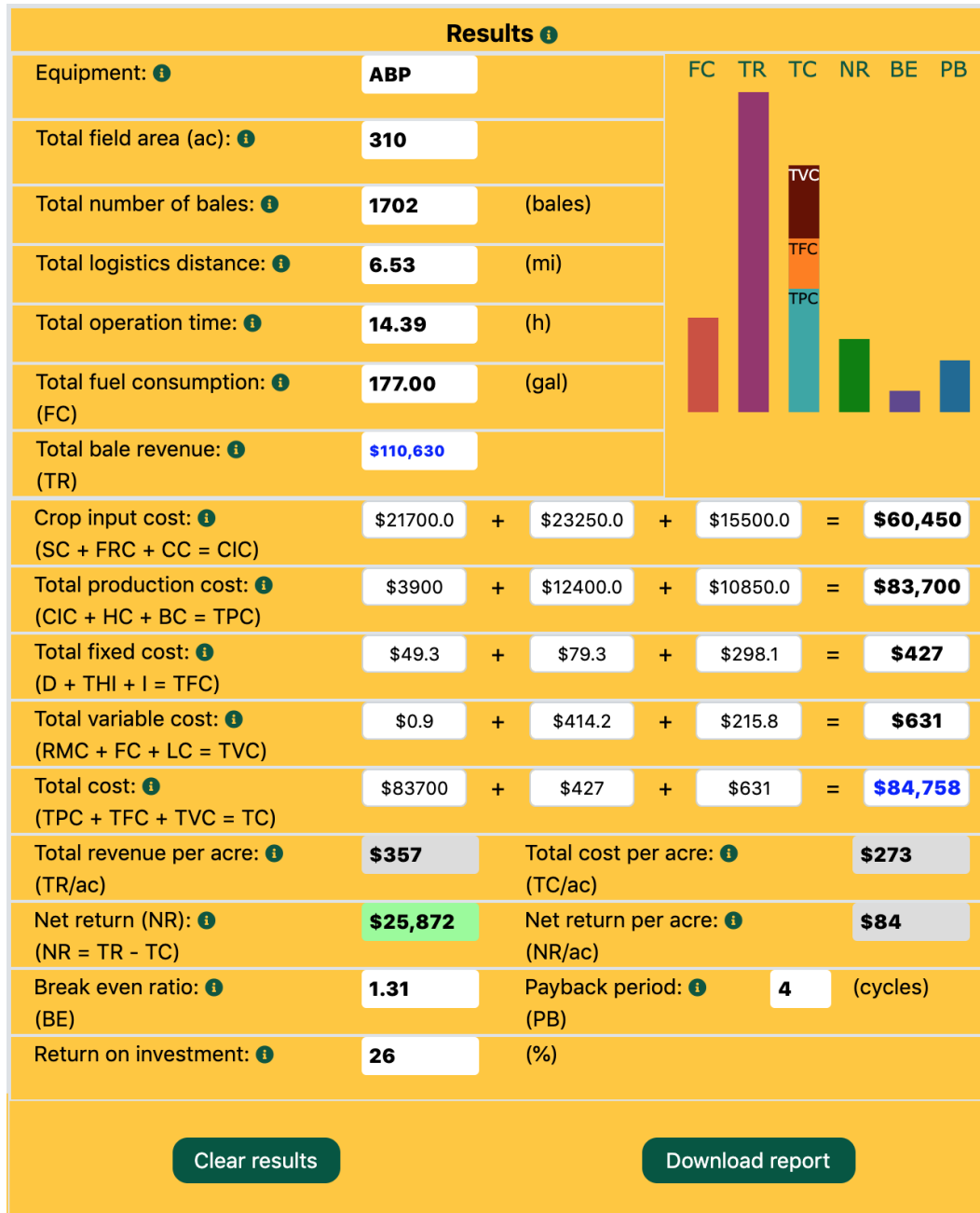
The screenshot shows a form titled "Inputs" with several input fields. The "Number of field units (#)" field is highlighted with a red rectangular box. This field is a number-box containing the value "1" and has small up and down arrow icons on its right side. Other fields include "Crop type" (Alfalfa), "Engine power (hp)" (80-149), "Machine age owned (years)" (1), "Annual usage (h)" (200), "Machine cost (\$)" (100000), "Forage yield (lb/ac)" (6500), "Bale mass (lb)" (1100), and "Field area unit (ac)" (30). Each of these other fields also has a corresponding number-box or slider control.

1. **Number-box input:** Values can be increased or decreased by clicking the up and down arrow present in the number-box.

This screenshot is identical to the one above, showing the "Inputs" form. However, in this image, a blue rectangular box is drawn around the up arrow icon on the right side of the "Number of field units (#)" field, illustrating how to increase the value.

Dynamic results - from the inputs

Steps 1, 2, and 3 generates live outcomes and dynamic plot on the results panel.



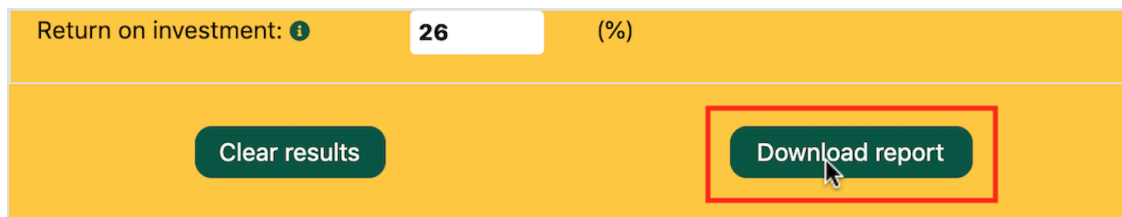
The output “Net return (NR)” box is color-coded (green - profit; red - loss) to readily observe the outcome. The per-unit relevant results such as (1) Total revenue per acre, (2) Total cost per acre, and (3) Net return per acre were also shown as gray output boxes.

The dynamic plot serves as a ready-to-observe tool of the generated results, which can be used to easily compare the contribution of the various cost components.

Step 4: Download report

A report containing selected input values and the generated outcomes, which can be used for record-keeping or comparison, can be accessed in a PDF format by following the instructions:

1. **Download report:** Click on the “Download report” button on the results panel to initiate the download process for the report.



1. **View report:** Once download is finished, click on the PDF file to view the report.

Forage Economics Calculator

Department of Agricultural and Biosystems Engineering, NDSU

Selected Inputs		Generated Results	
Crop type:	Alfalfa	Equipment:	ABP
Engine power (hp):	80-149	Total field area (ac):	60
Machine age owned (years):	1	Total number of bales:	444
Annual usage (h):	200	Total logistics distance (mi):	0.67
Machine cost (\$):	100000	Total operation time (h):	1.46
Forage yield (lb/ac):	6500	Total fuel consumption (gal):	22.51
Bale mass (lb):	1100	Total bale revenue:	\$20,150
Field area unit (ac):	60	Crop input cost:	\$11,505
Number of field units (#):	1	Total production cost:	\$15,930
Bales/trip:	8	Total fixed cost:	\$43
Machine speed (mph):	5.25	Total variable cost:	\$25
Bale sale price (\$/bale):	65	Total cost:	\$15,998
Seed cost (\$/ac):	70	Total revenue per acre:	\$342
Fertilizer cost (\$/ac):	75	Total cost per acre:	\$271
Chemical cost (\$/ac):	50	Net return:	\$4,152
Harvest cost (\$/ac):	40	Net return per acre:	\$70
Baling cost (\$/ac):	35	Break even ratio:	1.2
Fuel cost (\$/ac):	2.34	Payback period (cycles):	24
Labor cost (\$/ac):	15	Return on investment (%):	4

Subhashree et al., (2020). Forage Aggregation Economics Calculator. Department of Agricultural and Biosystems Engineering, North Dakota State University, Fargo, USA.

Generated on: Thu May 14 2020 16:14:23 GMT-0500 (Central Daylight Time)

Step 5: Reset input values

1. **Reset inputs:** Click on the “Reset” button to reset all the input values to the default input values.

Inputs ⓘ			
Crop type:	Alfalfa ▾	Engine power (hp):	80-149 ▾
Machine age owned (years):	1 ▾	Annual usage (h):	200 ▾
Machine cost (\$): ⓘ	100000	50000	150000
Forage yield (lb/ac):	6500	2500	36000
Bale mass (lb): ⓘ	1100	800	2000
Field area unit (ac):	60	20	640
Number of field units (#):	1		
Bales/trip: ⓘ	8	1	23
Machine speed (mph): ⓘ	5.25	4	8
Bale sale price (BP, \$/bale):	65	45	110
Seed cost (SC, \$/ac): ⓘ	70	10	500
Fertilizer cost (FRC, \$/ac): ⓘ	75	25	300
Chemical cost (CC, \$/ac): ⓘ	50	10	150
Harvest cost (HC, \$/ac): ⓘ	40	20	200
Baling cost (BC, \$/ac): ⓘ	35	15	150
Fuel cost (FC, \$/gal): ⓘ	2.34	1	10
Labor cost (LC, \$/h): ⓘ	15	12	30
<div style="border: 2px solid red; padding: 5px; display: inline-block; background-color: #2e7d32; color: white; border-radius: 10px; width: 100px; text-align: center;">Reset</div>			

Step 6: Clear result values

1. **Clear results:** Click on the “Clear results” button to clear all the result values and the plot.

Results ⓘ			
Equipment: ⓘ	<input type="text"/>	FC TR TC NR BE PB	
Total field area (ac): ⓘ	<input type="text"/>		
Total number of bales: ⓘ	<input type="text"/>	(bales)	
Total logistics distance: ⓘ	<input type="text"/>	(mi)	
Total operation time: ⓘ	<input type="text"/>	(h)	
Total fuel consumption: ⓘ (FC)	<input type="text"/>	(gal)	
Total bale revenue: ⓘ (TR)	<input type="text"/>		
Crop input cost: ⓘ (SC + FRC + CC = CIC)	<input type="text"/>	+	<input type="text"/>
Total production cost: ⓘ (CIC + HC + BC = TPC)	<input type="text"/>	+	<input type="text"/>
Total fixed cost: ⓘ (D + THI + I = TFC)	<input type="text"/>	+	<input type="text"/>
Total variable cost: ⓘ (RMC + FC + LC = TVC)	<input type="text"/>	+	<input type="text"/>
Total cost: ⓘ (TPC + TFC + TVC = TC)	<input type="text"/>	+	<input type="text"/>
Total revenue per acre: ⓘ (TR/ac)	<input type="text"/>	Total cost per acre: ⓘ (TC/ac)	<input type="text"/>
Net return (NR): ⓘ (NR = TR - TC)	<input type="text"/>	Net return per acre: ⓘ (NR/ac)	<input type="text"/>
Break even ratio: ⓘ (BE)	<input type="text"/>	Payback period: ⓘ (PB)	<input type="text"/> (cycles)
Return on investment: ⓘ	<input type="text"/>	(%)	
<input type="button" value="Clear results"/>		<input type="button" value="Download report"/>	

Any change in the inputs will bring the updated calculations and plots back.

APPENDIX C. FORAGE ECONOMICS CALCULATOR - STANDARD ECONOMICS CALCULATIONS

This appendix provides standard economic calculations including fixed and variable costs used in chapter 4 – Development of forage economics calculator web tool.

C.1. Total Fixed Cost

Total fixed cost (\$) is the sum of total depreciation, taxing, housing, and insurance, interest cost, and total field area rent and is estimated using the inputs, machine cost, interest rate, field area, and field area rent (Chapter 4: table 4.1): #5, #6, #9, #10).

$$\text{TFC (\$)} = D + \text{THI} + I + \text{TFAR} \quad (\text{C.1})$$

where, TFC = total fixed cost (\$), D = total depreciation cost (\$), THI = total taxing, housing, and insurance cost (\$), I = total interest cost (\$), and TFAR = total field area rent (\$).

C.1.1. Depreciation (D)

The average annual depreciation cost (\$/year) is calculated based on the machine cost, salvage value, and useful life of the machine (Bond and Jolley, 1991).

$$\text{Average annual depreciation} = \frac{\text{Machine cost} - \text{Salvage value}}{\text{Useful life of machine (year)}} \quad (\text{C.2})$$

Salvage value (\$) is the value of the machine at disposal and can be calculated as the percent of the machine cost. The salvage values as percentage for three different range of machine engine (30–79 hp, 80–149 hp, and > 150 hp) and annual usage hours (200, 400, and 600 h) were reported by the Iowa State University, extension and outreach (Edwards, 2015). The following second-order polynomial models with a good fit ($R^2 > 0.99$) were

developed from the above Iowa State University study using the inputs engine capacity (hp), annual usage (h), and machine age (years) as follows:

30–79 hp

$$200 \text{ h: } V_S = 0.09(A_M)^2 - 3.88(A_M) + 66.03 \quad (R^2 = 0.99)$$

$$400 \text{ h: } V_S = 0.09(A_M)^2 - 3.76(A_M) + 60.73 \quad (R^2 = 0.99)$$

$$600 \text{ h: } V_S = 0.09(A_M)^2 - 3.61(A_M) + 56.86 \quad (R^2 = 0.99)$$

80–149 hp

$$200 \text{ h: } V_S = 0.10(A_M)^2 - 4.23(A_M) + 69.89 \quad (R^2 = 0.99)$$

$$400 \text{ h: } V_S = 0.10(A_M)^2 - 4.25(A_M) + 69.45 \quad (R^2 = 0.99)$$

$$600 \text{ h: } V_S = 0.10(A_M)^2 - 4.23(A_M) + 68.89 \quad (R^2 = 0.99)$$

> 150 hp

$$200 \text{ h: } V_S = 0.12(A_M)^2 - 4.95(A_M) + 70.17 \quad (R^2 = 0.99)$$

$$400 \text{ h: } V_S = 0.12(A_M)^2 - 4.87(A_M) + 68.23 \quad (R^2 = 0.99)$$

$$600 \text{ h: } V_S = 0.12(A_M)^2 - 4.79(A_M) + 66.81 \quad (R^2 = 0.99)$$

where, V_S is the salvage value percentage (%) and A_M is the machine age (1 – 15) in years.

$$\text{Salvage value (\$)} = V_S \times \text{Machine cost} \quad (\text{C.3})$$

The useful life of the machine in years is calculated using the hours of use until wear-out and the annual usage (h). The hours of use until wear-out are assumed to be 10,000 h, and this assumption is based on the probability that the machine will become obsolete after this time of usage. machine will become obsolete after this time of usage.

$$\text{Useful life of machine (year)} = \frac{10,000 (h)}{\text{Annual usage (h/year)}} \quad (\text{C.4})$$

Substituting eq. (C.3) and eq. (C.4) in eq. (C.2) determines the average annual depreciation cost. determines the average annual depreciation cost.

$$\text{Depreciation hourly cost (\$/h)} = \frac{\text{Average annual depreciation (\$)}}{\text{Annual usage (h)}} \quad (\text{C.5})$$

$$\text{Total depreciation cost (\$)} = \text{Depreciation hourly cost} \times \text{Total operation time} \quad (\text{C.6})$$

Hourly depreciation cost (\$/h) is determined using average annual depreciation cost (\$) and annual usage (h) (eq. (C.5)). Total depreciation cost is determined using hourly depreciation cost (\$/h) and total operational time (h) (eq. (C.6)).

C.1.2. Taxing, Housing, and Insurance (THI)

The annual property tax, housing, and insurance (THI) costs are determined by multiplying the THI percentage fixed for the specific type of machine by the average investment in the machine. The average investment is the average value of machine cost and salvage value (eq. (C.7)). The total taxing, housing, and insurance percentage is considered as 1.33% for tractor (Bond and Jolley, 1991).

$$\text{Average annual THI cost} = \frac{\text{Machine cost} + \text{Salvage value}}{2} \times 1.33\% \quad (\text{C.7})$$

$$\text{THI hourly cost (\$/h)} = \frac{\text{Average annual THI cost}}{\text{Annual usage}} \quad (\text{C.8})$$

$$\text{Total THI cost (\$)} = \text{THI hourly cost} \times \text{Total operation time} \quad (\text{C.9})$$

THI hourly cost (\$/h) is determined using average annual THI cost (\$) and annual usage (h) (eq. (C.8)). The total depreciation cost is determined using hourly THI cost (\$/h) and total operational time (h) (eq. (C.9)).

C.1.3. Interest (I)

The machine when purchased using a loan, the interest rate is charged against the average value of the machine cost and salvage value. This amount is the money paid to

the lender as interest payments for the borrowed capital (Bond and Jolley, 1991). The interest rate is fed by the user into the calculator (Chapter 4: table 4.1): #6).

$$\text{Average annual interest cost (\$)} = \frac{\text{Machine cost} + \text{Salvage value}}{2} \times \text{Interest rate (\%)} \quad (\text{C.10})$$

$$\text{Interest hourly cost (\$/h)} = \frac{\text{Average annual interest cost}}{\text{Annual usage}} \quad (\text{C.11})$$

$$\text{Total interest cost (\$)} = \text{Interest hourly cost} \times \text{Total operation time} \quad (\text{C.12})$$

Interest hourly cost (\$/h) is determined using average annual interest cost (\$) and annual usage (h) (eq. (C.11)). Total interest cost is determined using hourly interest cost (\$/h) and total operational time (h) (eq. (C.12)) .

C.1.4. Total Field Area Rent (TFAR)

Total field area rent cost is the product of field area unit, number of field units, and field area rent per acre, (Chapter 4: table 4.1): #9, #10, #14).

Substituting the component costs from equations eq. (C.7), eq. (C.10), and eq. (C.13) along with total field area rent in eq. (C.2) determines the total fixed cost.

C.2. Total Variable Cost

Total variable cost is the sum of total repair and maintenance, total fuel, total labor cost, and total bale transportation cost. Inputs used to estimate the total variable cost are machine age, fuel cost, labor cost, bale transportation distance, bale transportation cost (Chapter 4: table 4.1): #20 – #24), and operation time (Chapter 4: eq. 4.3).

$$\text{TVC (\$)} = \text{RMC} + \text{TFC} + \text{TLC} + \text{TBTC} \quad (\text{C.13})$$

where, TVC = total variable cost (\$), RMC = total repair and maintenance cost (\$), FC = fuel cost (\$), LC = labor cost (\$), and TBTC = total bale transportation cost (\$).

C.2.1. Repair and Maintenance (RMC)

The accurate prediction of repair and maintenance cost (\$) is difficult since the repair cost of the machine depends on other external factors such as the purpose of use, terrain, soil, and operating conditions. The annual repair and maintenance cost can be determined using the machine cost (\$), total accumulated repair (TAR), machine age (year), and annual usage (h).

$$\text{Average annual RMC (\$)} = \text{Machine cost} \times \frac{\text{TAR}}{\text{Machine age}} \quad (\text{C.14})$$

A series of varying total accumulated repairs (TAR) equations based on the type of equipment has been developed by the University of Idaho, Washington State University, and Oregon State University (Painter, 2011). The TAR equation for a 4-wheel drive tractor is as follows: The TAR equation for a 4-wheel drive tractor is as follows:

$$\text{Total accumulated repairs} = 0.003 \times \left(\frac{\text{Annual usage} \times \text{Machine age}}{1000} \right)^{2.0} \quad (\text{C.15})$$

Substituting eq. (C.15) in eq. (C.14) estimates the annual repair and maintenance cost.

$$\text{RMC hourly (\$/h)} = \frac{\text{Average annual RMC}}{\text{Annual usage}} \quad (\text{C.16})$$

$$\text{Total RMC (\$)} = \text{RMC hourly cost} \times \text{Total operation time} \quad (\text{C.17})$$

RMC hourly (\$/h; eq. (C.16)) is determined using average annual RMC (\$) and annual usage (h). Total RMC cost (eq. (C.17)) is determined using hourly RMC (\$/h) and total operational time (h).

C.2.2. Total Fuel Cost (TFC)

Total fuel cost (\$) is calculated as a product of input fuel cost per gallon (Chapter 4: table 4.1): #20) and the calculated fuel consumption (Chapter 4: eq. 4.4 and 4.5).

C.2.3. Total Labor Cost (TLC)

Total labor cost (\$) is the product of the number of laborers, labor cost per hour (Chapter 4: table 4.1): #21 and #22), and the estimated operation time (Chapter 4: eq. 4.3).

C.2.4. Total Bale Transportation Cost (TBTC)

The total cost for transporting the bales from the field to a storage unit is estimated as a product of the following inputs, bale transportation cost per unit mile and distance (Chapter 4: table 4.1): #23 and #24).

Substituting the component costs from equation eq. (C.17) along with total fuel cost, total labor cost and total bale transportation cost in eq. (C.13) determines the total variable cost.

APPENDIX D. FORAGE ECONOMICS CALCULATOR - HTML, CSS, AND JS SOURCE CODE

This appendix provides source codes for Chapter 4 “ Development of forage economics calculator web tool”. The source code for HTML, CSS, and JS are provided below.

D.1. Cascading Style Sheet (CSS) for Styling Calculator

```
1 html,
2   body {
3     overflow-x: hidden;
4     scroll-behavior: smooth;
5   }
6
7   .nav {
8     height: 100%;
9     width: 0;
10    position: fixed;
11    z-index: 1;
12    top: 0;
13    left: 0;
14    background-color: #111;
15    opacity: 0.9;
16    overflow-x: hidden;
17    padding-top: 60px;
18    transition: 0.7s;
19  }
20
21  .nav a {
22    display: block;
23    padding: 20px 30px;
24    font-size: 25px;
25    text-decoration: none;
26    color: #ccc;
27  }
28
29  .nav a:hover {
30    color: #fff;
31    transition: 0.4s;
32  }
33
34  .nav .close {
35    position: absolute;
36    top: 0;
37    right: 22px;
38    margin-left: 50px;
39    font-size: 30px;
40  }
41
42  .slide a {
43    color: #000;
44    font-size: 36px;
45  }
46
47  #content {
48    padding: 20px;
```

```

50     transition: margin-left 0.7s;
51     overflow: hidden;
52     width: 100%;
53 }
54
55 .submenu {
56     height: 50%;
57 }
58
59 @media (max-width: 767px) {
60     .hidden-xs {
61         display: none !important;
62     }
63 }
64
65 .service-icon {
66     background-color: #fff;
67     color: #1D809F;
68     height: 7rem;
69     width: 7rem;
70     display: block;
71     line-height: 7.5rem;
72     font-size: 2.25rem;
73     box-shadow: 0 3px 3px 0 rgba(0, 0, 0, 0.1);
74 }
75
76 .masthead {
77     color: #FFC82E;
78     background-image: url(Images/NDSU_temp.jpg);
79     background-repeat: no-repeat;
80     background-attachment: scroll;
81     background-position: center center;
82     background-size: cover;
83     min-height: 100vh;
84 }
85
86 #manualsec {
87     text-align: center;
88     color: #FFC82E;
89     background-image: url(Images/NDSU_temp.jpg);
90     background-repeat: no-repeat;
91     background-attachment: scroll;
92     background-position: center center;
93     background-size: cover;
94     min-height: 100vh;
95 }
96
97 .paddingsec {
98     padding-bottom: 0.5%;
99 }
100
101 .img-fluid {
102     opacity: 1.0;
103     filter: alpha(opacity=100);
104 }
105
106 .img-fluid:hover {
107     opacity: 0.5;
108     filter: alpha(opacity=40);
109 }
110
111 /* Container holding the image and the text */
112 .container {
113     position: relative;
114     text-align: center;
115     color: white;

```

```

116 }
117
118 /* Bottom left text */
119 .bottom-left {
120     position: absolute;
121     bottom: 8vh;
122     left: 14vw;
123 }
124
125 .bottom-left-two {
126     position: absolute;
127     bottom: 2vw;
128     left: 9vw;
129 }
130
131 .portfolio-item {
132     display: block;
133     position: relative;
134     overflow: hidden;
135     max-width: 530px;
136     margin: auto auto 1rem;
137 }
138
139 .portfolio-item .caption {
140     display: flex;
141     height: 100%;
142     width: 100%;
143     background-color: rgba(33, 37, 41, 0.2);
144     position: absolute;
145     top: 0;
146     bottom: 0;
147     z-index: 1;
148 }
149
150 .portfolio-item .caption .caption-content {
151     color: #fff;
152     margin: auto 2rem 2rem;
153 }
154
155 .portfolio-item .caption .caption-content h2 {
156     font-size: 0.8rem;
157     text-transform: uppercase;
158 }
159
160 .portfolio-item .caption .caption-content p {
161     font-weight: 300;
162     font-size: 1.2rem;
163 }
164
165 @media (min-width: 992px) {
166     .portfolio-item {
167         max-width: none;
168         margin: 0;
169     }
170
171     .portfolio-item .caption {
172         -webkit-transition: -webkit-clip-path 0.25s ease-out, background-color 0.7s;
173         -webkit-clip-path: inset(0px);
174         clip-path: inset(0px);
175     }
176
177     .portfolio-item .caption .caption-content {
178         transition: opacity 0.25s;
179         margin-left: 5rem;
180         margin-right: 5rem;
181         margin-bottom: 5rem;

```

```

182 }
183
184 .portfolio-item img {
185   -webkit-transition: -webkit-clip-path 0.25s ease-out;
186   -webkit-clip-path: inset(-1px);
187   clip-path: inset(-1px);
188 }
189
190 .portfolio-item:hover img {
191   -webkit-clip-path: inset(2rem);
192   clip-path: inset(2rem);
193 }
194
195 .portfolio-item:hover .caption {
196   height: 70%;
197   width: 83%;
198   background-color: rgba(29, 128, 159, 0.9);
199   -webkit-clip-path: inset(2rem);
200   clip-path: inset(2rem);
201 }
202 }
203
204 .masthead .masthead-subheading {
205   font-size: 1.5rem;
206   font-style: italic;
207   line-height: 1rem;
208   margin-bottom: 25px;
209   font-family: "Droid Serif", -apple-system, BlinkMacSystemFont, "Segoe UI", Roboto, "Helvetica
    Neue", Arial, sans-serif, "Apple Color Emoji", "Segoe UI Emoji", "Segoe UI Symbol", "
    Noto Color Emoji";
210   color: #FFC82E;
211 }
212
213 .masthead .masthead-heading {
214   font-size: 2rem;
215   font-weight: 700;
216   line-height: 2rem;
217   margin-bottom: 2rem;
218   font-family: "Montserrat", -apple-system, BlinkMacSystemFont, "Segoe UI", Roboto, "Helvetica
    Neue", Arial, sans-serif, "Apple Color Emoji", "Segoe UI Emoji", "Segoe UI Symbol", "Noto
    Color Emoji";
219 }
220
221 .row-fluid [class*="span"] {
222   margin-left: 0;
223 }
224
225 .big-banner {
226   /* The image used */
227   background-image: url(Images/NDSU-temp.jpg);
228
229   /* Full height */
230   height: 100vh;
231
232   /* Center and scale the image nicely */
233   background-position: center;
234   background-repeat: no-repeat;
235   background-size: cover;
236   background-color: transparent;
237 }
238
239 .slidecontainer {
240   height: 25px;
241   /* Width of the outside container */
242 }
243

```

```
244 .slider:hover {
245     opacity: 1;
246 }
247
248 .slider::-webkit-slider-thumb {
249     -webkit-appearance: none;
250     appearance: none;
251     position: relative;
252     width: 15px;
253     height: 15px;
254     border-radius: 50%;
255     background: #0A5640;
256     cursor: pointer;
257 }
258
259
260 .slider {
261     -webkit-appearance: none;
262     height: 5px;
263     border-radius: 5px;
264     background: #d3d3d3;
265     outline: none;
266     opacity: 0.7;
267     -webkit-transition: .2s;
268     transition: opacity .2s;
269 }
270
271 .slides {
272     display: flex;
273     align-items: center;
274     justify-content: center;
275 }
276
277 @media all and (max-width: 768px) {
278     #sliderset {
279         padding-left: 120px;
280     }
281 }
282
283 @media all and (max-width: 768px) {
284     #HayMount {
285         max-height: 100%;
286         max-width: 100%;
287     }
288 }
289
290 @media all and (max-width: 768px) {
291     #myChart1 {
292         max-width: 100%;
293         max-height: 40%;
294     }
295 }
296
297 .header {
298     height: 10vh;
299 }
300
301 @media all and (max-width: 700px) {
302     .header {
303         height: 20vh;
304         font-size: 10px;
305     }
306 }
307
308 #container {
309     max-width: 90vw;
```

```

310
311 @media screen and (min-aspect-ratio: 13/9) {}
312
313 @media screen and (max-aspect-ratio: 13/9) {}
314
315 }
316
317 .box {
318     padding: 0 5px 0 5px;
319 }
320
321 div.tooltip-inner {
322     text-align: left;
323     -webkit-border-radius: 0px;
324     -moz-border-radius: 0px;
325     border-radius: 5px;
326     margin-bottom: 6px;
327     background-color: #0A5640;
328     color: white;
329     font-size: 14px;
330     max-width: 400px;
331     /* opacity: 1; */
332 }
333
334 div.tooltip.show {
335     opacity: 0.95;
336 }
337
338
339 .padding-0 {
340     padding-bottom: 0;
341 }
342
343 .bullelements {
344     font-size: 2vh;
345 }
346
347 .containerflex {
348     display: flex;
349     height: 240px;
350     justify-content: space-between;
351     align-items: flex-end;
352 }
353
354 .btn:focus {
355     outline: none;
356 }
357
358 .rowht{
359     height: 48px;
360 }
361
362 /* toggle in label designing */
363 .toggle {
364     position : relative ;
365     display : inline-block;
366     width : 50px;
367     height : 25px;
368     background-color: red;
369     border-radius: 30px;
370     border: 2px solid gray;
371 }
372
373 /* After slide changes */
374 .toggle:after {
375     content: ' ';

```

```

376     position: absolute;
377     width: 23px;
378     height: 23px;
379     border-radius: 50%;
380     background-color: gray;
381     /* top: 0.5px; */
382     left: 1px;
383     transition: all 0.5s;
384 }
385
386 /* Toggle text */
387 P {
388     font-family: Arial, Helvetica, sans-serif;
389     font-weight: bold;
390 }
391
392 /* Checkbox checked effect */
393 .checkbox:checked + .toggle::after {
394     left: 25px;
395 }
396
397 /* Checkbox checked toggle label bg color */
398 .checkbox:checked + .toggle {
399     background-color: green;
400 }
401
402 /* Checkbox vanished */
403 .checkbox {
404     display: none;
405 }

```

D.2. JavaScript - User-Defined Functions for Calculation Operation

```

1 function calculate() {
2
3
4     var remember = document.getElementById("switch").checked
5
6     var tAr = document.getElementById('Ar'); //string values stored
7     var tBt = document.getElementById('Bt');
8     var tBy = document.getElementById('By');
9     var tSp = document.getElementById('Sp');
10    var tUn = document.getElementById('Un');
11    var tLo = document.getElementById('BLT');
12    var tUnLo = document.getElementById('BULT')
13
14    var fAr = parseFloat(tAr.value) * 0.404686; //ac to ha conversion
15    var fBt = parseFloat(tBt.value);
16    var fBynb = parseFloat(tBy.value) * 0.000112085; // lb/ac to kg/m2 conversion 0.000112085
17    var fBynb1 = parseFloat(tBy.value) * 0.1; // Mg/ha to kg/m2 conversion 0.1
18    var fBy = parseFloat(tBy.value) * 0.00112085; // lb/ac to Mg/ha conversion 0.000112085
19    var fSp = parseFloat(tSp.value) * 1.60934; // mph to km/hr conversion
20    var fUn = parseFloat(tUn.value);
21    var fLo = parseFloat(tLo.value);
22    var fUnLo = parseFloat(tUnLo.value);
23    var ArF = 10;
24
25    document.getElementById('TVGt').setAttribute('fill', "#fff");
26    document.getElementById('TFCt').setAttribute('fill', "#000");
27    document.getElementById('TPGt').setAttribute('fill', "#000");
28
29
30    // ABP row

```

```

31 var checkStatus = document.getElementById("ckb").checked
32 if (checkStatus == false) {
33     document.getElementById("ABP").disabled = true;
34     document.getElementById("nABP").innerHTML = 0;
35     document.getElementById("ABP").min = 0;
36     document.getElementById("ABP").value = 0;
37     document.getElementById("ABPMc").style.color = "grey";
38     document.getElementById("nABP").style.color = "grey";
39     document.getElementById("minABP").style.color = "grey";
40     document.getElementById("ABP").style.background = "grey";
41     document.getElementById("maxABP").style.color = "grey";
42     document.getElementById("ABPinfo").style.color = "grey";
43     document.getElementById("ABParrow").style.color = "grey";
44     document.getElementById("EquipLabel").style.color = "grey";
45     document.getElementById("ABPRes").style.color = "grey";
46     document.getElementById("EqTyp_ABP").style.color = "grey";
47     document.getElementById("PLabel").style.color = "grey";
48     document.getElementById("PB_info").style.color = "grey";
49     document.getElementById("PB_ABP").style.background = "#FFC82E";
50     document.getElementById("PB_ABP").style.color = "grey";
51     document.getElementById("ROILabel").style.color = "grey";
52     document.getElementById("ROI_info").style.color = "grey";
53     document.getElementById("ROI_ABP").style.color = "grey";
54     document.getElementById("ROI_ABP").style.background = "#FFC82E";
55     document.getElementById("EquipPlot").value = "Tractor"
56     document.getElementById("minBt").value = 1
57     document.getElementById("Bt").min = 1
58     document.getElementById("Bt").max = 2
59     document.getElementById("maxBt").value = 2
60     document.getElementById("Equip").value = "Tractor"
61 } else {
62     document.getElementById("ABP").disabled = false;
63     document.getElementById("ABP").min = 10000;
64     document.getElementById("ABPMc").style.color = "black";
65     document.getElementById("nABP").style.color = "#0A5640";
66     document.getElementById("minABP").style.color = "black";
67     document.getElementById("ABP").style.background = "#d3d3d3";
68     document.getElementById("maxABP").style.color = "black";
69     document.getElementById("ABPinfo").style.color = "#0A5640";
70     document.getElementById("ABParrow").style.color = "black";
71     document.getElementById("EquipLabel").style.color = "black";
72     document.getElementById("ABPRes").style.color = "#0A5640";
73     document.getElementById("EqTyp_ABP").style.color = "black";
74     document.getElementById("PLabel").style.color = "black";
75     document.getElementById("PB_info").style.color = "#0A5640";
76     document.getElementById("PB_ABP").style.background = "white";
77     document.getElementById("PB_ABP").style.color = "black";
78     document.getElementById("ROILabel").style.color = "black";
79     document.getElementById("ROI_info").style.color = "#0A5640";
80     document.getElementById("ROI_ABP").style.color = "black";
81     document.getElementById("ROI_ABP").style.background = "white";
82     document.getElementById("EquipPlot").value = "Tractor and ABP";
83     document.getElementById("minBt").value = 3
84     document.getElementById("Bt").min = 3
85     document.getElementById("Bt").max = 23
86     document.getElementById("maxBt").value = 23
87     document.getElementById("Equip").value = "Tractor and ABP"
88 }
89 // Total field area
90 totArval = parseFloat(tAr.value * fUn);
91 totFAr.value = totArval.toFixed(0);
92
93 // Number of bales
94 var tBm = document.getElementById('Bm');
95 var fBm = parseFloat(tBm.value);
96

```



```

97  if (remember == false) {
98      var fBmc = fBm * 0.454; //lbs to kg conversion
99      var arHaEq = 10000;
100     var swath = 9;
101     var HeadPass = 2;
102     var area = fAr * arHaEq; // m2
103     var L = Math.sqrt(area); //m
104     var W = area / L; //m
105     var IL = (L - (swath * HeadPass * 2));
106     var IW = (W - (swath * HeadPass * 2));
107     var N = (IL * IW) * fBynb / fBmc;
108     var nbales = Math.round(N);
109     NB.value = nbales * fUn;
110 } else {
111     var fBmc = fBm; // kg
112     // alert("fBmc = " + fBm);
113     var arHaEq = 10000;
114     var swath = 9;
115     var HeadPass = 2;
116     var area = tAr.value * arHaEq; // m2
117     var L = Math.sqrt(area); //m
118     var W = area / L; //m
119     var IL = (L - (swath * HeadPass * 2));
120     var IW = (W - (swath * HeadPass * 2));
121     var N = (IL * IW) * fBynb1 / fBmc;
122     var nbales = Math.round(N);
123     NB.value = nbales * fUn;
124 }
125
126 //Total grain yield
127 var GrY = document.getElementById("GY").value;
128 var TGYv = GrY * tAr.value * fUn;
129 TGY.value = TGYv;
130
131
132 // Logistics distance
133 var LogisDis = Math.pow(((fAr * fBy) / (17.879 * (fBt + 0.895))), 1.377) * fUn;
134 var LogisDis1 = Math.pow(((tAr.value * tBy.value) / (17.879 * (fBt + 0.895))), 1.377) * fUn;
135 if (remember == false) {
136     LD.value = (LogisDis * ArF * 0.621371).toFixed(2);
137 } else {
138     LD.value = (LogisDis1 * ArF).toFixed(2);
139 }
140
141 // Bale collection operation time
142 var optTime = Math.pow(((fAr * fBy) / (-46.003 + (fBt * 80.230) + (fSp * 15.052))), 1.381) *
    fUn;
143 var optTime1 = Math.pow(((tAr.value * tBy.value) / (-46.003 + (fBt * 80.230) + (tSp.value *
    15.052))), 1.381) * fUn;
144 if (remember == false) {
145     var OTval = (optTime) * ArF;
146     OT.value = OTval.toFixed(2);
147 } else {
148     var OTval = (optTime1) * ArF;
149     OT.value = OTval.toFixed(2);
150 }
151
152 // Bale consumption fuel consumption
153 var FuelConsp
154 if (remember == false) {
155     if (fBt == 1 || fBt == 2) {
156         FuelConsp = Math.pow(((fAr * fBy) / (-5.913 + (fBt * 13.164) + (fSp * 2.777))), 1.414);
157     } else {
158         FuelConsp = Math.pow(((fAr * fBy) / (-4.991 + (fBt * 1.165) + (fSp * 4.827))), 1.242);
159     }
160     FuelConspUn = (FuelConsp * ArF * 0.264172) * fUn;

```

```

161 } else {
162   if (fBt == 1 || fBt == 2) {
163     FuelConsp1 = Math.pow(((tAr.value * tBy.value) / (-5.913 + (fBt * 13.164) + (tSp.value *
164       2.777))), 1.414);
165   } else {
166     FuelConsp1 = Math.pow(((tAr.value * tBy.value) / (-4.991 + (fBt * 1.165) + (tSp.value *
167       4.827))), 1.242);
168   }
169   FuelConspUn = (FuelConsp1 * ArF) * fUn;
170 }
171 FCP.value = FuelConspUn.toFixed(2);
172
173
174 // Total bale operation time – collection, loading, and unloading
175 var LUnL = ((fLo + fUnLo) * nbales * fUn) / 60; // loading and unloading operation time –
176   converting min to h
177 var totOpTime = LUnL + OTval;
178 TBOT.value = totOpTime.toFixed(2);
179
180 // Total fuel consumption – collection, loading, and unloading
181 // Loading and unloading fuel consumption
182 // Refer to equations 5, 6, and 7 in the – A simulation study paper
183 var CTval = 111.855 * 20 / 100; // 150 hp is 111.855 kw and load of 20 % (1 bale/trip) is
184   assumed (eq. 5)
185 var EFval = 1.047 * Math.log(20) - 1.711
186 var CFval = CTval / EFval;
187 var FCons
188 if (remember == false) {
189   FCons = CFval * LUnL * fUn * 0.264172; // converting litre to gal
190 }
191 else {
192   FCons = CFval * LUnL * fUn; // litre
193 }
194 var totFconsp = FCons + FuelConspUn
195 TBFC.value = totFconsp.toFixed(2);
196
197 //Total bales revenue
198 var tBc = document.getElementById('Bc');
199 var fBc = parseFloat(tBc.value);
200 var TBRv = (fBc * nbales * fUn).toFixed(0);
201 var TBRcs = Number(TBRv).toLocaleString('en');
202 if (TBRcs.length > 6) {
203   TBR.style.fontSize = "10px";
204 } else {
205   TBR.style.fontSize = "13px";
206 };
207 TBR.value = '$' + TBRcs
208
209 //Total grain revenue
210 var Gpr = parseFloat(document.getElementById('GP').value);
211 var TGRv = TGYv * Gpr;
212 var TGRcs = Number(TGRv).toLocaleString('en');
213 if (TGRcs.length > 6) {
214   TGR.style.fontSize = "10px";
215 } else {
216   TGR.style.fontSize = "13px";
217 };
218 TGR.value = '$' + TGRcs
219
220 // Total bale transportation cost
221 var tBtc = document.getElementById('BTC').value;
222 var fBtc = parseFloat(tBtc);
223 var tBtd = document.getElementById('BTD').value;

```

```

223 var fBtd = parseFloat(tBtd);
224 TBTC.value = fBtc * fBtd;
225
226
227 // Getting index value of the age in years
228 var ageyrs = document.getElementById("AgeYrs");
229 var ageyF = parseFloat(ageyrs.value);
230 var opt = ageyrs.options[ageyrs.selectedIndex].value;
231
232 // Getting index value of the engine power input
233 var EngP = document.getElementById("EHp");
234 var optEP = EngP.options[EngP.selectedIndex].value;
235
236 // Getting index value of the annual usgae in hours
237 var AnHrs = document.getElementById("AnnHrs");
238 var optAH = AnHrs.options[AnHrs.selectedIndex].value;
239
240 // Getting the input tractor price value
241 var MPrice = document.getElementById("Mp").value;
242
243 // Getting the loan interest rate
244 var Irval = document.getElementById("Ir").value;
245
246 //alert(Irval);
247
248 //-----Tractor fixed cost and RMC function
249
250 /***** Total fixed cost (TFC) - Tractor *****/
251 var checkStatus = document.getElementById("ckb").checked
252
253 var TFCres = [0, 0, 0, 0];
254
255 /***** Total fixed cost calculation for tractor */
256 function TFCval(af, bf, cf) {
257     var salvg = af * Math.pow(ageyF, 2) - bf * ageyF + cf;
258     var salval = MPrice * salvg * 0.01;
259     var uselif = 10000 / optAH;
260     var deprv = (((MPrice - salval) / uselif) / optAH) * totOpTime);
261     var deprval = (((MPrice - salval) / uselif) / optAH);
262     var THlv = (((((parseFloat(salval) + parseFloat(MPrice)) / 2) * 0.0133) / optAH) * totOpTime)
263     );
264     var THlval = (((((parseFloat(salval) + parseFloat(MPrice)) / 2) * 0.0133) / optAH));
265     var INTv = (((((parseFloat(salval) + parseFloat(MPrice)) / 2) * (Irval / 100)) / optAH) *
266     totOpTime);
267     var INTval = (((((parseFloat(salval) + parseFloat(MPrice)) / 2) * (Irval / 100)) / optAH));
268     var TFCv = (parseFloat(deprv) + parseFloat(THlv) + parseFloat(INTv)).toFixed(0);
269     TFCres[0] = deprv;
270     TFCres[1] = THlv;
271     TFCres[2] = INTv;
272     TFCres[3] = TFCv;
273     return TFCres;
274 }
275
276 if (optEP == 0 && optAH == 200) {
277     TFCval(0.0896, 3.8793, 66.025)
278 } else if (optEP == 0 && optAH == 400) {
279     TFCval(0.0893, 3.7568, 60.73)
280 } else if (optEP == 0 && optAH == 600) {
281     TFCval(0.0866, 3.6077, 56.856)
282 } else if (optEP == 1 && optAH == 200) {
283     TFCval(0.0998, 4.2295, 69.889)
284 } else if (optEP == 1 && optAH == 400) {
285     TFCval(0.1, 4.2478, 69.449)
286 } else if (optEP == 1 && optAH == 600) {
287     TFCval(0.1, 4.25, 69.0)

```

```

286 } else if (optEP == 2 && optAH == 200) {
287   TFCval(0.1197, 4.9515, 70.168)
288 } else if (optEP == 2 && optAH == 400) {
289   TFCval(0.1186, 4.8668, 68.225)
290 } else if (optEP == 2 && optAH == 600) {
291   TFCval(0.116, 4.7858, 66.809)
292 }
293
294 var Dep_val = parseFloat(TFCres[0]);
295 var THI_val = parseFloat(TFCres[1])
296 var INT_val = parseFloat(TFCres[2]);
297 var THI_I_val = ((parseFloat((TFCres[1])) + parseFloat(TFCres[2]))).toFixed(0);
298
299
300
301 var Dep_valout = parseFloat(TFCres[0]).toFixed(0);
302 var THI_val = parseFloat(TFCres[1])
303 var INT_val = parseFloat(TFCres[2]);
304 var THI_I_valout = ((parseFloat((TFCres[1])) + parseFloat(TFCres[2]))).toFixed(0);
305
306 // Land rent cost
307 var Lrv = document.getElementById("Far");
308 var LrCal = (parseFloat(tAr.value) * Lrv.value).toFixed(1);
309 LRC.value = '$' + LrCal;
310
311 // Total fixed cost
312 var TTFCs = (parseFloat(Dep_val) + parseFloat(THI_I_val) + parseFloat(LrCal)).toFixed(0);
313 var TFCcs = Number(TTFCs).toLocaleString('en');
314 if (TFCcs.length > 6) {
315   TFC.style.fontSize = "10px";
316 } else {
317   TFC.style.fontSize = "13px";
318 };
319
320 // No-cost (FAR, FRC, CC, LC = 0$): Total fixed cost
321 NCTFC = parseFloat(TFCres[3]).toFixed(0); // tractor
322
323
324 //*****RMC - Tractor *****/
325 var Xv = ((optAH * opt) / 1000);
326 var TAR = (0.003 * Math.pow(Xv, 2));
327 var RMCv = (((MPrice * TAR) / opt) / optAH) * totOpTime).toFixed(1);
328
329 //

```

```

330
331 // Labor cost:
332 var Lcv = document.getElementById("Lc");
333 var NL = document.getElementById("NL");
334 var LcCal = (parseFloat(Lcv.value) * totOpTime * parseFloat(NL.value));
335 // LC.value = '$' + (LcCal).toFixed(1);
336 TLC.value = '$' + (LcCal).toFixed(1);
337
338 // Fuel cost:
339 var Fcv = document.getElementById("Fc");
340 var FcCal = (parseFloat(Fcv.value) * totFconsp);
341 TotFuC.value = '$' + (FcCal).toFixed(1);
342 var FCLCval = FcCal + LcCal;
343 FCLC.value = '$' + (FCLCval).toFixed(1);
344
345 // Total bale transportation cost
346 var fBtc = parseFloat(document.getElementById("BTC").value);
347 var fBtd = parseFloat(document.getElementById("BTD").value);
348 var TBTCval = fBtc * fBtd;
349 TBTCv.value = '$' + TBTCval;

```

```

350
351 // Total variable cost (Tractor)
352 var TVCv = (parseFloat(RMCv) + parseFloat(FCLCval) + parseFloat(TBTCval)).toFixed(0);
353 var TVCcs = Number(TVCv).toLocaleString('en');
354 if (TVCcs.length > 6) {
355     TVC.style.fontSize = "10px";
356 } else {
357     TVC.style.fontSize = "13px";
358 };
359
360 // Seed cost:
361 var Arv = parseFloat(document.getElementById("Ar").value);
362 var SCv1 = parseFloat(document.getElementById("Sc").value);
363 var selectIndex = document.getElementById("drop").selectedIndex;
364 if (selectIndex == "0" || selectIndex == "1") {
365     SCv = SCv1 / 5;
366 } else {
367     SCv = SCv1
368 }
369 // var SCv = parseFloat(document.getElementById("Sc").value);
370 var SCcal = SCv * Arv * fUn;
371 SC.value = '$' + (SCcal).toFixed(1);
372 TSC.value = '$' + (SCcal).toFixed(0);
373
374 // Fertilizer cost:
375 var FRCv = parseFloat(document.getElementById("Frc").value);
376 var FRCcal = FRCv * Arv * fUn;
377 FRC.value = '$' + (FRCcal).toFixed(1);
378 TFRc.value = '$' + (FRCcal).toFixed(0);
379
380 // Chemical cost:
381 var CCv = parseFloat(document.getElementById("Cc").value);
382 var CCcal = CCv * Arv * fUn
383 CC.value = '$' + (CCcal).toFixed(1);
384 TCC.value = '$' + (CCcal).toFixed(0);
385
386 // Crop input cost:
387 var CICv = (parseFloat(SCcal) + parseFloat(FRCcal) + parseFloat(CCcal)).toFixed(0);
388 var CICcs = Number(CICv).toLocaleString('en');
389 if (CICcs.length > 6) {
390     CIC.style.fontSize = "10px";
391 } else {
392     CIC.style.fontSize = "13px";
393 };
394 CIC.value = '$' + CICcs;
395
396 // No-cost (FAR, FRC, CC, LC = 0$): Crop input cost
397 NCCIC = parseFloat(SCcal);
398
399 // Harvest cost:
400 var HCv = parseFloat(document.getElementById("Hc").value);
401 var HCcal = HCv * Arv * fUn;
402 HC.value = '$' + (HCcal).toFixed(1);
403 THC.value = '$' + (HCcal).toFixed(0);
404
405 // Baling cost:
406 var BLv = parseFloat(document.getElementById("Bl").value);
407 var BLcal = (BLv * Arv * fUn)
408 BL.value = '$' + (BLcal).toFixed(1);
409 TBC.value = '$' + (BLcal).toFixed(0);
410
411 // Crop input cost
412 CICa.value = document.getElementById('CIC').value;
413
414 // Total production cost
415 var TPCv = (parseFloat(HCcal) + parseFloat(BLcal) + parseFloat(CICv)).toFixed(0);

```

```

416 var TPCcs = Number(TPCv).toLocaleString('en')
417 if (TPCcs.length > 6) {
418     TPC.style.fontSize = "10px";
419 } else {
420     TPC.style.fontSize = "13px";
421 };
422 TPC.value = '$' + TPCcs;
423
424 var Dep_val = parseFloat(TFCres[0]);
425 var THI_val = parseFloat(TFCres[1]);
426 var INT_val = parseFloat(TFCres[2]);
427 var THI_I_val = ((parseFloat((TFCres[1])) + parseFloat(TFCres[2]))).toFixed(0);
428
429 // ABP Depreciation, taxing, housing, insurance, interest, and total fixed cost
430 var ABPPrice = document.getElementById("ABP").value;
431 var salvPercABP = 69;
432 var salvalABP = ABPPrice * salvPercABP * 0.01;
433 var uselifeABP = 10000 / optAH;
434 var deprABPv = (((((ABPPrice - salvalABP) / uselifeABP) / optAH) * totOpTime) + (Dep_val)).
    toFixed(0);
435 // var deprABPval = (((((ABPPrice - salvalABP) / uselifeABP) / optAH)));
436 var THI_ABpv = ((((((parseFloat(salvalABP) + parseFloat(ABPPrice)) / 2) * 0.0133) / optAH) *
    totOpTime) + (THI_val));
437 // var THI_ABpv = ((((((parseFloat(salvalABP) + parseFloat(ABPPrice)) / 2) * 0.0133) / optAH)
    ));
438 var INT_ABpv = ((((((parseFloat(salvalABP) + parseFloat(ABPPrice)) / 2) * (Irval / 100)) /
    optAH) * totOpTime) + (INT_val));
439 // var INT_ABpv = ((((((parseFloat(salvalABP) + parseFloat(ABPPrice)) / 2) * (Irval / 100)) /
    optAH)));
440 var THI_I_ABpv = (parseFloat(THI_ABpv) + parseFloat(INT_ABpv)).toFixed(1);
441 var TTFC_ABp = (parseFloat(deprABPv) + parseFloat(THI_I_ABpv) + parseFloat(LrCal)).toFixed(0);
442
443 /*****RMC - ABP *****/
444 var Xv = ((optAH * 1) / 1000); // opt = 1; Machine years owned assumed = 1
445 var TAR = (0.003 * Math.pow(Xv, 2));
446 var RMC_ABp = parseFloat((((ABPPrice * TAR) / opt) / optAH) * totOpTime).toFixed(1);
447 var RMC_ABpv = (parseFloat(RMC_ABp) + parseFloat(RMCv)).toFixed(1);
448
449 // Total variable cost (ABP)
450 var TVC_ABpv = (parseFloat(RMC_ABpv) + parseFloat(FCLCval) + parseFloat(TBTCval)).toFixed(0);
451 var TVC_ABpCs = Number(TVC_ABpv).toLocaleString('en');
452 if (TVC_ABpCs.length > 6) {
453     TVC.style.fontSize = "10px";
454 } else {
455     TVC.style.fontSize = "13px";
456 };
457
458 // Total cost (Tractor)
459 TFCv = TTFCs;
460 var TCv = (parseFloat(TPCv) + parseFloat(TVCv) + parseFloat(TFCv)).toFixed(0);
461 var TCcs = Number(TCv).toLocaleString('en');
462 if (TCcs.length > 6) {
463     TC.style.fontSize = "10px";
464 } else {
465     TC.style.fontSize = "13px";
466 };
467 TC.value = '$' + TCcs;
468
469 TotFC.value = '$' + TFCv;
470 TotVC.value = '$' + TVCv;
471 TotPC.value = '$' + TPCv;
472
473 // Total cost (ABP)
474 var TC_ABpv = (parseFloat(TPCv) + parseFloat(TVC_ABpv) + parseFloat(TTFC_ABp)).toFixed(0);
475 var TC_ABpCs = Number(TC_ABpv).toLocaleString('en');
476 if (TC_ABpCs.length > 6) {

```

```

477 TC.style.fontSize = "10px";
478 } else {
479 TC.style.fontSize = "13px";
480 };
481
482 // Total revenue per acre
483
484 var drpOp = document.getElementById("drop").selectedIndex
485
486 if (drpOp == 0) { document.getElementById("FrgePlot").value = "Alfalfa" }
487 else if (drpOp == 1) { document.getElementById("FrgePlot").value = "Alfalfa mix" }
488 else if (drpOp == 2) { document.getElementById("FrgePlot").value = "Barley" }
489 else if (drpOp == 3) { document.getElementById("FrgePlot").value = "Corn" }
490 else if (drpOp == 4) { document.getElementById("FrgePlot").value = "Grain mix" }
491 else if (drpOp == 5) { document.getElementById("FrgePlot").value = "Grass" }
492 else if (drpOp == 6) { document.getElementById("FrgePlot").value = "Grass mix" }
493 else if (drpOp == 7) { document.getElementById("FrgePlot").value = "Millet" }
494 else if (drpOp == 8) { document.getElementById("FrgePlot").value = "Oats" }
495 else if (drpOp == 9) { document.getElementById("FrgePlot").value = "Wheat" }
496 else if (drpOp == 10) { document.getElementById("FrgePlot").value = "Others" }
497
498 // Crop type styling options
499 if (drpOp == 2 || drpOp == 3 || drpOp == 4 || drpOp == 7 || drpOp == 8 || drpOp == 9) {
500 document.getElementById("GYtext").style.color = "black";
501 document.getElementById("GYInfo").style.color = "#0A5640";
502 document.getElementById("GPtext").style.color = "black";
503 document.getElementById("GPInfo").style.color = "#0A5640";
504 document.getElementById("GY").style.background = "#d3d3d3";
505 document.getElementById("GP").style.background = "#d3d3d3";
506 document.getElementById("minGP").style.color = "black";
507 document.getElementById("maxGP").style.color = "black";
508 document.getElementById("minGY").style.color = "black";
509 document.getElementById("maxGY").style.color = "black";
510 document.getElementById("markGP").style.color = "black";
511 document.getElementById("markGY").style.color = "black";
512 document.getElementById("nGP").style.color = "#0A5640";
513 document.getElementById("nGY").style.color = "#0A5640";
514 document.getElementById("TGYText").style.color = "black";
515 document.getElementById("TGYInfo").style.color = "#0A5640";
516 document.getElementById("TGY").style.color = "black";
517 document.getElementById("TGYUnit").style.color = "black";
518 document.getElementById("TGY").style.background = "white";
519 document.getElementById("TGY").value = TGYv;
520 document.getElementById("TGRText").color = "black";
521 document.getElementById("TGRText").style.color = "black";
522 document.getElementById("TGRInfo").style.color = "#0A5640";
523 document.getElementById("TGR").style.background = "white";
524 document.getElementById("TGR").style.color = "#0000FF";
525 document.getElementById("TGR").value = '$' + TGRcs;
526 document.getElementById("TypePlot").value = "Grain and Forage"
527 }
528 else if (drpOp == 0 || drpOp == 1 || drpOp == 5 || drpOp == 6) {
529 document.getElementById("GYtext").style.color = "grey";
530 document.getElementById("GYInfo").style.color = "grey";
531 document.getElementById("GPtext").style.color = "grey";
532 document.getElementById("GPInfo").style.color = "grey";
533 document.getElementById("GY").style.background = "grey";
534 document.getElementById("GP").style.background = "grey";
535 document.getElementById("nGY").style.color = "grey";
536 document.getElementById("GY").style.color = "grey";
537 document.getElementById("minGY").style.color = "grey";
538 document.getElementById("maxGY").style.color = "grey";
539 document.getElementById("nGY").innerHTML = 0;
540 document.getElementById("GY").min = 0;
541 document.getElementById("GY").max = 0;
542 document.getElementById("nGP").style.color = "grey";

```

```

543 document.getElementById("GP").style.color = "grey";
544 document.getElementById("minGP").style.color = "grey";
545 document.getElementById("maxGP").style.color = "grey";
546 document.getElementById("markGP").style.color = "grey";
547 document.getElementById("markGY").style.color = "grey";
548 document.getElementById("nGP").innerHTML = 0;
549 document.getElementById("GP").min = 0;
550 document.getElementById("GP").max = 0;
551 document.getElementById("TGYText").style.color = "grey";
552 document.getElementById("TGYInfo").style.color = "grey";
553 document.getElementById("TGY").style.color = "grey";
554 document.getElementById("TGYUnit").style.color = "grey";
555 document.getElementById("TGY").style.background = "#FFC82E";
556 document.getElementById("TGY").value = "___";
557 document.getElementById("TGRText").style.color = "grey";
558 document.getElementById("TGRInfo").style.color = "grey";
559 document.getElementById("TGR").style.color = "grey";
560 document.getElementById("TGR").value = "___";
561 document.getElementById("TGR").style.background = "#FFC82E";
562 document.getElementById("TypePlot").value = "Forage"
563 }
564
565 // Crop type javascript options
566 if (drpOp == 2 || drpOp == 3 || drpOp == 4 || drpOp == 7 || drpOp == 8 || drpOp == 9) {
567     TRev = (parseFloat(TBRv) + parseFloat(TGRv)).toFixed(0);
568 } else if (drpOp == 0 || drpOp == 1 || drpOp == 5 || drpOp == 6) {
569     TRev = TBRv;
570 }
571
572 TRevc = Number(TRev).toLocaleString('en');
573 if (TRevc.length > 6) {
574     TotRev.style.fontSize = "10px";
575 } else {
576     TotRev.style.fontSize = "13px";
577 };
578 TotRev.value = '$' + TRevc;
579
580
581
582 var TRACv = (TRev / Arv).toFixed(0);
583 var TRACcs = Number(TRACv).toLocaleString('en');
584 if (TRACcs.length > 6) {
585     TRAC.style.fontSize = "10px";
586 } else {
587     TRAC.style.fontSize = "13px";
588 };
589 TRAC.value = '$' + TRACcs;
590
591 // Total cost per acre (Tractor)
592
593 var TCACv = (TCv / Arv).toFixed(0);
594 var TCACcs = Number(TCACv).toLocaleString('en');
595 if (TCACcs.length > 6) {
596     TCAC.style.fontSize = "10px";
597 } else {
598     TCAC.style.fontSize = "13px";
599 };
600
601 // Total cost per acre (ABP)
602
603 var TCAC_ABpv = (TC_ABpv / Arv).toFixed(0);
604 var TCAC_ABpcs = Number(TCAC_ABpv).toLocaleString('en');
605 if (TCAC_ABpcs.length > 6) {
606     TCAC_ABpv.style.fontSize = "10px";
607 } else {
608     TCAC_ABpv.style.fontSize = "13px";

```



```

609 };
610
611
612 // Net return (tractor)
613 var NPv = (parseFloat(TRev) - parseFloat(TCv));
614 var NPcs = Number(NPv).toLocaleString('en');
615 if (NPcs.length > 6) {
616     NP.style.fontSize = "10px";
617 } else {
618     NP.style.fontSize = "13px";
619 };
620
621
622 // Net return (ABP)
623 var NP_ABPv = (parseFloat(TRev) - parseFloat(TC_ABPv)).toFixed(0);
624 var NP_ABPcs = Number(NP_ABPv).toLocaleString('en');
625 if (NP_ABPcs.length > 6) {
626     NP.style.fontSize = "10px";
627 } else {
628     NP.style.fontSize = "13px";
629 };
630
631 if (checkStatus == false) {
632     if (NPv < 0) {
633         document.getElementById('NP').style.backgroundColor = "#FFA07A";
634     } else {
635         document.getElementById('NP').style.backgroundColor = "#98FB98";
636     }
637 } else if (checkStatus == true) {
638     if (NP_ABPv < 0) {
639         document.getElementById('NP').style.backgroundColor = "#FFA07A";
640     } else {
641         document.getElementById('NP').style.backgroundColor = "#98FB98";
642     }
643 }
644 // No-cost (FAR, FRC, CC, LC = 0$):
645 // Total fixed cost - No cost
646 NCTFC = parseFloat(TFCres[3]).toFixed(0); // tractor
647 var NCTFC_ABP = (parseFloat(deprABPv) + parseFloat(THI_I_ABPv)); // ABP
648 // Total variable cost - No cost
649 NCTVC = (parseFloat(RMCv) + parseFloat(FcCal) + parseFloat(TBTCval)).toFixed(0); // tractor
650 var NCTVC_ABP = (parseFloat(RMC_ABPv) + parseFloat(FcCal) + parseFloat(TBTCval)).toFixed(0); //
651     ABP
652 // Total production cost - No cost
653 NCTPC = (NCCIC + parseFloat(HCcal) + parseFloat(BLcal)).toFixed(0); // tractor
654 // Total cost - No cost
655 NCTCv = parseFloat(NCTFC) + parseFloat(NCTPC) + parseFloat(NCTVC); // tractor
656
657 NCTC_ABPv = parseFloat(NCTFC_ABP) + parseFloat(NCTPC) + parseFloat(NCTVC_ABP);
658 // Net revenue - No cost
659 var NCNRv = (parseFloat(TRev) - parseFloat(NCTCv)); // tractor
660 var NCNRcs = Number(NCNRv).toLocaleString('en'); // tractor
661 var NCNR_ABPv = (parseFloat(TRev) - parseFloat(NCTC_ABPv)).toFixed(0); // tractor
662 var NCNR_ABPcs = Number(NCNR_ABPv).toLocaleString('en'); // tractor
663
664 // Harvest and collection cost
665 var HCCv = parseFloat(HCcal + BLcal + TBTCval + FCLCval + TFCres[3]).toFixed(0);
666 var HCC_ABPv = parseFloat(HCcal + BLcal + TBTCval + FCLCval + deprABPv + THI_I_ABPv).toFixed(0)
667 ;
668 var HCCPrv = parseFloat(HCCv / TCv * 100).toFixed(0);
669 var HCCABPPrv = parseFloat(HCC_ABPv / TC_ABPv * 100).toFixed(0);
670 var HCCAcv = parseFloat(HCCv / Arv).toFixed(0);
671 var HCCABPAcv = parseFloat(HCC_ABPv / Arv).toFixed(0);
672
673 // Net return per acre (tractor)
674 var NPACv = (TRACv - TCACv).toFixed(0);

```

```

673
674 // Net return per acre (ABP)
675 var NPAC_ABPv = (TRACv - TCAC_ABPv).toFixed(0);
676
677
678 // Break even (tractor)
679 var BEv = TRev / TCv;
680
681 // Break even (ABP)
682 var BE_ABPv = TRev / TC_ABPv;
683
684
685 // Payback and ROI (tractor)
686 if (NPv > 0) {
687     var PBv = (MPrice / NPv).toFixed(1);
688     PB.value = PBv;
689     var ROIv = (NPv / MPrice * 100).toFixed(0);
690     if (ROIv == Number.POSITIVE_INFINITY || ROIv == Number.NEGATIVE_INFINITY) {
691         ROIv = 0
692     }
693     ROI.value = ROIv;
694 } else {
695     PB.value = "----";
696     ROI.value = "----";
697 }
698
699
700 if (NCNRv > 0) {
701     // alert("positive")
702     var NCPBv = (MPrice / NCNRv).toFixed(0); // "No-cost" pay back (tractor)
703     var NCROIv = (NCNRv / MPrice * 100).toFixed(0); // "No-cost" ROI (tractor)
704     // NCPB.value = NCPBv;
705     if (NCROIv == Number.POSITIVE_INFINITY || NCROIv == Number.NEGATIVE_INFINITY) {
706         NCROIv = 0
707     }
708     // NCROI.value = NCROIv;
709 } else {
710     // alert("negative")
711     // NCPB.value = "----";
712     // NCROI.value = "----";
713 }
714
715 // Payback and ROI (ABP)
716 if (NCNR_ABPv > 0) {
717     var PB_ABPv = ((parseFloat(MPrice) + parseFloat(ABPPrice)) / (NP_ABPv)).toFixed(0);
718     PB.value = PB_ABPv;
719
720     var ROI_ABPv = ((NP_ABPv) / (parseFloat(MPrice) + parseFloat(ABPPrice)) * 100).toFixed(0);
721     ROI.value = ROI_ABPv;
722
723     var NCPB_ABPv = ((parseFloat(MPrice) + parseFloat(ABPPrice)) / (NCNR_ABPv)).toFixed(0); // "
724     var NCROI_ABPv = ((NCNR_ABPv) / (parseFloat(MPrice) + parseFloat(ABPPrice)) * 100).toFixed(0)
725     ; // "No-cost" ROI
726     // NCPB.value = NCPBv;
727     // NCROI.value = NCROIv;
728 } else {
729     PB.value = "----";
730     ROI.value = "----";
731 }
732
733 // Payback and ROI for ABP equipment only
734 var PBeqp = (parseFloat(ABPPrice) / parseFloat(NPv)).toFixed(1);
735 var ROIEqp = ((parseFloat(NPv) / parseFloat(ABPPrice)) * 100).toFixed(0);
736
737 var PBeqp_abp = (parseFloat(ABPPrice) / parseFloat(NP_ABPv)).toFixed(1);

```

```

737 var ROleqp_abp = ((parseFloat(NP_ABpv) / parseFloat(ABPPrice)) * 100).toFixed(0);
738
739
740 if (checkStatus == false) {
741     Dep.value = '$' + Dep_valout;
742     THI_I.value = '$' + THI_I_valout;
743     TFC.value = '$' + TFCcs;
744     RMC.value = '$' + RMCv;
745     TVC.value = '$' + TVCcs;
746     TotFC.value = '$' + TFCv;
747     TotVC.value = '$' + TVCv;
748     TotPC.value = '$' + TPCv;
749     TC.value = '$' + TCcs;
750     TCAC.value = '$' + TCACcs;
751     NP.value = '$' + NPcs;
752     NPAC.value = '$' + NPACv;
753     BE.value = BEv.toFixed(2);
754     if (NPv > 0) {
755         PB.value = PBv;
756         ROI.value = ROIv;
757     } else {
758         PB.value = "___";
759         ROI.value = "___"
760     }
761     EqTyp.value = "Tractor"
762     PB_ABp.value = "___";
763     ROI_ABp.value = "___";
764     // NCNR.value = '$' + NCNRcs;
765     // NCPB.value = NCPBv;
766     // NCROI.value = NCROIv;
767     HCC.value = '$' + HCCv;
768     HCCPc.value = HCCPrv + '%';
769     HCCPac.value = '$' + HCCAcv;
770 } else if (checkStatus == true) {
771     Dep.value = '$' + deprABpv;
772     THI_I.value = '$' + THI_I_ABpv;
773     TFC.value = '$' + TTFC_ABp;
774     RMC.value = '$' + RMC_ABpv;
775     TVC.value = '$' + TVC_ABpCs;
776     TotFC.value = '$' + TTFC_ABp;
777     TotVC.value = '$' + TVC_ABpCs;
778     TotPC.value = '$' + TPCv;
779     TC.value = '$' + TC_ABpCs;
780     TCAC.value = '$' + TCAC_ABpCs;
781     NP.value = '$' + NP_ABpCs;
782     NPAC.value = '$' + NPAC_ABpv;
783     BE.value = BE_ABpv.toFixed(2);
784     PB.value = PB_ABpv;
785     ROI.value = ROI_ABpv;
786     EqTyp.value = "Tractor and ABP"
787     PB_ABp.value = PBeqp_abp;
788     ROI_ABp.value = ROleqp_abp;
789     // NCNR.value = '$' + NCNR_ABpCs;
790     // NCPB.value = NCPB_ABpv;
791     // NCROI.value = NCROI_ABpv;
792     HCC.value = '$' + HCC_ABpv;
793     HCCPc.value = HCCABPPrv + '%';
794     HCCPac.value = '$' + HCCABPacv;
795 }
796
797
798 //Plot
799 var HT = 210;
800 var yval = 25;
801 var FCmax = 600;
802 var PBmax = 25;

```

```

803 var BEmax = 20;
804
805
806
807 // Fuel consumption plot (FC)
808 if (parseFloat(FuelConsp) < FCmax) {
809     var FCperc = FuelConsp / FCmax;
810     var FCHt = (FCperc * HT).toFixed(0);
811     document.getElementById("TCr").setAttribute("y", yval);
812     document.getElementById("TCr").setAttribute("height", HT);
813     document.getElementById("FCr").setAttribute("height", FCHt);
814     document.getElementById("FCr").setAttribute("y", Math.abs((parseFloat(HT) - FCHt)) +
        parseFloat(yval));
815 } else {
816     document.getElementById("TCr").setAttribute("y", yval);
817     document.getElementById("TCr").setAttribute("height", HT);
818 }
819
820 // Cost related plot (TR, TC, NR)
821 var dperc1
822 var dHT1
823 var dperc3
824 var dHT3
825 var yoff = 10;
826 var SumTC = parseFloat(TFCv) + parseFloat(TVCv);
827
828 var TVCperc = (TVCv * 50) / SumTC;
829 var TFCperc = (TFCv * 50) / SumTC;
830
831 //     alert("SumTC = " + SumTC);
832 //     alert("TFCv = " + TFCv);
833 //     alert("TFCperc = " + TFCperc);
834
835 if (parseFloat(NPv) > 0) {
836     dperc1 = (TCv * 100 / TRev).toFixed(0);
837     dHT1 = (dperc1 * 0.01 * HT).toFixed(0);
838     dHTVC = ((dHT1 * TVCperc) / 100).toFixed(0);
839     var yval1 = Math.abs((HT - dHT1)) + yval;
840     var yvalTPC = yval1 + dHT1 / 2 + yoff;
841     var yvalTFC = yval1 + (TVCperc * dHT1 * 0.01) + yoff;
842     var yvalTVC = yval1 + yoff;
843
844     document.getElementById("TRr").setAttribute("y", yval);
845     document.getElementById("TRr").setAttribute("height", HT);
846
847     document.getElementById("TCr").setAttribute("height", dHT1);
848     document.getElementById("TCr").setAttribute("y", yval1);
849
850     document.getElementById("TPCr").setAttribute("height", dHT1 / 2);
851     document.getElementById("TPCr").setAttribute("y", yval1);
852
853     document.getElementById("TPCt").setAttribute("y", yvalTPC);
854     document.getElementById("TFCt").setAttribute("y", yvalTFC);
855     document.getElementById("TVCT").setAttribute("y", yvalTVC);
856
857
858
859     document.getElementById("TVCr").setAttribute("height", dHTVC);
860     document.getElementById("TVCr").setAttribute("y", yval1);
861
862     dperc3 = (NPv * 100 / TRev).toFixed(0);
863
864     document.getElementById("NRr").style.fill = "green"
865 } else {
866     dperc1 = (TRev * 100 / TCv).toFixed(0);
867     dHT1 = (dperc1 * 0.01 * HT).toFixed(0);

```

```

868 dHTVC = ((HT * TVCperc) / 100).toFixed(0);
869 var yval2 = Math.abs((HT - dHT1)) + yval;
870 yvalTPC = yval + HT / 2 + yoff;
871 yvalTFC = yval + (TVCperc * HT * 0.01) + yoff;
872 yvalTVC = yval + yoff;
873
874 document.getElementById("TCr").setAttribute("y", yval);
875 document.getElementById("TCr").setAttribute("height", HT);
876
877 document.getElementById("TRr").setAttribute("height", dHT1);
878 document.getElementById("TRr").setAttribute("y", yval2);
879
880 document.getElementById("TPCr").setAttribute("height", HT / 2);
881 document.getElementById("TPCr").setAttribute("y", yval);
882
883 document.getElementById("TPCr").setAttribute("y", yvalTPC);
884 document.getElementById("TFCr").setAttribute("y", yvalTFC);
885 document.getElementById("TVCr").setAttribute("y", yvalTVC);
886
887
888 document.getElementById("TVCr").setAttribute("height", dHTVC);
889 document.getElementById("TVCr").setAttribute("y", yval);
890
891 dperc3 = (Math.abs(NPv) * 100 / TCv).toFixed(0);
892 document.getElementById("NRr").style.fill = "red"
893 }
894 dHT3 = (dperc3 * 0.01 * HT).toFixed(0);
895 document.getElementById("NRr").setAttribute("height", dHT3);
896 document.getElementById("NRr").setAttribute("y", Math.abs((HT - dHT3)) + yval);
897
898 // Payback period plot (PB)
899
900 if (PBv < PBmax) {
901     var PBperc = PBv / PBmax;
902     var PBHt = (PBperc * HT).toFixed(0);
903     document.getElementById("PBr").setAttribute("y", yval);
904     document.getElementById("PBr").setAttribute("height", HT);
905     document.getElementById("PBr").setAttribute("height", PBHt);
906     document.getElementById("PBr").setAttribute("y", Math.abs((parseFloat(HT) - PBHt)) +
907         parseFloat(yval));
908 } else {
909     document.getElementById("PBr").setAttribute("y", yval);
910     document.getElementById("PBr").setAttribute("height", HT);
911 }
912
913 // Break even ratio plot (BE)
914
915 if (BEv < BEmax) {
916     var BEperc = BEv / BEmax;
917     var BEHt = (BEperc * HT).toFixed(0);
918     document.getElementById("BEr").setAttribute("y", yval);
919     document.getElementById("BEr").setAttribute("height", HT);
920     document.getElementById("BEr").setAttribute("height", BEHt);
921     document.getElementById("BEr").setAttribute("y", Math.abs((parseFloat(HT) - BEHt)) +
922         parseFloat(yval));
923 } else {
924     document.getElementById("BEr").setAttribute("y", yval);
925     document.getElementById("BEr").setAttribute("height", HT);
926 }
927
928 } // end of function calculate ()

```

D.3. JavaScript - User-Defined Functions for Data Visualization

```
1 function chartDeets1() {
2
3   var TPCch = parseInt(document.getElementById("TPC").value.replace('$', '').replace(/\\,/g, ''));
4   var TBRch = parseInt(document.getElementById("TBR").value.replace('$', '').replace(/\\,/g, ''));
5   var TCch = parseInt(document.getElementById("TC").value.replace('$', '').replace(/\\,/g, ''));
6   var NRch = parseInt(document.getElementById("NP").value.replace('$', '').replace(/\\,/g, ''));
7   var Cropch = document.getElementById("FrgePlot").value;
8   var Croptypch = document.getElementById("TypePlot").value;
9   var Equiptypch = document.getElementById("EquipPlot").value;
10  var TRACch = document.getElementById("TRAC").value;
11  var TCACch = document.getElementById("TCAC").value;
12  var NPACch = document.getElementById("NPAC").value;
13  var BEch = document.getElementById("BE").value;
14  var PBch = document.getElementById("PB").value;
15  var ROIch = document.getElementById("ROI").value;
16
17  Cropchd.value = Cropch;
18  Croptypchd.value = Croptypch;
19  Equiptypchd.value = Equiptypch;
20  TRACchd.value = TRACch;
21  TCACchd.value = TCACch;
22  NPACchd.value = NPACch;
23  BEchd.value = BEch;
24  PBchd.value = PBch;
25  ROIchd.value = ROIch;
26
27  var ctx = document.getElementById("myChart1");
28
29  Chart.defaults.global.elements.rectangle.borderWidth = 2;
30
31  Chart.plugins.register({
32    beforeDraw: function (chartInstance) {
33      var ctx = chartInstance.chart.ctx;
34      ctx.fillStyle = "white";
35      ctx.fillRect(0, 0, chartInstance.chart.width, chartInstance.chart.height);
36    }
37  });
38  if (window.bar !== undefined)
39    window.bar.destroy();
40  window.bar = new Chart(ctx, {
41    // var myChart1 = new Chart(ctx, {
42    type: 'bar',
43    data: {
44      labels: ["Total revenue (TR)", "Total cost (TC)", "Net Return (NR)"],
45      datasets: [{
46        label: '',
47        backgroundColor: ["green", "red", "blue"],
48        data: [TBRch, TCch, NRch],
49      }],
50      borderWidth: 10,
51    },
52    options: {
53      tooltips: {
54        callbacks: {
55          dataset: [1, 2, 3],
56          label: function (tooltipItem) {
57            return "$" + Number(tooltipItem.yLabel);
58          }
59        }
60      },
61      responsive: false,
62      title: {
63        display: true,
```

```
64     text: 'Forage economics calculator web tool'
65   },
66   legend: {
67     display: false,
68   },
69   scales: {
70     xAxes: [{
71       barThickness: 80, // number (pixels) or 'flex'
72       maxBarThickness: 80 // number (pixels)
73     }],
74     yAxes: [{
75       gridLines: {
76         color: "black",
77         borderDash: [2, 5],
78       },
79       ticks: {
80         beginAtZero: true
81       },
82       scaleLabel: {
83         display: true,
84         labelString: "U.S. Dollars ($)",
85       }
86     }
87   }
}
```

APPENDIX E. BIOMASS YIELD PREDICTION - SHAPEFILE CREATION AND SATELLITE DATA COLLECTION

This appendix provides the procedure for creating shapefile using open-source QGIS software and javascript source codes for extracting Landsat and Sentinel satellite images from Google Earth Engine (GEE) using cloud mask function used in Chapter 5 “Biomass yield prediction for pastures using remotely sensed vegetation index and climate data through machine learning”.

E.1. Creating Shapefile Using QGIS Software

A georeferenced web map service layer can be traced to produce shapefile with vector features using the following steps.

1. Create a georeferenced shapefile, Layer → Create Layer → New Shapefile Layer
2. In the new shapefile layer dialog box, enter the file name (.shp), select geometry type as “Polygon”, and select the coordinate system and save this layer (fig.E1.A).
3. The shapefile is added to the layers box on the left hand side, right click on the created layer and select “Toggle Editing” (fig.E1.B).
4. Select the “Add Polygon” to digitize the polygon. Click a set of points on the perimeter of the desired polygon, when the last point is clicked enter the id number of the created polygon (fig.E1.C).
5. If needed, more polygons can be added to the same layer and once done, right click on the shapefile layer on the left hand side and click the “Toggle Editing” button again to finish editing the shapefile layer.

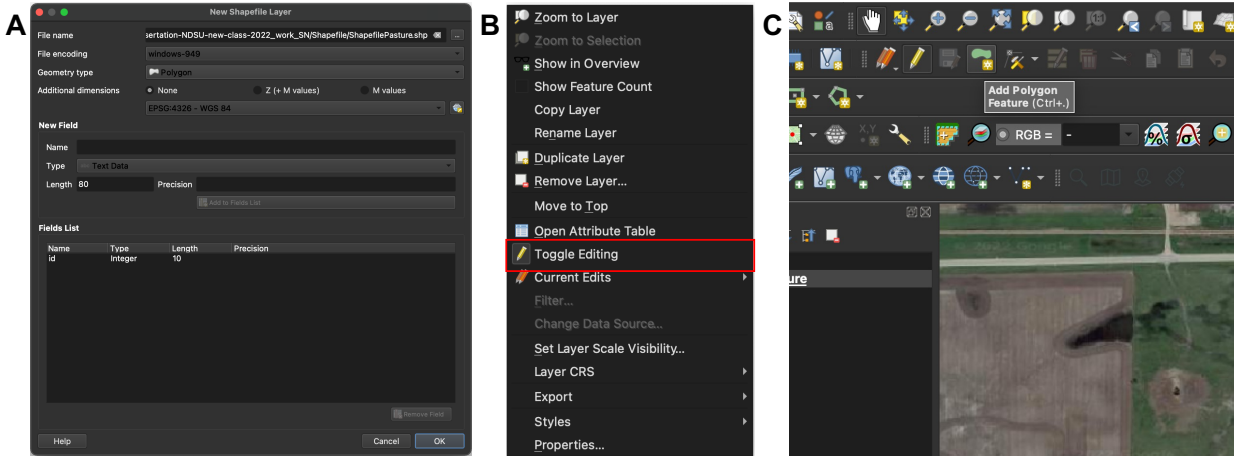


Figure E1. Creating polygon shapefile using QGIS software.

E.2. Collecting Landsat and Sentinel Data From the GEE Archive

```

1 # Cloud mask function
2 var cloudMaskL457 = function(image) {
3   var qa = image.select('pixel_qa');
4   var cloud = qa.bitwiseAnd(1 << 5)
5     .and(qa.bitwiseAnd(1 << 7))
6     .or(qa.bitwiseAnd(1 << 3));
7   var mask2 = image.mask().reduce(ee.Reducer.min());
8   return image.updateMask(cloud.not()).updateMask(mask2);
9 };
10
11 # Selecting Landsat or Sentinel archive
12 var dataset = ee.ImageCollection('LANDSAT/LT05/C01/T1_SR')
13   .filterDate('2012-05-01', '2012-08-31')
14   .map(cloudMaskL457);
15 var year = '2017'
16 var landsat = dataset.median().clip(geometry);
17 print(geometry);
18
19 # Visualizing satellite image on base map
20 var visParams = {
21   bands: ['B3', 'B2', 'B1'],
22   min: 0,
23   max: 3000,
24   gamma: 1.4,
25 };
26 Map.setCenter(-100.91386732871885, 46.770380732680884, 15);
27 Map.addLayer(landsat, visParams, '2003');
28
29 # Exporting the selected image to Google drive
30 Export.image.toDrive({
31   image: landsat,
32   description: year,
33   scale: 30,
34   region: geometry
35 })

```

APPENDIX F. BIOMASS YIELD PREDICTION - R SOURCE CODES FOR SATELLITE BAND EXTRACTION, DATA SIMULATION AND MACHINE LEARNING APPROACHES

This appendix provides R source codes for the Chapter 5 “Biomass yield prediction for pastures using remotely sensed vegetation index and climate data through machine learning”. The R codes for satellite data extraction, data simulation, feature selection, and machine learning are shown below.

F.1. User-Defined Function to Extract the Raster (Satellite) Image Values Based on the Pasture Shapefile

```
1 extrctSatVal <- function(flder, shpfl, src){
2 all_landsat_bands <- list.files(flder, pattern = ".tif$", full.names = TRUE) # dollar sign at the
  end to get all files end with tif
3 landsatval <- data.frame()
4 field_boundary <- st_read(shpfl) # boundary file
5 for(i in 1: length(all_landsat_bands)){
6 filnme <- all_landsat_bands[i] # tiff file
7 img <- stack(filnme)
8 excl1 <- filnme; excl2 <- str_remove(excl1, sprintf("%s/", flder)); exclf <- str_remove(excl2, ".
  tif")
9 band_vals <- cbind(Date = as.Date(exclf, "%Y_%m_%d"), field_boundary, exact_extract(img, field_
  boundary, 'mean'), Source = src) # zonal statistics
10 landsatval <- rbind(landsatval, band_vals)
11 }
12 return(landsatval)
13 }
14
15 flderIn <- "/Volumes/GoogleDrive/Shared drives/1 Subhashree NDSU PhD Work/1_ForageYieldPrection_
  Data/Data/DrToledoData/1_CubeSat/2018"
16 shpflIn <- "/Volumes/GoogleDrive/Shared drives/1 Subhashree NDSU PhD Work/1_ForageYieldPrection_
  Data/Data/ShpflPasture_MGP/PasturesArea4.shp"
17
18 resVal <- extrctSatVal(flderIn, shpflIn, "DT")
19 head(resVal)
20
21 write.csv(resVal, file="/Volumes/GoogleDrive/Shared drives/1 Subhashree NDSU PhD Work/1_
  ForageYieldPrection_Data/Data/DrToledoData/1_CubeSat/2018/CubeSatSatDT2018.csv", row.names =
  T) # Exporting extracted values as .csv file
```

F.2. Band Data Simulation Using Loess Fit Performed for Each Pasture

```

1 # Loess random sampling function
2 DataSimUsingLoess <- function(dat, xv, yv, smpl, repl, sd_p){
3   ranx <- seq(min(dat %>% dplyr::select(xv)), max(dat %>% dplyr::select(xv)), by = 1)
4   fitd <- loess(paste(yv, "~", xv), data = dat)
5   predl <- predict(fitd, ranx, se = T)
6   lcl <- predl$fit - qt(0.975, predl$df)*predl$se # https://stackoverflow.com/questions/22717930/how-to-get-the-confidence-intervals-for-lowess-fit-using-r
7   lcu <- predl$fit + qt(0.975, predl$df)*predl$se
8   predsSDl <- as.data.frame(cbind(ranx, predl$fit, lcl, lcu))
9   colnames(predsSDl) = c("ranx", "fit", "lwr", "upr")
10  predsSDl$spd <- sd(c(predsSDl$fit, predsSDl$lwr, predsSDl$upr))
11  predsSDl$spd2 <- (predsSDl$fit - predsSDl$lwr)/1.75
12  big_data <- data.frame()
13  for (i in 1:nrow(predsSDl)) {
14    spd <- (predsSDl$fit[i] - predsSDl$lwr[i])/1.75
15    nfit <- rnorm(repl, predsSDl$fit[i], spd)
16    xp <- rep(predsSDl$ranx[i], repl)
17    yp <- rep(predsSDl$fit[i], repl)
18    cl <- rep(predsSDl$lwr[i], repl)
19    cu <- rep(predsSDl$upr[i], repl)
20    dat1 <- as.data.frame(cbind(xp, yp, cl, cu, nfit))
21    dat1$i <- i # keeping track of iterations
22    big_data <- rbind(big_data, dat1)
23    # datalist[[i]] <- dat1 # add to the list
24  }
25  colnames(big_data) <- c("DOY", "FittedYield", "ConfLow", "ConfUp", "RandYield", "i")
26  return(big_data)
27 }
28
29 PID <- "MGP"; yr <- 2006 # change
30 Sdat <- Vdat %>% filter (Pasture == PID)
31 head(Sdat)
32
33 xf <- "DOY"; yf <- "SWIR2"; datf <- Sdat # change inputs
34 res <- DataSimUsingLoess(datf, xf, yf, 200, 4, 1.75)
35 out <- res %>% dplyr::select("DOY", "RandYield")
36
37 # Exporting the generated random band data into csv
38 out$Year <- yr; out$Pasture <- PID; out$variable <- yf; out$Date <- format(as.Date(out$DOY,
39   origin = "2006-01-01"))
40 outf <- out[, c(4, 3, 6, 1, 5, 2)]
41 outf; head(outf)

```

F.3. Combining Simulated Band Data Into a Data Frame and Filtering Using Date

```

1 # Importing simulated band values
2 fllder <- selectDirectory(caption = "Select Directory", label = "Select", path = getActiveProject
3   ())
4 AlBands <- list.files(fllder, pattern = ".csv$", full.names = TRUE)
5 Blue <- read.csv(AlBands[1]); Green <- read.csv(AlBands[2]); NIR <- read.csv(AlBands[3]); Red <-
6   read.csv(AlBands[4]);
7   SWIR <- read.csv(AlBands[5]); SWIR2 <- read.csv(AlBands[6])
8 identical(Blue[,1:4], Green[,1:4]); identical(Green[,1:4], Red[,1:4]); identical(Red[,1:4], NIR
9   [,1:4]); identical(NIR[,1:4], SWIR[,1:4]); identical(SWIR[,1:4], SWIR2[,1:4])
10
11 # Combined band values data frame
12 dbnds <- as.data.frame(cbind(Blue[, 1:4], Blue[,6], Green[,6], Red[,6], NIR[,6], SWIR[,6], SWIR2
13   [,6]))
14 colnames(dbnds) <- c("Pasture", "Year", "Date", "DOY", "Blue", "Green", "Red", "NIR", "SWIR", "
15   SWIR2")

```

```

11 dbnds$Date <- mdy(dbnds$Date)
12 dbnds <- dbnds %>% filter(Pasture == "MGP")
13
14 # Importing live biomass data
15 pth <- file.choose()
16 datBm <- read.csv(pth)
17 datBm$Year <- as.numeric(datBm$Year); datBm$DOY <- as.numeric(datBm$DOY); datBm$Date <- mdy(datBm
    $Date)
18 LvB04 <- datBm %>% filter(Year == 2006)
19
20 StDt <- LvB04$Date[1]
21
22 if( LvB04$Date[1] < dbnds$Date[1]){
23   StDt <- dbnds$Date[1]
24 } else{
25   StDt <- LvB04$Date[1]
26 }
27
28 if( LvB04$Date[nrow(LvB04)] < dbnds$Date[nrow(dbnds)]){
29   EnDt <- LvB04$Date[nrow(LvB04)]
30 } else{
31   EnDt <- dbnds$Date[nrow(dbnds)]
32 }
33
34 StDt; EnDt
35
36 LvB04F <- LvB04 %>% filter(Date >= StDt & Date <= EnDt)
37 dbndsF <- dbnds %>% filter(Date >= StDt & Date <= EnDt)
38 #str(LvB04F); str(dbndsF)
39 identical(LvB04F[,4], dbndsF[,4])
40
41 datb <- cbind(LvB04F[, 1:4], LvBiom = LvB04F[ncol(LvB04F)], dbndsF[5: ncol(dbndsF)]); colnames(
    datb)[5] <- "LvBiom"

```

F.4. Estimating Vegetation Indices

```

1 # 1. Visible band vegetation indices
2 Blv <- datb$Blue; Grv <- datb$Green; Rdv <- datb$Red; Nirv <- datb$NIR; Swv <- datb$SWIR; Sw2v <-
    datb$SWI2
3
4 # 2. Red chromatic color coordinate
5 datb$RCC <- Rdv/(Rdv + Grv + Blv)
6
7 # 3. Green chromatic color coordinate
8 datb$GCC <- Grv/(Rdv + Grv + Blv)
9
10 # 4. Blue chromatic color coordinate
11 datb$BCC <- Blv/(Rdv + Grv + Blv)
12
13 # 5. Excessive green index
14 datb$ExG <- 2*Grv - Blv - Rdv
15
16 # 6. Excessive green index v2
17 datb$ExG2 <- (2*Grv - Blv - Rdv)/(Rdv + Grv + Blv)
18
19 # 7. Excess red index
20 datb$ExR <- (1.4*Rdv - Grv)/(Rdv + Grv + Blv)
21
22 # 8. Excess green minus excess red index
23 datb$ExGR <- datb$ExG2 - datb$ExR
24
25 # 9. Green red vegetation index
26 datb$GRVI <- (Grv - Rdv)/(Grv + Rdv)
27

```

```

28 # 10. Green blue vegetation index
29 datb$GBVI <- (Grv - Blv)/(Grv + Blv)
30
31 # 11. Blue red vegetation index
32 datb$BRVI <- (Blv - Rdv)/(Blv + Rdv)
33
34 # 12. Green red ratio
35 datb$G.R <- Grv/Rdv
36
37 # 13. Green-Red difference
38 datb$G_Rdiff <- Grv - Rdv
39
40 # 14. Blue-Green difference
41 datb$B_Gdiff <- Blv - Grv
42
43 # 15. Visible-band difference vegetation index
44 datb$VDVI <- (2*Grv - Rdv - Blv)/(2*Grv + Rdv + Blv)
45
46 # 16. Visible atmospherically resistant index
47 datb$VARI <- (Grv - Rdv)/(Grv + Rdv - Blv)
48
49 # 17. Modified green red vegetation index
50 datb$MGRVI <- (Grv^2 - Rdv^2)/(Grv^2 + Rdv^2)
51
52 # 18. Color index of vegetation
53 datb$CIVE <- 0.441*Rdv - 0.881*Grv + 0.385*Blv + 18.787
54
55 # 19. Woebbecke index
56 datb$WI <- (Grv - Blv)/(Rdv - Grv)
57
58 # 20. Coloration index
59 datb$CI <- (Rdv - Blv)/Rdv
60
61 # 21. Normalized difference vegetation index
62 datb$NDVI <- (Nirv - Rdv)/(Nirv + Rdv)
63
64 # 22. Green normalized difference vegetation index
65 datb$GNDVI <- (Nirv - Grv)/(Nirv + Grv)

```

F.5. Machine Learning - Recursive Feature Elimination and Random Forest

```

1 %-----
2 # Recursive feature elimination
3 set.seed(1234)
4
5 # Define the control using a random forest selection function
6 control <- rfeControl(functions = rfFuncs, # random forest
7                       method = "repeatedcv", # repeated cv
8                       repeats = 2, # number of repeats
9                       number = 10) # number of folds
10
11 trainY <- as.matrix(datT %>% dplyr::select(LvBiom)) # converting y to a matrix otherwise error
12           produced
13 trainX <- datT %>% dplyr::select(Blue:Min_Wind_Chill)
14
15 # str(trainX); str(trainY)
16 # class(trainY)
17
18 # Run RFE
19 RFESys <- system.time(result_rfe1 <- rfe(x = trainX,
20                                         y = trainY,
21                                         sizes = c(1:13),
22                                         rfeControl = control))

```

```

23 # Print the results
24 Impvar <- as.matrix(varImp(result_rfe1))
25 datImp <- result_rfe1$variables
26 %-----
27 # Splitting dataset into training and testing
28 set.seed(1234)
29 ind <- sample(2, nrow(datT), replace = T, prob = c(0.70, 0.30))
30 trainB <- datT[ind == 1,]
31 testB <- datT[ind == 2,]
32 %-----
33 # Machine learning - Random forest
34 AlRanked <- RfeFR
35
36 trainS <- trainB %>% dplyr::select(LvBiom, AlRanked)
37 testS <- testB %>% dplyr::select(LvBiom, AlRanked)
38
39 #str(trainS); str(testS)
40
41 m1 <- randomForest(formula = LvBiom ~ .,
42                   data = trainS, do.trace = F)
43 # m1;
44 # plot(m1)
45
46 # number of trees with lowest MSE
47 ntre <- which.min(m1$mse); ntre
48
49 model_caret <- caret::train(LvBiom ~ ., data=trainS,
50                             method = "ranger",
51                             trControl = trainControl(method="cv", number = 10),
52                             num.trees = ntre,
53                             importance = 'impurity')
54
55 saveRDS(model_caret, "RF_model.rds")
56
57 # Predicting accuracy of the training data
58 rfs <- predict(model_caret, trainS)
59 rmse <- sqrt(mean((trainS$LvBiom - rfs)^2))
60 R2 <- round(cor(trainS$LvBiom, rfs)^2,2)
61
62 # Predicting accuracy of the testing data
63 rfs <- predict(model_caret, testS)
64 rm <- Metrics::rmse(testS$LvBiom, rfs)
65 R2 <- round(cor(testS$LvBiom, rfs)^2,2)
66 me <- Metrics::mae(testS$LvBiom, rfs)

```

APPENDIX G. RANGEFORAGE WEB TOOL - R SOURCE CODES FOR USER INTERFACE AND SERVER

This appendix provides R source codes for the Chapter 6 “Development of a user-friendly rangeland forage yield prediction web tool”. The R codes for the user interface and server side are presented below.

G.1. User Interface R Code for Tool Development

```
1 ui <- fluidPage(  
2   theme = shinytheme("darkly"),  
3   fluidPage(  
4     tags$style(  
5       HTML(  
6         ,  
7         #sidebar {  
8           background-color:#006633;  
9           color: white;  
10        }  
11        .navbar{  
12          background-color: #ffcc00 !important;  
13          color: #006633;  
14          font-weight:bold;  
15        }  
16        .navbar-nav: hover {  
17          color: black;  
18        }  
19        body, label, input, button, select {  
20          font-family: "Arial";  
21        }'  
22      )  
23    ),  
24    navbarPage(  
25      theme = "cerulean",  
26      # <--- To use a theme, uncomment this  
27      "Forage yield prediction calculator",  
28      tabPanel("Calculator",  
29        sidebarLayout(  
30          ## adding sidebar panel in page layout for picking data  
31          sidebarPanel(  
32            id = "sidebar",  
33            fileInput(  
34              "shpFile",  
35              "Upload shapefile (.shp file)",  
36              multiple = T,  
37              accept = c(".shp", ".cpg", ".dbf", ".prj", ".qpj", ".shx")  
38            ),  
39            fileInput(  
40              "rstFile",  
41              "Upload raster (.tif file)",  
42              multiple = F,  
43              accept = c(".tif")  
44            ),  
45            sliderInput(  
46              "C1",
```

```

47     div(HTML("Average turf soil temperature (&degF:")),
48         min = 0,
49         max = 100,
50         value = 50
51     ),
52     sliderInput(
53         "C2",
54         div(HTML("Average bare soil temperature (&degF)")),
55         min = 0,
56         max = 100,
57         value = 50
58     ),
59     fluidRow(
60         column(12, actionButton("Pred", "Estimate biomass"),
61             align = "center"),
62     )
63 ), # end sidebarPanel
64 mainPanel(leafletOutput("map"), ## Basic map for user to explore
65     fluidPage(fluidRow(
66         column(6,
67             tableOutput("values1"), align = "center"),
68         column(6,
69             tableOutput("values2"), align = "center"),
70     ),
71     fluidRow(column(12, textOutput("ResOut"), align = "center")))
72 ) # End sidebarLayout 1
73 ), # End tab panel 1
74 tabPanel("Data visualization",
75     sidebarLayout(
76         ## adding sidebar panel in page layout for picking data
77         sidebarPanel(
78             id = "sidebar2",
79             shinyjs::useShinyjs(),
80             fluidRow(
81                 column(6,
82                     checkboxInput("gciID", "GCI", FALSE)),
83                 column(6,
84                     checkboxInput("msaviID", "MSAVI", FALSE)),
85             ),
86             fluidRow(
87                 column(6,
88                     checkboxInput("gndviID", "GNDVI", FALSE)),
89                 column(6,
90                     checkboxInput("saviID", "SAVI", FALSE)),
91             ),
92             fluidRow(
93                 column(6,
94                     checkboxInput("rccID", "RCC", FALSE)),
95                 column(6,
96                     checkboxInput("ndviID", "NDVI", FALSE)),
97             ), # end sidebarPanel
98         ## Main Panel 2
99         mainPanel(
100             textOutput("outT"),
101             leafletOutput("mapn"),
102             tableOutput("table3"),
103         )
104     ) # End sidebarLayout 2
105 ), # End tabPanel 2
106 tabPanel("About", "This panel is intentionally left blank")
107 ) # close navbarPage
108 ) # style fluidPage
109 ) ## close ui

```


G.2. Server R Code for Tool Development

```
1 server <- function(input, output, session) {
2   uploadShpfile <- reactive({
3     if (!is.null(input$shpFile)) {
4       shpDF <- input$shpFile
5       prevWD <- getwd()
6       uploadDirectory <- dirname(shpDF$datapath[1])
7       setwd(uploadDirectory)
8       for (i in 1:nrow(shpDF)) {
9         file.rename(shpDF$datapath[i], shpDF$name[i])
10      }
11      shpName <-
12        shpDF$name[grep(x = shpDF$name, pattern = "*.shp")]
13      shpPath <- paste(uploadDirectory, shpName, sep = "/" )
14      setwd(prevWD)
15      shpFile <- shapefile(shpPath)
16      # shpFile <- st_read(shpPath)
17      return(shpFile)
18    } else {
19      return()
20    }
21  })
22
23  output$map <-
24    renderLeaflet({
25      ## begin rendering leaflet and store as 'map' in server output
26      leaflet() %>% addProviderTiles(providers$Esri.NatGeoWorldMap) %>% ## Add basemap
27        addScaleBar() %>% #add dynamic scale bar
28        addDrawToolbar(
29          polylineOptions = FALSE,
30          circleOptions = FALSE,
31          polygonOptions = TRUE,
32          markerOptions = FALSE,
33          circleMarkerOptions = FALSE,
34          rectangleOptions = FALSE,
35          singleFeature = FALSE,
36          editOptions = editToolbarOptions()
37        ) %>%
38        setView(lat = 46.769,
39              lng = -100.916,
40              zoom = 10)
41    }) ## close map
42
43  observeEvent(input$shpFile, {
44    crd <- coordinates(uploadShpfile())
45    ltln <- crd[1,]
46    leafletProxy("map") %>%
47      addPolygons(data = uploadShpfile()) %>%
48      flyTo(lat = ltln[2],
49          lng = ltln[1],
50          zoom = 15)
51  })
52
53  img <- reactive({
54    f <- input$rstFile
55    raster::raster(f$datapath)
56  })
57
58  observeEvent(input$rstFile, {
59    rst <- img()
60    spts <- rasterToPoints(rst, spatial = TRUE)
61    llpts <- spTransform(spts, CRS("+proj=longlat +ellps=WGS84 +datum=WGS84 +no_defs +towgs84
        =0,0,0"))

```

```

62   crd <- coordinates(1lpts)
63   xmin <- min(crd[,1]); xmax <- max(crd[,1]); ymin <- min(crd[,2]); ymax <- max(crd[,2])
64   x <- xmin + (xmax - xmin)/2
65   y <- ymin + (ymax - ymin)/2
66   leafletProxy("map") %>%
67     clearImages() %>%
68     addRasterImage(img(), project = F) %>%
69     flyTo(lat = y,
70          lng = x,
71          zoom = 15)
72   })
73
74   # Reading the tif file as raster brick for extracting bands
75   rstack <- reactive({
76     req(input$rstFile)
77     f <- input$rstFile
78     raster::brick(f$datapath)
79   })
80
81   # Extracting bands to show in table
82
83   extB <- reactive({
84     req(uploadShpfile(), rstack())
85     valB <- exactextractr::exact_extract(rstack(), uploadShpfile(), 'mean')
86     return(valB)
87   })
88
89   estimatedBands <- reactive({
90     req(extB())
91     val <- extB()
92     dataIn <- data.frame(
93       "Bands (mean, um)" = c("Blue",
94                             "Green",
95                             "Red",
96                             "Near infrared"),
97       Value = as.character(c(round(val[[1]]),
98                             round(val[[2]]),
99                             round(val[[3]]),
100                            round(val[[4]]))),
101       stringsAsFactors = FALSE,
102       check.names = FALSE)
103   })
104
105
106   estimatedVI <- reactive({
107     req(extB())
108     val <- extB()
109     Blv <- val[[1]]
110     Grv <- val[[2]]
111     Rdv <- val[[3]]
112     Nirv <- val[[4]]
113     SAVI <- ((Nirv - Rdv) / (Nirv + Rdv + 0.5)) * (1.5)
114     MSAVI <- (2 * Nirv + 1 - sqrt((2 * Nirv + 1) ^ 2 - 8 * (Nirv - Rdv))) / 2
115     GNDVI <- (Nirv - Grv) / (Nirv + Grv)
116     GCI <- (Nirv) / (Grv - 1)
117     NDVI <- (Nirv - Rdv) / (Nirv + Rdv)
118     RCC <- Rdv / (Rdv + Blv + Grv)
119     cat("RCC = ", RCC, "\n")
120     dataIn <- data.frame(
121       "Vegetation index" = c("SAVI",
122                             "MSAVI",
123                             "GNDVI",
124                             "GCI",
125                             "NDVI",
126                             "RCC"),
127       Value = as.character(c(

```

```

128     round(SAVI, 3),
129     round(MSAVI, 3),
130     round(GNDVI, 3),
131     round(GCI, 3),
132     round(NDVI, 3),
133     round(RCC, 3)
134  )),
135   stringsAsFactors = FALSE,
136   check.names = FALSE
137 )
138 })
139
140 # Show the values in an HTML table -----
141
142 # Bands variable table
143 output$values1 <- renderTable({
144   estimatedBands()
145 })
146
147 # VI table
148 output$values2 <- renderTable({
149   estimatedVI()
150 })
151
152 # Result output
153
154 Resv <- reactive({
155   req(extB())
156   val <- extB()
157   Blv <- val[[1]]
158   Grv <- val[[2]]
159   Rdv <- val[[3]]
160   Nirv <- val[[4]]
161   SAVI <- ((Nirv - Rdv) / (Nirv + Rdv + 0.5)) * (1.5)
162   MSAVI <- (2 * Nirv + 1 - sqrt((2 * Nirv + 1) ^ 2 - 8 * (Nirv - Rdv))) / 2
163   GNDVI <- (Nirv - Grv) / (Nirv + Grv)
164   GCI <- (Nirv) / (Grv - 1)
165   NDVI <- (Nirv - Rdv) / (Nirv + Rdv)
166   RCC <- Rdv / (Rdv + Blv + Grv)
167   cat("RCCresv = ", RCC, "\n")
168   Inp <- data.frame(cbind(
169     "SAVI" = round(SAVI, 3), "MSAVI" = round(MSAVI, 3), "GNDVI" = round(GNDVI, 3), "GCI" = round
170     (GCI, 3),
171     "NDVI" = round(NDVI, 3), "RCC" = round(RCC, 3), "Blue" = round(Blv, 3), "NIR" = round(Nirv,
172     3), "AvgT_Soil" = input$C1, "AvgB_Soil" = input$C2))
173   model_caret <- readRDS("RF_TrainModel_CubeSat.rds")
174   rfs <- round(predict(model_caret, Inp), 2)
175   return(rfs)
176   print(Inp)
177 })
178
179 observeEvent(input$Pred, {
180   output$ResOut <- renderText({
181     paste("Biomass yield prediction = ", Resv(), "kg/ha" )
182   })
183 })
184 # tabPanel 2 -----
185
186 # Text heading output
187 output$outT <- renderText({
188   if(input$gndviID == TRUE){
189     "Vegetation index selected: green normalized difference vegetation index (GNDVI)"
190   } else if(input$ndviID == TRUE){
191     "Vegetation index selected: normalized difference vegetation index (NDVI)"
192   }
193 })

```

```

192 } else if(input$saviID == TRUE){
193   "Vegetation index selected: soil adjusted vegetation index (SAVI)"
194 } else if(input$rccID == TRUE){
195   "Vegetation index selected: red chromatic coordinate (RCC)"
196 } else if(input$msaviID == TRUE){
197   "Vegetation index selected: modified soil adjusted vegetation index (MSAVI)"
198 } else if(input$gciID == TRUE){
199   "Vegetation index selected: green chlorophyll index (GCI)"
200 }else{
201   "Vegetation index selected:"
202 }
203 })
204
205 # Estimating VIs
206
207 uploadShpfileRead <- reactive({
208   if (!is.null(input$shpFile)) {
209     shpDF <- input$shpFile
210     prevWD <- getwd()
211     uploadDirectory <- dirname(shpDF$datapath[1])
212     setwd(uploadDirectory)
213     for (i in 1:nrow(shpDF)) {
214       file.rename(shpDF$datapath[i], shpDF$name[i])
215     }
216     shpName <-
217       shpDF$name[grep(x = shpDF$name, pattern = "*.shp")]
218     shpPath <- paste(uploadDirectory, shpName, sep = "/")
219     setwd(prevWD)
220     shpFile <- st_read(shpPath)
221     return(shpFile)
222   } else {
223     return()
224   }
225 })
226
227 ras <- reactive({
228   req(uploadShpfileRead(), rstack())
229   shp1 <- sf::st_transform(uploadShpfileRead(), crs(rstack()))
230   m1 <- raster::mask(rstack(), shp1)
231   return(m1)
232 })
233
234 ndviV <- reactive({
235   ndvi <- (ras()$nir - ras()$red)/(ras()$nir + ras()$red)
236   return(ndvi)
237 })
238
239 gndviV <- reactive({
240   gndvi <- (ras()$nir - ras()$green)/(ras()$nir + ras()$green)
241   return(gndvi)
242 })
243
244 gciV <- reactive({
245   gci <- ras()$nir/(ras()$green - 1)
246   return(gci)
247 })
248
249 rccV <- reactive({
250   rcc <- ras()$red/(ras()$red + ras()$green + ras()$blue)
251   return(rcc)
252 })
253
254 saviV <- reactive({
255   savi <- ((ras()$nir - ras()$red) / (ras()$nir + ras()$red + 0.5)) * (1.5)
256   return(savi)
257 })

```

```

258
259 msaviV <- reactive({
260   msavi <- (2 * ras()$nir + 1 - sqrt ((2 * ras()$nir + 1)^2 - 8 * (ras()$nir - ras()$red))) / 2
261   return(msavi)
262 })
263
264
265 # Raster base map
266 output$mapn <-
267   renderLeaflet({
268     ## begin rendering leaflet and store as 'map' in server output
269     leaflet() %>% addProviderTiles(providers$Esri.NatGeoWorldMap) %>% ## Add basemap
270     addScaleBar() %>% #add dynamic scale bar
271     addDrawToolbar(
272       polylineOptions = FALSE,
273       circleOptions = FALSE,
274       polygonOptions = TRUE,
275       markerOptions = FALSE,
276       circleMarkerOptions = FALSE,
277       rectangleOptions = FALSE,
278       singleFeature = FALSE,
279       editOptions = editToolbarOptions()
280     ) %>%
281     setView(lat = 46.769,
282            lng = -100.916,
283            zoom = 10)
284   }) ## close map
285
286 VIdisp <- function(vInf){
287   rst <- vInf
288   spts <- rasterToPoints(rst, spatial = TRUE)
289   llpts <- spTransform(spts, CRS("+proj=longlat +ellps=WGS84 +datum=WGS84 +no_defs +towgs84
290     =0,0,0"))
291   crd <- coordinates(llpts)
292   xmin <- min(crd[,1]); xmax <- max(crd[,1]); ymin <- min(crd[,2]); ymax <- max(crd[,2])
293   x <- xmin + (xmax - xmin)/2
294   y <- ymin + (ymax - ymin)/2
295   pal <- colorNumeric("RdYlGn", values(vInf), na.color = "transparent")
296   leafletProxy("mapn") %>%
297     clearImages() %>%
298     addRasterImage(vInf, colors = pal, project = F) %>%
299     setView(lat = y,
300            lng = x,
301            zoom = 20) %>%
302     addLegend(pal = pal, values = values(vInf), title = "Vegetation index", position = "
303       bottomright")
304
305 varVI <- c("gciID", "msaviID", "saviID", "rccID", "ndviID", "gndviID")
306
307 DisEnbFnc <- function(inPID, ViD, IndFn){
308   if(inPID == TRUE){
309     VIdisp(IndFn)
310     sel <- ViD
311     if (sel == ViD){
312       selt <- varVI[-which(varVI==ViD)]
313     }
314     shinyjs::disable(as.character(selt[1]))
315     shinyjs::disable(as.character(selt[2]))
316     shinyjs::disable(as.character(selt[3]))
317     shinyjs::disable(as.character(selt[4]))
318     shinyjs::disable(as.character(selt[5]))
319   }
320   else {
321     selt <- varVI[-which(varVI==ViD)]
322   }

```

```

322     shinyjs::enable(as.character(selt[1]))
323     shinyjs::enable(as.character(selt[2]))
324     shinyjs::enable(as.character(selt[3]))
325     shinyjs::enable(as.character(selt[4]))
326     shinyjs::enable(as.character(selt[5]))
327     leafletProxy("mapn") %>%
328       clearImages() %>%
329       clearControls() %>%
330       setView(lat = 46.769,
331             lng = -100.916,
332             zoom = 11)
333   }
334 }
335
336 observeEvent(input$gndviID, DisEnbFnc(input$gndviID, "gndviID", gndviV()))
337 observeEvent(input$ndviID, DisEnbFnc(input$ndviID, "ndviID", ndviV()))
338 observeEvent(input$gciID, DisEnbFnc(input$gciID, "gciID", gciV()))
339 observeEvent(input$saviID, DisEnbFnc(input$saviID, "saviID", saviV()))
340 observeEvent(input$rccID, DisEnbFnc(input$rccID, "rccID", rccV()))
341 observeEvent(input$msaviID, DisEnbFnc(input$msaviID, "msaviID", msaviV()))
342
343 shpAr <- reactive({
344   req(uploadShpfileRead())
345   Ar <- sf::st_area(uploadShpfileRead())
346   return(Ar)
347 })
348
349 DatViz <- reactive({
350   req(uploadShpfileRead())
351   Ar <- sf::st_area(uploadShpfileRead())
352   ArF <- round(Ar/10000, 2)
353   dataIn <- data.frame(
354     "Area (ha)" = as.character(ArF),
355     "Minimum" = as.character(0),
356     "Mean" = as.character(0),
357     "Maximu" = as.character(0),
358     stringsAsFactors = FALSE,
359     check.names = FALSE)
360 }
361 )
362
363 # VI table
364 output$table3 <- renderTable({
365   DatViz()
366 })
367
368 } ## close server
369
370
371 shinyApp(ui = ui, server = server) ## Run the app locally

```